

Development of spectroscopic techniques for the measurement of Respirable Crystalline Silica

STACEY, Peter

Available from the Sheffield Hallam University Research Archive (SHURA) at:

<http://shura.shu.ac.uk/32066/>

A Sheffield Hallam University thesis

This thesis is protected by copyright which belongs to the author.

The content must not be changed in any way or sold commercially in any format or medium without the formal permission of the author.

When referring to this work, full bibliographic details including the author, title, awarding institution and date of the thesis must be given.

Please visit <http://shura.shu.ac.uk/32066/> and <http://shura.shu.ac.uk/information.html> for further details about copyright and re-use permissions.

Development of spectroscopic techniques for the measurement of Respirable Crystalline Silica

Peter Robert Stacey

A thesis submitted in part fulfilment of the requirements of
Sheffield Hallam University for the degree of Doctor of Philosophy

May 2022

In collaboration with the Health & Safety Executive.

I hereby declare that:

1. I have not been enrolled for another award of the University, or other academic or professional organisation, whilst undertaking my research degree.
2. None of the material contained in the thesis has been used in any other submission for an academic award.
3. I am aware of and understand the University's policy on plagiarism and certify that this thesis is my own work. The use of all published or other sources of material consulted have been properly and fully acknowledged.
4. The work undertaken towards the thesis has been conducted in accordance with the SHU Principles of Integrity in Research and the SHU Research Ethics Policy.
5. The word count of the thesis is 29318 (excluding articles).

Name	<i>Peter Stacey</i>
Date	<i>01/05/22</i>
Award	<i>Doctor of Philosophy</i>
Faculty	<i>Materials Engineering Research Institute</i>
Director(s) of Studies	<i>Professor Christopher Sammon</i>

Acknowledgements

I would like to thank the director of studies Professor Christopher Sammon and my University supervisor Dr Francis Clegg for their leadership, support, and encouragement over the many years of study at Sheffield Hallam University.

I would also like to thank my colleagues at the Health and Safety Executive (HSE).

Professor Andrew Curran (Chief Scientific Advisor for HSE) for sponsoring these studies, and my managers Dr Stephen Kinghorn-Perry, Mr Laurie Davies and Dr Duncan Rimmer for their support.

Also, Dr Jackie Morton, for acting as the industrial supervisor for the university and the following colleagues for their helpful suggestions and policy and regulatory reviews; Dr Susan Hambling, Margaret Wade, Ian Pengelly, Owen Butler, Shirley Haslett, Claire McNicholas, Tracy Hamilton, and Richard Broughton and anyone else who may have contributed. In addition, I would like to thank Lidia Malecka for help with some of the graphics work in the articles, Dr Timothy Yates for help developing the Matlab script, Samantha Hall and Steven Stagg for their help and for collecting aerosol samples of artificial and natural stones, George Alliot and Kieth Birkitt for their photographs of the filters, Matthew Jackson and James Staff for checking results and all the inspectors who helped; in particular, Cliff Seymour, Trevor Lowe and Vincent Fowler.

Most of all I wish to thank my wife Nicola for her patience and support, her parents Christopher and Diana Worsell for providing me with a place to stay in Sheffield when I needed to analyse samples at the university, without which it might not have been possible to complete this work, and my parents Frederick and Cherry for their encouragement.

This thesis is my own work

Disclaimer

Whilst the work was conducted on behalf of HSE, the opinions expressed in the thesis and articles are those of the author's alone and do not necessarily reflect the views of HSE.

© Crown copyright 2023

Abstract

Inhalation of aerosols containing respirable-sized crystalline silica (RCS) is a significant hazard for hundreds of thousands of workers in Great Britain (GB), which can cause lung cancer and silicosis. There are elevated levels of disease attributed to exposure to RCS in GB. Personal aerosol monitoring provides an indication of a person's exposure to RCS, which correlates to the potential risk of ill-health. RCS is often measured in a portion of the aerosol collected in the workplace using X-ray diffraction (XRD) or Fourier Transform Infrared (FTIR) instruments. Uncertainty of XRD or FTIR measurements can exceed international requirements for occupational hygiene analyses at RCS concentrations where there remains a significant risk to worker health. This thesis investigates the application of Raman spectroscopy to improve sensitivity and limits of detection (LOD) for RCS measurements and chemometric methods to improve FTIR measurements when interference is present.

For Raman spectroscopy, a feasibility study was undertaken employing optimal measurement conditions and artificial dust mixtures. This study was developed into a method to assess in-respirator samples of RCS from a breathing manikin challenged with a simulated work task. RCS inward leakage ratios (ILRs) based on mass concentration were compared with particle mass and number concentration ILRs from particle counting instruments. The performance of Raman spectroscopy was compared with XRD to assess its limitations when measuring sub-fractions of quartz and RCS in 119 samples from stonemasonry activities. For FTIR, the performance of chemometric methods were compared when measuring artificially prepared mixtures with kaolinite interference and the measurement uncertainty of a Principal Component Regression method was evaluated using real mine dusts.

This work was the first to demonstrate the potential of Raman spectroscopy for quantitative measurements of RCS at low concentrations (less than $1\mu\text{g.m}^{-3}$). When measuring respirable quartz, Raman response is directly proportional to the mass of analyte when the depth of the sample is a couple of layers. For the quartz standard A9950, this depth is less than $5\mu\text{m}$ (which equates to about 3.6 layers of particles $1.39\mu\text{m}$ in diameter). An increase in Raman response/ μg

was observed at mass loadings above this particle density. The change in the Raman band response is coincident with the depth of sample deposit where significant attenuation of the XRD response would occur due to absorption by multilayers of particles. The Raman band integrated area obtained similar mass values to that measured with XRD integrated intensity when analysing sub-fractions of dusts with differing particle size. Measurements of 119 stone dust samples highlighted the advantage of Raman spectroscopy to quantify quartz with zircon. For FTIR, a multicomponent chemometric analysis of aerosol particulate on filters, was demonstrated, which substantially improves the accuracy of FTIR measurements of quartz in mine dusts. Nevertheless, the measurement of RCS remains potentially challenging due to the range of industries and exposures.

This Raman spectroscopy work supported other Health and Safety Executive research to investigate differences between emissions of natural and artificial stones. The short sampling times for laboratory-based experiments would have resulted in many of the samples reporting below or at the LOD of current measurement techniques. Therefore, the use of Raman spectroscopy made the findings of the research more comprehensive.

Chapter. 1	Introduction	1
1.1	Overview	2
1.2	What is crystalline silica?	4
1.2.1	Crystalline structure of quartz and cristobalite	4
1.3	Health effects of prolonged exposure to Respirable Crystalline Silica (RCS)	8
1.3.1	Classification of respirable crystalline silica as a carcinogen	8
1.3.2	Silicosis	9
1.3.3	The relationship between the measurement metric and incidence of silicosis	9
1.4	Regulation of exposure to respirable crystalline silica (RCS) in Great Britain	11
1.4.1	Monitoring for personal exposure to aerosols containing RCS	12
1.5	Current analytical methodology for monitoring exposure to RCS	13
1.5.1	Collecting a personal worker sample from an aerosol containing RCS	13
1.5.2	Analytical techniques for measuring respirable crystalline silica	18
1.5.3	X-ray diffraction (XRD) measurement of RCS	19
1.5.4	Infrared analysis	27
1.6	Application of Raman spectroscopy for the measurement of RCS	30
1.6.1	What is Raman spectroscopy?	30
1.6.2	Similarities and differences between IR and Raman spectroscopy	31
1.6.3	Optical vibrations for α -quartz and α -cristobalite	34
1.6.4	Measurement of crystalline material	36
1.6.5	Raman band intensity and quantitative measurement of RCS particulate on filters	37
1.6.6	Use of Raman for quantitative analysis	39

1.6.7	Raman measurement of crystalline silica and airborne particulate	40
1.6.8	The Raman instrument used for measurement of RCS.....	42
1.7	Performance of XRD and Infrared methods for RCS measurement.....	47
1.7.1	Typical limits of detection of current analytical methods for RCS	47
1.7.2	Estimates of RCS measurement uncertainty.....	49
1.7.3	Measurement uncertainty for direct on-filter methods	52
1.7.4	Differences between analytical approaches for measuring RCS.....	53
1.7.5	Differences between process recovery approaches for RCS methods	54
1.7.6	Relationship between XRD and FTIR instrument response and RCS particle diameter	56
1.7.7	The effect of interference on the measurement of RCS	56
1.7.8	Impact of interference on RCS measurement	62
1.8	Approaches for removal of spectral diffraction line interference	64
1.8.1	Current practice for measurements of RCS on aerosol filters	64
1.8.2	Potential of chemometric models to remove FTIR spectral interference for RCS.	64
1.8.3	Potential for removal of diffraction line interference for RCS from XRD scans	66
1.9	Discussion and conclusion	67
1.10	Aims and Objectives.....	70
Chapter. 2	Sample concentration methods.....	71
2.1	Method	72
	<i>First test method</i>	72
	<i>Second test method</i>	72
2.2	Results	73
2.3	Discussion and conclusion	74
Chapter. 3	Feasibility study for Raman microscopy measurement of RCS .	75

Chapter. 4	A Raman spectroscopy method for measurement of respirable crystalline silica collected on aerosol filters inside respiratory equipment.	86
Chapter. 5	Change in Raman response with particle size and the measurement of samples from stonemasonry activities.	104
Chapter. 6	A comparison between partial least squares and principal component regressions for analysis of particulate in coal dust.	130
Chapter. 7	Application of a Principal Component Regression (PCR) chemometric method for the quantification of RCS (quartz), in coal dusts.....	154
Chapter. 8	Discussion and conclusions	179
8.1	Discussion	180
8.1.1	Quantitative measurement of RCS.....	180
8.1.2	Influence of absorption	186
8.1.3	Influence of particle density	187
8.1.4	Improvements in the limit of detection (LOD)	188
8.1.5	Measurement of samples collected from inside a respirator	194
8.1.6	<i>Comparison with particle number and mass metrics</i>	195
8.1.7	<i>Comparability of Raman with XRD measurements of RCS</i>	197
8.1.8	<i>Dealing with spectral interferences</i>	200
8.1.9	Regulatory measurement at concentrations lower than the current WEL in Great Britain.	204
8.2	The potential for further improvements for RCS measurements and future work.	207
8.3	Conclusion.....	211

Table of Figures

Figure 1. The fundamental arrangement of atoms in crystalline silica.	6
Figure 2. Arrangement of tetrahedrons for α -quartz along the c and a crystal plane. An idealised image of a quartz crystal is shown on the right-hand side with the direction of the 'c' and 'a' axis.	6
Figure 3. The crystal habit of α -cristobalite showing the 'c' and 'a' axis of symmetry and approximate positions of tetrahedra in the unit cell.	7
Figure 4. The risk of the incidence of silicosis using the International Labour Organisation (ILO) classification in workers with 15 years employment for respirable crystalline silica concentrations from 0.3 mg.m^{-3} to 0.02 mg.m^{-3}	10
Figure 5. Schematic diagram of the SIMPEDS respirable cyclone sampler showing the cyclonic action around the vortex finder creating a moment of inertia.	15
Figure 6. Picture of and a schematic diagram of the HSE miniature respirable sampler with the foam selector for in-respirator aerosol sampling.	16
Figure 7. A schematic representation of the action of a cascade impactor. The arrows represent the path of particles of different diameters. W denotes the diameter of the inlet and S is the stopping distance of the particle.	18
Figure 8. Arrangement in a Bragg Brentano focusing X-ray diffraction instrument.	21
Figure 9. Schematic for the process of diffraction in a crystalline material.	21
Figure 10. X-ray diffraction scans of α -quartz and α -cristobalite measured using copper radiation (1.54 \AA).	22
Figure 11. Schematic of the Michelson interferometer for an FTIR instrument.	27
Figure 12. An infrared spectrum for respirable α -quartz collected onto a polyvinylchloride (PVC) filter.	28
Figure 13. An infrared spectrum for respirable α -cristobalite collected onto a polyvinylchloride (PVC) filter.	29

Figure 14. Jablonski diagram representing the energy transitions for different types of photon scattering.	31
Figure 15. Infrared and Raman active vibrations for a three atom molecule.	33
Figure 16. A schematic representation of the components of a Raman spectrometer connected to a microscope.	42
Figure 17. An illustration of the different sampling volumes obtained for microscope objectives with high and low numerical apertures.	46
Figure 18. Processes and contributors to uncertainty when measuring respirable crystalline silica.	50
Figure 19. Range of z-scores obtained from laboratories using direct on-aerosol filter (DOF) and indirect (ID) analysis approaches when using X-ray diffraction (XRD) or Fourier Transform Infrared (FTIR) spectroscopy.	54
Figure 20. The X-ray diffraction pattern of anorthite ($\text{CaAl}_2\text{Si}_2\text{O}_8$). The positions for the three main intensities of α -quartz are shown.	59
Figure 21. The X-ray diffraction pattern of albite ($\text{NaAlSi}_3\text{O}_8$) with a trace anorthite ($\text{CaAl}_2\text{Si}_2\text{O}_8$) and mica. The positions for the three main intensities of α -quartz are shown.	59
Figure 22. The X-ray diffraction pattern of microcline (KAlSi_3O_8) with a minor amount of albite ($\text{NaAlSi}_3\text{O}_8$). The positions for the three main intensities of α -quartz are shown.	60
Figure 23. FTIR absorbance spectrum for respirable anorthite dust collected onto a PVC filter.	60
Figure 24. FTIR absorbance spectrum for respirable albite dust collected onto a PVC filter.	61
Figure 25. FTIR absorbance spectrum for respirable microcline dust with a minor amount of albite collected onto a PVC filter.	61
Figure 26. A comparison of the percent variation of XRD results for α -quartz from their gravimetric loaded mass values for the plasma and furnace ashing indirect measurement approaches.	73

Figure 27. A representation of the size of an airy disc for high and low numerical aperture objectives showing the extension beyond the wavelength limited focal area and destructive interference occurring at P1.....	182
Figure 28. (A) The pattern observed when aluminium was removed from the surface of a polytetrafluorethylene filter when its surface was mapped using a 785 nm laser at 100 % power for three accumulations of 7 seconds at each position with a x20 objective and numerical aperture of 0.4. (B) The hole formed in a gold coated polycarbonate filter placed on a silver filter when measured with the same parameters at 10 % power.	183
Figure 29. The approximate diameter of the area contributing most photons collected by a x20 objective (NA 0.4) (between the dotted lines) when measuring the surface of a quartz plate in 1 μm steps over a metal foil.	184
Figure 30. The cumulative average Raman band integrated area for the measurement of quartz powder A9950 over a 15 mm diameter deposit on silver filters (A) and the measurement of quartz collected with the HSE miniature sampler onto 13 mm diameter quartz fibre filters (B).	185
Figure 31. A test of the X-ray diffraction limit of detection from 11 μg to 1 μg for the measurement of quartz standard A9950 deposited into an 15 mm diameter area onto 0.45 μm pore size silver filters.	190
Figure 32. Comparison between X-ray diffraction (XRD) and Raman spectroscopy measurements of respirable crystalline silica collected on impactor samples by stone type (sandstone, engineered stone, diorite and sintered stone).	198

List of Tables

Table 1. Polymorphs of crystalline silica and their occurrence in the workplace.	5
Table 2. Significant reflections of α -quartz and α -cristobalite when using copper radiation ($K\alpha_1$ 1.54 Å), their angles of 2θ , relative intensity and Miller indices.	23
Table 3. The observed Raman and infrared wavenumbers and their associated Mulliken symbols for α -quartz and α -cristobalite.	35
Table 4. Current analytical methods for RCS and their limits of detection in terms of the mass (μg) collected on an aerosol sampling filter and mass concentration for various sampling times (h) when using a respirable sampler with a flow rate of 2.2 L min^{-1} .	48
Table 5. Common materials found in workplaces and potential silicate interferences.	58
Table 6. Statistics from the second comparison comparing filter treatment processes for the indirect analysis method when measuring filters with a loading $10 \mu\text{g}$ of α -quartz	74
Table 7. Limits of detection obtained in this work compared with other recent studies.	192
Table 8. Metrics and particle diameter range for instruments used to compare inward leakage ratios.	195
Table 9. Trend line coefficients and coefficients of determination for a comparison of XRD with Raman measurements of RCS on Sioutas impactor samples from four stone types.	199

Chapter. 1 Introduction

1.1 Overview

Products and materials containing crystalline silica are widely used and found in many workplaces. As a result, many hundreds of thousands of workers are exposed to aerosols containing respirable crystalline silica (RCS) which, if inhaled, potentially causes disabling lung diseases such as silicosis and lung cancer. Internationally, the measurement of a sample of aerosol collected on a filter is one established approach to assess a worker's personal occupational exposure to this hazardous substance. Raman spectroscopy was investigated to assess its potential to provide new measurement capabilities that were beyond the performance of the established methods utilising X-ray diffraction (XRD) and Fourier transform infrared (FTIR) analysis.

Chapter 1 provides background, describes the limitations of current methodologies, the potential for Raman spectroscopy to provide a method with lower limits of detection and strategies that are available to potentially deal with the influence of interference on a measured RCS value.

Chapter 2 describes some pre-experimental work to investigate which sample concentration process provides more precise results.

Chapters 3, 4 and 5 demonstrate the development of Raman spectroscopy as a technique for the measurement of RCS, from initial tests under ideal conditions to a method capable of measuring regulatory samples collected from stonemasonry activities. These Chapters also show the improvement in the limits of detection (LOD) for RCS measurement found for both Raman spectroscopy and XRD methods.

Chapter 3 describes a feasibility study which applied favourable measurement conditions to assess the potential of Raman spectroscopy to measure RCS collected on filters. In addition, tests in Chapter 3 also challenged the Raman spectrometer to artificially prepared matrices to assess potential difficulties when measuring workplace samples with components that might absorb Raman photons. For example, absorption from hematite; that is found in samples from foundries.

Chapter 4 summarises the development of a Raman spectroscopy method, its improved LOD compared with established XRD and FTIR methods and its capability to measure RCS aerosol collected from miniature respirable samplers placed inside respiratory protective equipment. In addition, the laboratory-based experiments provided the opportunity to compare instruments measuring both mass and particle number metrics for the assessment of leakage into the respirator and their potential application for determination of respirator inward leakage ratios. The Raman spectroscopy method meets the criteria for its application as a regulatory method.

Chapter 5 takes the Raman spectrometer development a step further by exploring the relationship between the median particle diameter of the collected aerosol and instrument response, and its application when measuring RCS in 119 samples collected when cutting and polishing natural and engineered stones. Particle diameter can theoretically affect the Raman response. The change in instrument response with the median particle diameter of the collected aerosol is a common problem for most techniques measuring RCS. The Chapter demonstrates the stability of the Raman response within the respirable-sized particle diameter range (from μm to nm), the comparability of results with XRD in both calibration and stone samples and its advantages when measuring RCS in some matrices.

Differences between potential approaches to deal with matrix interference are the subject of Chapters 6 and 7. Developments in FTIR technology have reduced the size and cost of these instruments which provide quick measurements and are now portable. The magnitude of the effect of interfering minerals in the sample on the accuracy of results is one issue that is uncertain. Rapid multicomponent analysis of hazardous particulate on the same filter sample is a potential advantage of FTIR, which is demonstrated by Chapters 6 and 7. Chapter 6 investigated the difference in performance between partial least squares (PLSR) and principal component (PCR) regression chemometric methods demonstrating their similarity in performance when using a similar number of principal components. Chapter 7 applied an adapted version of the PCR model to the analysis of quartz, kaolinite and coal dust in a range of coal

mine dusts from Australia, South Africa and the United Kingdom. This approach was taken to demonstrate the advantage of using filter samples, containing artificially prepared mixtures of minerals generated in a laboratory, to develop a model that was applicable to a wide variety of different mine dusts.

1.2 What is crystalline silica?

Silica is one of the most abundant mineral groups found in the earth's upper continental crust¹ and consists of silicon (Si) and oxygen (O) atoms with the stoichiometric formula SiO_2 . Silica exists in both an amorphous (non-crystalline) and crystalline state; where the arrangement of atoms forms a symmetrical repeated pattern. There are many different forms of crystalline silica that are known as polymorphs. Polymorphs are molecules that have the same elemental composition with different crystal structures. Crystalline silica is widely found in manufactured products and raw materials in the construction, masonry, ceramics, chemicals, glass and metallurgical industries.² Table 1 lists crystalline forms of silica and their relative abundance in workplace samples.

The scope of this thesis focuses on the α -quartz and α -cristobalite crystalline polymorphs of silica. α -Quartz and α -cristobalite are the most commonly encountered polymorphs in the workplace and an overwhelming majority of exposures are to aerosols containing α -quartz.³

1.2.1 Crystalline structure of quartz and cristobalite

Structures of crystalline silica are built on tetrahedral arrangements of atoms consisting of a silicon (Si) connected to four oxygen atoms (O).⁴ A representation of the basic tetrahedron arrangement of atoms is shown in Figure 1.

Table 1. Polymorphs of crystalline silica and their occurrence in the workplace.

Silica polymorph (Crystal Structure)	Stability temperature range ⁴	Abundance in the workplace
α -Quartz (Trigonal)	From room temperature to 573 °C	Commonly found in workplace environments as a constituent of many natural and manufactured materials. The most abundant form of crystalline silica. ^{3, 4}
β -Quartz (Hexagonal)	573 °C to 870 °C	Rare – not stable at room temperature.
α -Cristobalite (Tetragonal)	From room temperature to 275 °C	Infrequently found in workplaces as a result of a processes involving heating quartz or amorphous silica above 1000 °C. α -Cristobalite occurs in ceramic, refractories, furnace insulation material, and calcined diatomaceous earth. ⁵ In nature, it occurs in some igneous rocks, bentonite clays and in some volcanic ash. ⁶ It is occasionally found in some imported bentonite clay.
β -Cristobalite (Cubic)	1470 °C to 1670 °C	Not often found in the workplace. Has been noted as a by-product of the de-vitrification of alumina silicate glass fibre insulation in furnaces. ⁷
α -Tridymite (Orthorhombic)	From room temperature to 117 °C	Rare. It was found in samples of dust from town gas facilities in the 1970s in association with α -cristobalite and most recently as a trace contaminant of mineral dust added to some artificial stone work tops. ⁸ It is found in some volcanic rocks.
β -Tridymite (Hexagonal)	870 °C to 1470 °C	Not encountered in workplaces.
Keatite	Stable at room temperatures	Its occurrence is not noted in workplaces. It is considered as a metastable phase of α -cristobalite. ⁹
Coesite and Stishovite		Not found in the workplace. These highly dense forms of crystalline silica are formed at high pressures and are found in rocks at the edge of meteor impact craters. ⁴

Note: α refers to the low temperature form and β to the high temperature form.

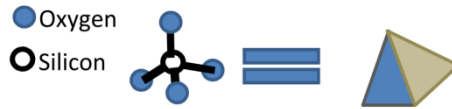


Figure 1. The fundamental arrangement of atoms in crystalline silica.

The structure for α -quartz was first determined in 1913.¹⁰ α -Quartz has a trigonal crystal system in the hexagonal group within which the unit cell has three molecules of SiO_2 (Si_3O_6). A set of three tetrahedra are arranged in a spiral along the 'c' axis, which contains the highest symmetry, to form the unit cell (Figure 2).¹¹ The unit cell has three fold symmetry along its 'c' axis which intersects the silicon atoms and two axis of two fold symmetry. Each unit cell is joined to others that run as a helical spiral along the c axis of the crystal. For α -quartz, the angle of the silicon and oxygen (Si-O-Si) bonds linking each tetrahedra is 144° . Six helical spirals join together which permits a six-sided column of space to form within the spirals.

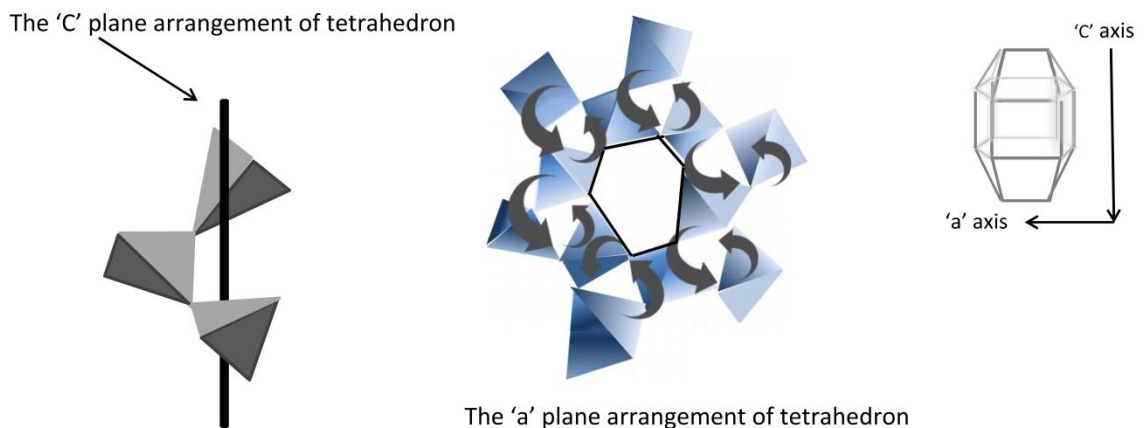


Figure 2. Arrangement of tetrahedrons for α -quartz along the c and a crystal plane. An idealised image of a quartz crystal is shown on the right-hand side with the direction of the 'c' and 'a' axis.

The low temperature α -cristobalite structure is tetragonal where neighbouring oxygen atoms are in a pseudo body centred cubic arrangement.¹² The crystal habit of α -cristobalite is represented in Figure 3, where the crystal is orientated from point to point on the 'c' axis of highest symmetry. There are twelve atoms in the unit cell (Si_4O_8) which has a more open structure when compared with α -

quartz.⁴ Therefore, four sets of tetrahedra are arranged in a spiral along the 'c' axis. The unit cell has four fold symmetry along its 'c' axis and four two fold axis of symmetry along the 'a' axis. For α -cristobalite, the Si-O-Si bond angle connecting each tetrahedra is from 144° to 147° , although some reported values are higher.¹³ The helices of tetrahedra are either left or right handed for both α -quartz and α -cristobalite

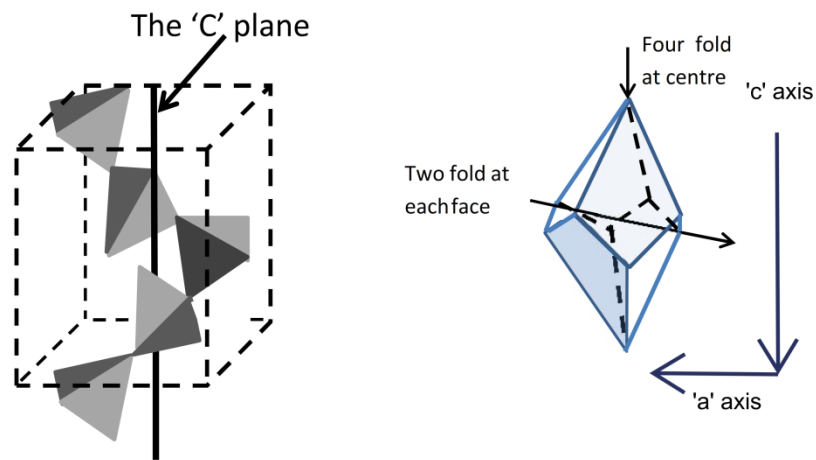


Figure 3. The crystal habit of α -cristobalite showing the 'c' and 'a' axis of symmetry and approximate positions of tetrahedra in the unit cell.

1.3 Health effects of prolonged exposure to Respirable Crystalline Silica (RCS)

Processing and handling of materials containing crystalline silica can result in aerosols containing particles that are respirable. The term 'respirable' refers to a health-related particle size definition, used in occupational hygiene, for the sizes of particles that penetrate into the alveoli of the lung; which is defined as a cumulative log distribution of particles with an aerodynamic median (50%) diameter of 4 μm and 0.1% at 16 μm .¹⁴ It is the inhalation of respirable-sized crystalline silica into the gaseous exchange region of the lung (alveoli) that can cause silicosis;¹⁵ which is one of the oldest occupational diseases.^{16, 17} Other diseases with sufficient evidence of association with the inhalation of crystalline silica are lung cancer,^{18, 19} and chronic obstructive pulmonary disease (COPD).¹⁷ The potential for incidence of lung disease from RCS is relatively high, even when the airborne concentrations are reduced, because large numbers of workers are exposed to aerosols containing crystalline silica. In 2022, it is estimated that about, 560,000 workers are potentially exposed to crystalline silica in Great Britain¹⁹ and 1.7 million in the United States of America.¹⁷

1.3.1 Classification of respirable crystalline silica as a carcinogen

The international agency for cancer research has classified crystalline silica dust as 'Group 1, carcinogenic to humans' whereas amorphous silica is not.²⁰ It is estimated that 907 cancer registrations were attributable to exposure to crystalline silica in the UK in 2005.²¹ The European Community classified respirable crystalline silica as a carcinogen when generated from a work process and a binding worker exposure limit for an aerosolised concentration 0.1 mg.m^{-3} was introduced in the European Union on the 17th of January 2020.²²

1.3.2 Silicosis

Silicosis is the main health effect associated with exposures in the workplace and is a disabling disease which often first materialises as shortness of breath known as a dyspnoea.²³ It is characterised as a nodular fibrosis of the lung tissue caused by the inhalation of dusts containing crystalline silica.¹⁷ There are three types of silicosis termed chronic, accelerated, or acute. Chronic silicosis is generally attributed to long term exposures of about 20 years. Accelerated silicosis is thought to occur between 2 to 5 years and is characterised by worker exposures to very high concentrations of airborne particles. Cases of accelerated silicosis were recently associated with exposures to emissions from working with artificial stones.²⁴ Acute silicosis develops rapidly and has been attributed to exposure from particles of freshly fractured crystalline silica.^{23, 25} There is no cure for silicosis and the only available treatment is a lung transplant.²⁴

1.3.3 The relationship between the measurement metric and incidence of silicosis

The toxicity of crystalline silica has been reported to vary between relatively pure samples of the same polymorph from different sources,^{26, 27} when mixed with different minerals,³ with particle size and when freshly fractured.²⁸ There is no conclusive evidence for differences in toxicity between quartz and cristobalite.¹⁵ Generally, the toxicity increases as particle size decreases which leads to increase in surface area and potential interactions with cells.¹⁵ However, the respirable mass of crystalline silica rather than a metric associated with the sizes of particles (e.g. particle number concentration or surface area) is used for measurements to assess the exposures of workers to aerosols containing crystalline silica.

The selection of respirable mass as the metric of choice was made from early research conducted in British coal mines. Research showed a better correlation with incidence of pneumoconiosis and dust exposure for respirable mass concentration (associated with lung burden) with a coefficient of determination of 0.8, compared with particle number concentration measurements with a coefficient of determination of 0.4.²⁹⁻³¹

Epidemiological studies reviewed by the Health and Safety Executive (HSE)¹⁵ showed that the quality and robustness of predictions for the incidence of silicosis in epidemiological studies varied. Data from a study of British coalminers in Scotland³² and subsequently reassessed by other researchers¹⁵ was used by HSE to describe the relationship between mass concentrations of respirable crystalline silica and the probability of the incidence of silicosis. Figure 4 shows that RCS concentrations over 15 years of daily personal exposure have a distinct relationship with the potential incidence of ill health and that there remains a risk of silicosis at relatively low concentrations of RCS.

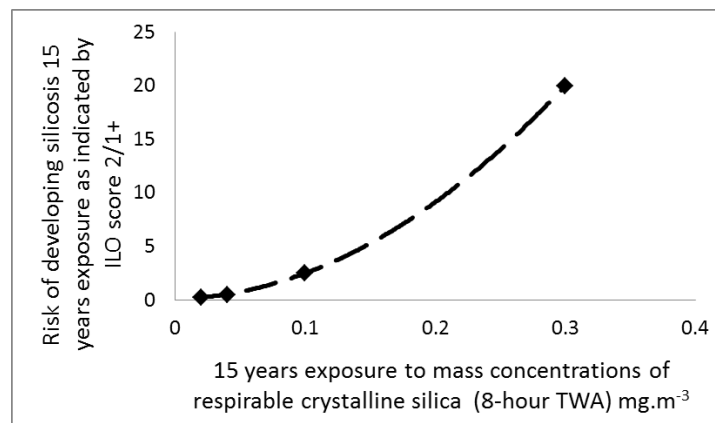


Figure 4. The risk of the incidence of silicosis using the International Labour Organisation (ILO) classification in workers with 15 years employment for respirable crystalline silica concentrations from 0.3 mg.m⁻³ to 0.02 mg.m⁻³.

(Reproduced from data in EH75 Respirable Crystalline Silica, Variability in fibrogenic potency and exposure-response relationships for silicosis. Health and Safety Executive; 2003)

The risk evaluation for developing silicosis is based on the 2/1 International Labour organisation (ILO) classification of lung radiographs for the profusion of opacities in the lung. A classification of 1/0 results in higher estimates of relative risk of ill health.

1.4 Regulation of exposure to respirable crystalline silica (RCS) in Great Britain

Exposures to RCS in Great Britain are regulated by the control of substances hazardous to health regulations (COSHH).³³ Employers (the duty holders) have a duty to prevent or adequately control worker exposure to hazardous substances and the key focus for controlling occupational exposures at work is effective risk management. The duty holder must apply good control practices and also ensure worker exposures do not exceed a workplace exposure limit (WEL) of 0.1 mg.m^{-3} below the current WEL. No regulatory distinction is made between mixed exposures to different polymorphs of crystalline silica in Great Britain.

The principles of good practice for controlling exposures are stated in the Control of Substances Hazardous (COSHH) to health regulations.³⁴ As Figure 4 shows, there remains a risk to worker health when workers are exposed to airborne concentrations of RCS. Schedule 2A of COSHH includes a principle that exposures must be controlled by measures proportionate to the health risk. For RCS, this includes reducing exposure to RCS concentrations to levels below 0.1 mg.m^{-3} , until the cost becomes disproportionate. The first step in the hierarchy of controls for controlling exposures is to substitute raw materials containing crystalline silica with ones containing a less hazardous material; although, this is not always practical because of the widespread occurrence of crystalline silica in nature. So, replacing a high with a low crystalline silica content material is another approach, which can be employed. Where, substitution of materials is not possible, engineering controls (e.g. such as water suppression or dust extraction) are often needed to reduce exposures.

Unfortunately, there are many processes that generate RCS, and where airborne levels of RCS remain high despite following the principles of good practice given in the COSHH regulations.^{33, 34} High exposures can occur, even when controls are applied and are often associated with work involving powered tools or energetic processes. In these instances, respiratory protective

equipment (RPE) is required to manage any residual risk in addition to the use of engineering and organisational controls.

1.4.1 Monitoring for personal exposure to aerosols containing RCS

The establishment of WELs are intended to prevent excessive exposures to airborne hazardous substances. The COSHH Approved Code of Practice³⁴ (ACOP) provides the following examples when exposure monitoring is necessary:

- When the risk assessment (regulation 6 of COSHH) shows that an initial exploratory monitoring exercise is necessary to reach an informed and valid judgement about the risks.
- To ensure a WEL or any (in-house) working standard is not exceeded.
- When failure or deterioration of the control measures is suspected that could result in a serious health effect.
- As an additional check on the effectiveness of any control measures to ensure exposures are prevented or reasonably controlled and prevent any subsequent risk to the health of a person.
- When any change occurs in the conditions affecting employees' exposure which affects the risk assessment and could mean that adequate control is no longer being maintained.

1.5 Current analytical methodology for monitoring exposure to RCS

1.5.1 Collecting a personal worker sample from an aerosol containing RCS

A sample of the aerosol is collected using a respirable sampler which separates the larger non-respirable aerosolised particles from the smaller respirable sized fraction, which is then measured. The respirable aerosol sampler is placed within a worker's breathing zone; which is defined as a hemisphere with a radius of about 30 cm centred on the midpoint of a line joining the ears and the face.³⁵ The correct flow rate of aerosol through the sampler is critical to the selection of the correct particle size fraction. A calibrated pump draws the aerosol at a specified flow rate through an inlet of the sampler, into the physical process used to separate the respirable fraction and onto a collection medium. Cyclonic action, foams sieves, and impactors are three physical approaches that are used to separate the respirable fraction.³⁶ The respirable dust is usually collected on a filter or foam for subsequent analysis. Common filters are organic membranes made from polyvinylchloride (PVC), mixtures of cellulose esters (MCE) and polycarbonate (PC).³⁷ Silver metal filters are also used to obtain a low background for X-ray diffraction methods.³⁷

Moment of inertia is the principle mechanism that is used to separate particles for each of these three aerosol sampling approaches.

For a moving body round an axis, the moment of inertia (I) is the ratio of angular momentum (L) with angular velocity (ω).

The angular momentum is related to mass by $L = mvr$ where m is the mass of the particle, v is its velocity and r is the radius of the particle from its axis of rotation. When the mass is high the angular momentum and moment of inertia will be high.

The separation efficiency of particles is governed by the Stokes number Sk .

$$Sk = \frac{\rho_p C_c d_p^2 U}{18\mu d_b} \quad (1)$$

Where:

ρ_p = the particle density, C_c = slip correction, d_p = the diameter of the particle, U = the relative velocity of the air, μ = the air viscosity, d_b = the body diameter

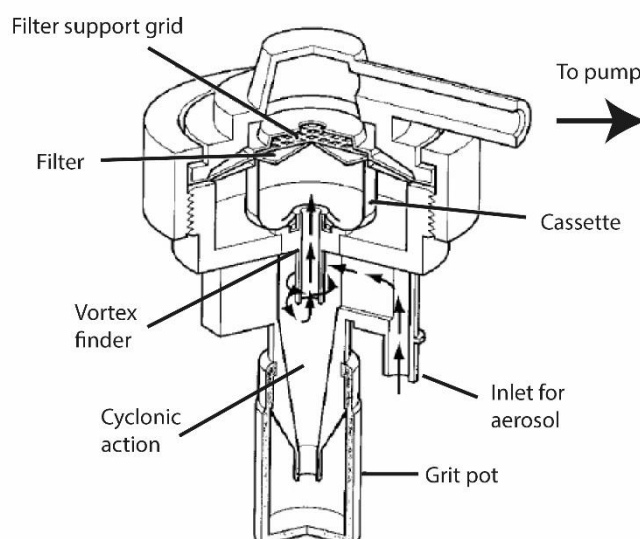
The particle will transit across the air stream and potentially impact on the separation medium referred to as the body when the Stokes number is greater than 1.^{38, 39}

1.5.1.1 Cyclonic action

The Safety in Mines Personal Dust Sampler (SIMPEDS) is described here as an example of a respirable sampler that uses cyclonic action. The SIMPEDS⁴⁰ is based on a design of cyclones, used for personal sampling, collectively known as the Higgins-Dewell. The first Higgins-Dewell personal cyclone sampler for occupational hygiene measurements of respirable dust was called the British Cast Iron Research Association sampler (BCIRA).⁴¹ The respirable sampler uses cyclonic action (Figure 5) to separate the respirable-sized fraction from particles with larger aerodynamic diameters in the aerosol entering the inlet. The aerosol is brought tangentially into the cylinder body and directed past a vortex finder, which is a short pipe projecting from the centre of the top of the cyclone. Moment of inertia is induced by the tangential flow of aerosol perpendicular to a vortex finder. A separation of particles is achieved by giving larger particles sufficient inertia to cross the air flow at a specific flow rate. The main forces acting on the particle are described by the Stokes number which is a ratio of the centripetal force and buoyancy forces acting on the particle.^{38, 39} The forces acting on a particle following a circular path are drag, buoyancy and centrifugal force and the balance between these forces determines the equilibrium orbit adopted by the particle. Drag acts on a particle as it is pulled from its orbit towards the vortex finder inlet and into a filter cassette.

The larger diameter particles with more mass will spin towards the outer sides of the sampler whilst the smaller and lighter diameter particles to enter the vortex finder in the middle of the cyclone body and into a cassette that holds a filter. Small aerosol particles can charge easily and adhere to the walls of the

filter cassette, especially when the filter cassette is made from polycarbonate.⁴² For the SIMPEDS, the cassette that holds the filter was specially designed to reduce losses of dust adhering to the walls in front of the filter.⁴³ This design facilitates what is known as a direct on-aerosol filter analysis approach since the whole sample is captured on the filter and no procedure is needed to recover dust deposited on other parts of the cyclone surfaces.



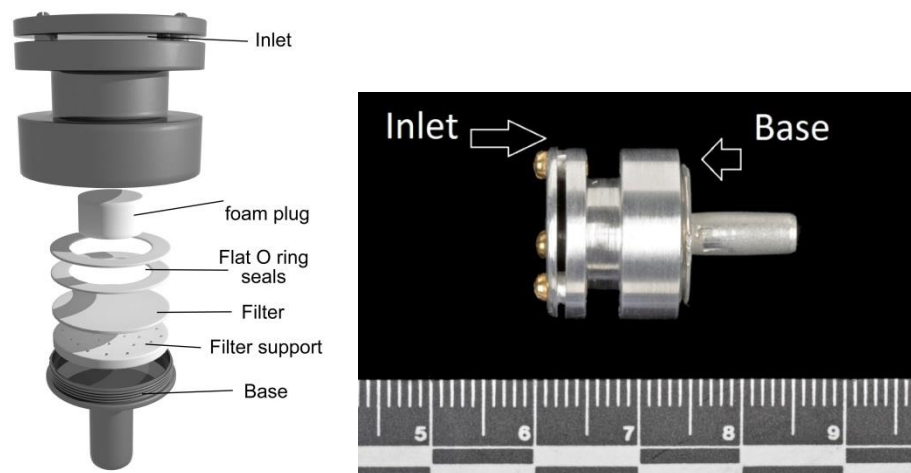
Crown copyright © 2021 Reproduced from MDHS 14 with the permission of the Health and Safety Executive.

Figure 5. Schematic diagram of the SIMPEDS respirable cyclone sampler showing the cyclonic action around the vortex finder creating a moment of inertia.

1.5.1.2 Foams

Foams were developed at the HSE to work with samplers that collect the larger sized inhalable fraction.⁴⁴ Inhalable refers to a health-related particle diameter definition for those particles that penetrate the nose and mouth; which includes the respirable fraction. The foam provides a complex path of cells. Smaller particles have a tendency to follow the air flow whilst larger particles with more mass have a larger moment of inertia and are collected by the foam.³⁹ The smaller sized particles continue to follow the flow of air, pass through the foam and are collected on a filter for subsequent analysis. The advantage of the use of foams as a particle size selector is that they provide a cheap alternative to

the respirable cyclone. If placed in the inlet of an inhalable sampler, both the inhalable and respirable fractions are measurable, since the foam collects the larger inhalable size particles and can be retrieved for analysis. Recently, a miniature respirable sampler was designed to collect particulate leaking into respirators using a polyurethane foam plug (Figure 6).^{45, 46}



Crown copyright © 2021. Reproduced with the permission of the Health and Safety Executive.

Figure 6. Picture of and a schematic diagram of the HSE miniature respirable sampler with the foam selector for in-respirator aerosol sampling.

1.5.1.3 *Impactors*^{38, 47}

Multiple particle size fractions are separated from an aerosol and collected using Cascade impactors. Cascade impactors contain several stages that collect particulate by impaction. An aerosol is pulled through an inlet nozzle which increases the speed of particles. A flat surface of an impaction stage, placed in front of the nozzle, deflects the stream of air containing the particles entering the sampler. Larger particles with more mass deviate from the stream of aerosol and impact onto the flat surface. The smaller particles will maintain their momentum and follow the air flow through to the next section with another impactor stage or through a filter. Impactors are often used to remove the unwanted larger sized particles from the aerosol of interest (e.g. for monitoring diesel exhaust). Three critical parameters that influence the median particle

diameter collected on the impaction substrate are the area of the inlet, the distance from the inlet to the impactor plate, (known as the stopping distance) and the air flow Reynolds number. The deceleration of a particle into the impaction filter is determined by the stopping distance (S) which is defined as equal to the flow velocity U_0 multiplied with the particles relaxation time (τ) (the time taken to adjust to new forces acting on it).

$$\tau = \frac{\rho_p d_p^2 C_c}{18\mu} \quad (2)$$

Where ρ_p is the density of the particle, d_p is its diameter, C_c is the Cunningham correction factor and μ is the viscosity of the medium within which the particle is travelling. The stokes number (Sk) is used to connect the inertia of a particle to its position travelling in a stream of air at a certain position from the centre of the impactor inlet (Figure 7).

$$Sk = \frac{S}{W/2} \quad (3)$$

Where W is the diameter of the inlet.

There is a particle stopping distance for each position of the flow of air crossing the diameter of the inlet. The further a particle with a specific diameter is away from the centre of the inlet air stream the longer is the stopping distance. Therefore, the impactor plate will collect a selection of particle sizes above a specific value. The median stopping distance (S_{50}) represents the design parameter for the collection of 50% of particles of a specific diameter. Impactors are often used because the S_{50} provides precise cuts of particle diameters. Values of Sk_{50} are relatively consistent for ratios larger than 0.5 for round and 1 for rectangle impactors.

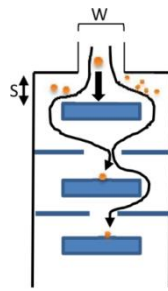


Figure 7. A schematic representation of the action of a cascade impactor.
The arrows represent the path of particles of different diameters. W
denotes the diameter of the inlet and S is the stopping distance of the
particle.

1.5.2 Analytical techniques for measuring respirable crystalline silica

When required under COSHH airborne concentrations of RCS are measured.^{48,}
⁴⁹ There are few analytical techniques that measure a property that is specific to crystalline silica. Analytical techniques that measure elemental silicon generally rely on the insolubility or solubility of crystalline silica in various acids or fluxes to improve their selectivity.^{50, 51} These chemical methods are no longer used for the occupational hygiene measurement of RCS because of the widespread presence of insoluble and flux reactive silicates in workplace atmospheres (like those from mineral feldspar group), and the varying degrees of reaction with amorphous silica.⁵⁰ Three techniques most commonly applied for the specific measurement of crystalline silica are; X-ray diffraction (XRD) which specifically measures crystalline material, Fourier Transform infrared spectroscopy (FTIR), which measures the molecular rotations and vibrations of molecules and colorimetric analysis, which measures the magnitude in colour of a molybdenum complex formed with the silanol groups on the surface of SiO_2 particles in water.⁵² The colorimetric method is no longer widely used because of its considerable variability,⁵³ sensitivity of response to particle size, the need to reflux in phosphoric acid to remove some interfering silicates, the incomplete dissolution of some silicates, and the slight solubility of the crystalline silica in phosphoric acid (10% to 20%).⁵⁴

Internationally, two analytical approaches are employed for the measurement of RCS. These are known as the direct on-aerosol sampling filter^{37, 55} and the indirect methods.^{56, 57} The indirect analysis approach recovers the aerosol collected on the aerosol filter and deposits it onto another (usually smaller filter) for analysis. The direct on-aerosol sampling filter approach measures the dust collected on the aerosol filter without any processing. The regulatory method used in Great Britain is known as Methods for the Determination of Hazardous Substances (MDHS) 101, which uses a direct on-aerosol sampling filter approach with FTIR or XRD.⁵⁵

1.5.3 X-ray diffraction (XRD) measurement of RCS

X-rays are electromagnetic waves that are classically described by a sine wave that repeats every 2π radians. X-ray diffraction is an analytical technique that measures the X-ray radiation scattered from atoms in a material. The X-ray radiation penetrates the material and some is scattered by atoms at different positions within its structure. For XRD, the wavelength of these X-rays does not change (X-ray radiation does not lose any energy), and the process is called elastic scattering.

Instruments with Bragg-Brentano focusing geometry are most often used for the measurement of RCS (Figure 8). The geometry of the instrument is arranged so that X-ray radiation from the sample is focused onto a detector. The detector receives different phases of the X-ray electromagnetic sine waves emerging from multiple points within the material; all with the same amplitude.

Constructive interference is the term given to the effect that results in a detected intensity, where sine wave phases of multiple X-rays coincide providing an increase in their amplitude. This amplification is the effect called diffraction. Constructive interference occurs when the radiation wavelengths (λ) are in alignment i.e. a whole number (n) of 2π radians (Equation 4). The diffraction effect is demonstrated in Figure 9, for a crystal where atoms have a regular arrangement.

$$\Delta = n\lambda \quad (4)$$

Destructive interference occurs when the X-rays, scattered from different planes of atoms, are out of phase i.e. the average phase shift for the X-ray radiation wavelengths is π radians.

Bragg's law (Equation 5) demonstrated that the short wavelength of the X-ray radiation is closely related to the distance between atoms in crystals, which can serve as natural X-ray gratings. Strong amplification of the X-ray radiation occurs at specific angles (θ) when atoms are arranged in a regular structure like a crystal. The reflections will occur at position of θ when,

$$\sin \theta = \frac{n\lambda}{2d} \quad (5)$$

Where d is the interatomic distance between atoms in a plane. Therefore, the diffracted intensity occurring at a particular position of θ is dependent on the regular arrangement of planes of atoms within the structure of the irradiated material. The diffracted intensity is therefore related to the dimensions of atomic structure; which is termed its crystallinity.

Traditionally, the angle of X-ray source irradiating the sample is fixed and intensities are measured at specific positions of two theta (2θ) as the detector is moved in an arc. In modern instruments, the sample position is fixed and the X-ray source and detector have a 1:1 (theta/theta) movement.

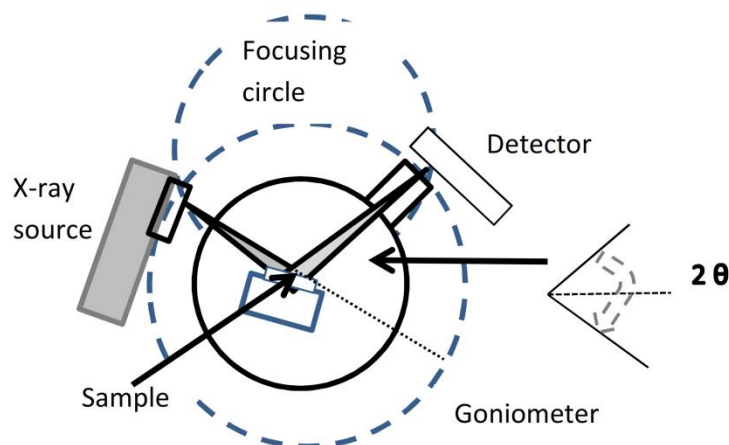


Figure 8. Arrangement in a Bragg Brentano focusing X-ray diffraction instrument.

The term 2θ is the angle between the directions of X-ray radiation passing through the sample (dotted line) and the detector.

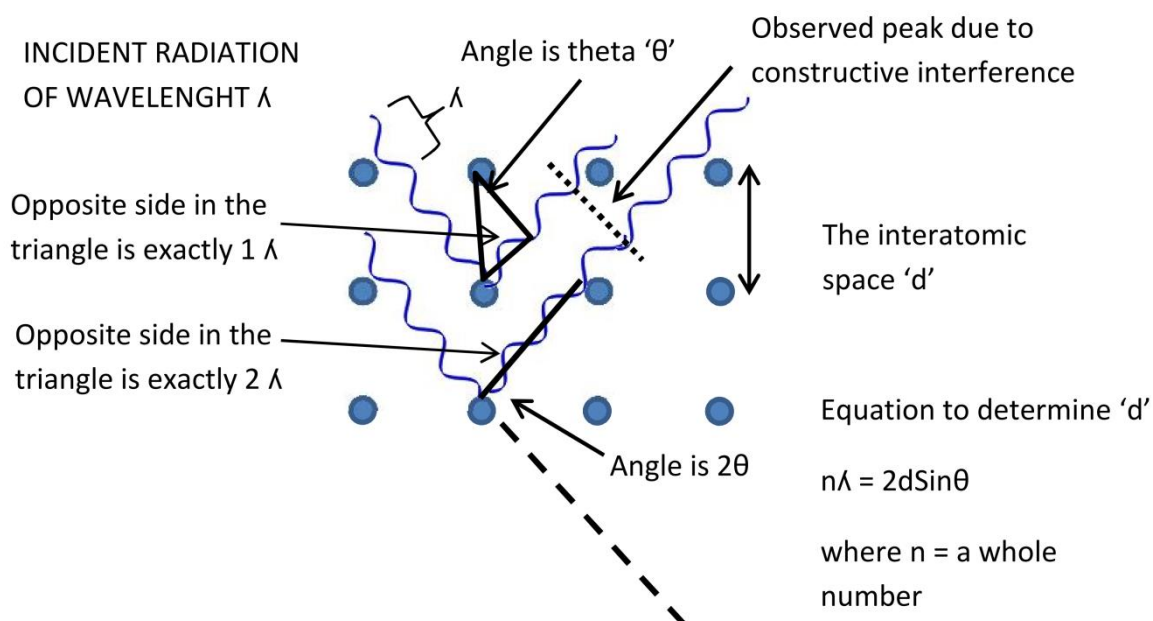


Figure 9. Schematic for the process of diffraction in a crystalline material.

A pattern of diffraction intensities is usually distinct to each component and can distinguish between polymorphs of substances, like those found for RCS. Generally, amorphous materials record a very broad background at low angles of 2θ . Examples of the diffraction intensity 2θ positions and their Miller indices

for α -quartz and α -cristobalite are shown in Table 2. The Miller indices is a notation describing a plane of atoms in a unit cell contributing to a particular XRD reflection. XRD scans for reference samples of α -quartz and α -cristobalite are shown in Figure 10.

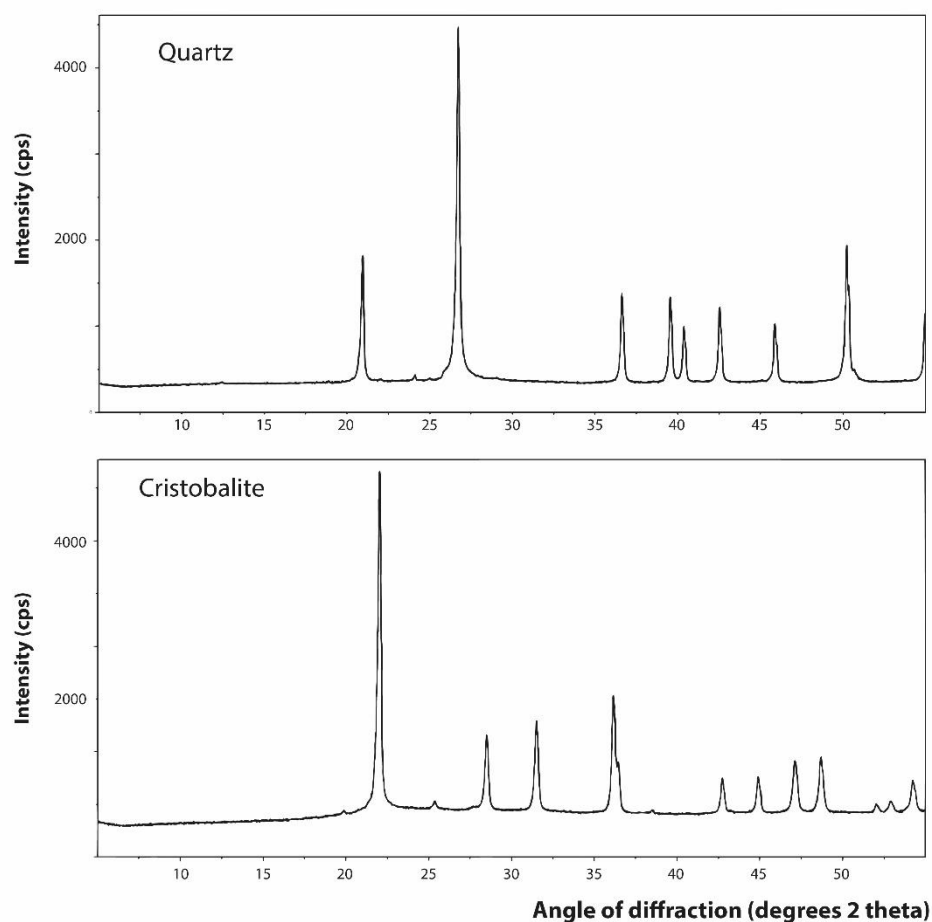


Figure 10. X-ray diffraction scans of α -quartz and α -cristobalite measured using copper radiation (1.54 Å).

Table 2. Significant reflections of α -quartz and α -cristobalite when using copper radiation ($K\alpha_1$ 1.54 Å), their angles of 2θ , relative intensity and Miller indices.

α -Quartz			α -Cristobalite		
Angle of 2θ	Relative Intensity	Miller Indices Notation	Angle of 2θ	Relative Intensity	Miller Indices Notation
20.9	14.2	100	22.0	100	110
26.6	100	101	28.5	9.1	111
36.5	9.8	110	31.5	10.2	210
39.4	9.1	102	36.2	13.2	020
40.2	4.6	111	36.4	4.9	112
42.4	3.8	020	38.5	0.1	021
45.7	2.9	201	40.6	0.0	120
50.1	18.7	211	42.7	2.4	121
50.6	0.5	003	43.2	0.1	013
55.2	2.3	310	47.1	5.2	113

Three diffraction angles with Miller indices of 100, 101 and 211 are measured for α -quartz. The principal 101 diffraction angle for quartz, positioned at a 2θ position of 26.6 degrees, has about 5 x more intensity than the secondary 100 and 211 diffraction angles at 2θ positions of 20.9 and 50.1 degrees. The less sensitive secondary diffraction positions are used because some matrix components will have XRD intensity that coincides with the principal reflections of α -quartz or α -cristobalite. Use of less intense diffraction positions or correction of the most intense for an interference introduces additional measurement errors and increases the limits of detection.

1.5.3.1 XRD and quantification for RCS

Several major factors affect the intensity of the diffracted X-rays⁵⁸, however, many are constant and the intensity of the XRD diffraction angle ($I_{(hkl)\alpha}$) is more simply related to an equation (6) involving the quantity of analyte in the sample and the attenuation of the detected signal due to absorption of X-rays from the sample matrix (μ_s).

$$I_{(hkl)\alpha} = I_{(hkl)\alpha}^0 K \frac{(\mu/\rho)_\alpha}{(\mu/\rho)_s} X_\alpha \quad (6)$$

Where X_α is the mass proportion of crystalline component α in the sample, K is a constant for instrumental and experimental factors, $(\mu/\rho)_s$ is the mass absorption coefficient of the sample where p is the sample density and $(\mu/\rho)_\alpha$ is the mass absorption coefficient of the analyte where p is the density of the analyte.

The simplest case occurs when the absorption of the sample matrix is the same as the analyte and the phase quantity is related to the ratio of the measured analyte intensity proportion and that of the pure phase ($I_{(hkl)\alpha}^0$).

$$X_\alpha = K \frac{I_{(hkl)\alpha}}{I_{(hkl)\alpha}^0} \quad (7)$$

X-ray intensity decreases exponentially as the depth of the sample (L) increases due to absorption of radiation by the sample (Equation 8).

$$I = I^0 \exp^{-(\mu/\rho)_s L} \quad (8)$$

Ultimately, the depth of the sample reaches a point where the contribution of X-ray intensity is not sufficiently distinguishable from the instrument noise at a particular distance from the sample surface.⁵⁹ This sample distance is termed 'infinitely thick'.⁶⁰ Most filter samples with aerosol particulate will never reach an infinitely thick depth because they are presented to the instrument as scattered particles on a filter surface or as layers a few μm in depth. A calibration based on standards of pure analyte is often applied to the measurement of RCS in samples from a variety of workplace atmospheres with different absorption

characteristics. Absorption of X-rays is minimal when the sample is a single layer of dust on an aerosol filter, however, there is a depth of sample when absorption becomes significant and a linear calibration relationship between X-ray intensity and mass of pure analyte per unit area is no longer true. For the measurement of RCS on-filters, Smith estimated that the correction for X-ray absorption was not necessary in most cases; which is when the sample loading on a 25 mm diameter aerosol sampling filter was less than 2000 µg.⁶¹ This was a theoretical estimate based on a single layer of particles with a uniform diameter of 2.5 µm covering a circular area with an effective diameter of 20 mm. More recently, Mecchia *et al.*⁶⁰ found, by experiment, that the critical mass for a 10% deviation from a linear relationship between intensity and mass could be as low as 900 µg, for a deposit on a 25 mm diameter filter with typical a mass absorption coefficient of 100 cm²/g. The critical mass was lower for deposit areas of 10 mm or 15 mm in diameter, which is obtained on some small diameter aerosol filters or when using an indirect recovery based method.⁵⁶

Copper is the most common material used to generate X-rays for the measurement of RCS, although it can cause fluorescence in samples containing significant amounts of iron (e.g. from foundries), which absorbs X-rays. Mecchia *et al.*, found significant attenuation of X-ray response occurs at loadings as low as 200 µg in artificial quartz mixtures with 80% hematite.⁶⁰ A correction is applied for the reduced transmission of the copper radiation based on the measurement of the intensity of a diffraction angle of the substrate beneath the sample deposit.^{37, 62-64} The equation for intensity $I_{(hkl)\alpha}$ and its relationship with the proportion of analyte (X_α) when using Bragg Brentano diffraction geometry is detailed in equation 9.

$$I_{(hkl)\alpha} = \frac{k_\alpha}{(\mu/\rho)_s} X_\alpha [1 - \exp(-2(\mu/\rho)_s D_{sample} / \sin \theta_{(hkl)\alpha})] \quad (9)$$

Where k_α is the calibration constant of the phase α , D_{sample} is the surface density of the sample in terms of its mass per unit area and $\sin \theta_{(hkl)\alpha}$ is the angle of reflection.⁶⁰ The correction method proposed by Leroux *et al.*,⁶² is universally adopted in most analytical methods for RCS^{37, 56, 57, 64} where silver filters or aluminium plates are employed as supporting substrates. The intensity for a

particular diffraction angle of RCS is corrected by measuring the attenuation of a silver or aluminium reflection through the sample or sample and aerosol sampling filter; when using a direct on-aerosol filter measurement method. Equations 10 and 11 are applied in international methods for RCS measurement.

$$I_{corr(hkl)\alpha} = I_{(hkl)\alpha} F \quad (10)$$

Where $I_{corr(hkl)\alpha}$ is the corrected intensity and F is an absorption correction factor.

$$F = (R \ln T)/(1 - T^R) \quad (11)$$

and $R = \sin\theta_{Ag} / \sin\theta_{(hkl)\alpha}$ and T is the transmittance of X-rays through the sample. $\sin\theta_{Ag}$ and $\sin\theta_{(hkl)\alpha}$ refer to the sine of the Bragg angles of the silver reference and analyte diffraction positions respectively.

The integrated area of the reflection is used for quantitative analysis because that is less sensitive to changes in particle size than the height of the diffraction intensity.⁶⁵ The profile of the diffraction intensity tends to get wider and flatter as the crystallinity decreases.

Sensitivity is an important issue for the measurement of RCS. For example, the anti-scatter slits, which are often set to a narrow angle to improve resolution of the diffraction intensity, are set to illuminate as much of the sample as possible without introducing additional X-ray noise from the sample holder.⁵⁵ This strategy serves to improve the representativeness of the measurement and the intensity at the expense of its resolution. The amount of energy used to produce X-rays is also another factor that can improve sensitivity⁶⁰ and the instrument at HSE is often set to its maximum power input of 55 Kv and 50 mA for the measurement of RCS on filters and uses a broad focus tube to provide more X-ray energy over the sample area than other varieties of X-ray tube.

1.5.4 Infrared analysis

Fourier transform infrared (FTIR) is one of the most widely used instruments employed for RCS analysis. FTIR measures the absorbance when photons from an infrared (IR) source are passed through or reflected from a substance. A schematic block diagram of a typical arrangement for a FTIR instrument is shown in Figure 11.

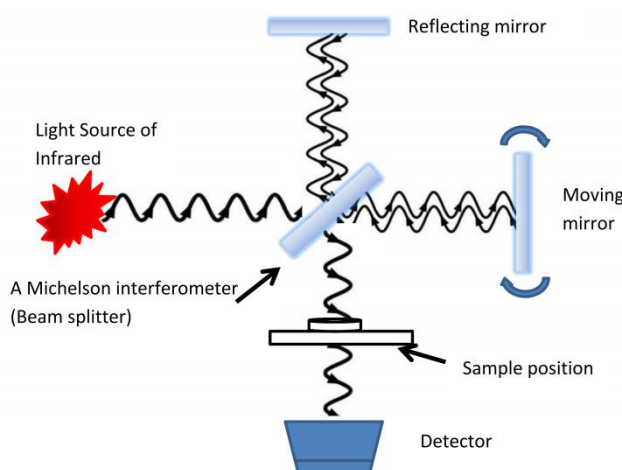


Figure 11. Schematic of the Michelson interferometer for an FTIR instrument.

FTIR in transmission mode is the most common instrumental arrangement used for RCS analysis, although some recent work has applied diffuse reflection infrared Fourier transform spectroscopy (DRIFTS).⁶⁶ Infrared (IR) radiation has a broad spectrum of radiation that is longer in wavelength than visible light. The range of wavenumbers ($1/\lambda$) used in instruments to measure quartz is in the middle IR range from 200 to 4000 cm^{-1} . Many bonds in molecules will transform into an excited state when irradiated with electromagnetic radiation (light) if the photon energy can be accommodated within the energy states of the molecule. The frequency of the electromagnetic light energy results in atomic vibrations where molecules will bend, stretch or waggle. Energy is absorbed if the frequency of the resulting vibration matches that of the incident electromagnetic radiation. The magnitude of the energy change is described by the Bohr frequency condition,

$$h\nu = \Delta E \quad (12)$$

where h is Plank's constant, ν is the frequency of the energy and ΔE is the change in energy states.⁶⁷

IR absorbance bands are only observed with an accompanying change of dipole to a molecular vibration. A dipole moment on a molecule will vary when bonds are given energy and stretch or bend asymmetrically. The wavelength of the incident photon energy causes an oscillating dipole and generates an electromagnetic wave of the same frequency as the photon that causes the vibrations. The absorbance for α -quartz is related to the asymmetric Si-O-Si stretching and Si-O bending vibrations of the silicon and oxygen atoms.⁶⁸ α -Quartz has two characteristic bands at 800 cm^{-1} and 780 cm^{-1} and significant secondary bands at 694 cm^{-1} and 512 cm^{-1} . The background corrected heights of the two bands at 800 cm^{-1} and 780 cm^{-1} are used for quantification (Figure 12).

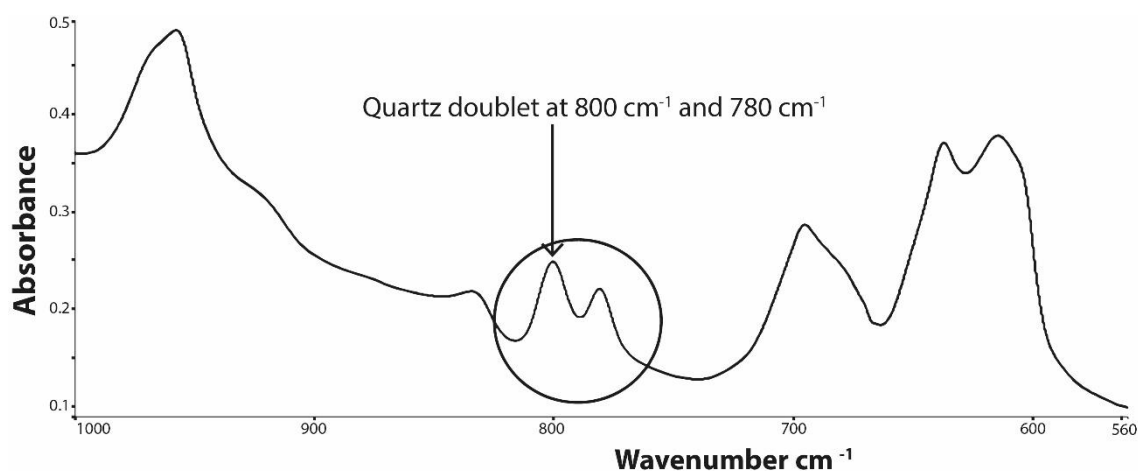


Figure 12. An infrared spectrum for respirable α -quartz collected onto a polyvinylchloride (PVC) filter.

α -Cristobalite has a significant band at 800 cm^{-1} and minor bands at 620 cm^{-1} and 490 cm^{-1} (Figure 13). The background corrected band heights at 800 cm^{-1} and 620 cm^{-1} are measured.⁵⁵ Band height is more commonly used for quantification because the peak area is more influenced by changes in response due to changes in particle size of the measured aerosol.^{65, 68} Many of

the band widths of α -quartz, α -cristobalite and amorphous silica coincide between 900 cm^{-1} to 780 cm^{-1} and many silicate minerals will have bands within the silica spectral region because the SiO_4 tetrahedron is also a fundamental structural unit of this class of minerals.^{68,69}

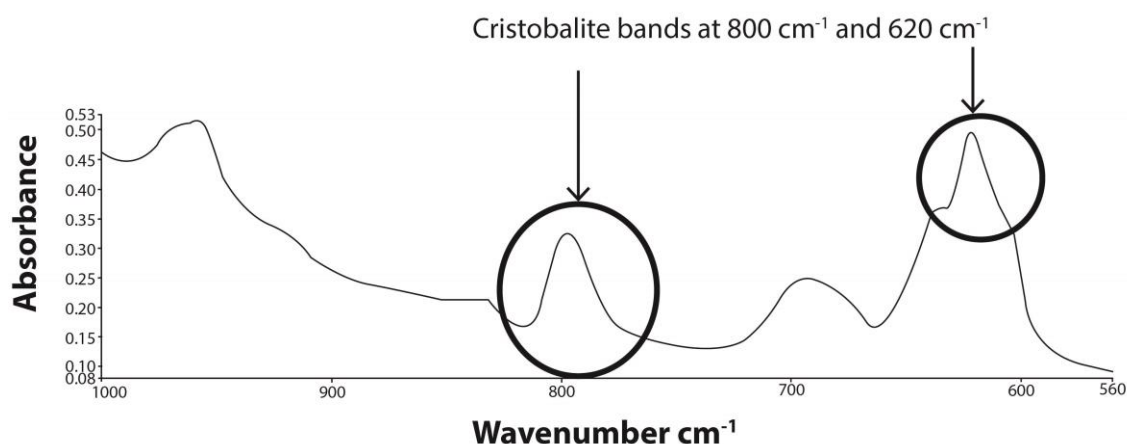


Figure 13. An infrared spectrum for respirable α -cristobalite collected onto a polyvinylchloride (PVC) filter

In theory, the relationship between the analyte concentration and absorbance follows a linear relationship described by the Beer-Lambert Law in equation 13.

$$\text{Absorbance (A)} = \epsilon Lc \quad (13)$$

Where ϵ is the molar extinction coefficient, L is the optical path length and c is the concentration of substance. In practice, the relationship between absorbance and concentration is linear for loadings less than 1.5 mg when measuring RCS on 25 mm diameter aerosol filters. This is because the filter area is much larger than the infrared beam area on the surface of the filter. Dust collecting outside the infrared beam area is not measured at high mass loadings, resulting in a reduced response per unit mass of RCS loaded on the filter. Attenuation of the infrared response can occur in the presence of 'dark' particles, although this is not generally a problem with occupational hygiene samples and FTIR is widely used for measuring RCS in coal⁵⁶ and foundry environments.

1.6 Application of Raman spectroscopy for the measurement of RCS

1.6.1 What is Raman spectroscopy?

'Raman' is a light scattering effect that was first theoretically described by Smekal in 1923.⁷⁰ Smekal proposed that the frequency of the light (ν) interacting with a gas molecule will lose or, if the atoms in a molecule were already in an excited state, gain energy ($\nu \pm \nu_1$) where ν_1 is the energy lost or gained. The observation of this effect was first reported by Raman and Krishnan who used visible light and mercury lamps to investigate the scattering of light from gases and dust free liquids. Raman and Krishnan were attempting to build upon the recent work of Compton, who discovered the scattering of X-rays from electrons in an atom resulting in a loss of energy.⁷¹ Landsberg and Mandelshtam first observed the scattering effect for optical light now known as 'Raman', when studying crystals of quartz. The observations made by Landsberg and Mandelshtam, which they termed as 'the combination of light scattering effect', were reported a couple of months later than Raman.⁷² The two discoveries demonstrated that the shift in wavelength due to the interactions of light within a molecule is universally found in gases, liquids and solids.

Atoms in molecules will vibrate when irradiated with electromagnetic radiation (laser energy). Most of the energy from the light source is transmitted through the molecule. A small proportion (estimated as 1% to 5%) interacts with atomic nuclei and electrons providing them with momentum to a virtual energy state. The nuclei and electrons then return to their ground state as a photon is scattered from the molecule. The vast majority of these photons (estimated as 99%) are scattered with the same energy as the incident photons. This unaltered photon energy (when absorbed photon energy is equivalent to the emitted) is termed Rayleigh or elastic scattering. The magnitude of the energy (E) transferred to and from the atom would correspond to the Bohr frequency condition $h \nu$, where h is Planck's constant. A small proportion of the scattered photon energy gains or loses energy where $E = h \nu \pm \nu_1$ and is termed as

Raman or inelastic scattering. Most incident and scattered radiation are of almost identical magnitude even when an energy change has occurred. Anti-Stokes scattering occurs when the electrons are already in an elevated state which results in the emission of a photon of higher energy (shorter wavelength) since it is a combination of the pre-existing and the excited state. Photons from Stokes energy transitions are of longer wavelengths because a loss of energy occurs in the process. The difference between the wavelength of the exciting laser radiation and the emitted photon is known as the Stokes shift.

A simplified schematic representation of these effects is shown in the Jablonski diagram in Figure 14.

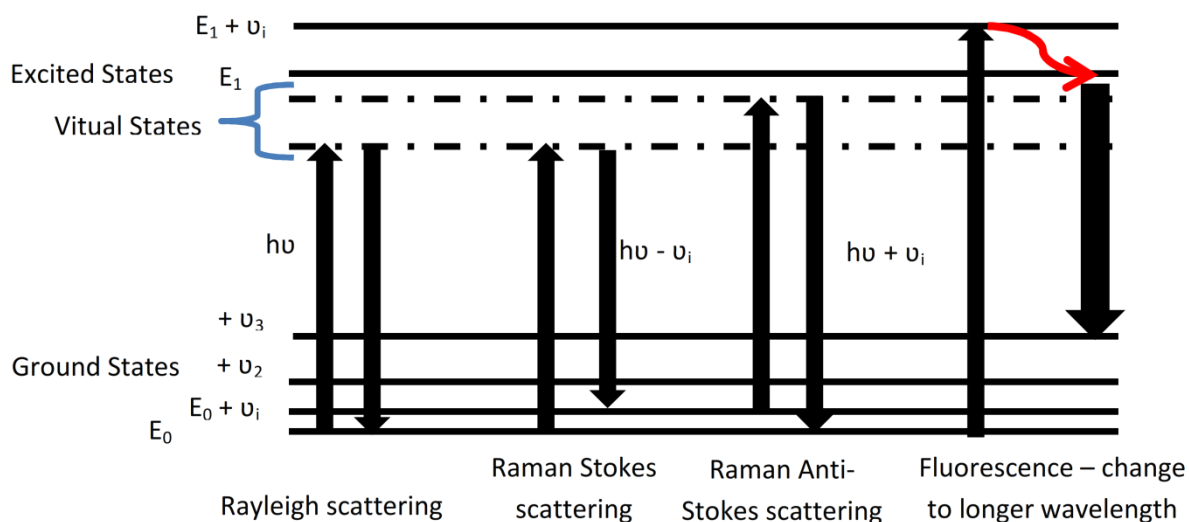


Figure 14. Jablonski diagram representing the energy transitions for different types of photon scattering.

1.6.2 Similarities and differences between IR and Raman spectroscopy

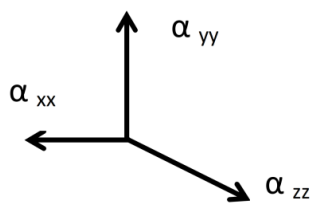
Both, Raman scattering and IR absorption involve the displacement of electrons and nuclei with an applied electric field. A vibrating dipole is caused when electrons and nuclei are sufficiently displaced. The induced dipole (P) creates its own electromagnetic field that interacts with the applied field (E). At low field strengths, the magnitude of the dipole is proportional to the applied field and its polarisability (α).⁷³

$$P = E\alpha \quad (14)$$

Polarisability is the proportionality constant for the distortion of the electron cloud.⁷³⁻⁷⁵ IR absorption occurs when the vibrations of molecules resonate with the applied field and energy transitions occur in the ground state ($E_0 \pm \nu_1$). In Raman scattering, the energy transitions reach a virtual state (Figure 14). Raman scattering occurs more from a change of polarisability rather than a change in dipole. In the molecule, polarisability (α) is a tensor that acts in a three dimensional space as the product of two or more vector quantities. This can be written as:

$$\begin{pmatrix} P_x \\ P_y \\ P_z \end{pmatrix} = \begin{pmatrix} E_x \\ E_y \\ E_z \end{pmatrix} \begin{pmatrix} \alpha_{xx} & \alpha_{yx} & \alpha_{zx} \\ \alpha_{xy} & \alpha_{yy} & \alpha_{zy} \\ \alpha_{xz} & \alpha_{yz} & \alpha_{zz} \end{pmatrix} \quad (15)$$

Where the dominant tensors are, α_{xx} , α_{yy} and α_{zz} since the others will work against each other. In a three dimensional system the dominant tensors can be represented as coordinate vectors:



The magnitude of the tensor is proportional to the inverse of the square root of the polarisation.

$$\frac{1}{\sqrt{\alpha_{xx}}} + \frac{1}{\sqrt{\alpha_{yy}}} + \frac{1}{\sqrt{\alpha_{zz}}} = 1 \quad (16)$$

Therefore, the larger the polarisation potential the smaller is the change in tensor direction. Raman scattering occurs when the ratio of the rate of change of the polarisability with the rate of change of the nuclear displacement ($\frac{d\alpha}{dq}$) is greater than zero. Vibrations that fluctuate with small changes of polarisation result in infrared absorption and are generally antisymmetric. The vibration is Raman active when the tensor direction is symmetric or either α_{yx} and α_{xy} , or α_{xz} and α_{zx} or α_{zy} and α_{yz} are unchanged.⁷⁵ Therefore, molecular vibrational symmetry significantly determines whether a vibration is Raman or IR active.

An example is given in Figure 15 which shows some nuclei displacements (q) from equilibrium ($q = 0$) for a simple three atom molecule. The magnitude of the

polarisation potential is usually displayed as an ellipsoid; however, for convenience in figure 15 they are shown as arrows. The molecular vibrations that result in Raman scattering or IR absorbance do not coincide when the molecule has a centre of symmetry. This circumstance is called the rule of mutual exclusion.

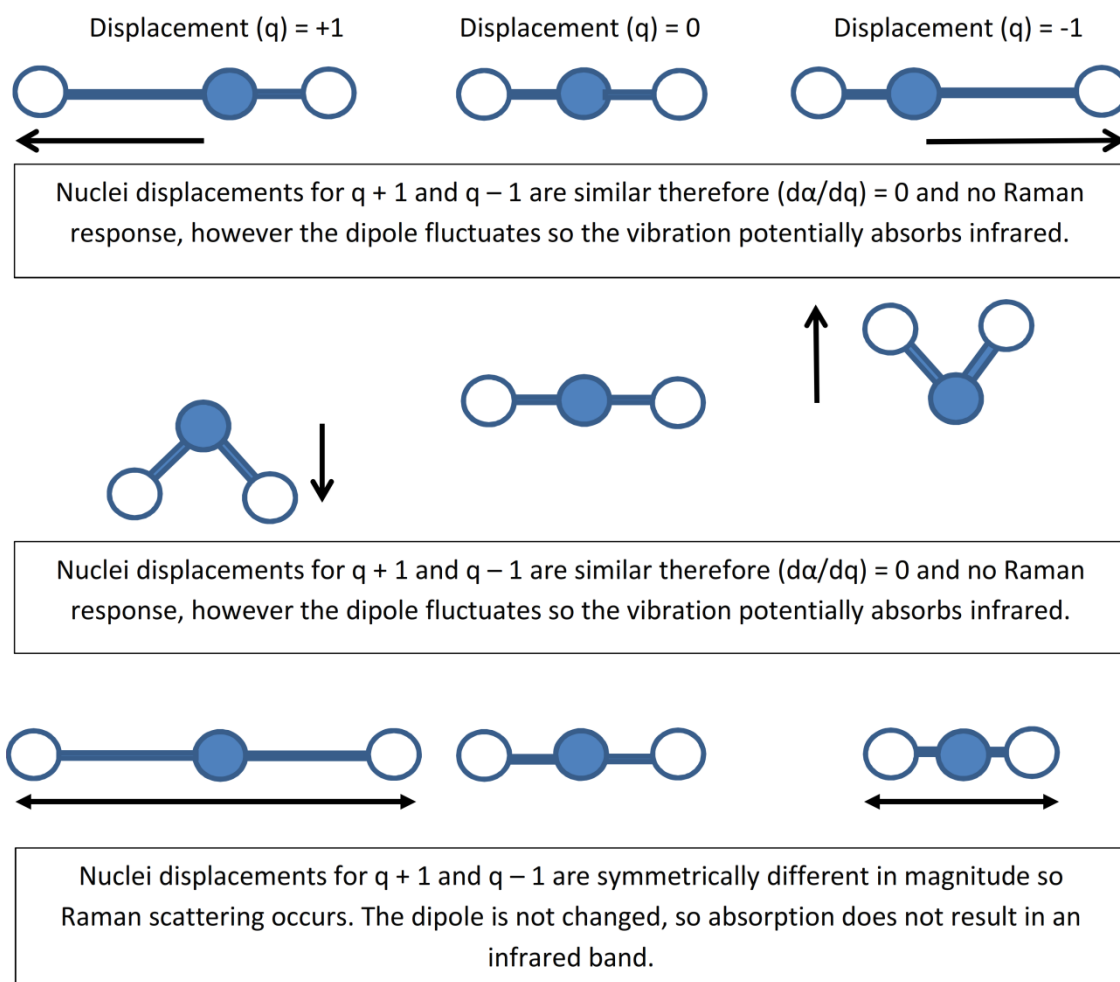


Figure 15. Infrared and Raman active vibrations for a three atom molecule.

1.6.3 Optical vibrations for α -quartz and α -cristobalite

Differences between Raman and IR bands for α -quartz and α -cristobalite have been studied extensively.^{11, 76-79} In a crystal, modes of vibration depend on the atomic structure and lattice dynamics.⁷⁶ The unit cell of α -quartz has nine atoms implying 27 (3n) possible vibrational vectors (x, y or z direction, equation 15), within its trigonal hexagonal structure. Active vibrations are described by group theory and the composition of their irreducible representations.⁸⁰ For α -quartz, its optical zone centre phonons are described by the Mulliken symbols $4A_1 + 4A_2 + 8E$ where A_1 denotes the number of symmetric vibrations (Raman active), A_2 the number of antisymmetric vibrations with respect to the principle c axis (IR active) and E, the number of doubly degenerate vibrations (both IR and Raman active).^{11, 77}

α -Cristobalite has a tetragonal structure with a unit cell of 12 atoms. The vibrations described by group theory and Mulliken symbols are $4A_1 + 4A_2 + 8E + 5B_1 + 4B_2$ where the B_1 and B_2 modes are potentially Raman active as their vibrations are symmetrical to the perpendicular 'a' axis.⁷⁹ A summary of the observed IR and Raman active vibrations with their associated Mulliken symbol identified in literature is provided in Table 3.^{77, 78, 81} Not all vibrations are observed.

Spectra for the principle Raman bands for α -quartz and α -cristobalite are shown in Chapter 3. For α -quartz, the principal Raman signal at 464 cm^{-1} is associated with the flexing positions of the Si-O-Si bonds connecting each tetrahedron⁸¹ as the helices stretches and relaxes in sequence with the wavelength of the laser radiation. The Si atoms remain relatively static within their structure.⁸¹ For α -cristobalite, the principal band at $\sim 410\text{ cm}^{-1}$ (reported range 411 cm^{-1} to 418 cm^{-1}) is attributed to A_1 mode and probably corresponds to the A_1 modes found for α -quartz⁸² although other researchers have attributed this band to lattice O-Si-O bending vibrations.⁷⁸

Table 3. The observed Raman and infrared wavenumbers and their associated Mulliken symbols for α -quartz and α -cristobalite.

α -Quartz		α -Cristobalite	
Raman wavenumber cm^{-1}	Infrared wavenumber cm^{-1}	Raman wavenumber cm^{-1}	Infrared wavenumber cm^{-1}
128 (E)	128 (E)	121 (B_1)	
207 (A_1)			147 (E)
263 (E)	263 (E)	233 (A_1)	
354 (A_1)		275 (E)	276 (E)
	364 (E)	286 (B_2)	
394 (E)	394 (A_2)		300 (A_2)
402 (E)		368 (A_1)	
464 (A_1)		380 (E)	380 (E)
697 (E)	695 (E)	416 (A_1)	
	777 (A_2)	485 (E)	480 (E)
797 (E)	797 (E)		495 (A_2)
807 (E)			625 (A_2)
1066 (E)		785 (B_1)	
1083 (A_1)		796 (E)	798 (E)
1161 (E)		1076 (A_1)	
1232 (E)		1086 (B_1)	1100 (E)
			1144 (A_2)
		1188 (B_2)	
		1193 (E)	1196 (E)

1.6.4 Measurement of crystalline material

A phonon is a name given to a collective vibration of atoms in a lattice. In a crystal solid, a phonon vibration, instigated by the electromagnetic radiation of the laser, will propagate as a vector involving an atomic plane in the crystal lattice. The crystal lattice is the basic arrangement of atoms and a reciprocal lattice is the mathematical description (Fourier transform) of the space for the projection of wave vectors from the crystal lattice. Within the reciprocal lattice, a Brillouin zone is a three dimensional space that represents a range within the unit cell that characterises a change in angular frequency of the vibration of atoms initiated by the phonon. The observed frequency of vibration of the atoms will depend on the masses of atoms involved. Large atoms will have lower frequencies of vibration than smaller ones and will appear almost stationary when close to the edge of a Brillouin zone. Optical photons are characterised by higher vibrational energies. There is a directional dependence of the phonon and photon vectors and the wave vector and conservation of energy is preserved in both processes.⁸³ Only the photon wavelengths emitted close to the centre of the Brillouin zone are observed in the Raman spectrum and the band profile is therefore dependent of the structure of the material. More crystalline materials will have narrower Raman band widths than less crystalline materials.

There is no consistently defined reciprocal space in an amorphous material, although vibrations do occur within the arrangement of atoms. Fused quartz is an amorphous version of crystalline quartz. The amorphous variety contains the same elements with the same masses and bonds as the crystalline form, although some of the bond lengths and positions are different because the material has lost its defined structure. The observed spectrum for fused quartz results in a very broad band near the principal band for α -quartz at 464 cm^{-1} which would suggest that the Brillouin zone had substantially increased compared to the crystalline material; so that more of the possible photon wavelengths from the Brillouin zone edge to its centre are sampled.⁸⁴

1.6.5 Raman band intensity and quantitative measurement of RCS particulate on filters

Raman scattering occurs when an electromagnetic field is applied, displaces electrons and nuclei and causes a change of polarisability. The polarisability over all states yields the intensity for the Stokes bands $I_{(v-v_j)}$

$$I_{(v-v_j)} = \frac{2^7 \pi^5}{9 \lambda^4} \frac{(3a^2_{Ij} + 2/3 \gamma_{Ij}^2) I_p}{(1 - \exp(-h\nu_j/kT))} \quad (17)$$

Where I_p is the incident intensity and a and γ_{Ij} are the average and anisotropic (property that allows change) parts of the polarisability tensor $\left(\frac{d\alpha}{dq}\right)$.⁸⁰ Temperature is a factor that is included in the denominator and the intensity of Stokes and anti-Stokes lines increases with temperature. Planck attributed the increase in scatter to the higher amplitudes of nuclei vibrations.⁸⁰ An external standard, such as a silicon plate can mitigate any change in response in quantitative or qualitative analysis, due to different ambient temperatures,⁸⁵ although it has also been observed that high quality quantitative analysis is achievable without spectral standardisation.⁸⁶

The Raman scattering of near infrared radiation from powders and pressed pellets was described by Schrader *et al.*^{87, 88} The equation for the Raman radiation scattered from the surface of a sample $J_{Scattered}$ in an antiparallel direction (180°) is shown in equation 18 i.e. reflected back from the surface of the sample. The equation is applicable to $J_{Scattered}$ observed by Raman instruments with microscope attachments and accounts for the interaction of the incident and reflected radiation in its surroundings.

$$J_{Scattered} = \Phi \frac{sk}{\alpha} \cdot \frac{k \sinh^2 kd + (\alpha + r) \sinh kd \cosh kd - krd}{[(\alpha + r) \sinh kd + k \cosh kd]^2} \quad (18)$$

Where $k^2 = 2r\alpha + \alpha^2$, α is the absorption coefficient, r is the elastic scattering coefficient, s is the Napierian Raman scattering coefficient, d is the depth of sample and Φ is the applied flux. The absorption coefficient (α) is sample matrix specific and is the arithmetic average of that reducing the exciting and emitted Raman radiation. The effect of matrix absorption and instrumental factors can

usually be reduced through the use of internal standards⁸⁹, although, the addition of an internal standard has the effect of diluting the analyte concentration reducing the sensitivity of the measurement. Schrader demonstrated that Raman intensity increases as the depth of sample (in millimetres) increases and then reaches a plateau.⁸⁸ An influence on the scattered intensity is the elastic scattering coefficient (r), which is inversely proportional to the size of the particles i.e. larger particles have more intensity. Despite this, many articles have reported different relationships with intensity for larger particles.⁹⁰⁻⁹³ Some of these differences were attributed to the limited analysis volume of the instrument's optics,^{92, 94} which has been confirmed using Monte Carlo simulation studies.⁹⁵ The distribution of photons is fairly localised for small particles and close to the surface of the particle, whereas it has a broader range of scattering angles and its origin is deeper for larger sized particles.⁹⁵ The influence of particle size on the Raman response when measuring respirable-sized particulate on a filter was unknown.

Instrumental factors also have a role in the observed intensity. Raman band response observed by the detector through the instrument is dependent on a number of other factors which includes, the wavenumber of the energy source ($\bar{\nu}_0$); the Raman shifted wavenumber ($\Delta\bar{\nu}$); the applied power of the energy source (Φ); the cross sectional area of the laser beam on the sample (A); the depth of the sample (d); the number of molecules per unit volume irradiated (N); and the differential Raman photon scattering cross-section (the proportion of photons ($J_{scattered}$) effectively scattered by the incident radiation) (β)

$$I = \frac{\Phi}{A} d (\bar{\nu}_0 - \Delta\bar{\nu})^4 N \beta (\bar{\nu}_{ref} - \Delta\bar{\nu})^{-4} \quad (19)$$

The efficiency of the Raman scattering is proportional to the fourth power of the incident radiation $(\bar{\nu}_0 - \Delta\bar{\nu})^4$ i.e. Lasers with shorter (ultraviolet) provide more intensity than those with longer (infrared) wavelengths. The formula $(\bar{\nu}_{ref} - \Delta\bar{\nu})^{-4}$ accounts for the changes in intensity due to deviations in polarisation. Crystals can orientate themselves in certain directions according to a preferred crystallographic plane, which can affect some observed intensities⁹⁶, since the polarisation is not always identical from each crystal face. For example, the

mineral talc has a thin plate like shape has a tendency to orientate itself along its flattest surface. Preferred crystal orientation is likely to occur when crystals are deposited on a flat surface (like a filter for collecting aerosol). If repeatable, the preferred orientation may provide consistent intensities for quantitative measurements of RCS particles collected on a filter. Preferred orientation is also reduced by decreasing the particle size i.e. when potentially measuring respirable-sized particles. Rotating the sample or taking multiple measurements can also average out this effect.⁹⁷ The intensity is directly proportional to the power of the laser and the area illuminated, if polarisation and internal field effects are ignored or assumed to be relatively consistent.

$$I = \frac{\Phi}{A} ds \quad (20)$$

Where $s = (\bar{\nu}_0 - \Delta\bar{\nu})^4 N \beta (\bar{\nu}_{ref} - \Delta\bar{\nu})^{-4}$

Therefore, three preeminent factors relating to Raman intensity from equation 20 are the cross-sectional area, the laser flux, and the depth of the sample. Equation 20 assumes that the number of molecules (per unit volume) is constant, which is not necessarily the case in every analysed volume or when using a mapping process to combine accumulated spectra; so N and β are other factors that are potentially variable from spectra to spectra when measuring samples of aerosol particulate collected on a filter. Accurate quantification is more likely if the sample deposit is homogeneously distributed over a consistent area to ensure a relationship between the density of particles within the illuminated area and concentration on the filter. In addition, the depth of a sample over a 5 mm, 10 mm or 15 mm diameter area can be controlled so that it is a thin layer,⁶⁰ which should reduce matrix effects such as fluorescence, or absorption, which may influence Raman band intensity.

1.6.6 Use of Raman for quantitative analysis

Raman spectroscopy was considered as a practical quantitative technique from the 1990s^{89, 98} which evolved from the investigation of quantitative methods for near infrared (NIR) spectroscopy and the use of chemometric methods to interrogate spectra.^{89, 97, 98} The leap forward in the application of Raman was

the development of Fourier Transform (FT-Raman) instruments which increased sensitivity of the optical conductance by two orders of magnitude compared with dispersive spectrometers⁸⁸. In 2003, Pelletier referred to around 200 articles describing quantitative applications for Raman,⁹⁸ Early quantitative applications were focused on the measurement of organic chemicals (e.g. benzene) and plastics.

A review of quantitative Raman methods, in 2013, included 101 references.⁹⁷ Ensuring the representativeness of the sample measurement was a key feature. These methods focus on three approaches, (a) averaging of Raman spectra collected at many different locations on a sample, (b) rotation of a sample during spectral collection and (c) simultaneous Wide Area Illumination (WAI) for spectral collection. Areas of application include; pharmaceuticals, petrochemicals, chemical, cosmetics, clinical and agricultural. A single method for the quantification of the herbicide Paraquat was classified as an environment application. WAI is not necessarily useful for the measurement of RCS on filters since it requires the use of lower magnification lens when compared with a microscope or probe. Raman line intensity is decreased at lower magnifications due to the smaller angles for light collection.⁹⁹ Powered rotation of the sample (b) was attempted in initial experiments but was not adopted due to the greater noise from the undulating background at a microscopic level and the reduced intensity compared with a focused spot approach at higher magnifications. The collection of multiple spots was selected to enhance the representativeness of analysis across the sample deposition area.

1.6.7 Raman measurement of crystalline silica and airborne particulate

1.6.7.1 *Crystalline silica measurement*

Previous work has focused on the identification of polymorphs in materials. Polymorphs of silica (including those of microcrystalline silica) were distinguished in bulk material when using Raman spectroscopy.¹⁰⁰ Raman spectroscopy, using an argon laser, was also investigated as a potential technique to identify the mineral content of rocks on moons or planets¹⁰¹ and to identify gem quality microcrystalline and amorphous silica from Romania.¹⁰²

Quantitatively, a method was developed for opaline in silica nodules of rock of volcanic origin utilising a rotating stage to obtain an average signal from the sample surface. Calibrations were made for quartz, cristobalite, coesite and calcite mixtures.¹⁰³

1.6.7.2 *Airborne particulate*

Raman spectroscopy was used for the identification and characterisation of airborne particulate.¹⁰⁴⁻¹¹⁰ Potgieter-Vermaak and Van Grieken¹¹¹ evaluated individual aerosol particles collected on a number of filter materials with 514 nm argon and 785 nm infrared lasers. A minimum of 50 particles were characterised on each filter using an acquisition time between 10 to 40 s. Identification of particles was limited by the spectral database. The contribution of the background was reduced by using an objective with a higher magnification and numerical aperture to reduce the measured volume. Other research focuses on the measurement of soot or diesel particulate.^{105, 110, 112-116} As early as 1997, Keller and Heintzenberg¹¹⁴ reported initial results for a quantitative method for elemental carbon on polycarbonate filters. More recently, Grafen *et al.*¹¹³ developed a continuous monitoring system for soot particles which uses a stainless steel filter tape. A near infrared laser at 785 nm with a power of 80 mW was used to analyse the deposit area of 6.5 mm in diameter. The laser beam of about 100 μm in diameter was moved across the filter during measurement. The concentration of soot was reported in terms of the number of particles per cm^2 . Later, Whelan employed a 633 nm laser at 100% power to measure respirable coal and diesel particulate using a 5x objective and a 400 second count time and obtained a measurement precision of 10% and less when rotating the sample.⁷⁴

There are few articles describing quantitative methods for particulate analysis. Some application articles focused on identifying the proportion of particles in the collected aerosol.^{104, 112, 115} Catelani *et al.* determined the percentage of particles in samples of airborne dust collected on polycarbonate filters from two ambient monitoring sites in Italy using a point count method.¹¹² Quartz compositions by number ranged from 4.5% – 12%. The chemical composition of marine aerosols over the Pacific Ocean were also recently examined.¹⁰⁴

Aluminium foil on a 'PIXE streaker' sampler was used as a collection substrate for a direct-on aerosol sampling filter analysis approach. The PIXE sampler is an impactor designed to collect the 2.5 μm to 10 μm aerodynamic diameters. Particles within this size range bounce off the impactor and are collected on a slowly moving substrate. None of these articles attempted to quantify the mass of crystalline silica within the matrix and their potential for a precise quantitative analysis by mass on filters was not reported.

1.6.8 The Raman instrument used for measurement of RCS

A Raman spectrometer, connected to a microscope, was used for this research, which is described below (Figure 16). In summary, photons from a laser source are directed towards a dichroic (notch) filter which allows only changed wavelengths to pass through and reflects the laser wavelength to the microscope. A microscope objective directs the light to the sample and captures a portion of the scattered photons. The scattered photons are returned to the dichroic filter which passes the changed wavelengths to a slit and a collimator in front of a diffraction grating. The diffraction grating splits and spreads the constituent wavelengths onto a detector.

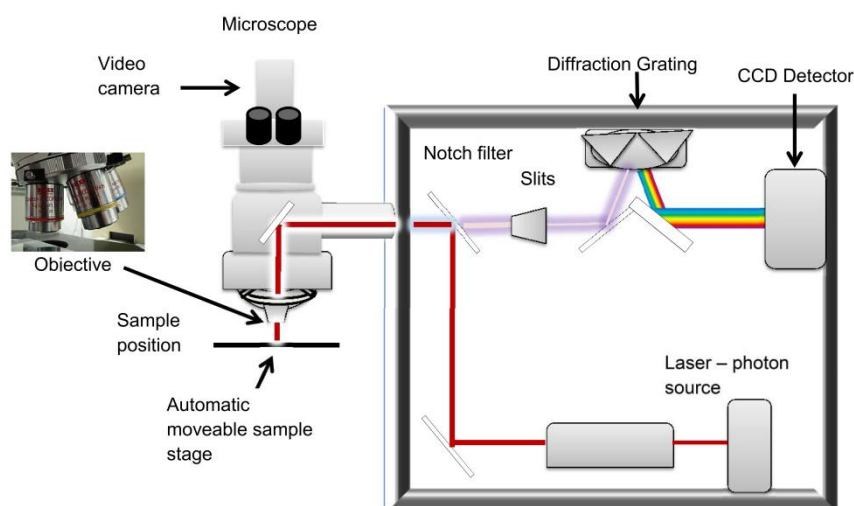


Figure 16. A schematic representation of the components of a Raman spectrometer connected to a microscope.

1.6.8.1 *The laser source*

A high intensity source of photons is needed because Raman is a weak effect when compared with absorption or Rayleigh scattering. Lasers are a high intensity source of photons and have narrow band width when compared with lamp sources; which improves the resolution of the Raman spectral band. The improved resolution and intensity when using lasers, compared with lamp sources, increased the ability of Raman to cope with mixtures of powders from a variety of sources.

Raman band intensity is related to the laser wavelength. Shorter wavelengths have more energy and provide more scattered intensity (equation 19). Although, one issue with Raman measurement is the potential for the laser photon energy to induce fluorescence rather than Raman scatter because of the amount of energy applied to obtain sensitive measurements. When it occurs, the magnitude of the fluorescence is greatly in excess of any Raman scatter and can swamp the Raman bands. Higher energy lasers can also be more prone to inducing photodecomposition of the sample. Although less intense, a laser with a longer wavelength can be operated at a higher power and have a lower propensity to cause fluorescence or photodecomposition.¹¹⁷

Near infrared (NIR) lasers were developed in the 1980s and were adopted for Raman spectroscopy because their longer wavelengths (785 nm and 1064 nm), when compared with the wavelengths from Ne-He (633nm) and Ar⁺ (488 nm and 514 nm), reduced the probability of electronic transitions from the ground state associated with the fluorescence effect.¹¹⁸ A NIR laser at 785 nm was used for this research because it would potentially be more useful for workplaces samples, which may contain components that fluoresce. The full laser power of 110 mW on the sample was used because the material of interest in this work and filter substrate is relatively inert to heat and may dissipate some localised heating effects. Lower power may also be useful to reduce the opportunity for fluorescence, if this remained problematic in a particular sample. However, this would also reduce the measurement sensitivity. An alternative is to add multiple spectra with a reduced collection

time to enable the same overall exposure and to keep within the working response of the detector.

1.6.8.2 *Dichroic notch filters*

Dichroic notch or edge filters direct the photons from the laser source to the microscope and the sample. These dichroic filters are able to efficiently exclude the Rayleigh scatter (unchanged wavelengths) whilst allowing the Raman shifted photons through the dispersion grating when the photons are returned from the sample via the microscope objective.^{73, 119} Notch or edge refers to the wavelength profile of excluded photons.

1.6.8.3 *Dispersion grating components*

The returned light is passed through a slit which has a role in resolution and intensity of the Raman bands. Wider slits permit more photons to enter and increase intensity, whereas narrower slits can improve resolution and potentially decrease fluorescence.

The Raman photons are then passed through a collimator and a dispersion grating. The dispersion grating is a set of finely spaced lines positioned on a reflective surface.⁷³ The angle of diffraction is dependent on the wavelength of the photon. Constructive or destructive interference occurs as the photons are reflected from the depth of the surface. The dispersion (spread of wavelengths) is related to the groove density and the working wavelength of the laser. Wavelength of the laser source can affect the dispersion of the Raman shifted wavelengths onto the detector. When using short UV wavelength lasers, it is possible to collect the whole Raman spectrum onto the detector; however, longer laser wavelengths will have a greater spread of Raman shifted wavelengths. A selected portion of the whole spectral range provides better spectral resolution when using NIR lasers. Gratings with lower numbers of grooves per mm have higher intensities; however, this advantage can be offset because background interference can be more significant in real samples. This research applied a grating with 1200 lines.mm⁻¹.

1.6.8.4 *The detector*

One of the most significant advances for Raman spectroscopy was the development of charged coupled device (CCD) detectors.¹²⁰ CCD detectors have substantially reduced measurement times and permitted the measurement of the whole spectrum separated by a diffraction grating. However, the resolution of the whole spectrum range (200 cm^{-1} to 3800 cm^{-1}) is usually low due to the size of the detector area. The highest resolution is obtained for specific band width regions within the whole spectrum. Early, CCD detectors were found to have good efficiency when combined with the use of red light sources.¹²¹

1.6.8.5 *The microscope objective and role in intensity and sampling (measurement) volume*

Microscopes were first combined with Raman spectrometers in the later 1970s and early 1980s.¹²² The focusing of the laser energy into a small area using an objective lens is an advantage for quantitative Raman analysis because it improves the efficiency of the photon collection. The higher magnification objective usually has a higher numerical aperture, which is the angle between the centre of the focal plane on the sample and the edge of the objective lens. Higher intensities are usually obtained because the collection angle is increased and the laser flux is concentrated into a smaller area. However, the focal volume is smaller than that obtained using an objective with a lower numerical aperture (Figure 17). A sampling strategy that is representative of the sample is an important consideration for repeatable quantitative analysis. Lower magnification objectives with lower numerical apertures collecting from a larger focal volume can facilitate a more representative measurement and the greater depth of field can potentially reduce variability in intensity due to focusing errors e.g. with an automated stage and focus.

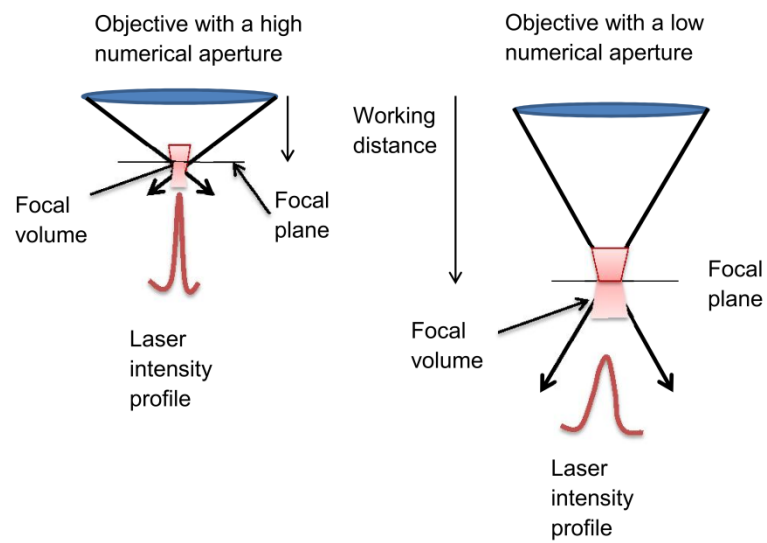


Figure 17. An illustration of the different sampling volumes obtained for microscope objectives with high and low numerical apertures.

1.7 Performance of XRD and Infrared methods for RCS measurement

The standards required for the performance of analytical methods for occupational hygiene monitoring when measuring exposure limits are described by the European standard EN482¹²³ and BS ISO 20581.¹²⁴ Both documents have the same three stipulated requirements:

- The measurement range of the method must be from 0.1 to 2 times the exposure limit.
- The expanded relative uncertainty of the measurement (including sampling) should be less than or equal to 30% when measuring from 0.5 to 2 times the exposure limit.
- The expanded relative uncertainty (including sampling) should be less than or equal to 50% when measuring from 0.1 to 0.5 times the exposure limit.

For RCS the limit of detection dictates the lower limit of the measurement range for precision studies.

1.7.1 Typical limits of detection of current analytical methods for RCS

Table 4 shows the limits of detection (LOD) when measuring samples of pure analyte (quartz or cristobalite) on clean filters for a range of established international X-ray diffraction and infrared analytical methods. The LOD is shown in terms of mass (μg) collected and the mass concentration (in $\mu\text{g.m}^{-3}$) for a SIMPEDS respirable sampler operating at 2.2 L.min^{-1} when sampling for a half (4h) and a quarter (2h) of a working shift. When the sampling time is decreased the LOD in terms of concentration increases and instruments may only be able to detect concentrations at which there remains a significant silicosis risk.

The uncertainty of weighing is a factor that may affect the reliability of estimates for the LOD for the direct on-filter methods; since the known measured mass for

Table 4. Current analytical methods for RCS and their limits of detection in terms of the mass (μg) collected on an aerosol sampling filter and mass concentration for various sampling times (h) when using a respirable sampler with a flow rate of 2.2 L min^{-1} .

Method Code	NIOSH ⁺ 7500 ⁵⁷	OSHA ⁺⁺ ID142 ⁵⁶	ISO 16258-2:2015 ⁶⁴	HSE 101 ⁵⁵	ISO 16258-1:2015 ³⁷	HSE 101 ⁵⁵	ISO 19087:2018 ¹²⁵	NIOSH 7603 ¹²⁶
Measurement approach	Indirect	Indirect	Indirect	Direct	Direct	Direct	Both	Direct
Technique	XRD	XRD	XRD	XRD	XRD	FTIR	FTIR	FTIR
Analysis filter	Silver	Silver	Silver	PVC	Various	PVC	PVC	KBr pellet
Validation range (μg)	20 to 2000	10 to 2000	Not stated	20 - 2000	Not stated	20 to 2000	Not stated	30 to 250
LOD (μg)	5	10 ^{**}	3 to 9 [*]	5 to 10	3 to 9 [*]	4	10	10
Volume of air (L)	528 L for a respirable sampler collecting a 4 h (half shift) sample at a flow rate of 2.2 L.min^{-1}							
LOD ($\mu\text{g.m}^{-3}$)	0.01	0.02	0.006 to 0.02	0.02 to 0.04	0.006 to 0.02	0.01	0.02	0.02
Volume of air (L)	264 L for a respirable sampler collecting a 2 h (quarter shift) sample at a flow rate of 2.2 L.min^{-1}							
LOD ($\mu\text{g.m}^{-3}$)	0.02	0.04	0.01 to 0.04	0.04 to 0.08	0.01 to 0.04	0.02	0.04	0.04

^{*}Estimated for a range of international methods. The LOD values are for the measurement of α -quartz without any matrix. The LODs are likely to be greater when interference is present due to bias. The LOD values quoted for XRD are for the measurement of the most intense reflection at a 2θ angle of 26.6 degrees. The LODs for the secondary XRD reflections of α -quartz were estimated between 10 μg to 20 μg for the 2θ reflection at 20.9 degrees and between 15 μg to 35 μg for the 2θ reflection at 50.1 degrees ³⁷.

^{**} Defined as a reliable limit. ⁺The National Institute for Occupational Safety and Health of the United States of America (USA). ⁺⁺ The Occupational Safety and Health Administration for the United States of America (The regulatory body in the USA).

The HSE code of practice for monitoring of toxic substances proposes a sampling time of 2 h for a continuous process with minimal variability ¹²⁷.

calibration samples is determined gravimetrically. Weighing of PVC filters is reported to have a precision of 5 µg with a limit of quantification of 14 µg.¹²⁸ Clean room environments are needed to further reduce variability.¹²⁹

A third consideration is the influence of interferences in real matrices which may increase the LOD.¹³⁰

1.7.2 Estimates of RCS measurement uncertainty

An accuracy range has traditionally been used to determine the reliability of a measured value; which includes estimates of both the relative standard deviation and bias calculated from a method validation process.¹³¹ Estimates of measurement uncertainty provide an indication of the range for the likelihood of the occurrence of a 'true' result for each reported exposure concentration. Generally, the relative error (uncertainty) of a measurement increases as the mass collected on filter decreases over the analytical mass range of interest (0.1 to 2x the WEL)¹³², which leads to wider uncertainty estimates for the RCS at concentrations lower than the WEL^{130, 133} especially when collected for less than a full shift. Previously, uncertainties for RCS measurements have been estimated from proficiency testing,¹³⁰ laboratory quality control data¹³⁴ and some method validation studies.^{8, 135, 136}

For RCS, method validation studies are generally conducted to derive measurement uncertainties using ideal samples of pure analyte. This is because of the many different workplace environments and the difficulty in applying a secondary technique to establish a known value in a matrix, with a sufficient degree of certainty. Measurement uncertainty of hazardous particulate in aerosols comprises two main elements termed the analytical and sampling uncertainties. Each of these elements includes the individual errors that contribute to the reliability of a reported measured value in an individual laboratory. The analytical uncertainty includes those processes specific to the analysis of the analyte in the collected sample whilst the sampling uncertainty includes those process specific to the collection of the aerosol onto a medium that is suitable for subsequent analysis. The temporal and spatial variability of the aerosol in the workplace are not included in this process because these

factors are characterised by further measurement or other occupational assessment processes.^{127, 137}

The many individual components contributing to the reliability (uncertainty) of a measured value for RCS analysis are described in Figure 18.

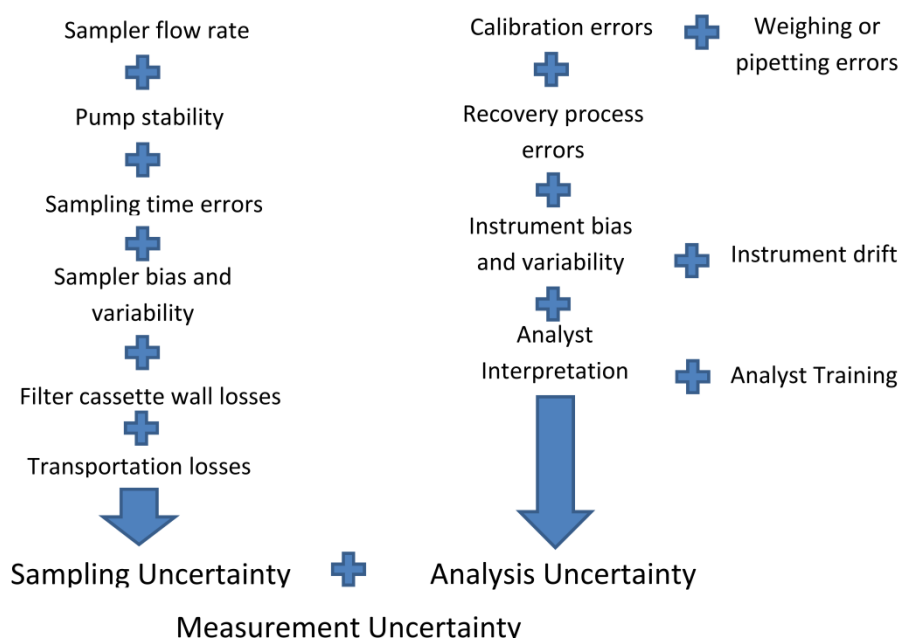


Figure 18. Processes and contributors to uncertainty when measuring respirable crystalline silica.

Annex D of the international guidance for the measurement of respirable crystalline silica¹³⁸ identifies the following components that are relevant:

The components of the uncertainty of sampling (u_s) are mainly linked to:

- a) Volume of sampled air;
- b) Efficiency of the sampler; and
- c) Transportation and storage of samples.

The components of the uncertainty of analysis (u_A) are mainly those linked to:

- a) Analytical method precision;
- b) Correction for the recovery or bias of the method;
- c) Instrumental drift; and
- d) Purity of the calibration powder.

An expanded uncertainty (U) is calculated by combining each component as the square root of the sum of squares and multiplying by a factor 2 which is applied to estimate the 95% level of confidence (equation 21).

$$U = 2 \times \sqrt{u_A^2 + u_S^2} \quad (21)$$

Few method validation studies have assessed the expanded uncertainty for RCS measurement methods. Only, four publications were found that investigated indirect XRD analysis approaches for RCS measurements.^{8, 135, 136, 139} However, several of the standard uncertainty components in these studies were estimated or excluded. For example, few authors considered particle selection bias and variability of individual samplers beyond the use of a standard value of 5% which is applied for the variability of the sampling pump.^{8, 134, 136} Few studies have attempted to investigate uncertainty for specific respirable samplers³⁶ which is probably due to the need for specialist equipment and facilities.

As an aid for laboratories, ISO 24095 proposes a standard value of 10.1% for sampling uncertainty which is based on expert opinion. This consensus value includes the variability from the pump flow rate, variability of the individual samplers and potential bias from the EN481 convention. Taking the consensus value for sampling uncertainty into consideration, the analytical method uncertainty needs to be less or equal to 11.2%, when following equation 21, and when measuring a concentration from 0.5 to 2x the WEL; to comply with international standards that require the expanded uncertainty to be within 30%. Studies of proficiency testing (PT) data from laboratory measurements on samples of pure respirable α -quartz calibration dust indicate that the average standard deviation of RCS results between laboratories is likely to be between

10% to 15% at the lowest mass loading of 80 µg (equivalent to a 7h shift sample concentration of 0.076 mg.m⁻³).¹³² Another study of PT data involving samples with matrix indicates that the average analytical precision between laboratories over the whole analytical range could be as much as 19%.^{133, 139} However, this study is for indirect analysis approaches and includes all filter digestion approaches (plasma or furnace ashing or use of tetrahydrofuran), which were not considered separately.

A feasibility study, to reduce the permissible exposure limit in the United States conducted by the Occupational Health and Safety Administration, concluded that sufficient dust could be collected with existing samplers to exceed the limit of quantification at a concentration of 0.05 mg.m⁻³, so long as a half shift 4 h sample was collected.¹³⁴ In GB, there is no recommendation to sample for longer than a quarter of a shift (2 h) when the process is continuous and well-controlled.¹²⁷ Higher sampler flow rates or longer sampling times can increase the amount of dust collected on a filter, which can improve the measurement sensitivity and uncertainty. However, samplers with flow rates higher than 2.2 L.min⁻¹ are not commonly employed in the United Kingdom and cannot currently be used with direct on-filter methods like MDHS 101.⁵⁵

1.7.3 Measurement uncertainty for direct on-filter methods

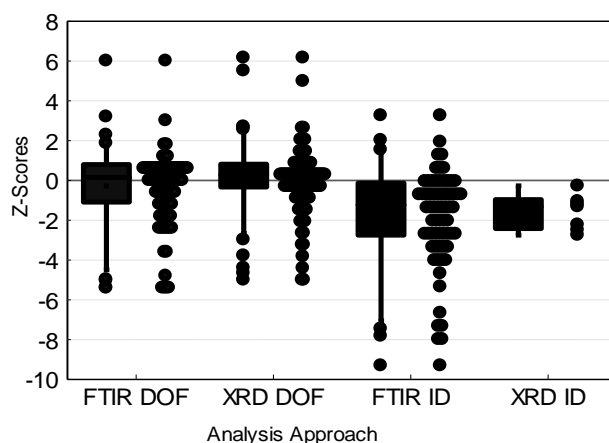
The generation of replicate test samples is a prerequisite of many method validation precision studies to determine analysis uncertainty; however, it is difficult to achieve replicates when using the direct on-filter approach applied by MDHS 101.⁵⁵ The calibration approach for a direct on-aerosol filter measurement approach is dependent on the generation of an aerosol and the use of the appropriate sampler to collect a proportion of the dust. For RCS, a portion of the aerosol is collected with a respirable sampler and collected onto a filter. The mass of analyte collect on the filter is determined gravimetrically and is therefore traceable to primary national mass standards. However, it is not currently possible to reliably replicate an aerosol. Replicate samples for proficiency testing programmes¹³² are generated using multi-sampler chambers with critical orifices behind each sampler to provide a uniform flow rate, however, these are not designed for small scale method validation studies. For

technical reasons, the availability of proficiency loadings below 50 µg (about half the current WEL in GB) are not common due to the difficulty of collecting replicates with an appropriate level of precision. Due to this, the American proficiency analytical testing (PAT) program changed its sample preparation from one involving aerosol sampling to a slurry pipetting procedure,¹³⁹ although this procedure cannot replicate the deposition on an aerosol filter which affects measurement sensitivity.¹³⁸

ISO 24095 provides an alternative approach to calculate the analytical method uncertainty, which is based on the determination of calibration uncertainty from the least squares linear trend line relationship between observed mass and instrument response. The calibration uncertainty is useful for the direct on-aerosol filter analysis methods because it does not need replicate samples, however, sufficient calibration samples are needed to accurately describe the variance. The example given in ISO 24095 is for an unweighted regression which is not necessarily a valid approach when applied to heteroscedastic precision, which is potentially the case for XRD measurements. The unweighted calibration uncertainty tends to provide unexpected large estimates for XRD analyses, however, it might be useful for FTIR where the homoscedastic (similar variance across the measured range) relationship is expected.

1.7.4 Differences between analytical approaches for measuring RCS

Between laboratory measurement precision estimates are an important consideration when assessing the practical performance of regulatory measurements. Precision between laboratories is often larger than the uncertainties derived from validation studies because they include a range of laboratory conditions. PT programmes provide a useful source of precision data for different methods since laboratories are measuring almost identical samples. The UK AIR (Air and Stack Emissions) PT programme provides participants with replicate calibration type samples of pure α -quartz on PVC filters collected with a respirable sampler. Results comparing the range of z-scores from participants using direct-on-filter (DO) and indirect (ID) RCS analysis methods from the AIR PT programme are shown in Figure 19. Information about the type of ashing approaches was not provided.



© Crown copyright (2022) Reproduced with the permission of the Health and Safety Executive.

Figure 19. Range of z-scores obtained from laboratories using direct on-aerosol filter (DOF) and indirect (ID) analysis approaches when using X-ray diffraction (XRD) or Fourier Transform Infrared (FTIR) spectroscopy.

A z-score represents the difference between a laboratory's results divided by the standard deviation set by the proficiency testing scheme. The standard deviation for PT was 10%, so a z-score less than 2 would imply the result had a difference of + 20%. The average z-scores were -0.27, 0.18, -1.72 and -1.58 for the FTIR DOF (n=83), the XRD DOF (n=109), the FTIR ID (n=67) and the XRD ID (n=7) respectively with standard deviations of 1.81, 1.59, 2.41 and 0.89. On average, the results for the indirect analysis approaches are lower than the target values when compared with those for the direct on-aerosol filter methods, indicating low recoveries of sample.

1.7.5 Differences between process recovery approaches for RCS methods

Selection of the best reproducible analytical approach is an important consideration when investigating new techniques to measure lower concentrations. Pipetting known masses of analyte from an aliquot of suspension is likely to achieve more consistent loadings at low masses, since a suspension can be accurately diluted by volume and pipetted. Although, calibration samples deposited from a suspension will not be suitable for a direct on-filter approach as they do not replicate the deposit profile of a collected

sample, which affects measurement sensitivity.³⁷ An indirect analysis approach has an advantage for low mass measurement as it permits analysts to concentrate the sample in order to improve sensitivity and to use a different filter than that used for the aerosol collection.

The three most common approaches described in indirect analysis methods for removing the organic aerosol sampling filter and recovering the aerosol dust for analysis are:

- 1) The use of a low temperature plasma asher, where the aerosol filter is placed in a glass bottle, ashed in the plasma asher to remove the organic filter, a small amount of isopropanol is added directly to the bottle which is then sonicated and the liquor and residue is washed into a filter funnel and filtered onto the analysis filter (usually silver for XRD);
- 2) The use of a furnace, where the aerosol filter is placed in a crucible and then into a furnace which is heated to a prescribed temperature and time. The crucible and residue are washed out into a beaker with isopropanol, which is sonicated and then transferred to a filter funnel for filtration onto the analysis filter; and
- 3) Use of THF to dissolve the filter, (this method was not employed in this study).

The furnace approach is considered a source of analytical error by some researchers investigating the NIOSH method¹⁴⁰ whilst others regard plasma ashing and furnace treatment as equivalent processes.¹⁴¹ An advantage of the furnace approach is that it can effectively remove anthracite (crystalline carbon) and kaolinite, which are both interferences with the most sensitive reflection of α -quartz.¹⁴² Indirect methods usually prescribe 600°C for the furnace temperature, 800°C when graphite is present^{57, 126} or 450°C to 800°C in other methods.⁶⁴ Higher furnace temperatures above 475°C can initiate a reaction between α -quartz and any calcite in the dust sample to form wollastonite (CaSiO_3).^{126, 143} Calcite is a common contaminant in many dusts, including from some coal mines. Another issue is the potential for α -cristobalite contamination from the devitrification of the furnace lining.⁷

1.7.6 Relationship between XRD and FTIR instrument response and RCS particle diameter

The use of different calibration materials with slightly different crystallinities and particle sizes was identified as a major source of variability for proficiency testing results.⁵³ Responses from both XRD and FTIR instruments are sensitive to changes in the average or median particle diameter of RCS, even within the limited respirable size range.⁶⁵ The relationship between particle diameter and instrument response was studied in different calibration powders^{65, 144-147} and dust from coal mines.¹⁴⁸ For FTIR, the absorbance band height increases as the particle size decreases from about 8 μm to 1 μm in diameter,^{68, 149} whereas XRD integrated area intensity measurements are more consistent over this particle size range.^{65, 145, 148} The measurement response for both FTIR⁶⁸ and XRD^{65, 148} decreases at particle diameters less than 1 μm due to a thin amorphous, or less ordered, layer on the surface of each particle of approximately 0.03 μm in depth.^{68, 150-153} The less crystalline surface contributes proportionately more, in terms of particle volume and mass, at particle diameters less than 1 μm , so that both the XRD and FTIR techniques give lower measurement responses for the mass of crystalline silica particles. The band response when using Raman spectroscopy is also potentially affected by the particle size,^{88, 90, 91, 94, 154} which may also affect the Raman measurement of RCS in workplace samples of respirable dust. Chapter 5 investigates the Raman response when the measurement is challenged with different median diameter dusts within the respirable particle size range and compares it with XRD.

1.7.7 The effect of interference on the measurement of RCS

FTIR or XRD methods can achieve an LOD between 3 μg and 10 μg when measuring pure quartz or cristobalite on clean 25 mm diameter polyvinylchloride (PVC) filters (Table 4). However, a potential major limitation is the influence of interfering minerals. The tetrahedral building block of silicon (Si) and oxygen (O) atoms in crystalline silica is also found in silicate mineral groups, such as feldspars, micas, zeolites and clays. These mineral structures can produce

FTIR absorbencies and XRD reflections that are close to or coincide with those of α -quartz and α -cristobalite.^{54, 55, 68, 138, 147, 153}

There is often potential for significant interference when measuring α -quartz because of its abundance in natural and synthetic materials in the workplace. For example, a common material like granite is widely used in construction, aggregate and stonemasonry industries. Granite dust (about 20% to 30% quartz) can contain significant amounts of feldspars such as, anorthite, orthoclase and albite and some mica, all of which are highlighted as potential interferences for FTIR⁵⁵ and XRD.^{147, 153} Artificial (engineered) stones, fabricated in factories to provide uniform work surfaces, can also contain feldspar minerals since powdered natural mineral dust is often added to the resin where α -quartz or α -cristobalite is present as a main phase or a contaminant of the added powder.^{8, 155} Major interferences such as zeolite and mullite¹⁵³ are found in dust from some ceramics manufacture and foundries. Ball clays, used in ceramics, can contain about 30% α -quartz, whilst kaolin may contain trace amounts (0% to 10%).

Table 5 lists the α -quartz content of common materials found in workplaces and potential interferences.

Table 5. Common materials found in workplaces and potential silicate interferences.

Material	Approximate α -Quartz Content. Mass Percent	Potential Interferences
Coal dust	Less than 10%, typically 5%*	Graphite, kaolinite and feldspars
Kaolin	Less than 10%	Kaolinite, muscovite, and other clays
Ball clay	Typically 20% to 30%	Kaolinite and other clays and some
Basalt	Up to 5%	Feldspars of the anorthite and albite series
Dolerite	Up to 15%	Feldspars of the anorthite and albite series
Diorite	Up to 20%	Feldspars, mostly anorthite
Flint	Greater than 90%	Some feldspar e.g. albite
Granite	20% to 45%	Feldspars, orthoclase, albite, anorthite, and muscovite.
Gritstone	70% to 90%	Some feldspars and sometimes mica
Limestone,	Less than 2%	No significant interference
Quartzite	Greater than 95%	No significant interference
Sandstone	70% to 90%	Trace of minor feldspars
Siltstone	50% to 90%	Clays
Slate	20% to 40%	Clays – illite and chlorite with orthoclase
Brick	Typically around 20% to 30%	Refractory silicates e.g. mullite
Artificial stones	0% to 95%	A range of feldspars and zeolite
Concrete	1% or less when brought to site in premanufactured pieces. Older concrete or when mixed on site – not detected to about 30%	No significant interference
Ceramics	5% to 45%	Refractory silicates e.g. mullite , poorly crystalline meta-kaolinite

*samples from coal mines can contain high proportions of α -quartz when the strata around the coal are worked on.

Granite dusts are a particular issue for quantitative measurement since the XRD scans of the three most common minerals found in these rocks have many diffraction intensities and FTIR absorbance bands that are close to those of quartz. XRD scans of relatively pure feldspars commonly found in granites are shown in Figures 20 to 22. The positions for the most significant α -quartz intensities are also shown.

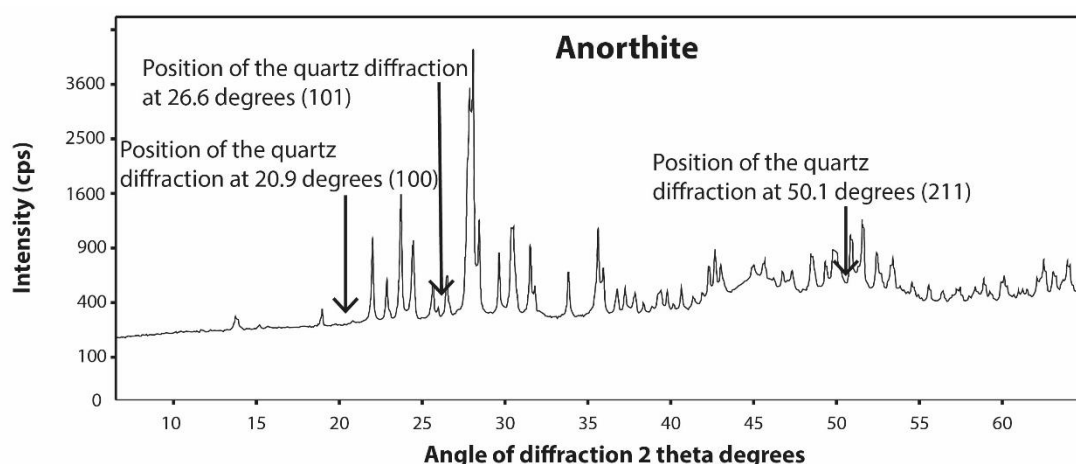


Figure 20. The X-ray diffraction pattern of anorthite ($\text{CaAl}_2\text{Si}_2\text{O}_8$). The positions for the three main intensities of α -quartz are shown.

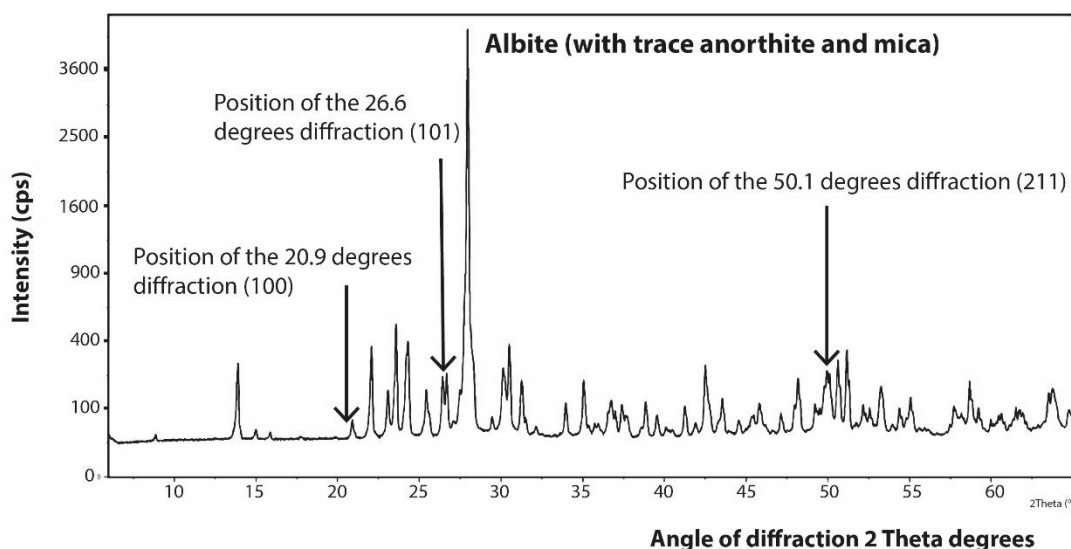


Figure 21. The X-ray diffraction pattern of albite ($\text{NaAlSi}_3\text{O}_8$) with a trace anorthite ($\text{CaAl}_2\text{Si}_2\text{O}_8$) and mica. The positions for the three main intensities of α -quartz are shown.

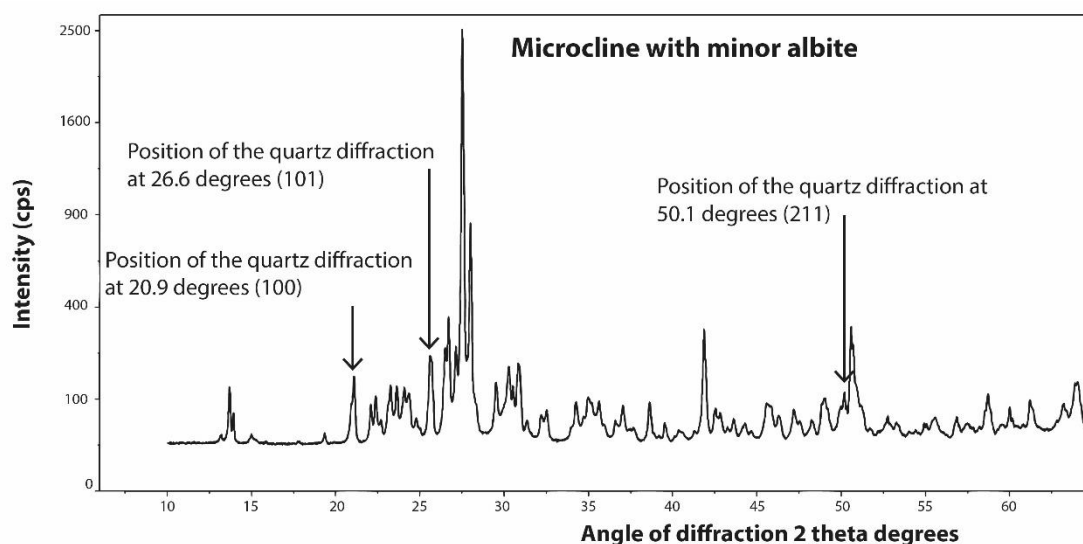


Figure 22. The X-ray diffraction pattern of microcline (KAlSi_3O_8) with a minor amount of albite ($\text{NaAlSi}_3\text{O}_8$). The positions for the three main intensities of α -quartz are shown.

Figures showing the FTIR absorbance bands for the same feldspar mineral dusts when collected on PVC filters are shown in Figures 23 to 25. The position of the 800 cm^{-1} wavenumber absorbance for α -quartz and α -cristobalite is shown.

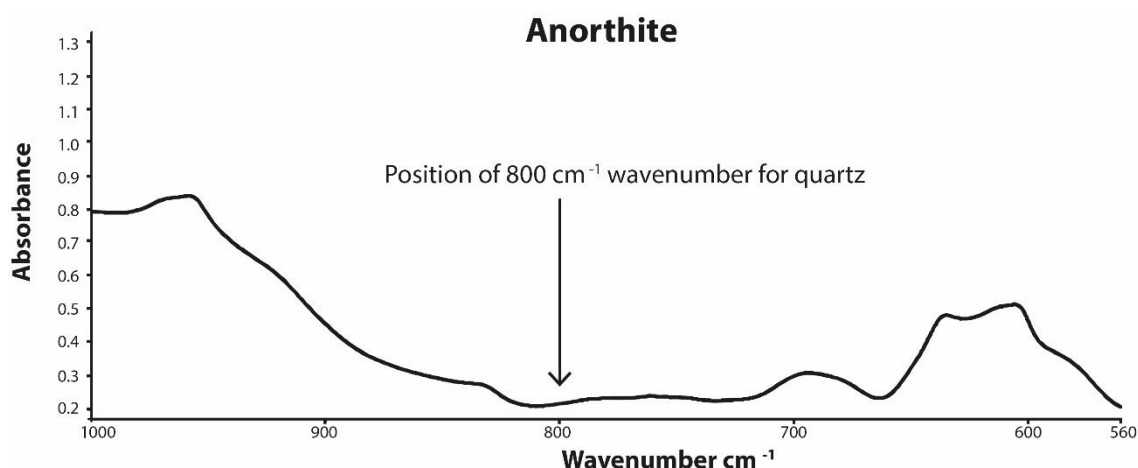


Figure 23. FTIR absorbance spectrum for respirable anorthite dust collected onto a PVC filter.

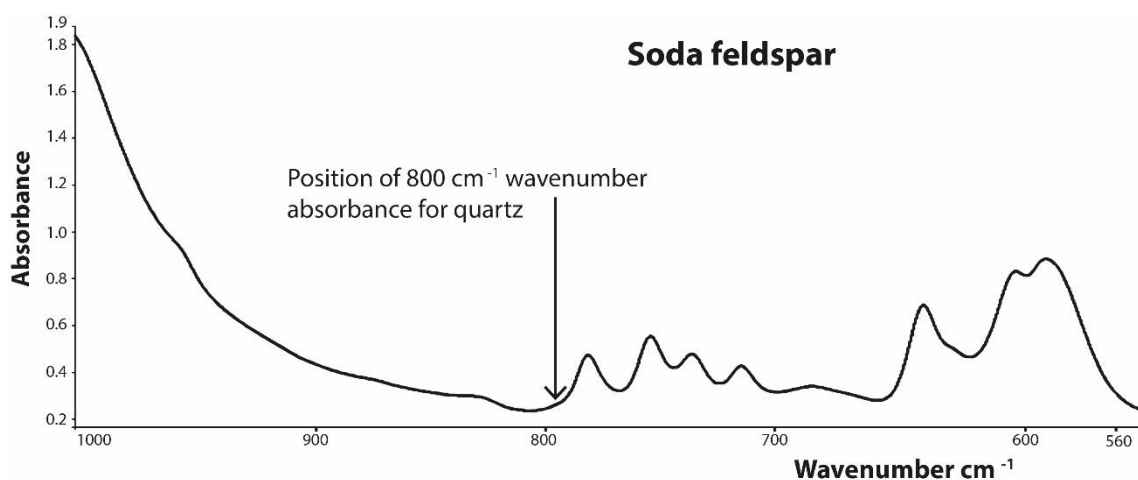


Figure 24. FTIR absorbance spectrum for respirable albite dust collected onto a PVC filter.

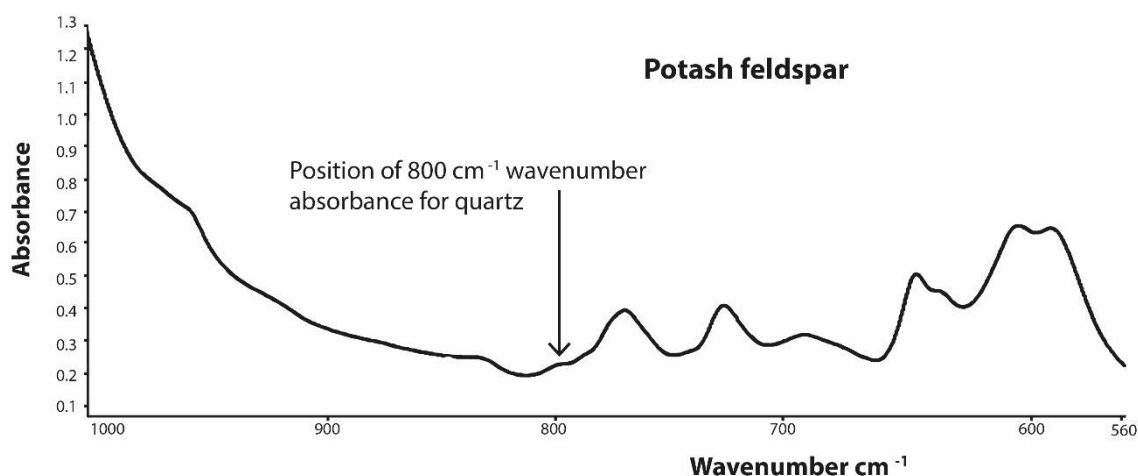


Figure 25. FTIR absorbance spectrum for respirable microcline dust with a minor amount of albite collected onto a PVC filter.

Many of the coincident reflections and absorbance bands from these interferences are relatively minor in magnitude when compared with the principal reflections and absorbance of α -quartz and α -cristobalite. This may indicate that these Feldspar minerals have a concentration threshold, below which their effect on the quantification of RCS is minimal.

1.7.8 Impact of interference on RCS measurement

The effect of the interference on XRD and FTIR measurements is seldom quantified. The American Proficiency Testing programme (PAT) includes test samples of α -quartz with coal dust, calcite, coal dust with talc and talc.⁵³ The average inter-laboratory precision for laboratories measuring RCS in the PAT scheme is about 19.9%.¹³⁹ This could be compared with the average inter-laboratory precision of about 8.5% (from 4% at high loadings 10% to 15% at low loadings) when measuring calibration type filters with pure quartz from the Workplace Analysis Scheme for Proficiency in the United Kingdom.¹³² Although, process recovery issues rather than interference could also be the reason for the higher average precision.

XRD is considered less susceptible to the presence of interferences than FTIR methods since the analyst may select an alternative reflection for quantification; however a secondary 100 or 211 reflections result in a loss of sensitivity and increase uncertainty.⁸ Sample treatment is a strategy for the removal of interference when using indirect XRD analysis methods.^{49, 57, 64, 126, 153, 156} Phosphoric acid digestions have been applied to remove silicate and other interferences; however, they do not always result in complete removal, may etch the crystalline silica (10% to 20%)^{54, 153} and add additional uncertainty. Conversely, a limited study did not find line interference a serious issue when measuring samples from 11 industries using the direct on-aerosol filter approach.¹⁵⁷ Although, other work found serious interference with the 101 and 211 reflections in samples containing, aragonite, graphite, mullite and muscovite¹⁴⁷ collected from foundries and potteries.

For FTIR, the minerals; anorthite, albite, orthoclase, kaolinite and muscovite are listed as common interferences in MDHS 101. Mullite, pyrophyllite, montmorillonite and vermiculite are also listed by other researchers in Japan.¹⁵⁸ However, no interference in foundry samples was reported by Foster and Walker⁶⁸ and no significant difference between XRD and FTIR results was found when measuring brick and tile (n=62) foundry (n=96) and potteries (n=106).¹⁴⁷ Kaolinite is a major interference in many workplace samples and is often found in coal dusts.^{56, 142} The presence of kaolinite was found to cause a

positive bias between 0% and 23%¹⁴² for FTIR measurement of RCS. Chapter 6 describes the relationship between bias and the proportion of kaolinite in the sample when using the MDHS 101 method.

1.8 Approaches for removal of spectral diffraction line interference

1.8.1 Current practice for measurements of RCS on aerosol filters

For FTIR, there are currently five approaches suggested for the removal of spectral interference. Firstly, the direct calibrations of mixtures of each component,¹⁵⁶ secondly, subtraction of a reference spectrum of pure analyte (if a non-linear baseline is found), thirdly calibration of and subtraction of the reference spectrum of the interference,¹²⁵ fourthly best expert judgement and finally chemometric methods. The reference subtraction method was found to be superior compared with the use of absorption ratios when applying synthetic mixtures of pure minerals.¹⁵⁸ A scaled absorbance subtraction approach for kaolinite, zeolite and some feldspars was applied for the direct on-filter FTIR analysis in MDHS 101.^{68, 147} However, the observed spectrum can be different from the stored reference, due to their differing crystallinity and slight changes in elemental composition, which affects the structure. It is also difficult to find quartz free standards and spectra of many natural materials. Residual absorbance can also occur because it is difficult to identify trace components due to the broad FTIR absorbencies, which may affect the accuracy of the subtraction. For example, some residual absorbance was found in spectra from potteries and brick manufactures and attributed to minor components such as illite not accounted for in the original spectra.⁶⁸

For XRD filter analysis, expert judgment is generally applied. Diffraction line interference is assessed by comparing their relative intensities with those of a reference pattern.³⁷ The integrated intensity can be calculated by adjusting the background positions for the change in intensity profile.

1.8.2 Potential of chemometric models to remove FTIR spectral interference for RCS.

Currently, quantitative methods use the Beer-Lambert Law assumption and a simple regression between two sets of coordinates, where x is the mass of analyte and y is the measured response. This is done for practical reasons. Standards of pure α -quartz or α -cristobalite are used for calibration due to the

wide variety of workplace conditions. A further development is the Multivariate Linear Regression (MLR) calibration examining a range of absorbance bands within spectra:

$$y_j = c + \sum_{i=1}^k m_i x_i + \varepsilon_{ij} \quad (22)$$

Where y_j is the predicted value, c is the intercept coefficient, m_i is the slope coefficient for the absorbencies considered x_i and ε_{ij} is the error in y and x .¹⁵⁹

Chemometrics is a potential multivariate solution for FTIR and Raman spectra because the process can interrogate the whole spectra to distinguish the most important features. Other approaches are operator dependent (reference spectra scaling), require knowledge of what is present, or rely on individual measurements of significant components which can introduce error. Chemometrics uses a mathematical process known as principal component analysis (PCA) to assess the influence of different infrared active components in spectra^{160, 161} and then applies MLR to quantify one or several components.¹⁵⁹ Two common chemometrics processes are principal component regression (PCR) and partial least squares regression (PLSR).

PCA is a way of reducing large amounts of data to a limited number of characteristic vector quantities¹⁶² known as principal components (PC). This provides a vector value (score) for each matrix component of interest by fitting a line to the variables and determining the distance of a point to an origin. The maximum spectral variability is the most characteristic feature. In PCR, a MLR then establishes a relationship between the mass of analyte in the matrix and the most correlated vector values suppressing collinearity¹⁵⁹ (e.g. a residue of the filter background with analyte loading). A PLSR examines both spectral and concentration data.¹⁶³ Both processes use MLR, however, PLSR contains correlates between vector scores obtained from the spectra and the vector scores from the variability in analyte mix and mass loadings. PLSR models can potentially be derived that use fewer principal components than the PCR model, because the concentration of a component can be given a low weighting if the derived scores poorly describe the observed variability in the spectra. This may

reduce the variability of results obtained when the models are challenged with dusts from different atmospheres as there is a lower potential for the spectral components to be affected by interference.

In 1994, PLSR was applied to resolve quartz and cristobalite in mixtures with fused amorphous silica using an indirect potassium bromide (KBr) disc method.^{69, 164} The goal of more recent work (from 2013) was to develop and demonstrate the capability of portable infrared instruments to provide on-site end-of-shift or end-of-task measurements.^{128, 165, 166} Chemometric models reduce the need for expert operator interpretation of spectra when interference is present and instruments are taken to or based at a workplace. Ashley *et al.*, compared four different portable instruments and found that they provided comparable results,¹⁶⁷ indicating that calibrations are potentially transferable, although, earlier work showed that resolution from some instruments might be an issue.¹⁶⁶ PLSR was recently applied for the measurement of quartz in Pittsburgh coal dust,^{168, 169 161} and for mixtures of quartz in calcite and dolomite using the KBr disc method.⁶⁶

1.8.3 Potential for removal of diffraction line interference for RCS from XRD scans

The analysis of components in bulk materials is the focus of computational methods to remove line interference from XRD scans. Two main approaches are the whole pattern fitting methods like Rietveld¹⁷⁰ and single intensity profile fitting methods.¹⁷¹ Neither of these have yet been applied to the measurement of respirable dust collected on filters. The Rietveld method was applied to measure the larger sized inhalable particulate fraction and wood dust on quartz fibre filters, however, some computational difficulties occurred when the intensity of coincident calcite and gypsum reflections were similar.¹⁷² The Rietveld method is less likely to work with respirable dust because of the potential for a larger proportion of amorphous material, and the difficulty of including an internal standard for accurate analysis in a sample of collected aerosol, which would dilute the concentration of analyte.

1.9 Discussion and conclusion

Inhalation of RCS can cause silicosis and cancer and large numbers of workers are potentially exposed to concentrations of RCS. Accurate measurements of RCS are needed to: support workplace exposure assessments; to help reduce incidence of disease by assessing the effectiveness of controls, protective equipment or regulatory interventions. The better the precision the easier it is to distinguish risks of exposure between materials, processes and similarly exposed groups of workers. There are some significant limitations with the reliability of the current analytical methodology using XRD and FTIR instruments; especially when there is a need to assess workplace exposures at RCS concentrations below those of the current WEL where there remains a risk to worker health. Accuracy of measurement is dependent on the instrument settings, method approach (direct on-aerosol filter or indirect), ashing approach (low temperature plasma ashing or furnace) and potentially the nature of interference.

These analytical and practical limitations can have a potential impact on the assessment of the:

- Risk of exposure when wearing respiratory equipment because a limit of detection less than one twentieth of that achievable with current analytical methodology is needed to assess whether a mask is effective at reducing exposures in the workplace to its assigned protection factor.
- Mass lung burden of RCS in groups of workers and their risks of ill health associated with their role, task or age, since lower limits of detection are needed to distinguish between working populations that are unexposed and exposed to RCS.
- The efficacy of controls when tested in research facilities and risks to health and contribution from task specific exposures, where accurate measurements of 1 h and less might be required.

Internationally, the main focus of work to improve the sensitivity of RCS measurement in the last 10 years has been on the development and testing of higher flow rate respirable samples to collect more dust for measurement.^{173, 174}

Often, when flow rates increase, the samplers increase in size and larger pumps are needed. Increased instrument sensitivity would enable the use of existing sampling equipment or potentially smaller miniature samplers⁴⁵ which would be a cheaper alternative for occupational hygienists. Low temperature FTIR has also been investigated by researchers in NIOSH but not developed further.¹⁷⁵

There are many methods that use Raman spectroscopy for quantitative work. However, despite its potential, there was little work describing the use of Raman spectroscopy for quantitative analysis of aerosol particulate and none for crystalline silica. Raman response is specific for the polymorphs of crystalline silica and the parameters that influence its magnitude are known (equations 18 to 20). For quantitative analysis, the Raman band response is dependent on the type of laser and energy applied, sample temperature, numerical aperture of the objective and particle size of the measured sample. Similar to electron microscopy techniques, a Raman microscope can potentially obtain a very low LOD because it measures a response from a small area of a sample on a substrate. However, for accurate quantitative analysis the representativeness of the measured sample is important and strategies are needed to accomplish repeatable results within a reasonable analysis time.

Any analytical method for workplace measurements must be as universally applicable as possible. For all the techniques discussed, the presence of spectral interference is a factor that may cause measurement inaccuracies when analysing some workplace samples. There are many minerals listed in RCS methods and articles that have FTIR absorption bands or XRD intensities coincident or close to those for α -quartz or α -cristobalite, although the magnitude of the effect of interference is less well established. Kaolinite is one common mineral which can potentially cause significant interference. Reference spectra subtraction methods were a useful approach to deal with interference, however, spectral discrepancies might remain. To ensure accuracy, other approaches might be needed when measuring samples from RCS concentrations below the WEL from some workplaces. Multivariate, chemometric methods are increasing available to analytical laboratories for

routine work, and may reduce intervention times to control exposures when used in conjunction with portable FTIR instruments. However, the performance of these chemometric methods when using the equipment most commonly employed in the UK is not fully established.

1.10 Aims and Objectives

The aims of the work, after considering the knowledge gaps, are firstly, to explore the potential of vibrational spectroscopy techniques to measure lower mass concentrations of respirable crystalline silica (RCS) and secondly to investigate chemometric methods for Fourier Transform Infrared (FTIR) and profile fitting for X-ray diffraction (XRD), to improve accuracy of these traditional techniques when interference is present.

The principle objectives were to:

- Investigate the potential of Raman spectroscopy to measure dust collected on filters containing RCS obtained from a miniature aerosol sampler developed by the author at the Health and Safety Executive.
- To investigate the performance of Raman spectroscopy:
 - a) when measuring aerosol particles from natural and industrial processes of the most common polymorphs of crystalline α -quartz and α -cristobalite;
 - b) when measuring different particle size fractions within the respirable range;
 - c) when measuring samples collected from behind respirators.
- To compare the performance of XRD and FTIR analytical techniques specified in international methods for RCS.
- To investigate the use of de-convolution data processing techniques to remove the effect of interfering components to improve both the existing and novel approaches.

This research is funded by the Health and Safety Executive (HSE) and supports a strategic programme of work to examine the effectiveness of respiratory protective equipment (RPE) when worn in the workplace.

Chapter. 2 Sample concentration methods

A short study was conducted to investigate the furnace and plasma ashing sample digestion approaches with the aim of determining which procedure provided the most precise results.

2.1 Method

First test method

The HSE α -quartz standard A9950 was loaded onto 30 PVC filters following the procedure in MDHS 101. A portion of an aerosol of A9950 was collected onto the filters using a SIMPEDS respirable sampler and the mass of loaded standard was determined gravimetrically. Fifteen filters were placed in porcelain crucibles and ashed in a furnace (Carbolite Ltd, Hope Valley, UK) at 450 °C. The other fifteen filters were placed in glass bottles and ashed using a low temperature plasma asher (Emitech K1050X, Quorum Technologies Ltd, Ashford, UK). The filters were ashed in air at 50% power (48 watts) for 12 h and then in oxygen for 4 h at 95% power (95 watts). About 5 mL of 99.9% purity isopropanol (Fisher Scientific UK Ltd,) was added to the bottle after it was removed from the asher and had cooled. The liquor and residue were sonicated for 3 mins and then filtered into a 15 mm diameter circular area on a 0.45 μm pore size silver filter. The samples from the furnace were filtered in a similar way. The recovered dust was deposited into a 15 mm diameter area onto silver filters and measured using XRD. The percentage difference from the gravimetric loading was plotted against the mass loading value and the values for the mean squared residual errors (MSRE) were compared using the F-test for each trend line relationship (furnace or plasma ashed samples) between response and loaded mass.

Second test method

In addition, a second comparison was performed with the lowest loading of 10 μg to ascertain if differences between methods were identifiable by XRD. Ten replicate samples were prepared for the plasma ashing process and ten for the furnace treatment. The test samples were prepared by pipetting 1 mL of a stock suspension of 11 $\mu\text{g}.\text{mL}^{-1}$ of the certified reference material NIST 1878a (96.7% crystalline) onto 25 mm diameter polyvinylchloride (PVC) filters. The deposited

mass was measured using XRD and the measurement approach described in MDHS 101.⁵⁵ The filters were ashed following the procedures described above. T-tests and F-tests were used to ascertain if the means and variances of the two sets of results (pre-process and post-process) were similar. Probabilities (p) less than 0.05 would indicate a difference at the 95% level of confidence.

2.2 Results

First test results

Figure 26 provided a visual comparison of the differences between the XRD and gravimetric mass results when using ashing approach specific calibrations. The standard error of the residuals was 18 μg for the furnace approach, which was almost more than twice the value of 11 μg when plasma ashing. The values for the MSRE were slightly significantly different ($p = 0.035$) at the 95% level of confidence. The plasma ashing process had more samples below a mass of 50 μg which should be a disadvantage as these would be expected to show greater variability because the measurement precision is considered poorer.

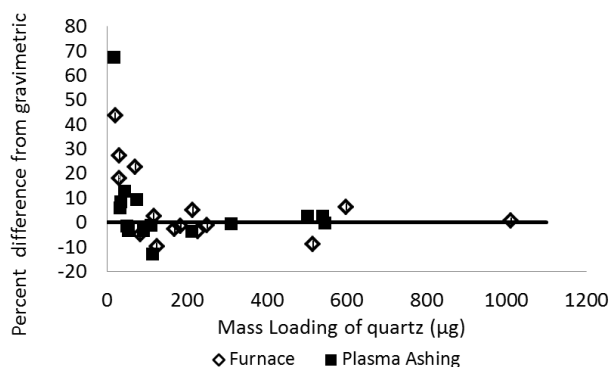


Figure 26. A comparison of the percent variation of XRD results for α -quartz from their gravimetric loaded mass values for the plasma and furnace ashing indirect measurement approaches.

Second test results

Results from the further study with ten replicate samples of 11 μg for each process are shown in Table 6. A high average value of 16 μg with a standard deviation of 7 μg was obtained for an initial set of ten post process furnace

samples. These were rejected due to potential contamination from the furnace lining. Hence, a metal plate was placed on the floor of the furnace and another set of ten samples were prepared for this process.

Table 6. Statistics from the second comparison comparing filter treatment processes for the indirect analysis method when measuring filters with a loading 10 µg of α-quartz .

Process	Before Process		After Process		Comparing pre with post process	
	Average (µg)	Standard deviation (µg)	Average (µg)	Standard deviation (µg)	t test probability	F test probability
Plasma ashing	10.3	0.73	9.95	0.49	0.16	0.11
Furnace with metal floor	10.2	0.90	10.9	1.49	0.19	0.08

2.3 Discussion and conclusion

These measurements were made on ideal samples and do not necessarily represent the performance of the method when measuring dust collected from respirable samplers (Figure 19). The standard deviations for both methods (pre and processed samples) are good (from 5% to 15%). These results indicate that two ashing processes can produce sets of results that are not significantly different from their unprocessed values. The F-test between processed plasma and furnace ashed samples was significantly different ($p < 0.01$), although, this might be due to the more variable aliquots for the furnace samples. The plasma ashing process generally produces results with smaller standard deviations and there is also less potential for sample contamination. Therefore, plasma ashing was used as the preferred processing technique in subsequent chapters.

Chapter. 3 Feasibility study for Raman microscopy measurement of RCS

Stacey, P., Mader, K. T., and Sammon, C.

Feasibility of the quantification of respirable crystalline silica by mass on aerosol sampling filters using Raman microscopy. (2017). *J. Raman Spectrosc.*, 48: 720– 725. doi: [10.1002/jrs.5113](https://doi.org/10.1002/jrs.5113).

Published Open Access Licence CC BY 4.0

Current citations = 13 (April 2022)

A small deposit area (5 mm in diameter) and high laser energy were applied to create advantageous conditions to assess the potential for quantitative measurement of respirable α -quartz and α -cristobalite deposited on silver filters close to and below the LODs of established analytical techniques. Samples of 20% quartz in hematite and 5% quartz in calcite were also measured to assess the performance in these challenging mixtures. Hematite, commonly found in foundry, brick manufacture and some mine samples, was selected because it may absorb the Raman response.

Feasibility of the quantification of respirable crystalline silica by mass on aerosol sampling filters using Raman microscopy

Peter Stacey,^{a*} Kerstin T. Mader^b and Christopher Sammon^b

Airborne respirable crystalline silica (RCS) is a hazard that can affect the health of workers, and more sensitive measurements are needed for the assessment of worker exposure. To assess the use of Raman microscopy for the analysis of RCS particulate collected on filters, aliquots of quartz or cristobalite suspended in isopropanol were pipetted onto silver filters. Samples were measured by arbitrarily selecting positions along the filter and collecting spectra at 50 discrete points. The calculated limits of quantification on test samples were between 0.066–0.161 and 0.106–0.218 μg for quartz and cristobalite, respectively. Three respirable quartz calibration dusts (A9950, NIST 1878 and Quin 1B) with different mass median aerodynamic particle sizes obtained similar Raman response relationships per unit mass. The difference between NIST 1878 and Quin 1B was not significant ($p = 0.22$). The intermediate measurement precision of replicate samples was 10–25% over the measured range for quartz (0.25–10 μg) and could potentially be improved. Results from mixtures of quartz and cristobalite were mostly within 10% of their theoretical values. Results from samples of 6% quartz in calcite were close to the theoretical quartz mass. The upper measurement limit for a mixture of 20% RCS in the light absorbing mineral hematite (Fe_2O_3) was 5 μg . These data show that Raman spectroscopy is a viable option for the quantification of the mass of respirable crystalline silica on filters with a limit of detection approaching 1/10th of that obtained with other techniques. The improvement in sensitivity may enable the measurement of particulate in samples from low concentration environments (e.g. inside a mask) or from miniature samplers operating at low flow rates. ©2017 Crown copyright. *Journal of Raman Spectroscopy* published by John Wiley & Sons, Ltd.

Keywords: respirable crystalline silica; workplace; Raman; limit of detection; quantification; particle size

Introduction

Respirable sized particles can penetrate to the alveoli of the lung.^[1] Their aerodynamic size range is defined by an International Organisation for Standardisation/Centre European de Normalisation/American Congress of Government Occupational Hygienists convention^[1] as those particles mostly $<16 \mu\text{m}$ with a 50% penetration cut-off value of $4 \mu\text{m}$. Inhalation of respirable particles from an aerosol containing crystalline silica is linked to diseases such as silicosis^[2] and cancer.^[3] In 2004, an estimated 907 cases of cancer in Great Britain were attributed to exposure from aerosols containing respirable crystalline silica (RCS) in the workplace.^[4] RCS is also thought to cause of chronic obstructive pulmonary disease.^[5] Quartz and cristobalite are two crystalline polymorphs of silica that are encountered in aerosols in the workplace. Quartz is a common component in many naturally occurring mineral products, whilst cristobalite is often present in industrial processes where a silica-containing material is heated to around 1000 °C. There is a requirement under the Great Britain's Control of Substances Hazardous to Health regulations^[6] to control exposure to below the current WEL for RCS of $100 \mu\text{g m}^{-3}$, as a time weighted average for an 8 h working shift.

X-ray diffraction (XRD) and infrared spectroscopy (IR) are two techniques specified by national analytical methods to measure RCS in dust collected on an air sample filter.^[7] Limits of detection (LOD) for XRD and IR reported for RCS measurements on laboratory test samples of pure analyte are between 3 and 10 μg .^[7] Aerosol samplers that typically operate at 2 l min^{-1} are not able to collect

sufficient sample for a quantifiable mass of RCS (20–30 μg) in less than 2 h^[7,8] when sampling an RCS concentration around the WEL. This level of analytical performance limits the capabilities of sampling to evaluate the protection and exposure of workers, e.g. to enable analysis of short-term or task-specific samples within the working shift or from some low concentration environments. Although airborne concentrations of RCS are generally low, there are industrial processes that may expose workers to high concentrations above the WEL, and the use of face filtering masks as respiratory protective equipment (RPE) is frequently employed to protect workers. The exposure of a worker wearing a mask is estimated by applying a correction factor to the results obtained from a personal sample taken outside of the mask. If the RPE is functioning as intended, the expected airborne concentration of RCS inside the mask will be between 0.2 and 1 times the LOD of current

* Correspondence to: Peter Stacey, Health and Safety Executive, Science Division, The Health and Safety Laboratory, Harpur Hill, Buxton SK17 9JN, UK. E-mail: peter.stacey@hsl.gsi.gov.uk

This is an open access article under the terms of the Creative Commons Attribution License, which permits use, distribution and reproduction in any medium, provided the original work is properly cited.

a Health and Safety Executive, Science Division, The Health and Safety Laboratory, Harpur Hill, Buxton SK17 9JN, UK

b Materials and Engineering Research Institute, Sheffield Hallam University, Sheffield, Howard Street, S1 1WB, UK

analytical techniques for a typical 960-l pumped air sample when collected at 2 l min^{-1} during an 8 h working day. A goal of this work was to investigate the use of alternative measurement techniques, with better LOD, to measure the very low airborne concentrations of RCS inside a mask. Ultimately, the aim is to find a technique sensitive enough to permit the analysis of samples to assess the workplace effectiveness of RPE.

Raman spectroscopy is sensitive to both chemical and morphological changes within a sample and is routinely used to distinguish between polymorphs, including those of microcrystalline silica.^[9] This technique was used to quantitatively analyse opaline in silica nodules of volcanic origin utilising a rotating stage to obtain an average signal from the sample surface and produce calibration curves by mass for quartz, cristobalite, coesite and calcite mixtures.^[10] Raman spectroscopy was also investigated as a potential technique to determine the mineral content of rocks on moons or planets.^[11] Only recently has Raman spectroscopy been used to characterise airborne particles of dust from samplers collecting particulate matter $<10\text{ }\mu\text{m}$ and particulate matter $<2.5\text{ }\mu\text{m}$ from ambient air.^[12–14] Potgieter-Vermaak and Van Grieken^[12] examined the suitability of a number of filter materials for the evaluation of individual aerosol particles using micro-Raman spectroscopy. Catelani *et al.* determined the percentage of particles in samples of airborne dust from two sites using a point count method.^[13] Quartz compositions by number ranged from 4.5% to 12%. The chemical composition of marine aerosols over the Pacific Ocean was also recently examined with an aluminium foil on a 'streaker' sampler being used as a collection substrate for an on-air-sample filter analysis approach.^[14] The work reported in this article investigates the use of a wide area coverage approach to quantification, where the Raman spectra of crystalline silica from many different fields of view are combined.^[15] The advantage of a wide-field measurement approach is that it reduces the variability of the analysis caused by the inhomogeneity of the sample deposit, which is a major factor affecting the reliability of Raman quantification.^[15]

Experimental

Reagents and test sample preparation

Suspensions of the NIST reference material 1878a for quartz and 1879 for cristobalite ($10\text{ }\mu\text{g ml}^{-1}$) were prepared in isopropanol (CAS 67-63-5). These suspensions were constantly agitated with a magnetic stirrer. Aliquots (0.1–2 ml) of these suspensions were deposited onto 25-mm diameter, 0.45- μm pore size silver filters (SKC Ltd., Bedford, UK). The deposit area was constrained to a 5-mm diameter area using a bespoke fluted filter funnel. A 5-mm diameter hole in a 25-mm diameter plastic washer was fitted beneath the filter to reduce the sintered suction area and the spread of the sample. Figure S1 shows the filtration equipment, mask and a sample of hematite dust on the deposit area of a silver

filter. The circumference of the deposit area was marked with a needle, before deposition. The scratched circumference clearly demarcated the deposit area from the blank filter in reflected white light under the microscope.

To assess if the Raman measurement is also affected by particle size differences, we compared two other quartz calibration powders with different mass median aerodynamic particle size distributions. The origin of the materials and differences in median aerodynamic particle size^[16] are listed in Table 1.

Raman measurement strategy

Raman spectra were collected from the 5-mm diameter deposit area using an In-Via Raman microscope (Renishaw Ltd., Gloucester, UK) with near infrared laser (785 nm) excitation, CCD camera and a grating with 1200 l mm^{-1} . Typical spectra for quartz and cristobalite standards on silver filters are shown in Fig. 1.

The sample deposit was located on a silver filter, and 50 fields of view were randomly selected from within the 5-mm diameter of the scratched circumference. Raman spectra were obtained from within each field of view using an $\times 20$ objective. The analysis area was estimated as $100\text{ }\mu\text{m}^2$, so approximately, 20% of the deposit area would be analysed from 50 sampling points. The spectrum for each sampling point was collected with 100% laser power with a 7-s exposure time and three accumulations. The integrated areas of the Raman peaks were obtained by fitting with a Gaussian line shape using the standard algorithms in the manufacturer's WIRE 4 software package. The areas under the peaks at 462 cm^{-1} for quartz and 410 cm^{-1} for cristobalite were quantified if they appeared within the spectra from each sampling point. The trend between accumulated area counts and theoretical mass was plotted for both polymorphs of crystalline silica.

The signal from a silicon wafer (Si) standard was measured using the integrated area at 520 cm^{-1} with an $\times 50$ objective at 10% laser power for 1 s once before and after each filter analysis. The results of these measurements were used as an external standard to compensate for fluctuations in laser intensity. Daily fluctuations in laser intensity were corrected using the ratio between the count collected when the silicon area was first measured and the average collected before and after each filter measurement.

Statistical evaluation

The difference in trend lines for the measured response and mass relationships between calibration dusts were determined using a *t* statistic calculated from the difference between the slopes of the lines and their standard errors.

An estimate of the intermediate precision was made by analysing five replicate mass loadings of quartz on silver filters at five different measurement levels, incorporating analyses conducted on different days by different researchers to account for any additional variability from the analysts.

Table 1. Origin and median aerodynamic sizes of respirable quartz calibration dusts tested to assess the influence of particle size on Raman response

Name	Origin	Aerodynamic size (μm)		Crystallinity percent
		Mass median	Number median	
NIST 1878a	National Institute for Science and Technology (United States of America)	3.72	1.52	93.7 ± 0.21
A9950	The Health and Safety Executive (Great Britain)	6.04	1.39	89.3 ± 1.86
Quin 1 Bulk	Institut National de Recherche et de Sécurité (France)	7.16	3.24	95.2 ± 2.51

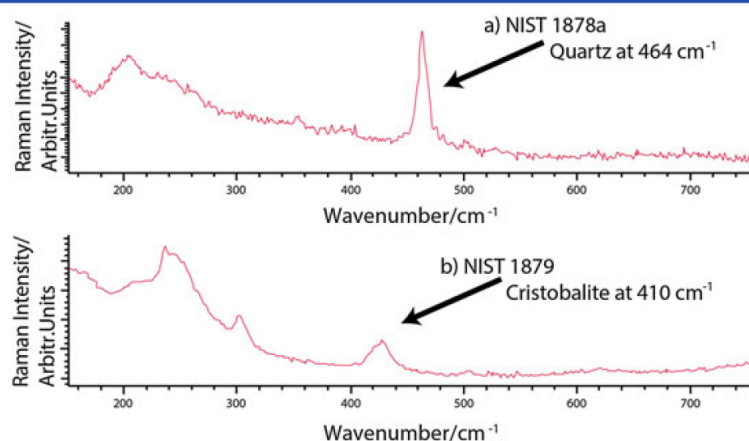


Figure 1. Spectra for quartz and cristobalite collected from a single field of view from a filter-containing 10 µg of analyte deposited in a 5-mm diameter area. [Colour figure can be viewed at wileyonlinelibrary.com]

Precision and bias of pipetting

Test samples, with mass loadings greater than 2 µg, were first measured using an XRD X-pert Pro MPD instrument (Panalytical Ltd., Cambridge, UK) with focusing Bragg–Brento geometry to provide a correction for pipetting errors. The silicon content of some of the highest loadings of reference material on silver filters was measured using inductively coupled plasma atomic emission spectroscopy (Perkin Elmer, Beaconsfield UK). The mass of quartz calculated from the silicon content measurement was used to assess bias in the pipetting. The LOD of this technique was calculated to be approximately 3 µg.

Limits of detection

Five blank 13-mm diameter, 5-µm pore size polyvinylchloride filters, (SKC Ltd., UK), commonly used for workplace aerosol sampling, were ashed at 600 °C in a furnace, ultrasonicated with isopropanol and filtered onto a 5-mm diameter area on the 0.45-µm pore size silver filters. The measurement strategy was then applied to analyse each of the five silver filters. The total area counts were recorded from any identifiable peaks found in the spectra that matched the quartz or cristobalite wavenumbers. The standard deviation was calculated from the accumulated counts from each of the five filters (Table 2).

These LOD values were compared with a procedure proposed in International Organisation for Standardisation 16258 to calculate an LOD^[8] from the variability of the background scatter. The standard deviation of the background scatter from a fitted trend line was calculated from spectra obtained from 11 randomly selected fields of view on two blank filters. The standard deviation was then multiplied by three times the response trend line coefficients for

quartz, or cristobalite. This provides an estimate of the LOD from the scatter of a scan from a single sampling point. Counting statistics will apply to obtain an LOD for the spectra from 50 sampling points, because the detection of a peak in a scan was also dependent on the subjective judgement of the individual analyst. For a Poisson distribution, commonly employed in counting statistics, a count of four is considered above a background level with a 99% level of confidence,^[17] so the estimated LOD for a single scan was also multiplied by four.

Simulated matrix samples

Mixtures of quartz and cristobalite were prepared by pipetting aliquots from a suspension of standard dust onto the same silver filter using the bespoke apparatus in Fig. S1 to test the performance of the measurement in a more complex situation. In addition, mixtures from suspensions of 20% quartz in hematite and 6% quartz in calcite were also studied to assess how Raman spectroscopy would perform as a quantitative tool in these challenging matrices. The hematite and calcite powders were the same as those previously used in a study of X-ray absorption.^[18] The recorded mass was compared with the theoretical mass of quartz deposited on the silver filter determined from the aliquot volume and the concentration of quartz in the suspension. The 95% level of confidence for each mass loading was calculated from the intermediate measurement precision.

Results and discussion

Variation of the Raman signal intensity of the silicon external standard measurement at the same position was <2% when collected sequentially. Repeatability in different positions within a few minutes was approximately 3%. This variability could be due to the sample not being perfectly flat or the presence of non-RCS dust particles. Precision of the measurement between days was approximately 20%. This large between day variation did not change the results for the mass of RCS because the measured value is corrected for the change in intensity, which is relatively consistent during the analysis. XRD analysis identified a pipetting bias between the samples. This was attributed to the use of an air rather than piston displacement pipette for some of the loadings. The

Table 2. Limits of detection for quartz and cristobalite

Analyte	Quartz mass (µg)	Cristobalite (µg)
Limits of detection from filter measurements	0.049	0.066
Limits of detection calculated from variability of the background scatter	0.020	0.032

measured mass value was verified using inductively coupled plasma atomic emission spectroscopy, and based on this, a correction was made to the theoretical loading value for some of the quartz samples. Figure 2 shows that the calibration over a mass range of 0.25–15 μg for quartz, and 1–10 μg for cristobalite was linear over the analytical range of test samples with a calculated coefficient of determination (r^2) of greater than 0.98. The quartz calibration includes 30 samples from two suspensions, and the cristobalite calibration includes 12 samples from two suspensions. Two quartz samples at 20 and 50 μg were also measured but are not included in the chart. The trend line including these two points with the rest of these data had a coefficient of determination of 0.98 indicating that the relationship between mass and response was potentially linear up to 50 μg . The average number of fields with a quantifiable peak measured at the lowest quartz loading of 0.250 μg was seven (14%).

LOD obtained using Raman spectroscopy

The LODs, determined using a blank filter measurement approach, were compared with an LOD calculated from the variability of the background noise (Table 1). The values given in Table 1 indicate a limit for quantification (the standard deviation multiplied by 10) for the measurement of quartz and cristobalite of approximately 0.066–0.161 and 0.106–0.218 μg , respectively. These values are approximately an order of magnitude less than typical LODs for RCS obtained using the XRD and IR analytical techniques (3–10 μg),

which are currently the industry standard for the determination of RCS. Raman microscopy also has the potential to reduce the LODs further by analysing a greater proportion of the sample area, i.e. scans from more sampling points and longer collection times. A calibration in terms of counts/sampling point permits the analyst some flexibility in their measurement approach when analysing samples from challenging low dust concentration environments because they would be able to collect more scans from sampling points to improve the LOD without having to recalibrate for the increase in measured area.

Precision of measurements on test filters

Intermediate precision for the analysis of quartz using Raman microscopy on replicate samples is shown in Fig. 3. The values in Fig. 3, which decrease from approximately 25% to 10% over the mass range of 0.25–10 μg , include a contribution due to pipetting precision and different analysts. An analytical precision of approximately 10% in the range of 2–10 μg is satisfactory for routine work and could be improved by collecting spectra from more fields of view, as some error will be due to the inhomogeneity of the deposit. Figure 3 also demonstrates the benefit of correcting for the laser intensity using the Si external standard. Some additional variability might be due to slight differences in the way the external standard measurement was collected by different researchers, as the intensity of the Si signal using Raman microscopy is dependent upon the sample orientation.

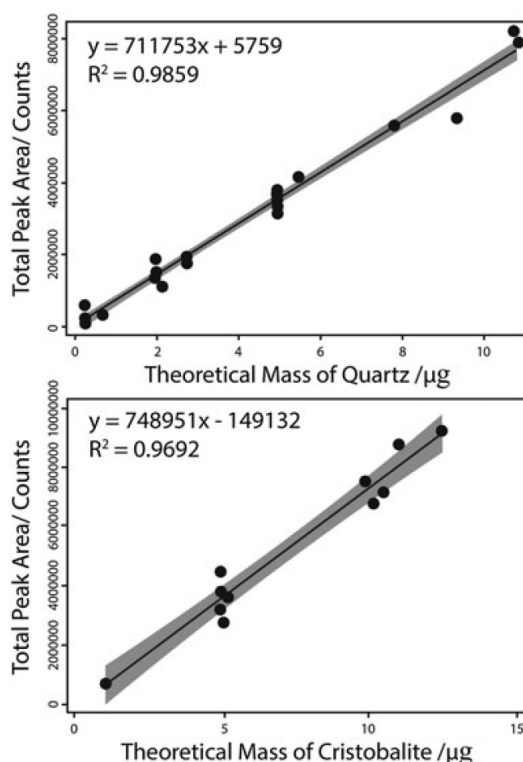


Figure 2. Trend line relationships for Raman response with mass of quartz (NIST 1878) and cristobalite (NIST 1879) loaded in 5-mm diameter area onto silver filters. The shaded area is the 95% confidence interval for each slope coefficient.

Effect of aerodynamic particle size on measurement response

The differences in measured response between three respirable quartz dust standards (NIST 1878a, A9950 and Quin 1 B) used for calibrations are shown in Fig. 4. The median number aerodynamic particle size values of the NIST 1878a and A9950 reference materials are very similar (1.4–1.5 μm), although A9950 contains a larger proportion of larger diameters by mass (Table S1), and they have different crystallinities (93.7% and 89.3%). Quin 1 B is a powder where its particle size distribution has both larger number and mass median particle sizes (3.2 and 7.1 μm , respectively) when compared with NIST 1878a and A9950 so would be most affected by any changes in Raman response due to particle size differences. The probability (p) that the standards with the largest differences in median aerodynamic diameter (NIST1878a and Quin B) were different was not significant ($p = 0.22$) when trend lines with an intercept were evaluated over the analysis range shown. The

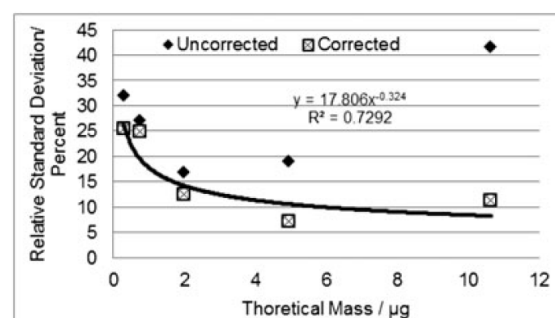


Figure 3. Intermediate measurement precision for Raman measurement of quartz (NIST SRM 1878) deposited into a 5-mm diameter area on silver filters.

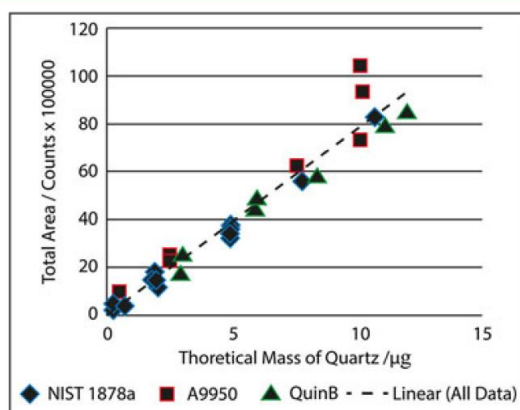


Figure 4. Comparison of the Raman response with mass when measuring respirable quartz calibration dusts NIST 1878a, A9950 and Quin 1B with different median number and mass aerodynamic particle sizes. [Colour figure can be viewed at wileyonlinelibrary.com]

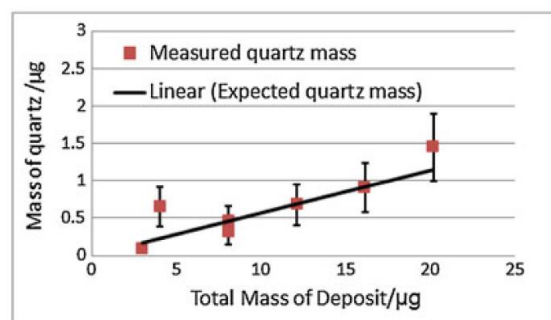
comparison between A9950 and NIST 1878a was borderline significantly different ($p = 0.04$); however, most values were close to the NIST 1878a trend line relationship below $10 \mu\text{g}$ and if a single value at the highest loading is removed the response relationship with mass loading from the two materials is not significantly different ($p = 0.08$). These results demonstrate that the difference in response due to aerodynamic particle size within the respirable size range will not significantly affect the reported result for most samples within the mass range $0.25\text{--}10 \mu\text{g}$. Conversely, XRD and IR measurements are affected by differences in median aerodynamic particle size of the powder within the limited respirable range.^[16] We reason that, when using a quantitative method based on the accumulated Raman spectra from random selection of a number of sampling points, the number distribution of particles is more critical than their mass distribution. In addition, because the test samples are prepared in terms of mass per unit volume, the number of particles per unit mass loaded on these filters is reduced when respirable quartz calibration dusts with larger particles are prepared. This potentially compensates for any change in Raman response because of the larger aerodynamic particle size. It should be noted that 'Quin 1B' is not intended for the preparation of calibration standards prepared from a suspension and represents a larger aerodynamic particle size distribution that would not routinely be expected on a sample filter collected using a respirable size selective aerosol sampler for occupational hygiene sampling.

Results from simulated mixtures

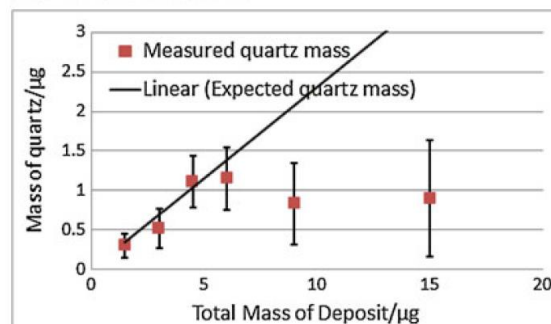
Four mixtures of pure cristobalite and quartz were measured (Table S2). Ratios of measured mass with the theoretical mass for three of the four samples were within 5% for both quartz and cristobalite. The fourth sample, with the highest loading, was slightly high approximately 20%. Measurement of mixtures of quartz and cristobalite were challenging because of the convolution of overlapping peaks within the spectrum (Fig. 1). There were some individual analyte differences where the use of peak fitting and Fourier self-deconvolution approaches may have improved the area measurement but were not used for these experiments.

Results from samples simulating more realistic sample mixtures of 6% quartz in calcite and 20% quartz in hematite are shown in

Fig. 5. The bar with each measurement represents the 95% level of confidence calculated from the intermediate precision. Whereas the calculated mass of quartz in calcite follows the line of expected mass, indicating that Raman would be able to reasonably measure quartz in matrix samples where calcite is a major component, (e.g. cement dust), the measured values obtained for 20% quartz in hematite tail-off when the total mass of deposit are $>5 \mu\text{g}$. This is because hematite is opaque to visible light, meaning that only signal from the surface of the deposits would be observed. Conversely, calcite is transparent to visible light, meaning the Raman signal comes from a greater depth of the deposited particles. The limit of $5 \mu\text{g}$ for hematite containing samples may therefore be an indicator of a critical mass, below which the particle density of the deposit on the filter is sufficiently dispersed not to affect the Raman signal collected from a sampling point. For this reason, Raman might not be a useful technique for heavily loaded samples from environments with high hematite or iron content, e.g. foundry or coal mine dust. Attenuation of signal from hematite and dark particles is not unexpected and is also an issue with XRD and IR analysis.^[7,8,19] There are several strategies to compensate for this. Firstly, the loadings can be managed by reducing sampling times to ensure the total mass is below the critical level. This requires vigilance on the part of the occupational hygienist taking the sample, who is often not the same person analysing the samples. Alternatively, silver filters are also used in XRD analysis as an internal standard to correct for the absorption. The use of an



(a) 6% Quartz in calcite



(b) 20% Quartz in hematite

Figure 5. A comparison of the theoretical with the Raman measured mass of quartz in mixtures of (a) calcite and (b) hematite deposited in a 5-mm diameter area on silver filters. The error bars are the 95% confidence intervals for the Raman measurement. [Colour figure can be viewed at wileyonlinelibrary.com]

internal standard in the Raman measurements was not investigated in this work.

Sample analysis strategy

Sample analysis time is critical to a client in terms of cost and promptness of response. Initially, the Raman analysis was performed manually, and each sample took about 2 h to analyse. However, use of software to automatically locate and analyse a sampling point can count twice as many fields in about half the time. Sample analyses times of greater than ½ h are not uncommon in occupational hygiene air sampling work.

The analytical approach most commonly employed in the Great Britain is a direct on-filter analysis in which the filter on which the sample is collected and analysed directly with no additional sample workup.^[7,8] In other methods, the dust from the air sample filter is recovered and redeposited onto an analysis filter for the instrument.^[19] A direct on-air sample analysis approach is preferable as there is less chance for gross errors because of losses of dust from the recovery process. So long as the mass loading is low (<20 µg) and does not contain signal attenuating components, a direct on-filter Raman technique should be possible. A recovery approach might be needed to remove particles affecting the measurement when loading densities of particles are high. Hematite and iron are soluble in dilute acids, and carbonaceous material can be removed through ashing. Various sample preparation approaches were evaluated to ash a number of surrogate realistic samples of dust on 13-mm diameter filters on polyvinylchloride or mixed cellulose ester filters. The amount of material deposited on a filter is a potentially critical factor for accurate analysis using Raman spectroscopy, so a method that efficiently removes the filter material is essential for an indirect analysis approach with a recovery step in the analytical process. The identification of a method to completely dissolve a filter and unwanted material remains an unresolved issue at this stage. An alternative approach for heavily loaded samplers might be to use an aliquot from a suspension of dust recovered from the air sample filter.

Conclusions

This article has demonstrated the potential advantageous application of Raman spectroscopy for quantification of the mass of quartz and cristobalite with an order of magnitude improvement in the LOD compared with those of current industry standard XRD and IR techniques. The improved sensitivity of the Raman spectroscopy method over traditional measurement approaches may offer an improvement in the capability of occupational hygiene exposure monitoring, enabling the development of new approaches for the measurement of low dust concentration environments and potentially the analysis of samples from miniature samplers at low flow rates. A direct on-air-sample filter approach where the sampled dust collected on the air sample filter without the need to recover it onto a separate analysis filter should be possible, but further work is needed. A limiting factor for Raman microscopy is the presence of light absorbing particles such as hematite. The analysis of quartz was limited to a total deposit mass of <5 µg when measured in a mixture of 80% hematite deposited in 5-mm diameter circle.

Acknowledgments

Acknowledgements are given to Deeba Zahoor who provided technical support for the Raman facility at Sheffield Hallam University and to Mr Ian Pengelly and Dr Jackie Morton at the Health and Safety Laboratory who reviewed the work, Ms Gillain Frost for her guidance on statistics and Mr Dean Turner for his graphics work.

Disclaimer

This publication and the work it describes were funded by the Health and Safety Executive (HSE). Its contents, including any opinions and/or conclusions expressed, are those of the authors alone and do not necessarily reflect HSE policy.

References

- [1] European Committee for Standardisation (CEN), EN 481, *Workplace Atmospheres: Size Fraction Definitions for Measurement of Airborne Particles in the Workplace*, CEN, Brussels, Belgium, **1993**.
- [2] Health and Safety Executive, EH75 respirable crystalline silica, variability in fibrogenic potency and exposure–response relationships for silicosis, HSE Books, **2012**.
- [3] International Agency for Cancer Research (IARC), Monographs on the evaluation of carcinogenic risks to humans, Volume 100, A review of human carcinogens, Part C Arsenic Metals Fibres and Dusts, World Health Organisation, Lyon, France, **2012**.
- [4] L. Rushton, S. Hutchings, L. Fortunato, C. Young, G. Evans, T. Brown, R. Bevan, R. Slack, P. Holmes, S. Bagga, J. Cherrie, M. Van Tongeren, *British J. Cancer* **2012**, *107*, 53–57.
- [5] E. Hnizdo, V. Vallyathan, *Occup. Environ. Med.* **2003**, *60*, 267.
- [6] Health and Safety Executive. Control of substances hazardous to health. Approved Code of Practice, HSE Books, **2013**.
- [7] Health and Safety Executive, Methods for the Determination of Hazardous Substances, Respirable Crystalline Silica, MDHS 101, Direct On-Filter Analyses by Infrared Spectroscopy and X-ray Diffraction. HSE Books, **2005**.
- [8] International Organisation for Standardisation. ISO 16258. Workplace air — analysis of respirable crystalline silica by X-ray diffraction — Part 1: direct on-filter method, Geneva Switzerland, **2015**.
- [9] K. Kingma, R. Hemley, *Am. Mineralogist* **1994**, *79*, 269.
- [10] N. Noguchi, K. Shinoda, K. Masuda, *J. Mineral. Petrol. Sci.* **2009**, *104*, 253.
- [11] A. Wang, B. Jolliff, L. Haskin, *J. Geophys. Res.* **1995**, *100*, 21,189–21,199.
- [12] S. Potgieter-Vermaak, R. Van Grieken, *Appl. Spectrosc.* **2006**, *60*, 39–47.
- [13] T. Catelani, G. Pratesi, M. Zoppi, *Aerosol Sci. Tech.* **2014**, *48*, 13.
- [14] C. Deng, S. Brooks, G. Vidaurre, D. Thorton, *Aerosol Sci. Tech.* **2014**, *48*, 193.
- [15] K. Shin, H. Chung, *Analyst* **2013**, *138*, 3335.
- [16] P. Stacey, E. Kauffer, J.-C. Moulut, C. Dion, M. Beauparlant, P. Fernandez, R. Key-Schwartz, B. Friede, D. Wake, *Ann. Occup. Hyg.* **2009**, *53*, 639–649.
- [17] M. Mecchia, C. Pretorius, P. Stacey, M. Mattenklott, E. Inccociati, in *ASTM International* (Eds: M. Harper, T. Lee), **2013**, West Conshohocken, PA, USA, pp. 139–168.
- [18] International Organisation for Standardisation, ISO 14966 determination of numerical concentration of inorganic fibrous particles — scanning electron microscopy method, Geneva, Switzerland, **2002**.
- [19] International Organisation for Standardisation, ISO 16258 workplace air — analysis of respirable crystalline silica by X-ray diffraction — Part 2: method by indirect analysis, Geneva, Switzerland, **2015**.

Supporting information

Additional Supporting Information may be found online in the supporting information tab for this article.

Correction to: Feasibility of the quantification of respirable crystalline silica by mass on aerosol sampling filters using Raman microscopy

Peter Stacey, Kerstin T. Mader, Christopher Sammon

*Health and Safety Executive, Science Division, Harpur Hill, Buxton, Derbyshire, SK17 9JN, United Kingdom

++Sheffield Hallam University, Materials and Engineering Research Institute, Sheffield, S1 1WB United Kingdom.

The total calculated area measured by the Raman spectroscopy mapping procedure was approximately 0.026 % and not 20 % as stated in the Raman measurement strategy section. However, visual observation on other filter types showed the area affected by the laser is larger than the theoretical focal area of 0.026%.

Poisson statistics were not applied to the values for the estimated limits of detection listed in Table 2. The sentence referring to Table 2 in the method section should read: 'For a Poisson distribution, commonly employed in counting statistics, a count of four is considered above a background level with a 99% level of confidence, so the estimated LOD for a single scan could potentially also be multiplied by four to provide a detectable value for the method'.

Supplementary Information

Feasibility of the quantification of respirable crystalline silica by mass on aerosol sampling filters using Raman microscopy

Peter Stacey, Kerstin T. Mader, Christopher Sammon

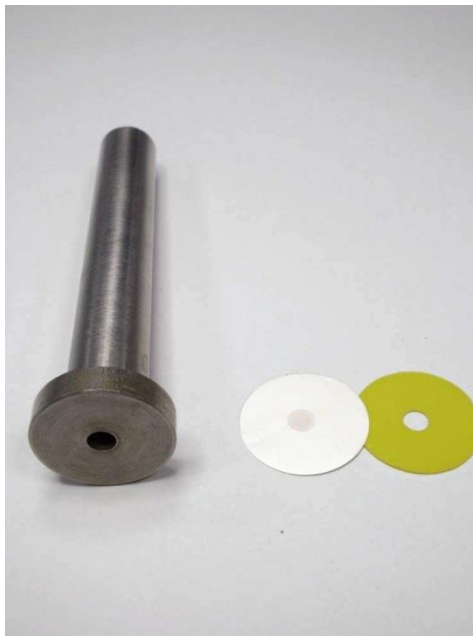


Fig S1. Filtering apparatus used for test samples showing a mask and filter with a 5 mm diameter deposit of hematite.

The table of data in the supplementary information Table S1 is supplied here graphically as charts for each calibration powder showing the differences between their particle diameter distributions.

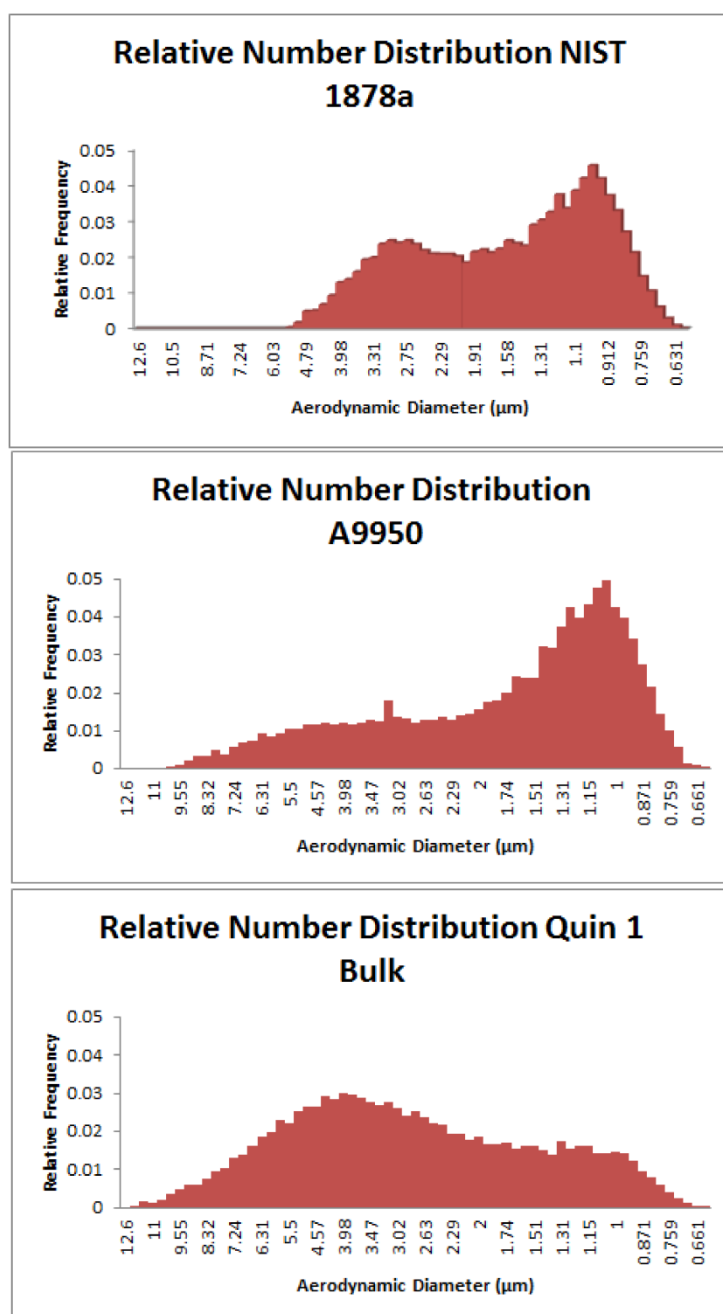


Figure S2. The number distribution of particles for the three α -quartz calibration dusts, NIST 1878a, A9950 and Quin1 Bulk, measured in the feasibility study. Original data is provided as Table S1.

Table S2: Ratio of Raman measurement mass values with the theoretical and those obtained using X-ray diffraction from four samples containing aliquot mixtures of α -quartz and α -cristobalite pipetted into a 5 mm deposit area on silver filters.

Sample	Ratio with theoretical mass value and theoretical mass (μg)			Ratio with X-ray diffraction mass value		
	α -Quartz	α -Cristobalite	Total	α -Quartz	α -Cristobalite	Total
A	0.95 (10.7)	0.87 (5.1)	0.92	0.95	0.95	0.95
B	1.08 (10.7)	1.28 (10.1)	1.18	1.00	1.04	1.02
C	1.24 (4.9)	1.07 (10.1)	1.13	1.39	1.03	1.14
D	0.96 (7.8)	1.00 (7.6)	0.98	1.11	0.92	1.02

This table is different from that supplied to the Journal. The table shows ratios with both the theoretical and the XRD values.

Chapter. 4 A Raman spectroscopy method for measurement of respirable crystalline silica collected on aerosol filters inside respiratory equipment.

Peter Stacey, Francis Clegg, Jackie Morton and Christopher Sammon

An indirect Raman spectroscopy method for the quantitative measurement of respirable crystalline silica collected on filters inside respiratory equipment.

Analytical Methods, 2020(12): p. 2757 - 2771.

<https://doi.org/10.1039/D0AY00165A>

Published Open Access Licence CC BY 4.0

Current citations = 6 (April 2022)

A quantitative method was developed to measure RCS collected from miniature in-respirator samplers. The LOD and analysis uncertainties were evaluated for a 10 mm diameter deposit area. The method was validated using samples of pure quartz and sandstone dust (with about 20% of a Feldspar contaminant), generated from a simulated work activity. Results were compared with the established X-ray diffraction methods; which were used as a benchmark.



Cite this: DOI: 10.1039/d0ay00165a

An indirect Raman spectroscopy method for the quantitative measurement of respirable crystalline silica collected on filters inside respiratory equipment†

Peter Stacey,^a Francis Clegg,^b Jackie Morton^a and Christopher Sammon^b

This article describes the development of an analytical method to measure respirable crystalline silica (RCS) collected on filters by a miniature sampler placed behind respirators worn by workers to evaluate their 'true' exposure. Test samples were prepared by aerosolising a calibration powder (Quin B) and by pipetting aliquots from suspensions of bulk material (NIST 1878a and Quin B) onto filters. Samples of aerosolised RCS collected onto polyvinyl chloride PVC filters were ashed and their residue was suspended in isopropanol and filtered into a 10 mm diameter area onto silver filters. Samples were also collected by the Health and Safety Executive's (HSE) miniature sampler from within the facepiece of a respirator on a breathing manikin during a simulated work activity. Results obtained using Raman spectroscopy were compared with X-ray diffraction (XRD) measurements, which was used as a reference method and a linear relationship was obtained. Raman has similar estimates of uncertainty when compared with the XRD methods over the measurement range from 5 to 50 μg and obtained the lowest limit of detection (LOD) of 0.26 μg when compared with XRD and Fourier Transform Infrared FTIR methods. A significant intercept and slope coefficient greatly influenced the higher LOD for indirect XRD method. The level of precision and low LOD for Raman spectroscopy will potentially enable workplace measurements at lower concentrations below the Workplace Exposure Limit (WEL) than are achieved using current analytical instrumentation. Different inward leakage ratio (ILR) measurement approaches were compared using six aerosolised sandstone dust tests. For the three highest inward leakage ratios the Portacount® obtained higher values than the RCS mass or the miniWRAS ratios, the latter of which reporting both particle number and quartz mass concentration. However, these limited ILR data were insufficient to establish statistical correlations between the measurement methods.

Received 26th January 2020
Accepted 20th April 2020

DOI: 10.1039/d0ay00165a

rsc.li/methods

Introduction

The term respirable refers to a health-related definition for the mass distribution of aerodynamic particle size diameters that are less than 16 μm and with a median aerodynamic diameter of 4 μm with the potential to penetrate to the alveoli of the lung.¹ The inhalation of respirable-sized crystalline silica (RCS) is a potential hazard to the health of thousands of workers in the United Kingdom because of the widespread use of materials containing crystalline silica. It is estimated that a total of 560 000 workers are potentially exposed to RCS in Great Britain (GB).² Crystalline silica is a common naturally occurring mineral and exposure to excessive levels of RCS generated when

working on materials containing crystalline silica can cause lung diseases, including silicosis³ and cancer.⁴

There are many processes which can generate RCS, especially those which involve working with powered tools on materials containing crystalline silica, where airborne levels of RCS remain high despite following the principles of good practice given in the Control of Substances Hazardous to Health (COSHH) regulations 2002.⁵ In addition to the use of engineering and organisational controls, Respiratory Protective Equipment (RPE) is often required to manage any residual risk and help ensure worker exposures are below the Workplace Exposure Limit (WEL).

Respirators are classified in terms of their assigned protection factors (APF). For example, in the United Kingdom, a type of RPE known as a Filtering Facepiece 3 (FFP3) respirator is allocated an assigned protection factor (APF) of 20. The value of 20 assumes that the respirator is capable of reducing airborne concentration inside the respirator by at least 1/20th of the concentration outside. APFs are based on the 5th percentile of

^aHealth and Safety Executive, Buxton Laboratory, Harpur Hill, Buxton, Derbyshire, SK17 9JN, UK. E-mail: peter.stacey@hse.gov.uk

^bSheffield Hallam University, Materials and Engineering Research Institute, Sheffield, S1 1WB, UK

† Electronic supplementary information (ESI) available. See DOI: 10.1039/d0ay00165a

workplace data and are intended to be a reasonable worst-case estimate of protection in the workplace. Some studies indicate that RPE does not always prevent exposures reaching regulatory exposure limits when used in workplace conditions.^{6–8}

Currently, there isn't a method which measures the personal RCS exposure a worker is subject to in their breathing zone inside a respirator. The exposure of a worker wearing RPE is routinely assessed by measuring the RCS concentration obtained from a sampler placed outside the RPE, but within the breathing zone of the worker.

A miniature respirable sampler was developed by the Health and Safety Executive (HSE) to collect dust after penetrating into a respirator to determine a more reliable measure of RCS exposure in the workplace. The HSE miniature sampler has the potential to provide a hazard specific measure of the worker's 'true' exposure^{9,10} and provide data for studies to investigate the APF when working with crystalline silica. Estimates indicate that the mass of RCS collected from within the facepiece of the FFP3 type respirator, will be below the limits of detection (LOD) of current X-ray diffraction (XRD) and Fourier-transform infrared (FTIR) analytical methods for RCS measurement, if the tight-fitting FFP3 respirator is performing to its APF specification. Raman spectroscopy was investigated as new approach to measure RCS at lower filter mass loadings levels¹¹ by micro-concentrating an aerosol sample onto a small measurement area (5 mm in diameter). A similar feasibility study using semi-portable Raman equipment was conducted by Zheng *et al.*¹² and both feasibility studies demonstrate that the Raman technique was more sensitive (reported LODs for RCS when using Raman are from 0.02 to 0.55 µg) than the established XRD and FTIR methods. LODs for RCS analysis when using current XRD and FTIR methods range from about 3 to 10 µg for both instruments^{13–15} on deposit areas that can range from 16 mm to about 22 mm in diameter. Wei *et al.*¹⁶ recently demonstrated a LOD of 0.33 µg for RCS using a cascade IR laser focused on a smaller deposit area (1.7 mm in diameter). An advantage of using Raman spectroscopy is that its measurement response more specifically measures the crystalline silica and is able to distinguish between different polymorphs. FTIR measures the absorption of energy from the vibrational and stretching frequencies of molecular bonds. Similar absorbance is found for amorphous silica, which is considered to have lower toxicity than crystalline silica,¹⁷ other polymorphs of crystalline silica and for some silicate minerals that have similar molecular silicon and oxygen bonds. This article describes the validation of a Raman spectroscopy analysis method for the measurement of aerosols of RCS using a silver filter as the analysis substrate. There are two main analytical approaches used in measurement methods for RCS. The first is known as a direct on-aerosol sampling filter analysis approach where the dust on, for example, a polyvinyl chloride (PVC) filter is analysed without further processing.¹⁵ The second is known as an indirect approach, where the sample dust is recovered from the aerosol sampling filter and deposited onto another filter for analysis by the instrument.^{18,19} The method employed for this work is an indirect analysis approach where the dust is recovered from a polyvinylchloride (PVC) filter and deposited onto the silver

filter. A silver filter is used routinely by some XRD methods for the measurement of aerosol particulate,¹⁹ therefore little modification of current sampling protocols would be necessary to adopt a Raman analysis approach and the filters can be analysed by both techniques for comparative purposes. The silver filter provides a relatively flat surface when compared with other membrane filters, which is important when using a microscope to focus on the aerosol particulate during Raman analysis. This substrate provides little interference for the most common polymorphs of crystalline silica (quartz and cristobalite) and may have the potential to provide a resonance enhanced Raman response when the particles are in close contact with its surface. XRD is the established technique currently employed for the measurement of RCS. XRD analysis is considered less prone to influence from other mineral interferences and changes in measurement response due to differences in the median particle sizes of the measured dust than FTIR, which is the other most commonly used technique. In this work, XRD is used as the reference method and the performance of Raman and XRD measurements were compared when measuring laboratory prepared test samples and when measuring samples from a simulated work task conducted in a calm air chamber.

Particle number concentration measurements are used to assess the fit of masks and respirators on an individual. However, workplace exposures are measured and assessed against exposure limits in terms of mass concentration and the relationship between the two when measuring workplace aerosols is not known. The APFs used for the classification of RPE for workplace provision is based on limited mass concentration inward leakage data, collected from the workplace supported by expert opinion. APFs provide information about the level of protection a type of RPE is expected to achieve in the workplace when compared with mass based exposure limits. Instruments measuring number concentration have been proposed for workplace studies,^{20,21} however, any estimates of APFs from these instruments would need to assume that the number concentration based leakage ratio is equivalent to the mass concentration based leakage ratio. In this article, RCS mass concentration inward leakage ratios (ILRs) were compared with those based on particle number concentration values from the Portacount® and miniWRAS instruments. The Portacount® is an instrument commonly used for fit-testing of tight-fitting negative pressure respirators and determines an inward leakage ratio based on a count of the number of particles outside the respirator to those inside the respirator while a series of fit-testing exercises are undertaken. The miniWRAS measures a wider particle size range and reports particle number concentration and mass if it is assumed the all the particles are spherical and have the same density.

Methods

An outline of the structure of the first three stages of this study is provided in Fig. 1. The first stage used the HSE miniature respirable sampler and compared the performance of XRD and Raman when measuring respirable and non-respirable

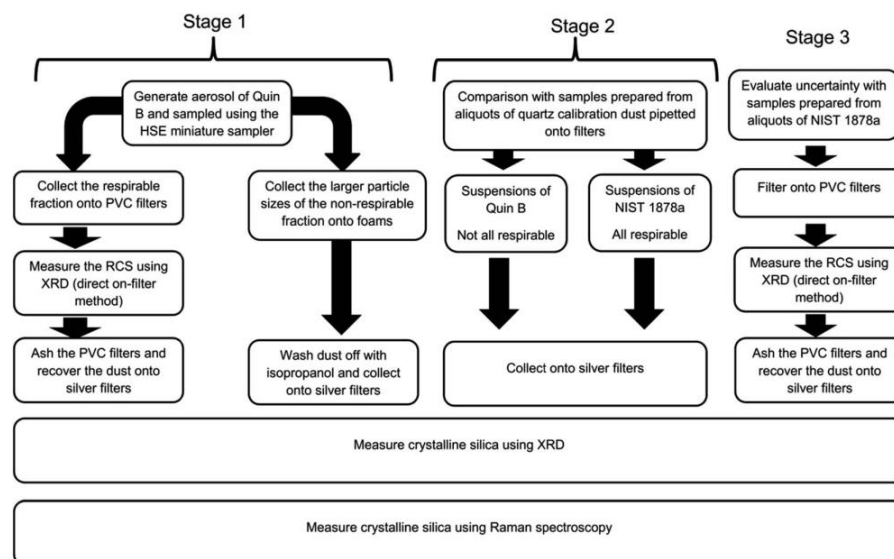


Fig. 1 The analytical measurement process.

samples of RCS collected from aerosols of calibration dust Quin B. Samples analysed were either deposited directly onto PVC filters or in-directly onto silver filters. The second stage compared the response trend lines of the aerosolised samples collected in the first stage with those of the bulk calibration material (Quin B) and that of a certified reference material of respirable sized quartz NIST 1878a that had been suspended in isopropanol and directly pipetted onto silver filters. For the third stage replicate samples of the certified reference material, NIST 1878a, were also prepared by directly pipetting aliquots from an isopropanol suspension on PVC filters to estimate and compare the uncertainty of the XRD and Raman methods.

Stage 1: aerosol preparation of samples using the HSE miniature sampler

Aerosols of respirable quartz (Quin B, Institut National de Recherche et de Sécurité (INRS), France) were generated and sampled onto 13 mm diameter 5 µm pore size polyvinyl-chloride (PVC) filters (SKC Ltd, Blandford Forum, Dorset, UK) using the HSE miniature sampler.⁹ The procedure to collect these calibration samples is described in HSE's method for the determination of hazardous substances (MDHS) 101 RCS.¹⁵ In brief, the quartz calibration powder of high crystallinity (Quin B) was placed in a glass bowl at the bottom of a bell-type jar and was aerosolised using a short burst of pressurised air. The jar was earthed to reduce agglomeration of particles. The aerosol was sampled using the HSE miniature sampler which was placed at the top of the jar. The HSE miniature sampler uses polyurethane foam (PUF) to first remove the larger sized particles (non-respirable) by filtration from the smaller respirable sized

ones, which pass through and are collected on a 13 mm diameter PVC filter. The selection of particles through the foam is dependent on the flow of air. The HSE miniature sampler was calibrated at its specified flow rate for the selection of respirable dust at 0.8 l min^{-1} using a TSI 4100 flow calibrator (TSI Inc, Shoreview, USA).⁹ The mass of quartz collected on each filter was determined gravimetrically using a balance with a readability of 6 decimal places (Sartorius UK Ltd, Epsom, UK). This was followed by direct on-aerosol filter XRD measurements using standard XRD flat sample holders, modified to include a mask with a 13 mm diameter hole to hold the filters steady at their centre. Each PVC filter was then placed in a glass bottle and ashed using a low temperature plasma asher (Emitech K1050X, Quorum Technologies Ltd, Ashford, UK). The filters were ashed in air at 50% power for 12 h and then in oxygen for 4 h at 95% power. About 5 ml of 99.9% purity isopropanol (Fisher Scientific UK Ltd) was added to the bottle after it was removed from the asher and had cooled. The isopropanol and residue were then sonicated for about five minutes and the suspension was filtered onto 0.45 µm pore size silver filters. The area of the sample deposit was constrained to 78.6 mm^2 using a bespoke 10 mm diameter filtration funnel. A washer, with a hole of the same diameter as the funnel, was placed under the filter to ensure the uniform spread of sample.

Non respirable dust collected on the PUF particle selectors was also prepared for Raman and XRD analysis. The sample foams were placed into glass bottles, covered with isopropanol and sonicated for 5 minutes. The foams were then washed with more isopropanol, removed from the bottle and the liquor was filtered, (as described above) onto a 10 mm diameter area on fresh silver filters.

Stage 2: comparison with standard materials NIST 1878a and Quin B

The preparation of calibration standards by pipetting aliquots of calibration dust onto a silver analysis filter is common practice in some measurement methods for RCS.^{18,19} This approach allows the deposition of a known amount of dust that is traceable to a calibrated metric. It is frequently used because the alternative method to prepare calibration filters, by collecting samples of aerosol onto filters, does not easily permit the preparation of replicate samples; as the aerosol generation cannot be accurately repeated. The bulk quartz power, NIST 1878a (National Institute for Science and Technology, United States) was selected because it is a quartz certified reference material that is completely respirable sized²² and closely represents the particle size of dust collected on the filter after the aerosol is separated into its respective fraction by a respirable sampler.

To test the difference between the response from the aerosol generated samples and a respirable quartz certified reference material, aliquots from a stock suspension of ($10 \mu\text{g ml}^{-1}$) NIST 1878a in isopropanol were pipetted onto silver filters to provide a trend line of mass and response. The slopes of the trend lines of the bulk materials were compared with the slope of the response from the respirable Quin B collected on the filters from the respirable sampler. A *t*-test was used to compare the similarity of the slopes of their mass response relationships to confirm that the two dusts were similar after their respective processing with a 95% level of confidence. The null hypothesis is that there is no difference between the slopes, so a probability value of less than 0.05 would indicate that there was a significant difference at the 95% level of confidence. A similar mass response trend line was developed directly from aliquots of the calibration material Quin B, which contains a significant proportion of particles that are not respirable for comparison with trend lines obtained for the quartz dust collected from the foam samples. Each trend line contained samples from two separate suspensions.

Stage 3: uncertainty and repeatability precision

The precision, from the measurement of different replicate samples, was calculated to estimate the uncertainty of the indirect analysis process over the mass loading range between 0.5 to 60 μg . Replicate samples were prepared by filtering aliquots from a suspension of quartz standard reference material (SRM) NIST 1878a in isopropanol ($10 \mu\text{g ml}^{-1}$) onto PVC filters using the same procedure described above. Five replicate aliquots were filtered at six mass loadings levels, by taking 0.05, 0.1, 0.5, 1, 2 and 5 ml aliquots of stock solution. A $0.45 \mu\text{m}$ pore size silver filter was placed behind the PVC sample filter to provide support, slow the filtration speed and to check for breakthrough of particles. The PVC filters were measured using XRD, and ashed following the same procedure for the test samples prepared from the respirable Quin B collected on filters. The residues were then transferred to silver filters using the procedure described previously and then quantified using XRD and Raman spectroscopy. The percent relative standard

deviations (RSD) for the mean mass value of the Raman measurements were compared with those obtained using XRD measurement of the most sensitive quartz reflection at a 2θ angle of 26.6 degrees made on the same samples. The repeatability precision was calculated from three repeated measurements on a single filter at each mass loading.

Calibration and Raman measurement conditions

Measurement conditions were based on those described in a feasibility study using 5 mm diameter deposit area.¹¹ An In-Via Raman microscope (Renishaw Ltd, Gloucester, UK) with near infrared laser (785 nm) excitation, CCD camera, and a grating with 1200 l mm^{-1} was used to collect Raman spectra between 314 and 906 cm^{-1} . This range was set to avoid the broad Raman band below 300 cm^{-1} , which was attributed to a trace of silver oxide. Raman spectra were collected from 50 to 90 points along a predetermined line using a $\times 20$ microscope objective with a numerical aperture of 0.4. The minimum area of the focused laser was about $4.5 \mu\text{m}^2$. An automated microscope stage and focus facilitated an operator free data collection process. The automated focus was set to operate for every third field of view position. Spectra were collected at each field of view position using the same laser power and exposure time. Each spectrum was collected by the instrument's laser at 100% power of 500 mW at its source with three accumulations of seven seconds. The integrated areas under the Raman response at 464 cm^{-1} for quartz was measured by fitting a Gaussian model using the standard algorithms in the manufacturer's WiRE 4 software package for each spectrum collected. The band fitting software in this package was also applied to model and subtract the presence of interference. The mean band area response was calculated for each sample. Spectra that were shown to have saturated the detector were excluded from this calculation. Trends lines were drawn to compare the average area counts and mass. A silicon (Si) wafer was measured before the analysis of a test sample and used as an external standard to compensate for daily fluctuations in laser intensity. The integrated area from the silicon wavenumber shift at 520 cm^{-1} was measured with a $\times 50$ objective at 10% laser power for 1 s. The average area measurement, calculated for each calibration and test sample, was corrected for fluctuations in laser intensity using the ratio between the area count collected when the silicon was first measured and the average collected on the day of the filter measurement.

X-ray diffraction measurements

The quantity of quartz in test samples was also determined using an X-pert Pro MPD instrument (PANalytical Ltd, Cambridge, UK) with focusing Bragg-Brentano geometry. The instrument used the second set of standard instrumental conditions described in Table A1 of the International Standards Organisation (ISO) standard method ISO 16258-1; 2015.¹⁴ The instrument was fitted with a broad focus copper tube set at 50 kW and 45 mA, automatic scattering and receiving slits set to provide an illumination length of 18 mm and an array detector with the detection area set at 2.12 degrees. The area of the most

intense 101 quartz reflection at a 2θ angle of 26.6 degrees was measured for 420 s for each 0.03 degree interval over the range 25.9–27.3 degrees. Tube drift was corrected using the measurement of an aluminium plate as an external standard.

Limit of detection of the Raman measurement

Ten clean PVC filters were prepared for analysis using a plasma asher and the procedure described for the preparation of filter samples from the HSE miniature sampler. The ashed residue of each PVC filter was suspended in isopropanol and then filtered into a 10 mm diameter area onto a 25 mm diameter 0.4 μm pore size silver filter. About 90 spectra were obtained from each filter and the area of any band at the position for the quartz shift close to $464 \pm 4 \text{ cm}^{-1}$ in each spectra was quantified using the instruments WIRE™ software. The limit of detection was calculated from the standard deviation of the average Raman area response of the detected quartz shift from ten silver filters. The calculated standard deviation was multiplied by three to estimate the 99% level of confidence.

Limit of detection for XRD analysis

The LOD values for the direct on-aerosol filter XRD measurement of the quartz on 13 mm diameter PVC filters and the indirect XRD measurement approach involving the deposition of the aerosol dust onto a silver filter were measured in two ways. For the direct method ten clean 13 mm diameter PVC filters were first measured by XRD. Subsequently, for the indirect method the same filters were then ashed, their residue suspended in isopropanol, filtered onto a 10 mm diameter area on a silver filter and measured by XRD again. The LOD values for both the direct and indirect measurement approaches were calculated from the average variation of the scatter in the XRD pattern for one degree around the primary quartz reflection at the 2θ angle of 26.6 degrees. The standard deviation of the area measurements of the blank filters was then multiplied by 3. For comparison, the LODs were also calculated following the approach in Stacey²³ to provide an LOD for each measured filter. Stacey²³ showed that direct measurement of the background scatter could provide LOD values that were comparable to the more traditional approach using the measured responses for each sample. A short Matlab script (Mathworks, Cambridge, United Kingdom) was used to fit a line of best fit with a polynomial equation to the scatter around the 2θ angle of 26.6 degrees. The standard deviation of the scatter was multiplied by 1.66 (3/2) to obtain the 99% level of confidence of positive scatter above the line of best fit. The LOD was calculated as a mass by multiplying the standard deviation with the calibration coefficients obtained from the fitted mass response trend lines.

Collection of samples from a simulated work activity

To assess the measurement procedure for inward leakage tests, samples were collected from aerosols generated from a simulated work activity in a calm air chamber. The calm air chamber consisted of three chambers, one on top of the other, with an air flow (about 0.4 m s^{-1}) from the top to the bottom. The work

activity involved the power cutting of a sandstone pavement block. Two square chambers, of approximately 1 m^3 , sit on top of each other separated by an aluminium honeycomb layer (approximately 6 cm deep) to improve laminar flow. A third, pyramid shaped chamber, is sited above the first two and incorporates a deionising fan to allow mixing and reduce charge, as described in previous work.^{9,24} In these experiments, a mitre saw with a diamond cutting disc was bolted to a frame in the top pyramid shaped chamber and the deionising fan was situated on top of the honeycomb directly below the simulated work task positioned between the two square boxes. A 'Sheffield' manikin head²⁵ was situated in the centre of the bottom chamber and connected to a breathing machine. The breathing machine had a sinusoidal breathing pattern, with tidal volume 1.5 l and rate of 20 breaths per minute (total respiratory minute volume 30 l min^{-1}). This breathing rate and volume were selected to represent a worker conducting sustained hand and arm work over a full shift with breaks.²⁶ The safety in mines personal dust, respirable sampler (SIMPEDS) is frequently used for routine workplace monitoring of respirable dust in the United Kingdom. Three SIMPEDS were positioned equidistant in a line across the chamber in front of the manikin to collect the respirable dust concentration of the chamber. The SIMPEDS were positioned between 10 to 30 cm from the FFP3 respirator placed on the manikin. The inlets for these SIMPEDS samplers were at the level of the mouth on the Sheffield manikin head. PVC filter samples from the SIMPEDS were measured for RCS using XRD and the routine HSE analytical method MDHS 101 (ref. 15) to obtain a measure of the RCS concentration in the chamber. This approach replicates the current standard practice to assess a workers' exposure to aerosols containing RCS, where the sample is collected outside the respirator using the SIMPEDS sampler. The loadings on the filters for the SIMPEDS were much higher than those measured from the HSE miniature sampler within the facepiece of the respirator, therefore the secondary and tertiary quartz XRD reflections at 2θ angles of 20.9 and 50.1 degrees were also quantifiable and measured using the direct on aerosol filter approach specified in MDHS 101. The average of two of the three measured reflections providing the most consistent values for each sample was reported as the mass of RCS from the SIMPEDS sampler. The average RCS value from all three SIMPEDS samplers was used to calculate the concentration of RCS inside the chamber. An FFP3 respirator was positioned over the nose and mouth of the Sheffield head. Two HSE miniature samplers were fixed within the facepiece of the respirator using the same procedure for fixing tubes from particle counting instruments to RPE for face-fit tests.¹⁰ The leakage of crystalline silica into the facepiece was calculated from the ratio of the concentration of RCS from the miniature sampler inside the facepiece, measured using Raman, and the average concentration of RCS on filters from the three SIMPEDS samplers that collected the aerosol concentrations outside the respirator. It has been shown that the performance of the SIMPEDS and HSE miniature sampler to collect respirable aerosol is not significantly different when measuring concentrations of RCS up to 4 mg m^{-3} and with $282 \mu\text{g}$ as a maximum mass collected on the PVC filter in the

miniature sampler. The trend lines diverge from the ideal 1 : 1 relationship at higher mass loadings.⁹

Particle size measurements for the simulated work activity

Two Portacount® (TSI Inc, Shoreview, USA) and two mini Wide Range Aerosol Spectrometer (miniWRAS) aerosol sizing instruments (GRIMM Aerosol Technik Ainring GmbH, Germany) were used in these tests for the comparison of inward leakage values. The Portacount® instrument, which measures the concentration of the number of particles, is commonly employed for inward leakage and face fit testing and has the smallest particle size measurement range. This instrument mostly counts particles from 0.02 μm to a particle diameter of 1 μm . The Portacount® instruments were operated from outside the chamber. One tube from the Portacount® instrument was fixed into the respirator whilst the other was positioned to sample the chamber atmosphere. The miniWRAS instruments were employed as they measure a much wider particle size range. They use two different detectors to cover the particle size range from 0.01 to 32 μm (particle diameter) in 42 sizing channels. This instrument counts the smaller and nano-sized particles (0.010 μm to 0.2 μm) using a unipolar diffusion charger with time multiplexed electrode and Faraday cup electrometer and uses an optical cell for the larger sized particles (0.25 μm to 35 μm). The mass concentration can be estimated if it is assumed that the particles are spheres with the same density. Two miniWRASs were placed inside the bottom of the chamber and operated remotely using wireless technology. The inlet for one miniWRAS was fed into the respirator positioned on the Sheffield manikin head whilst the other miniWRAS was set up to sample the concentration of dust inside the chamber. Potential losses of dust due to electrostatic attraction to the walls of the sampling tubes to the instrument were evaluated and minimised before the experiments. The mass median diameters of the aerosols were calculated by loading the raw data from the miniWRAS into a spreadsheet, converting each particle size bin into a particle volume, multiplying by the number of particles and then the density (2.65 g cm^{-3}) to obtain the mass distribution. Tablecurve 2D (version 5.01) software was used to fit

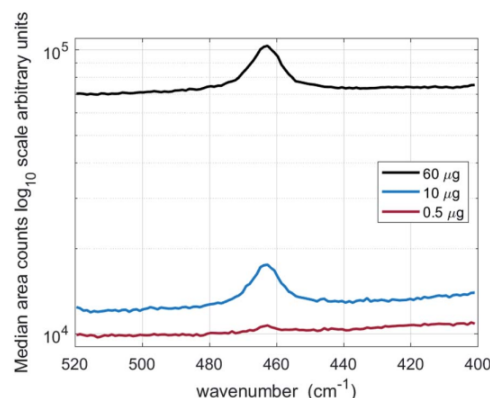


Fig. 2 Median of accumulated spectra from 90 fields of view for filters containing 60 μg , 10 μg and 0.5 μg of respirable quartz (NIST 1878a).

a curve to cumulative particle size model and calculate the median mass particle size diameter (MMD). Alarms were set on both the miniWRAS and Portacount® instruments to warn of very high concentrations that could lead to an increased risk of particle counting errors; for example, due to the coincidence of particles within the optical beam at high concentrations. In addition, a deionising fan was used during all experiments to reduce the potential for multiply charged particles and thus reduce counting errors for the electron mobility spectrometer, which is used in the miniWRAS to measure the smaller and nano-sized particles.

Results

Fig. 2 shows the median for the accumulated spectra for a sample of 60 μg , 10 μg and 0.5 μg of NIST 1878a deposited into a 10 mm diameter area onto a 0.45 μm pore size silver filter. Table 1 reports trend line coefficients and coefficients for determination (r^2) for the Raman measurements of crystalline silica (quartz) in NIST 1878a and Quin B and aerosolised sub-

Table 1 Load ranges, trend line equations and coefficients of determination for the Raman spectroscopy calibrations used in this study^a

Quartz dust	Calibration approach	<i>n</i>	Mass range (μg)	Trend line equation	Coefficient of determination
Quin B	Indirect – respirable dust recovered from aerosol sampling filter	11	13 to 106 (gravimetric mass)	$Y = 4964x$	0.97
	Indirect – non-respirable dust recovered from foam particle selectors	14	5 to 586 (gravimetric mass)	$Y = 5411x - 38\,099$	0.99
	Indirect – non-respirable dust recovered from foam particle selectors (limited mass range)	10	5 to 100 (gravimetric mass)	$Y = 4947x$	0.98
NIST 1878a	Measurement of aliquots from a suspension	14	5 to 60 (theoretical mass)	$Y = 5095x$	0.99
Quin B	Measurement of aliquots from a suspension	13	10 to 90 (theoretical mass)	$Y = 3994x$	0.98

^a *n* denotes the number of samples measured.

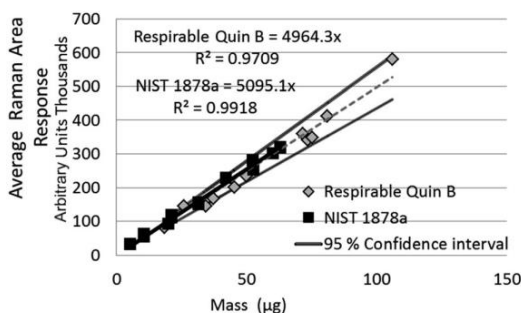


Fig. 3 The difference in average Raman area response at 464 cm^{-1} between two quartz calibration powders Quin B and NIST 1878a. Quin B was aerosolised and the respirable fraction was collected on PVC filters which were ashed and redeposited onto silver filters. Aliquots of the bulk powder of the certified reference material of respirable quartz (NIST 1878a) were filtered directly onto silver filters.

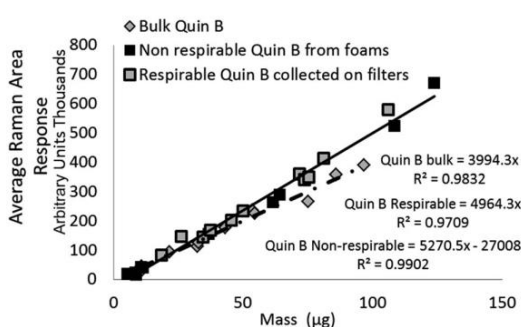


Fig. 4 The difference in Raman response between the respirable fraction of Quin B collected by the HSE miniature sampler, the non-respirable fraction of the Quin B collected by the foam particle separators and aliquots of the bulk powder Quin B filtered directly onto silver filters.

fractions of Quin B. An intercept is not given when it is not significantly different from zero with a 95% level of confidence.

The difference between the calibration trend line slopes for Raman measurement of NIST 1878a and aerosolised respirable

Quin B (Fig. 3) was not significant ($p = 0.33$). For ease of comparison, the 95% level of confidence is also shown in Fig. 3 for the respirable Quin B results. The other Raman mass response relationships, for the measurement of crystalline silica dust collected by the PUF foam (*i.e.* with particle sizes larger than respirable) and measurement of the bulk material Quin B (with a large proportion of non-respirable particles), are significantly different at the 95% level of confidence ($p < 0.05$). However, detector signal saturation occurred at loadings of the non-respirable Quin B above $100\text{ }\mu\text{g}$ when a counting time of seven seconds was applied so counting times were reduced for the highest loaded foam dust calibration samples with non-respirable Quin B to avoid the saturation. The counting time for the highest loaded foam dust calibration sample was 3 seconds for each accumulation. To comply with the calibration measurement conditions we assumed that the difference in response was proportional to the change in measurement time. Each measured band area was multiplied by $(7/n)$, where n is the counting time used to avoid saturation. A linear trend line relationship was observed over the whole mass range with a coefficient of determination of 0.99. When the mass range for the crystalline silica collected in the foams is restricted to samples below $100\text{ }\mu\text{g}$ the slopes of the trend lines for the measurement of respirable Quin B collected on the silver filters and the non-respirable Quin B (Fig. 4) are not significantly different ($p = 0.93$).

Table 2 reports the trend line equations and coefficients of determination for the XRD measurements at each stage of the measurement process (Fig. 1) when measuring quartz on the same samples. The trend line slope coefficient when comparing the Raman and XRD measurement values for respirable Quin B was 1.01 with a coefficient of determination of 0.98. The trend line slope coefficients for the mass response relationships of the direct on-aerosol filter XRD measurements of RCS on PVC filters and when collected indirectly onto silver filters, following sampling with the HSE miniature sampler of respirable Quin B are different at the 95%. The slope coefficients for XRD measurements of the bulk certified reference material of respirable quartz (NIST 1878a) pipetted onto silver filters were statistically similar with the respirable Quin B collected with the HSE miniature sampler when the PVC filters were ashed and

Table 2 Load ranges, trend line equations and coefficients of determination for the X-ray diffraction calibrations used in this study^a

Quartz dust	Calibration approach	<i>n</i>	Mass range (μg)	Trend line equation	Coefficient of determination
Quin B	Direct on-aerosol sampling filter (PVC)	17	13 to 106 (gravimetric mass)	$Y = 0.441x$	0.97
	Indirect – respirable dust recovered from aerosol sampling filter	17	13 to 106 (gravimetric mass)	$Y = 0.419x - 1.61$	0.99
	Indirect – non-respirable dust recovered from foam particle selectors (limited mass range)	14	5 to 586 (gravimetric mass)	$Y = 0.505x$	0.99
NIST 1878a	Measurement of aliquots from a liquid suspension	13	5 to 60 (theoretical mass)	$Y = 0.390x - 1.26$	0.99
Quin B	Measurement of aliquots from a liquid suspension	11	10 to 60 (theoretical mass)	$Y = 0.518x$	0.98

^a *n* denotes the number of samples measured.

Table 3 Limits of detection for quartz achieved for each technique and a comparison with values from recently published work. The entries in bold indicate those values that were measured by this work

Technique	Description	Number of measurements	Calculated limit of detection (μg)
X-ray diffraction	Direct on 13 mm diameter PVC aerosol filter	10	1.5 to 3
	Indirect 10 mm diameter area on silver filters	8	5.1 to 6.1
Raman	Indirect 10 mm diameter area on silver filters	10 \times 90 spectra	0.26
	Aliquots on 5 mm diameter areas ¹¹	5 \times 50 spectra	0.055
	1, 1.5 and 3 mm diameter areas ¹²	3 \times 15 spectra	0.055 to 3 ^a
Infrared	Direct on 9 mm diameter PVC aerosol filter ³⁶	12	0.5 to 1.5
	Cascade laser focused into 1.7 mm area deposit ¹⁶	Not known ^b	0.33

^a The limit of detection was dependent on the counting time (5 to 30 s) at each field of view. The LODs quoted are for a deposition method. Lower LODs were obtained using a focused collection approach. ^b A method limit of detection was estimated using Partial Least Squares (PLS) modelling.

then recovered onto silver filters ($p = 0.35$); but not with direct on-aerosol PVC filter measurements for respirable Quin B, the non-respirable Quin B collected on the foams, or the aliquoted bulk Quin B (all $p < 0.05$). The slope of the trend line obtained from aliquots of bulk Quin B was statistically similar to that of the non-respirable quartz collected on the foams ($p = 0.32$).

Limits of detection calculated for Raman, and XRD were compared with published values for infrared analysis in Table 3. Raman has the lowest calculated limits of detection for quartz. The intermediate precision for Raman measurement was between 4 to 11 percent relative standard deviation (RSD) (Fig. 5) over the measurement range 6 to 60 μg and increased to 45% at 0.50 μg . The trend line equation for the intermediate precision for the indirect Raman method was $y = 29.6x^{-0.44}$. The XRD limits of detection in terms of mass determined using the more traditional approach were 2.3 μg for the direct on-aerosol filter approach and 5.6 μg for the indirect analysis approach. The average standard deviation of the XRD background scatter determined using the Matlab calculation was 0.623 for direct on-aerosol filter measurement and 0.442 for the indirect analysis approach on a silver filter. The precision for XRD measurement (Fig. 6) was from 4 to 16% when measuring

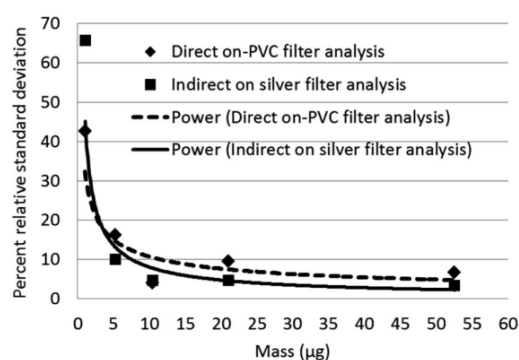


Fig. 6 Intermediate measurement precision of XRD measurement of certified reference material NIST 1878a (respirable quartz) for the principle quartz reflection at a 2θ angle of 26.6 degrees for the direct on-aerosol filter and the indirect measurement approaches.

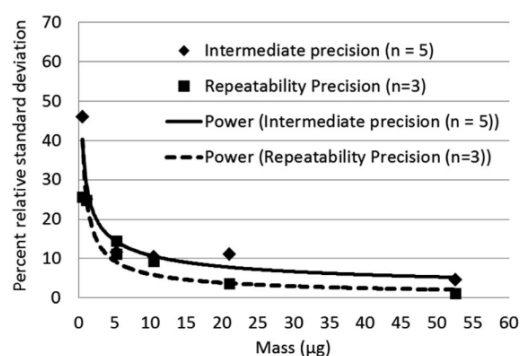


Fig. 5 Intermediate and repeatability measurement precision for Raman analysis of certified reference material NIST 1878a (respirable quartz) when sample is recovered from the aerosol PVC sampling filter and deposited onto a 10 mm diameter area on a silver filter.

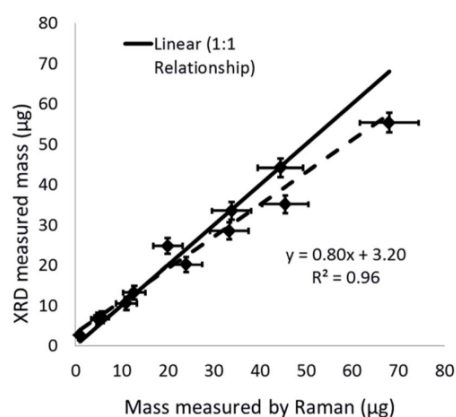


Fig. 7 A comparison of Raman and XRD measurements on the same samples when measuring the fraction of quartz collected from the particle size selective foams in miniature samplers placed inside a face filtering particulate respirator on a breathing manikin.

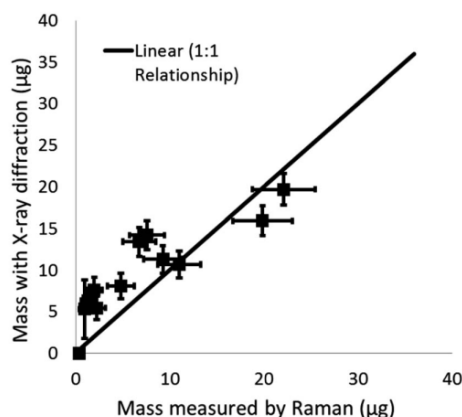


Fig. 8 A comparison of Raman and XRD measurements on the same samples when measuring the respirable crystalline silica (quartz) emitted from the cutting of a sandstone block and collected on the PVC filters from miniature samplers placed inside a face filtering particulate respirator on a breathing manikin.

with PVC filters for the direct on-aerosol filter approach and decreased to 3 to 10% RSD when measuring the quartz dust recovered on silver filters over the mass range 4 to 47 µg. The % RSD increased to 45 and 66% respectively for the PVC and silver filters with a loading of about 1 µg. The trend line equation for

the intermediate precision for the XRD indirect method was $y = 46.8x^{-0.76}$. No XRD precision measurements were obtained for mass loadings of quartz below 1 µg because these were not detected.

Simulated work activity

The proportion of crystalline silica in the stone was determined using the XRD Rietveld method with nickel oxide as an internal standard. The bulk sandstone used for cutting contained 89% crystalline silica (quartz) with 9% feldspar (microcline), and 2% mica (muscovite 2M1). XRD and Raman results for quartz collected on the PUF particle selector (*i.e.* non-respirable fraction) inside the HSE miniature sampler during tests in the calm air chamber are compared in Fig. 7. Mass loadings for these foam samples ranged from 0.87 to 63 µg. XRD and Raman measurements collected on the filters (*i.e.* the respirable fraction) in the miniature sampler inside the respirator are shown in Fig. 8; these, as anticipated, show lower mass loadings. If both the XRD and Raman results are exactly the same they should follow the ideal 1 : 1 relationship. The error bars in Fig. 7 and 8 show the 95% level of confidence for each of pair of measurements which were calculated from the intermediate precision for indirect analytical approach applied for each instrument.

On average, 95% of particles (by number) emitted from the cutting process and measured by the miniWRAS were less than 0.68 µm for the outside aerosol and 0.58 µm for the aerosol

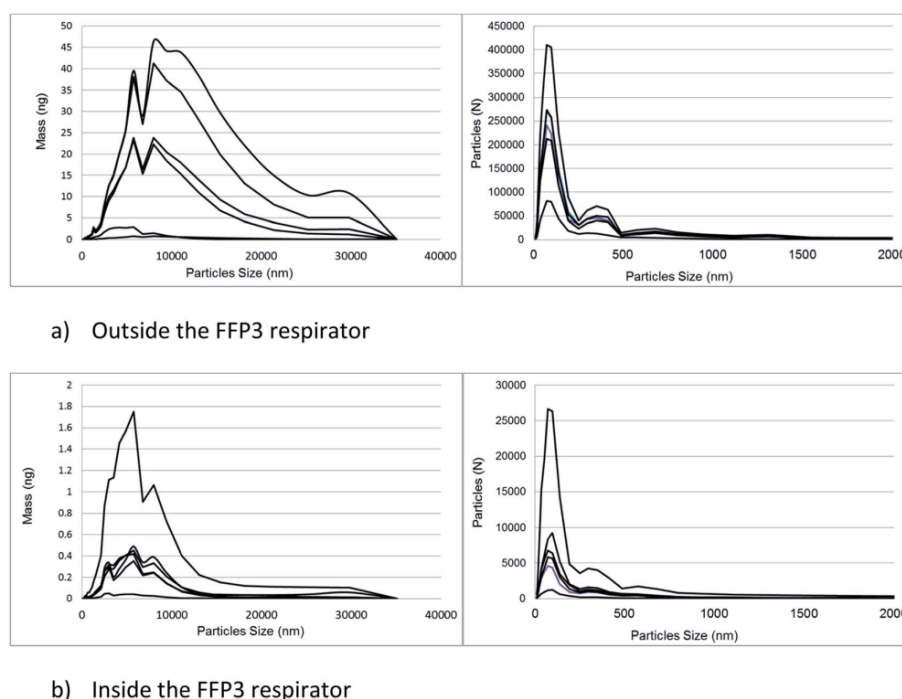


Fig. 9 A comparison of the mass and particle number distributions of the emission generated by cutting sandstone using a diamond blade.

inside the respirator (Fig. 9). The mass median diameters measured by the miniWRAS of the aerosol outside and inside the respirator were between 4.35 μm to 9.47 μm and 4.29 μm to 5.60 μm , respectively. The mass median diameter (MMD) inside the respirator increased as the outside concentration increased following the equation:

$$\text{MMD inside the respirator} = 0.212 (\text{MMD outside}) + 3.54 \quad (1)$$

The coefficient of determination was 0.89 and the MMD were reported in μm . The filter samples were weighed to determine the mass of respirable dust collected by the respirable samples positioned inside and outside the mask. The proportion of crystalline silica, determined using Raman spectroscopy, in the respirable dust samples collected inside the respirator (median = 34%) decreased with reducing mass and inward leakage ratio and was less than the proportion in the respirable dust samples outside (median = 73%). Fig. 9 shows the number and mass distribution of particle sizes detected by the miniWRAS in the aerosols outside and inside the respirator. Generally, the proportions of particle sizes inside and outside the respirator remained reasonably consistent over the whole particle size range. An example of this effect is provided in Fig. S1 (ESI[†]). An inward leakage ratio (ILR) is the ratio of the concentration of particles measured inside the respirator divided by the concentration of aerosol outside the respirator. Table 4 compares the percentage ILRs determined from the Raman measured RCS mass concentrations with the particle number concentration ratios measured by the Portacount[®] instrument and number and mass concentrations measured by the miniWRAS in terms of the percentage leakage into the respirator. The ILR values from the respirable dust measurements are not shown because the values for the in-mask samples are generally close to their limit of quantification; however, the ILR for the highest in-mask respirable dust sample collected from test 6 with a mass loading of 37 μg was 13.4.

The relationship between the ILRs based on the Raman measured RCS mass concentration and those determined using number concentration from the Portacount[®] instrument are shown in Fig. 10. Qualitatively, the three highest ILRs from the Portacount[®], which are calculated from the ratios of particle number concentrations, were much higher than the miniWRAS, measuring both number and mass concentrations and the

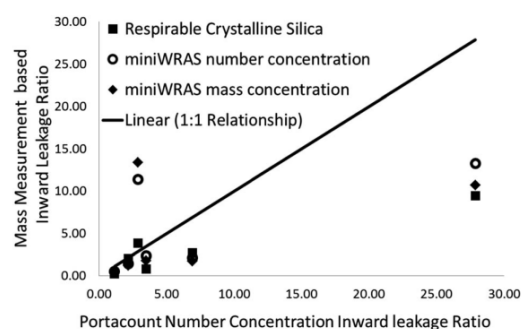


Fig. 10 Trend line between the percent inward leakage ratios (ILR) determined by the Portacount[®] instrument using particle number concentration and those determined measuring the mass of respirable quartz.

respirable crystalline silica concentration ILR values (Fig. 10). The highest particle concentration measured the Portacount[®] was 17 025 particles per cm^3 which is within the upper limit specified by the manufacturer of 2.5×10^5 particles per cm^3 . However, the miniWRAS obtained particle concentrations that were 2 \times to about 4 \times more than the Portacount[®]. The largest particle concentration measured by the miniWRAS was 50 000 particles per cm^3 .

Discussion

The advantage of Raman spectroscopy over XRD when measuring low concentrations of RCS collected from inside respirators are demonstrated in this work. The Raman obtains measurements that are comparable with XRD and has similar uncertainty estimates with a much lower LOD.

Raman photon scatter originates from a small fraction of the applied laser photons and the laser energy is potentially sufficient to cause photoluminescence (emission and fluorescence) effects in particles. The fluorescence effects are often much greater than the magnitude of the Raman bands and can swamp the detector; however, no samples in this work were not measurable because of fluorescence. In addition, other particles in close proximity of the analyte of interest may enhance the magnitude of the Raman shift or absorb the Raman photons as they are emitted. The measurement strategy applied in this work helps the Raman system overcome potential issues

Table 4 Inward leakage ratio (ILR) percentages calculated from each metric and instrument used in the calm air chamber experiments when challenged to an aerosol of sandstone dust generated using a power saw

Metric	Concentration of particles (Portacount [®] ILR) percent (%)	Concentration of particles (miniWRAS ILR) percent (%)	Respirable mass concentration (miniWRAS ILR) percent (%)	Respirable crystalline silica concentration (Raman ILR) percent (%)
Test 1	1.14	0.49	0.36	0.60
Test 2	2.16	1.42	1.18	1.97
Test 3	2.87	11.39	13.40	2.49
Test 4	3.49	2.36	1.79	1.06
Test 5	6.91	2.09	1.72	3.05
Test 6	27.88	13.25	10.71	6.69

associated with fluorescence and stray Rayleigh scattering. The choice of laser wavelength to reduce the risk of fluorescence, the averaging of accumulated micrometre area spectra, the spatial separation of particles and the characteristics of a respirable dust sample collected on a filter surface all play their role to reduce the effect of interference.

The accumulation and averaging of multiple micrometre area spectra across the surface of a uniformly distributed sample permits the exclusion of occasional spectra with saturation or too much interference; since the average should be relatively consistent, provided sufficient spectra are collected. Measuring low concentrations also improves the spatial separation of particles and reduces interference effects. For example, a feasibility study¹¹ measuring 20% quartz in a photon absorbing hematite (Fe_2O_3) mineral mixture in deposit areas of 5 mm in diameter showed that quartz was measurable to a specific particle density before absorption reduced the response. XRD measurement has similar issues with absorption in mixtures of hematite²⁷ which is overcome using a standard to correct for the reduced transmittance. The larger 10 mm diameter deposit areas applied in this work enables measurement of higher loadings that are more able to cope with routine sample deposits and the LOD is sufficient to enable an improved measurement despite a loss of sensitivity, due to a reduced particle density per unit mass, when compared with the feasibility study.¹¹ It's possible to exclude the occasional spectra with a high fluorescence and interference and still obtain an accurate result if the density of particles (and therefore the average) is reasonably consistent across the surface of the filter and sufficient spectra from a sample are analysed.

A major technical challenge is to determine, with reasonable accuracy, whether a respirator is performing to the APF it is expected to achieve in the workplace. Sensitive measurements are needed because of the small mass of RCS collected during sampling. Where high exposure to RCS is likely to occur, an FFP3 respirator or another type of respirator with an equivalent or higher APF may be worn during workplace tasks, in addition to other control measures. Therefore, potentially short sampling times and the low WEL for RCS ($100 \mu\text{g m}^{-3}$ as an 8 h time weighted average) highlight the importance of using a technique with a sufficiently low limit of detection. Table 3 shows that the Raman method has the lowest LOD for the measurement of RCS on test filters compared to XRD, FTIR, and cascade IR methods. In this study, the expected mass of RCS collected on a filter from the miniature sampler within the facepiece of tight-fitting respirator is above the Raman method limit of detection when a worker is wearing a respirator for 1 h, the respirator is performing to its APF of 20 and the challenge concentration of RCS outside the respirator matches expected concentration for the workplace exposure limit *i.e.* $1/8^{\text{th}}$ of $100 \mu\text{g m}^{-3}$ (the 8 h WEL). This theoretical calculation indicates that Raman spectroscopy is a technique that can be used to assess the applicability of the APF when sampling for an hour. In practice, the RCS concentrations are likely to be higher than this because respirators are generally worn for work tasks with the potential to produce the highest exposures despite the use of other control measures. Further improvements to the Raman

sensitivity and LOD beyond those achieved in this study are also potentially possible by collecting scans from more measurement points, by increasing measurement time in each measurement point¹² or, by further concentrating the sample into a smaller deposit area.¹¹ However, concentrating the sample into a smaller area may also increase the risk of interference, absorption and fluorescence from other particles. Zheng *et al.*¹² reported a direct proportional relationship between increases in sensitivity of the Raman response with decreasing circular deposit areas with diameters from 3 to 1 mm. A proportional relationship with deposit area is also shown when comparing our current work using 10 mm deposit area with our previous work on 5 mm diameter area (ESI Fig. S2†).¹¹ Therefore, analysts can potentially apply the technique to any deposit area size without further calibration by applying a predictable factor, assuming the particle density does not increase the risk of interfering factors.

An evaluation of this and recent work highlights the importance of the deposit area in determining the sensitivity and LOD for all the analysis techniques involved with the measurement of RCS (Table 3). Generally, the LOD is reduced as the deposit area decreases. Samples are usually collected and measured on 25 or 37 mm diameter filters. Concentrating the sample improves the response for techniques like Raman, which examine a small area in each field of view measured. Concentrating the sample into a 9 or 10 mm diameter area for XRD and IR analysis, also moves the whole sample within the full width of the infrared beam, which is between 7 mm to 9 mm or the area that provides most XRD response, which is about 15 mm in diameter. A deposit area of 10 mm in diameter should also reduce the possibility of obtaining a trend line relationship for XRD or IR with a significant negative intercept; since there is no potential for mass to be outside the analysis area that does not contribute to the measurement response. The change in LOD with measurement area suggests that LODs obtained by industry practitioners could be different from those stated in national or international methods for indirect RCS analysis, if the deposit area is not specified.

Comparison of the quantification of RCS determined by XRD and Raman (Fig. 7 and 8) from the calm air chamber experiments demonstrates that the results reported have a linear relationship. The slight differences between the Raman and XRD values are probably caused by the influence of a negative intercept coefficient, where the intercept was significantly different from zero, for one of the two measurement techniques. For example, Fig. 8 shows XRD measured values have a positive bias towards higher values when comparing XRD and Raman measurements on the same samples at low measurement levels less than $15 \mu\text{g}$. Although, the lowest mass for test samples with a measurable XRD response was about $1 \mu\text{g}$, the application of the intercept provides a higher estimated LOD of about 5 to $6 \mu\text{g}$ (Table 3). The observed number (about $1 \mu\text{g}$) does not agree with the calculated XRD LOD value of $5 \mu\text{g}$ to $6 \mu\text{g}$; which is similar to the LODs currently reported in analytical methodology.^{14,15,19} The LODs for the XRD methods were confirmed using the two different approaches discussed in the methodology section. Further investigation showed that, the variability of the X-ray scatter reflected from the filter and

sample holder obtained from measurements on the silver filters (for the indirect analysis approach) was lower than that obtained from measurements on the PVC filters (for the direct on-aerosol filter approach); which has a higher X-ray scatter but lower LOD. This seems to indicate that the over prediction of the LOD for the indirect XRD analysis approach is due to the application of the intercept coefficient for the XRD calibration trend line response and that in this instance a nonlinear trend line relationship might be more suitable to fit loadings close to the intercept. The XRD method adopted by the Occupational Safety and Health Administration (OSHA) in the United States uses a polynomial curve to fit logarithmically transformed data;¹⁸ which assumes the relationship between mass and XRD response is curved. Forcing the XRD results herein through zero produces a trend line $Y = 0.393$ with a coefficient of determination (r^2) of 0.99. The correspondence between the Raman and XRD values now converge around the 1 to 1 line for the ideal relationship (Fig. S3 ESI†).

Fig. 3 demonstrates a close match between the mass response of NIST 1878a and the aerosolised 'Quin B' when collected on a filter after the PUF particle selector. This level of significance ($p = 0.36$) demonstrates the suitability of this NIST 1878a as a standard for the indirect analysis method, where dust is recovered from the aerosol sampling filter and deposited onto another filter for analysis. The comparability of the NIST 1878a powder provides an opportunity for analysts to prepare calibration, replicate and quality control standards from a liquid suspension rather than employ a more elaborate and less repeatable process of collecting a dust sample from a generated aerosol. Moreover, an improved calibration approach is to include laboratory test samples prepared onto the filters used for collection of the aerosol and to develop a trend line with the intercept forced through zero or to model a curve towards zero at low mass loadings.

The samples with non-respirable quartz dust from the foams had the highest loaded masses measured by Raman and were used to assess the upper limits of measurement. A linear Raman measurement response was obtained up to 586 μg with a coefficient of determination of 0.99. Higher loaded masses (greater than 100 μg) were affected by high saturation of the detector and were only measurable by reducing the measurement time during data collection. A significant factor limiting the upper measurement threshold appears to be the saturation of signal at the detector rather than absorption of the Raman response due to the density and depth of the dust sample. A technique to compensate for this is to reduce the counting time during analysis and mathematically correct the measured area counts to comply with the measurement counting conditions for the calibration (Fig. 3). The laser energy could also be reduced; however, it would be more convenient if the detector were able to accommodate the increase in counts from the sample.

The response of many techniques measuring RCS is affected by differences in particle sizes²² however, previous work¹¹ has shown that Raman was not significantly affected when measuring Quin B and NIST 1878a, which have different mass median diameters (3.7 and 7.2 μm , respectively), over a limited mass measurement range with a maximum mass of 12 μg . In this work, the mass responses for the respirable and the non-

respirable fractions of Quin B collected by the miniature sampler are also not statistically different (Fig. 4) when the measured range is restricted to those samples less than 100 μg , however, the trend response for the bulk Quin B powder is significantly different. Many of the mass response values for the bulk Quin B coincide with the trend lines for the respirable and non-respirable Quin B collected by the miniature sampler at lower measured masses below 50 μg (Fig. 4). The mass response trend lines also tend to converge as they approach zero. There could be several reasons for this including; firstly, the particle size distribution of the bulk material will not be the same as the aerosolised dust because the heavier particles tend to fall out quicker, and secondly, the particle size distribution is also less diverse for lower mass samples improving the uniformity of the particle size distribution and consistency of measurements. For example, the d_{50} of the aerosol size distributions was reduced as the aerosol concentration decreased (Fig. 9). The advantage of a multiple point measurement approach (with each point having a small (micro) sampling area) is that it is likely to reduce the particle size dependence of the measurements when mass loadings are low. Each sampling point measured using Raman looks at a very small part of the available sample and the measurement will encounter larger numbers of smaller sized particles at low concentrations than the larger sized particles. The occurrence of larger sized particles in each measured sampling point increases at higher mass loadings, which may change the average sample response for sample masses higher than 50 μg . A multiple point micro measurement approach may also reduce the particle size dependency of the measurement response for other techniques *e.g.* XRD and FTIR.

This work demonstrates that Raman and XRD have the similar analytical uncertainty over the range from about 5 to 60 μg when measuring test samples (Fig. 5 and 6); however, Raman has a much lower LOD. The lower LOD enables Raman measurements of RCS to potentially meet all the European requirements in EN 482:2012 + A1:2015 (ref. 28) for the performance of occupational hygiene analytical methods when measuring regulatory limit values at mass loadings below those currently possible using traditional XRD and FTIR methods. EN 482:2012 + A1:2015 has three requirements for long term measurements to assess worker exposures against an occupational exposure limit. These are;

- The measurement range of the method must be from 0.1 to 2 times the exposure limit,
- The expanded relative uncertainty of the measurement (including sampling) should be less than or equal to 30% when measuring from 0.5 to 2 times the exposure limit,
- And the expanded relative uncertainty (including sampling) should be less than or equal to 50% when measuring from 0.1 to 0.5 times the exposure limit.

A Raman measurement at 10 μg on low particle density test samples free of interference meets all these requirements. This statement assumes the sampling errors are 11.8% as specified in ISO 24095,²⁹ the sampling and measurement precision are combined as the square root of the sum of squares and the uncertainty is multiplied by a coverage factor of 2. A mass of 10 μg would equate to an air concentration of about 10 $\mu\text{g m}^{-3}$ being

sampled for 7 h using a respirable sampler at a typical flow rate of 2.2 l min^{-1} . This theoretical concentration value of $10 \mu\text{g m}^{-3}$ is 10% of the WEL in GB and 20% of the current regulatory limit for RCS in the United States.³⁰ However, it is not currently known if the Raman approach will have the same level of performance with more complex dust mixtures with a greater particle density, and in samples collected with the types of aerosol samplers and filter diameters that are more commonly employed for work exposure assessments or reassurance testing.

Raman was successfully employed for the measurement of RCS within a facepiece respirator samples using mass measurement instruments.

The placing of an FFP3 respirator on a breathing manikin reduced the number of particles leaking into the masks across all particle sizes when compared with the number of particles in the chamber outside the respirator (Fig. 9). This general reduction in numbers of particles inside the facepiece of the FFP3 respirator compared with outside also resulted in a decrease in the mass median aerodynamic diameter inside the respirator due to a smaller number of larger particles that contributed most to the sample mass. For example, a single $10 \mu\text{m}$ diameter particle of quartz is about 1000 times heavier than a single particle with a diameter of $1 \mu\text{m}$; so, a relatively small number of larger particles of about $10 \mu\text{m}$ can have a significant impact in terms of mass. Whether a larger diameter particle (*e.g.* greater than $10 \mu\text{m}$ in diameter) is present inside an FFP3 respirator might be due to probability and not necessarily as a result of any particular property of the respirator. For example, there is a lower probability of observing larger diameter particles inside a respirator if they are not present in significant numbers in the outside aerosol. The relative consistency of the percentage proportions of particles inside and outside the respirator at each particle size range recorded by the miniWRAS is in contrast with other work,³¹ although charts in Rengasamy and Eimer³² indicate that the relative ILR can be fairly consistent in certain conditions over the nanoparticle size range when investigating leakage with sealed FFP3 respirators. In this study, there was no attempt to deliberately put a hole through the respirator and the most likely leakage route would have been around the nose piece and chin of the respirator through a soft rubber type of seal rather than through the valve.

A comparison of particle number concentration measurements using the Portacount® and mass concentration measurements of RCS using Raman spectroscopy is currently not generally applicable to workplace practice. Instruments reporting particle number concentration measurements are specifically used to help assess the fit of worker's RPE and mass based measurements are used to derive APFs to assess protection of RPE from work based tasks were exposures and exposure limits are measured in terms of their mass concentration. The Portacount® obtained higher ratios for the three highest ILRs (Fig. 10) than the RCS mass determined by Raman spectroscopy or the miniWRAS, which reports both number and mass concentrations.

All aerosol measuring instruments have errors associated with both the aerosol sampling and measurement which combine and contribute to the overall uncertainty of the reported concentration value. The uncertainty of an inward leakage ratio value is the addition of the uncertainty of both the

two measurements (outside and inside the mask). When a respirator is performing to its APF the leakage will be low and the in-mask measurement will usually make the largest contribution to the overall uncertainty of the ILR. The counting errors made by optical particle number concentration instruments like the Portacount® and the optical detector in the miniWRAS, used for the larger sized particles, are well established.³³ Optical particle sizing instruments are calibrated using uniform spheres with a specific refractive index. The calibration particles' characteristics may differ from the those measured from a workplace aerosol and the instruments often need a calibration that is specific for the expected matrix due to the nature of light scattered by the particles.³⁴ Large counting errors are also attributed to the coincidence of particles at high concentrations, the fluctuation of concentrations of particles in the size range just smaller than the lowest detectable particle size and Rayleigh scatter.³³ The miniWRAS uses an electrical mobility spectrometer to count particles at the lowest sizes, for particle sizes below $1 \mu\text{m}$, however, counting errors can also occur from multiply charged particles.³⁵ For this study, particle number concentrations were kept below thresholds specified by the manufacturer that cause an increase in the risk of particle coincidence, and a deionising fan was also included to reduce the potential for agglomeration of multiple charged particles. We discount the possibility that the Portacount® measured lower a concentration of particles outside the respirator due to the coincidence of particles (so increasing the ILR) because the concentrations measured are within the manufacturers' specification and the risk of this event significantly affecting the ratio is low. Differences between instruments are better explained by the different particle size measurement range and metric used by each instrument. For example, although the relative proportions of large and small particles leaking into a respirator in the tests were relatively consistent when using the miniWRAS over the whole particle size range, the increase in absolute number of smaller sized particles (less than $0.5 \mu\text{m}$ in diameter) is greater than the increase in absolute number of larger diameter particles (Fig. 9) when the particle concentration is higher *i.e.* for the higher ILR values. Therefore, the Portacount®, measuring the smallest size range in terms of particle number concentration (mostly less than $1 \mu\text{m}$) is potentially more sensitive when a leak occurs in these tests than the miniWRAS which measures particle diameters from $0.01 \mu\text{m}$ to $32 \mu\text{m}$.

Recently published work involving the measurement of artificial aerosols of salt (NaCl) has found that the Portacount® obtained ratios that were twice as high as those obtained with a flame photometer, which measures all particle sizes sampled containing NaCl.²¹ It was also confirmed that the particle size distribution inside the mask was similar to that found outside and when measuring particle size diameters below $10 \mu\text{m}$.²¹ These findings are similar to the observations in this work, which used more realistic aerosols of mineral dust generated from a simulated work task and the procedures applied in the workplace for the collection of samples to measure the mass concentration of RCS. This article highlights the advantage of using Portacount® instruments for its current employed purpose, which is for face fit testing in ambient environments, because its sensitivity when measuring small particle sizes is high. The main purpose of the RCS specific measurement by

Raman spectroscopy is not to assess fit but to determine the actual exposure of workers when wearing respirators. The hazard specific RCS measurement is potentially more accurate for this purpose when compared with a particle counting measurement that has to assume all the particles are RCS and have the same spherical shape and same density to convert a number to a mass concentration value.

However, the limited data from this study is insufficient to determine any true statistical correlation between particle number and mass based measurements, although large differences were observed between the other instruments and high Portacount® particle number ILRs in these tests. Further workplace and laboratory measurements are needed to confirm these data.

Conclusion

Raman spectroscopy is a viable technique for the analysis of RCS from low concentrations of dusts collected after penetrating the facepiece of a tight-fitting FFP3 respirator. This work also indicates the potential of Raman to provide workplace measurements of RCS at lower mass concentrations below the WEL than are currently possible with traditional analysis techniques (XRD and FTIR instruments) as Raman spectroscopy has the lowest reported LOD.

The sample deposit area is a significant factor that affects measurement sensitivity and LOD for all analytical techniques measuring RCS (*i.e.* XRD, IR and Raman). Smaller sample deposit areas improve measurement sensitivity because the sample either becomes more concentrated or more of the sample is within the analysis area of the instrument.

Results from XRD and Raman are comparable, and it is recommended that a zero intercept is included in the XRD trend line relationship or to model the intercept towards zero for low mass measurements.

Saturation of the detector, when the sample loading is high (about 100 µg), is a significant potential limitation for Raman measurement when measuring densely loaded samples.

An analytical approach based on the measurement of multiple micro-sized points within a sample may reduce the dependence of measurement response on particle size for some techniques.

An FFP3 respirator placed over the mouth of the breathing manikin reduced the particle number and mass concentrations within the respirator compared to outside across all measured particle sizes. A linear relationship was observed between the mass median diameter of the particles within the facepiece of an FFP3 respirator and the mass median diameter of the challenge aerosol outside the respirator.

Instruments reporting particle number concentration measurements are specifically used to help assess the fit of worker's RPE and mass based measurements are used to derive APFs which are used to assess protection of RPE from work based tasks. The limited data from this study suggest that these distinct roles are appropriate for each measurement metric. Further workplace and laboratory measurements are needed to confirm these comparisons of inward leakage data.

Disclaimer

This publication and the work it describes were funded by the Health and Safety Executive (HSE). Its contents, including any opinions and/or conclusions expressed, are those of the authors and do not necessarily reflect HSE policy.

Conflicts of interest

There are no known conflicts of interest.

Acknowledgements

Thanks to Ian Pengelly, Laurie Davies, Margaret Wade and Susan Hambling (Health and Safety Executive) for their technical and editorial reviews. Thanks also to Rhiannon Mogridge (Health and Safety Executive) for her support with the calm air chamber tests, calibrating the breathing manikin and looking after the Portacount® and miniWRAS instruments and to Timothy Yates for his support with developing the Matlab code.

References

- 1 CEN, EN 481:1993, *Workplace atmospheres—Size fraction definitions for measurement of airborne particles*, European Committee for Standardisation, Brussels, 1993.
- 2 T. Brown, J. W. Cherrie, M. Van Tongeren, L. Fortunato, S. Hutchings and L. Rushton, *The burden of occupational cancer in Great Britain lung cancer*, Health and Safety Executive, Bootle, Liverpool, 2012.
- 3 HSE, EH75, *Respirable Crystalline Silica, Variability in fibrogenic potency and exposure-response relationships for silicosis*, Health and Safety Executive, 2003, Report No. ISBN 978 0 7176 2191 0.
- 4 L. Rushton, S. J. Hutchings, L. Fortunato, C. Young, G. S. Evans, T. Brown, *et al.*, Occupational cancer burden in Great Britain, *Br. J. Cancer*, 2012, **107**(suppl. 1), S3–S7.
- 5 HSE, *The Control of Substances Hazardous to Health Regulations 2002 (as amended)*, Health and Safety Executive, Crown, Norwich, United Kingdom, 2005.
- 6 M. Hery, M. Villa, G. Hubert and P. Martin, Assessment of the performance of respirators in the workplace, *Ann. Occup. Hyg.*, 1991, **35**(2), 181–187.
- 7 S. Chazelet, P. Wild, E. Silvente and C. Eypert-Blaison, Workplace Respiratory Protection Factors during Asbestos Removal Operations, *Ann. Work Exposures Health*, 2018, **62**(5), 613–621.
- 8 S. Steinle, A. Sleenwenhoek, W. Mueller, C. J. Horwell, A. Apsley, A. Davis, *et al.*, The effectiveness of respiratory protection worn by communities to protect from volcanic ash inhalation; Part II: Total inward leakage tests, *Int. J. Hyg. Environ. Health*, 2018, **221**, 977–984.
- 9 P. Stacey, A. Thorpe, R. Mogridge, T. Lee and M. Harper, A New Miniature Respirable Sampler for In-mask Sampling: Part 1—Particle Size Selection Performance, *Ann. Occup. Hyg.*, 2016, **60**(9), 1072–1083.

- 10 R. Mogridge, P. Stacey and J. Forder, A New Miniature Respirable Sampler for In-mask Sampling: Part 2—Tests Performed Inside the Mask, *Ann. Occup. Hyg.*, 2016, **60**(9), 1084–1091.
- 11 P. Stacey, K. T. Mader and C. Sammon, Feasibility of the quantification of respirable crystalline silica by mass on aerosol sampling filters using Raman microscopy, *J. Raman Spectrosc.*, 2017, **48**(5), 720–725.
- 12 L. Zheng, P. Kulkarni, M. E. Birch, K. Ashley and S. Wei, Analysis of Crystalline Silica Aerosol Using Portable Raman Spectrometry: Feasibility of Near Real-Time Measurement, *Anal. Chem.*, 2018, **90**(10), 6229–6239.
- 13 ISO, ISO 19087:2018, *Workplace air—Analysis of respirable crystalline silica by Fourier-Transform Infrared spectroscopy*, International Organisation for Standardisation, Geneva, Switzerland, 2018.
- 14 ISO B, 16258-1, *Workplace Air – Analysis of Respirable Crystalline Silica using X-Ray Diffraction. Part 1. Direct-on-filter Method (ISO)*, ed. ISO, British Standards Institution, Chiswick, London, 2015.
- 15 HSE, *Methods for the Determination of Hazardous Substances, MDHS 101/2 Crystalline Silica in Respirable Airborne Dust, Direct On-Filter Analyses by Infrared Spectroscopy and X-Ray Diffraction*, Health and Safety Executive (HSE), Crown, Norwich, United Kingdom, 2014.
- 16 S. Wei, P. Kulkarni, K. Ashley and L. Zheng, Measurement of Crystalline Silica Aerosol Using Quantum Cascade Laser-Based Infrared Spectroscopy, *Sci. Rep.*, 2017, **7**(1), 13860.
- 17 J. K. McLaughlin, W. H. Chow and L. S. Levy, Amorphous silica: A review of health effects from inhalation exposure with particular reference to cancer, *J. Toxicol. Environ. Health*, 1997, **50**(6), 553–566.
- 18 OSHA, Method ID142, Crystalline Silica. Quartz and Cristobalite, in *Industrial Hygiene Chemistry Division*, ed. OSHA, Salt Lake Technical Center, Sandy, UT 84070-6406, United States, 2015.
- 19 NIOSH, *Silica, Crystalline, by XRD (filter redeposition) Method 7500*, ed. K. Ashley, Department of Health and Human Services, National Institute for Occupational Safety and Health, 2003.
- 20 S.-A. Lee, S. A. Grinshpun, A. Adhikari, W. Li, R. McKay, A. Maynard, *et al.*, Laboratory and Field Evaluation of a New Personal Sampling System for Assessing the Protection Provided by the N95 Filtering Facepiece Respirators against Particles, *Ann. Occup. Hyg.*, 2005, **49**(3), 245–257.
- 21 C. Sun, C. Thelen, I. Sancho Sanz and A. Wittmann, Evaluation of a New Workplace Protection Factor-Measuring Method for Filtering Facepiece Respirator, *Saf. Health Work*, 2020, **11**(1), 61–70.
- 22 P. Stacey, E. Kauffer, J.-C. Moulut, C. Dion, M. Beuparlant, P. Fernandez, *et al.*, An International Comparison of the Crystallinity of Calibration Materials for the Analysis of Respirable alpha-Quartz Using X-Ray Diffraction and a Comparison with Results from the Infrared KBr Disc Method, *Ann. Occup. Hyg.*, 2009, **53**(6), 639–649.
- 23 P. Stacey, A study to assess the performance of an “X-ray powder diffraction with Rietveld” approach for measuring the crystalline and amorphous components of inhalable dust collected on aerosol sampling filters, *Powder Diff.*, 2019, 1–9.
- 24 P. Stacey, T. Lee, A. Thorpe, P. Roberts, G. Frost and M. Harper, Collection Efficiencies of High Flow Rate Personal Respirable Samplers When Measuring Arizona Road Dust and Analysis of Quartz by X-ray Diffraction, *Ann. Occup. Hyg.*, 2014, **58**(4), 512–523.
- 25 CEN, EN 149:2001 + A1:2009, *Respiratory protective devices—Filtering half masks to protect against particles—Requirements, testing, marking*, Comité Européen De Normalisation, Brussels, Belgium, 2009.
- 26 ISO, ISO/TS 16976-1:2015, *Respiratory protective devices—Human factors. Part 1: Metabolic rates and respiratory flow rates*, International Standards Organisation, Geneva, Switzerland, 2015.
- 27 M. Mecchia, C. Pretorius, P. Stacey, M. Mattenklott and E. Incocciati, *X-Ray Absorption Effect in Aerosol Samples Collected on Filter Media*, ed. T. Lee and M. Harper, ASTM International, West Conshohocken, PA, United States of America, 2013.
- 28 CEN, EN 482:2012 + A1:2015, *Workplace exposure. General requirements for the performance of procedures for the measurement of chemical agents*, Comité Européen De Normalisation, Brussels, Belgium, 2015.
- 29 ISO, ISO 24095:2009, *Workplace air – Guidance for the measurement of respirable crystalline silica*, International Standards Organisation, Geneva, Switzerland, 2009, ISBN 978 0 580 58960 7.
- 30 Rules and Regulations, *Final Rule. Occupational Exposure to Respirable Crystalline Silica*, Occupational Safety and Health Administration, 2016.
- 31 W. C. Hinds and G. Kraske, Performance of Dust Respirators with Facial Seal Leaks: I. Experimental, *Am. Ind. Hyg. Assoc. J.*, 1987, **48**(10), 836–841.
- 32 S. Rengasamy and B. C. Eimer, Total Inward Leakage of Nanoparticles Through Filtering Facepiece Respirators, *Ann. Work Exposures Health*, 2011, **55**(3), 253–263.
- 33 A. E. Martens, Errors in Measurement and Counting of Particles Using Light Scattering, *J. Air Pollut. Control Assoc.*, 1968, **18**(10), 661–663.
- 34 N. Sang-Nourpour and J. S. Olfert, Calibration of optical particle counters with an aerodynamic aerosol classifier, *J. Aerosol Sci.*, 2019, **138**, 105452.
- 35 N. Takegawa and H. Sakurai, Laboratory Evaluation of a TSI Condensation Particle Counter (Model 3771) Under Airborne Measurement Conditions, *Aerosol Sci. Technol.*, 2011, **45**(2), 272–283.
- 36 T. Lee, L. Lee, E. Cauda, J. Hummer and M. Harper, Respirable Size-Selective Sampler for End-of-Shift Quartz Measurement: Development and Performance, *J. Occup. Environ. Hyg.*, 2017, **14**(5), 335–342.

Supplementary Information

An indirect Raman spectroscopy method for the quantitative measurement of respirable crystalline silica collected on filters inside respiratory equipment.

Peter Stacey, Francis Clegg, Jacqueline Morton and Christopher Sammon

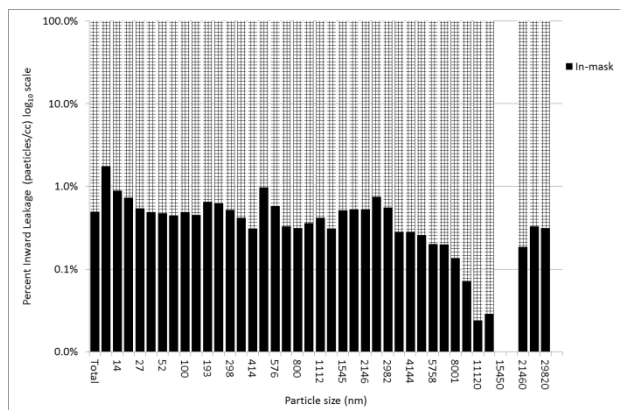


Figure S1. An example of the proportion of particles leaking into a respirator for each size range measured by the miniWRAS instrument.

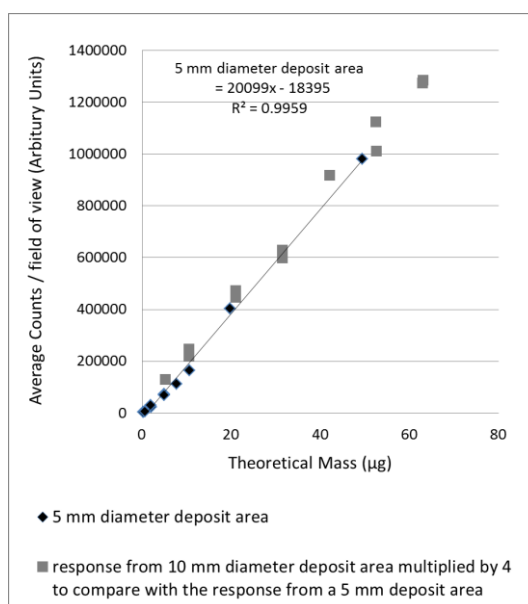


Figure S2: A comparison between the average response from a 5 mm deposit of NIST 1878a and the average response from a 10 mm deposit divided by the ratio of increase in deposit area.

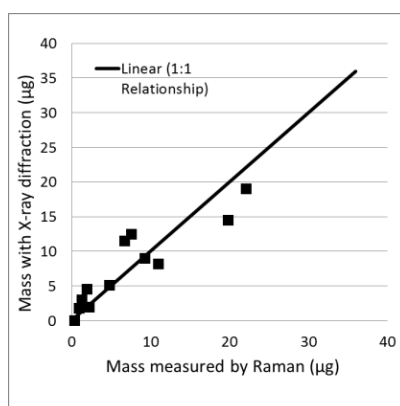


Figure S3. Comparability of Raman and XRD measurements when measuring respirable crystalline silica dust from the aerosol sampling filters and when the intercept is zero for both calibrations.

Chapter. 5 Change in Raman response with particle size and the measurement of samples from stonemasonry activities.

Stacey, P, Hall, S, Stagg, S, Clegg, F, Sammon, C.

Raman spectroscopy and X-ray diffraction responses when measuring health-related micrometre and nanometre particle size fractions of crystalline α -quartz and the measurement of α -quartz in dust samples from the cutting and polishing of natural and artificial stones. J Raman Spectrosc. 2021; 52: 1095– 1107.


<https://doi.org/10.1002/jrs.6110>.

Published Open Access Licence CC BY 4.0

Current citations = 7 (November 2022)

This work investigates the change in XRD and Raman response with decreasing median particle diameter from 0.50 μm to 7 μm . The sample deposit area was 15 mm in diameter which matches that used for many established XRD methods. Some 119 respirable stone dust samples were analysed and compared with an established regulatory XRD method used in the United States. Zircon, anorthite and rutile were three challenging potential interferences in the respirable dust samples.

Raman spectroscopy and X-ray diffraction responses when measuring health-related micrometre and nanometre particle size fractions of crystalline quartz and the measurement of quartz in dust samples from the cutting and polishing of natural and artificial stones

Peter Stacey^{1,2}  | Samantha Hall¹ | Stephen Stagg¹ | Francis Clegg² | Christopher Sammon²

¹Buxton Laboratory, Health and Safety Executive, Buxton, UK

²Materials and Engineering Research Institute, Sheffield Hallam University, Sheffield, UK

Correspondence

Peter Stacey, Buxton Laboratory, Health and Safety Executive, Harpur Hill, Buxton, Derbyshire SK17 9JN, UK.
Email: peter.stacey@hse.gov.uk

Funding information

Health and Safety Executive, Grant/Award Number: PH00760

Abstract

Around 560 000 workers in Great Britain are potentially exposed to respirable crystalline silica (RCS), which can cause disabling diseases, such as silicosis and lung cancer. These experiments assessed the performance of a new Raman spectroscopy method for measuring RCS, in samples of pure quartz powder with different median aerodynamic particle diameters and stone dusts from variety of natural and artificial stones. The relationship between the Raman response and particle size was characterised by measuring subfractions of the respirable quartz standard A9950 collected using the Sioutas impactor. Bulk samples of quartz standards A9950 and Quin B that provided the highest median particle size diameters were also measured. Health-related thoracic and respirable particle size fractions, and the environmental monitoring fractions of PM₁₀, PM_{2.5}, PM₁ and PM_{0.5}, were also collected during the powered cutting and polishing of sandstone and diorite (granite), engineered and sintered stones. All Raman spectroscopy results were compared with those from X-ray diffraction (XRD), which was used as the reference technique. The Raman spectroscopy response closely followed the predicted crystallinity of RCS for different particle diameters. Raman spectroscopy obtained slightly higher percentages than XRD for particle size fractions below 1 µm. The Raman spectroscopy and XRD results were highly correlated for the thoracic, respirable and impactor fractions. The coefficients of determination were between 0.98 and 0.95. The slope coefficients for the correlation were 1.11 for the respirable fraction and 1.07 for the thoracic fraction. Raman spectroscopy is a promising alternative to XRD for measurement of RCS with a much lower limit of detection of 0.21 µg compared with 1 µg.

This is an open access article under the terms of the Creative Commons Attribution License, which permits use, distribution and reproduction in any medium, provided the original work is properly cited.

© 2021 Crown copyright. *Journal of Raman Spectroscopy* published by John Wiley & Sons Ltd. This article is published with the permission of the Controller of HMSO and the Queen's Printer for Scotland.

KEYWORDS

artificial stone, measurement, nanometre, particle size, respirable crystalline silica

1 | INTRODUCTION

This study was designed to support research to compare the particle size emission profile of aerosols generated from the powered cutting and polishing of natural and artificial stones. Industrial processes, using materials containing crystalline silica, can generate aerosols containing respirable (respirable crystalline silica [RCS]) particles that are small enough to penetrate to the alveoli region of the lung and can cause diseases like silicosis^[1] and lung cancer.^[2] It is estimated that 560 000 workers are regularly exposed to RCS in Great Britain^[3] and 1.7 million in the United States.^[4] One approach to assess exposure to hazardous airborne substances is to measure the concentration of the material entering the breathing zone of a worker. A sample of the aerosol is collected, using a sampler that selects sizes of particles that are associated with the main health effect. There are several different health-related size fractions that are of interest to researchers when evaluating the occupational health risk from aerosols of dust. The three size fractions that are of significance in occupational hygiene are for particle diameters that can penetrate into the nose and throat (inhalable), the larynx (thoracic) and the alveoli (respirable).^[5] Respirable sized particles are associated with silicosis caused by inhalation of particles of crystalline silica. The respirable and thoracic fractions are subfractions of the inhalable dust that penetrate beyond the larynx and into the lung. The inhalable fraction contains particles that do not penetrate as far as the lung, where silicosis and lung cancer can occur, so this size fraction was not evaluated in this study. Differences between each particle size definition are shown in Figure S1.

The thoracic aerosol samplers are designed to select particles with a log-normal cumulative distribution of aerodynamic diameters that are less than 40 μm and have a median of 10 μm . Respirable samplers are designed to select particles with diameters of less than 16 μm and a median diameter of 4 μm . These particle size fractions differ from those used when measuring aerosol particulates in environmental atmospheres, which are termed PM10 for all particulate diameters less than 10 μm , PM2.5 for particulate diameters less than 2.5 μm and PM1 for particulate diameters less than 1 μm . Aerosol samplers in environmental monitoring are designed to select the particle diameters with a more refined size selection cut within a specific standard deviation.^[6] PM10 is comparable with the thoracic particle size health

fraction, and PM2.5 is used to specifically inform on the risks to health from those particles likely to penetrate to the gas exchange region (alveoli) of the lung.^[7] Particle size fractions of PM2.5 and PM1 (particles equal to or less than 2.5 or 1 μm) are also of interest because these particles have greater potential to deposit in the alveoli.

X-ray diffraction (XRD) and Fourier transform infrared spectroscopy (FTIR) are two techniques that are currently employed for the measurement of concentrations of RCS in workplace aerosols.^[8] Each technique employs a different principle of measurement. XRD measures the intensity of X-ray radiation diffracted from the arrangement of atoms within the structure of a crystalline component in the dust sample, whereas FTIR measures the absorbance of infrared radiation, which, for RCS, is related to the asymmetric Si–O–Si stretching and Si–O bending vibrations of the silicon and oxygen atoms in the crystalline silica.

Two significant factors that affect the accuracy of XRD and FTIR measurements of crystalline silica in dusts are the presence of interferences (i.e., other crystalline components with reflections or absorbance that coincides with those from crystalline silica) and the particle size and crystallinity of the measured material. The particle size of the RCS in a sample of dust affects the measurement response for both XRD and FTIR.^[9] FTIR absorbance increases as the particle size decreases from about 8 to 1 μm in diameter,^[10,11] whereas XRD integrated area intensity measurements are more consistent over this particle size range.^[9,12,13] The measurement response per unit mass of both FTIR^[10] and XRD^[9,12] shows an attenuation at particle diameters less than 1 μm . The reduction in measurement response for both XRD and FTIR is attributed to a thin amorphous, or less ordered, layer on the surface of each crystalline silica particle of approximately 0.03 μm in depth that transitions into a more crystalline centre.^[10,14–16] The less crystalline surface layer contributes proportionately more, in terms of particle volume and mass, at particle diameters less than 1 μm , so that both the XRD and FTIR techniques give lower measurement responses for the mass of crystalline silica particles. The mass of crystalline silica in the aerosol would be under-reported, if the reference material used for calibrating each instrument contained significant numbers of larger particles (equal or greater than 1 μm), than those in the collected aerosol.

Raman spectroscopy has been widely used for the characterisation of individual aerosol particles^[17–20],

however, it is a relatively new technique for the quantitative analysis of hazardous substances in aerosols collected for occupational hygiene exposure measurements.^[20–23]

The aim of this work is to assess if particle size is a factor that affects the Raman band intensity when using the specific analytical conditions proposed for a new method to measure aerosols of RCS collected onto filters.^[24] Another aim of this study is to compare results obtained using Raman spectroscopy, as a new method to measure RCS, with those obtained from the established technique of XRD for both laboratory generated samples and emissions collected during typical stone working activities.

Particle size can affect the measured Raman spectroscopy response, and micro-Raman spectroscopy is used as a technique to measure the particle size of nano-sized particles.^[25] The profile and position of the Raman band can change as the particle diameter decreases.^[26] The role of particle size and its effect on near infrared (NIR) Raman scattering in loose powders and tablets were described by Schrader et al.^[27,28] Equation 1 was used to explain the scattering of the Raman band intensity emitted from the substance in an anti-parallel direction from a sample, that is, with a measurement arrangement that is similar to the modern Raman spectrometers with microscope attachments used in this work.

$$J_{\text{Scattered}} = \Phi \frac{sk}{\alpha} \frac{k \sinh kd + (\alpha + r) \sinh kd \cosh kd - krd}{[(\alpha + r) \sinh kd + k \cosh kd]^2} \quad (1)$$

where $k^2 = 2r\alpha + \alpha^2$, α is the absorption coefficient, r is the elastic scattering coefficient, s is the Napierian (internal) scattering coefficient, d is the depth of sample and Φ is the applied flux. The elastic scattering coefficient (r) is inversely proportional to the diameter of the particles,^[28] which would imply that scattering would be greater in powders for larger diameter grains.

The principal theoretical findings of Schrader et al.^[28] were that Raman intensity should

- increase as the particle size increases;
- increase when the depth of the sample increases, which reaches a stationary value at small sample thickness for fine powders; and
- be independent of the size of grains when measuring small particles with optimised conditions (i.e., in cuvettes with reflective surfaces).

However, the intensity (I) of the Raman band response observed by the detector through the instrument is also dependent on a number of other factors (Equation 2), which includes the wavenumber of the energy source ($\bar{\nu}_0$); the Raman shifted wavenumber ($\Delta\bar{\nu}$); the reference wavenumber ($\bar{\nu}_{\text{ref}}$); the applied power of the energy source (Φ); the cross-sectional area of the laser beam on the sample (A); the depth of the sample (d); the number of molecules per unit volume irradiated (N); and the differential Raman photon scattering cross-section (the proportion of photons [$J_{\text{scattered}}$] effectively scattered by the incident radiation) (β):

$$I = \frac{\Phi}{A} d (\bar{\nu}_0 - \Delta\bar{\nu})^4 N \beta (\bar{\nu}_{\text{ref}} - \Delta\bar{\nu})^{-4} \quad (2)$$

Several practical studies have examined the effect of particle size on Raman response in crystalline powders or grains,^[29–33] and some of these articles^[30,32] show that smaller particles can lead to an increase of intensity, which is contrary to the findings of Schrader et al.^[28] Most of these previous studies involve particle sizes greater than 10 μm or particles compacted in pellets to examine the Raman response from pharmaceutical tablets, which is less relevant to the subject of this article.

This study examined aerosol particles scattered onto a thin reflective filter (silver) and focused on health-related particle size fractions and environmental sample fractions of aerosol particulates (0.5 to 10 μm). These diameters are much closer to the wavelength of the incident energy, that is, an NIR laser of 0.785 μm than particles studied in previous work.

2 | METHOD

The experiments were designed in three stages. First, a calibration was developed using the respirable quartz reference material A9950 (Health and Safety Executive [HSE], Buxton, UK). A9950 is a high purity quartz reference material with a crystallinity of 89.3%.^[9] Second, the measurement response for the XRD and Raman spectroscopy was compared for different size fractions of A9950 collected using a Sioutas impactor,^[34] and a calibration mass correction factor was determined to correct the measured mass for any reduction in XRD or Raman spectroscopy response at small particle diameters. Third, XRD and Raman spectroscopy measurements of crystalline silica were compared for samples of dust generated from the cutting and polishing of natural and artificial stones.

2.1 | Calibration of XRD and Raman spectroscopy instruments

Raman measurements were collected using an In-Via microscope (Renishaw Ltd, Gloucester, UK) with an NIR (785 nm) laser with a line output at 300 mW, and 110 mW on the sample, without attenuation. XRD measurements were obtained using an X-pert Pro MPD instrument (PANalytical Ltd, Cambridge, UK) with focusing Bragg–Brentano geometry and X-pert for Industry software (Malvern Panalytical Ltd, Malvern, UK).

XRD and Raman spectrometry measurement conditions and methods to determine the limits of detection (LODs) are described in previous articles^[21,35] and in the Supporting Information.

Calibration samples for XRD and Raman spectroscopy were prepared by filtering aliquots (0.25 to 9 ml) from a 201 $\mu\text{g ml}^{-1}$ suspension of A9950 in isopropanol into a 15-mm-diameter area on 0.45- μm -pore-size silver filters (SKC Ltd, Blandford Forum, Dorset, UK). A suspension of 14.7 $\mu\text{g ml}^{-1}$ was used for lower loadings. The area of the sample deposit was constrained to 176.7 mm^2 using a bespoke 15-mm-diameter filtration funnel. The preparation of calibration samples to aid a uniform deposit is described in previous articles.^[21,24] The mass of sample loaded onto the silver filters was kept below 1000 μg to avoid correcting for sample absorption when using XRD.^[36] The calibration response trend line was extended up to 1800 μg to examine the effect of the depth of sample on Raman band intensity.

2.2 | Generation of samples of A9950 to assess stability of the Raman band response

A Sioutas impactor aerosol sampler^[34] was used to collect aerosols of A9950 generated in a containment box within a fume cupboard. This impactor aerosol sampler selects particles following the particle selection criteria defined for environmental health-related monitoring. The Sioutas separates the captured aerosol into four fractions for particles between 10 and 2.5 μm , 2.5 and 1 μm , 1 and 0.5 μm and 0.5 and 0.25 μm . PM10 is the sum of all the fractions, whereas PM2.5 is the sum of the three fractions excluding the 10 to 2.5- μm cut. Particles less than 0.25 μm are captured on an exit filter.

The Sioutas impactor was calibrated to operate at its specified flow rate of 9 L min^{-1} using a TSI 4100 flow metre (TSI Inc, USA). Size fractions of A9950 were collected on 0.5- μm -pore-size polytetrafluoroethylene (PTFE) filters (SKC UK Ltd, Blandford Forum, UK)

placed on each impaction stage. Dust collected onto PTFE filters was washed into glass bottles with isopropanol and filtered into a 15-mm-diameter area on 0.45- μm -pore-size silver filters for analysis. An amount of isopropanol was placed into a borosilicate glass bottle, which was sufficient to cover a PTFE filter. PTFE filters containing sample were inserted into the glass bottle and wetted with the isopropanol. The filter was then held with tweezers close to the surface of the isopropanol, and the remaining dust was washed or scrapped into the liquor with a spatula. The filter, spatula and sides of the glass bottle were washed with isopropanol into the liquor. The suspension was then filtered onto silver filters following the previously described procedure.

The proportions of A9950 were then measured on each silver filter using XRD and Raman spectroscopy.

Twelve filters (three from each impactor stage) were used to assess the potential for loss of dust during the recovery and filtration processes. The weight of dust collected on the PTFE and silver filters was determined gravimetrically using a balance with a readability of six decimal places (Sartorius UK Ltd, Epsom, UK). The average recovery and its standard deviation were recorded for the 12 filters.

The XRD and Raman spectroscopy responses were also compared when measuring the respirable fraction of aerosolised quartz standard Quin B collected using the GK 2.69 respirable sampler (Mesa Labs, Lakewood, Colorado, USA) operating at a flow rate of 4.2 L min^{-1} . The GK 2.69 sampler was used with an adaptor for a 25-mm-diameter PVC filter in a conductive filter cassette. The PVC filters collected from the respirable sampler were placed into glass bottles and ashed using a low-temperature plasma asher (Emitech K1050X, Quorum Technologies Ltd, Ashford, UK). The filters were ashed in air at 50% power for 12 h and then in oxygen for 4 h at 95% power. About 5 ml of isopropanol was added to the bottle after it was removed from the asher. The liquor and residue were then sonicated for about 2 min and filtered into a 15-mm-diameter circular area on 0.45- μm -pore-size silver filters.

Bulk samples of A9950 and Quin B quartz reference materials were used to evaluate the measurement response for quartz dusts with median particle sizes from about 4 up to 7 μm . The quartz reference material Quin B (Institut National de Recherche et de Sécurité [INRS], France) has a crystallinity of 95.5% and a median particle size closest to the thoracic fraction (median diameter of 7.2 μm when measured using laser diffraction). The quartz reference material A9950 has a median diameter of 4.2 μm .

About 1 mg of bulk quartz power (A9950 or Quin B) was weighed into a glass bottle, sonicated for 2 min in

isopropanol and filtered into a 15-mm-diameter area on a pre-weighed silver filter. Three replicate samples were prepared for each powder.

A two-sided *t* test was used to compare if the XRD and Raman spectroscopy measurements made on the same samples were similar, for each size fraction, with a 95% level of confidence. A probability (*p*) value greater than 0.05 would indicate that the results for each instrument were not significantly different.

Laser diffraction particle size measurements were used to verify the particle size distribution of the A9950 collected by each particle size fraction. The particle size measurements were conducted by Particle Technology Ltd (Hatton, Derbyshire, UK) using a Horiba LA950 laser diffraction particle size analyser (Horiba UK Ltd, Northampton, UK). The laser diffraction instrument reports the volume distribution of sphere diameters.

The mass of the quartz particle and the mass of the crystalline quartz are different when particles are small, which may affect the instrument response.^[14,16] To compare the relationship between Raman response and crystallinity, the relative mass response for each particle size fraction was plotted with a line showing the proportion of crystalline quartz for particles with a disordered layer of 0.03 µm. The predicted crystallinity was calculated by making the assumption that these particles were spherical and by calculating the volume for the particle and the crystalline material, where the radius is reduced by 0.03 µm. The volume crystalline material was then divided by the total volume of the particle for each median particle size value from each size fraction. A volume spherical diameter is similar to that measured by a laser diffraction instrument and equates to an aerodynamic diameter for small particles.

A mass correction factor (\bar{X}) for the average difference in response per unit mass from the calibration was calculated for each impactor stage using the ratio:

$$\bar{X} = \frac{1}{n} \sum (M_T/m_I) \quad (3)$$

where M_T represents the mass of particles collected by an impactor size fraction, determined gravimetrically, m_I is

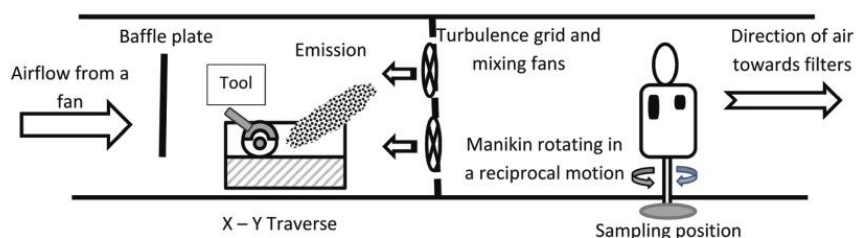
the mass reported using the instrument (XRD or Raman spectroscopy) and *n* is the number of ratios. This average ratio was applied to correct for any reduction in instrument response from the calibration at small particle diameters.

2.3 | Samples from cutting and polishing of stones

Cutting and polishing tests were conducted on sandstone, two engineered (resin-containing) stones, a natural stone known as diorite (which is an igneous rock related to granite) and a sintered stone. The mineral composition of each of these stones was measured using XRD and the Rietveld method with an internal standard. The generation of emissions from the powered cutting and polishing of stones was carried out in a dust tunnel (Figure 1), which is a long box about 1.5 m high and 1 m wide. The stones were held on a traverse, which moved the stone in the *x* and *y* directions whilst the stone was cut or polished. A fan moved air from outside the building through the dust tunnel past the traverse and towards a rotating manikin, which simulated the presence of a worker and was used as the sampling position. A turbulence grid with three ionising fans was positioned downstream of the emission and used to reduce eddies and improve mixing of the generated aerosols.

A GK 2.69 sampler with a cassette for a 37-mm-diameter PVC filter collected the respirable fraction, whilst another GK2.69 sampler operating at 1.6 L min⁻¹ collected the thoracic fraction.^[37] A Sioutas impactor operating at its specified flow rate of 9 L min⁻¹ was used to collect the environmental particle size fractions within PM10. The GK 2.69 samplers were placed on the front of the rotating manikin on the chest, and the Sioutas sampler was placed on its back at about the same height. Three replicate tests were performed with the GK 2.69 samplers and two with the Sioutas impactor. The filter samples from the respirable and thoracic samplers were ashed following the procedure previously described. The Raman band response for each impactor stage for each dust was compared with the response obtained from

FIGURE 1 Configuration of the dust tunnel, not to scale [Colour figure can be viewed at wileyonlinelibrary.com]



XRD (which is related to the crystallinity of the quartz particulate). In addition, the mass of quartz particulate collected in each impactor stage was estimated by applying the mass correction factor (\bar{X}) to the measured Raman band and XRD responses.

3 | RESULTS

The mass response trend lines achieved for Raman spectroscopy when pipetting aliquots of A9950 onto silver filters are shown in Figure 2. The stability of the average area responses from typical particle loadings from each stage from a Sioutas impactor is shown in Figure S3. Scanning electron microscope (SEM) images of the density of particles at various mass loadings are shown in Figure S4. Particles appeared to be a continuous layer from a loading of about 500 μg and are stacked on top of each other in the image at 1000 μg . The trend lines for XRD are shown in Figure S5. The maximum mass value for the XRD calibration was about 1000 μg because of the significant absorption of the X-ray response (about 20%) at higher mass loadings^[36] when quartz is deposited on a 15-mm-diameter area. The LODs from the two

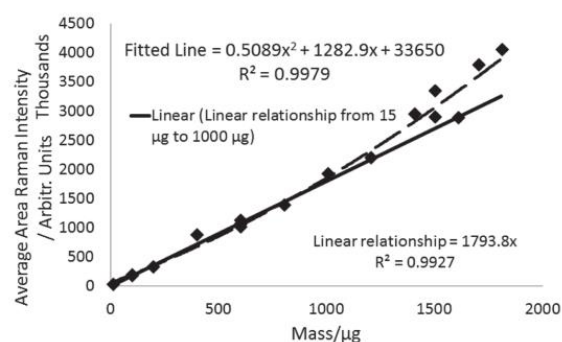


FIGURE 2 Relationship between Raman responses for a mass of quartz loaded into a 15-mm-diameter area onto a silver filter

approaches for the Raman spectroscopy and XRD measurements are listed in Table 1.

The average recovery of fractions of A9950 from 12 PTFE Sioutas impactor filters and onto the silver filters was $100 \pm 3.8\%$ (1σ). The mass loadings ranged from 890 to 1300 μg for the 2.5- to 10- μm impactor stage and from 102 to 120 μg for the 0.25- to 0.5- μm stage. The particle sizes of A9950 collected by each impactor filter and the bulk quartz reference dusts were measured using laser diffraction. They are also shown in Table 2 with the average percentage mass response from each technique, the standard deviation of the replicate analyses and the t -test probability value for each set of techniques.

Figure 3 shows the change in instrument response per unit mass for each measured particle size fraction. A curve for the predicted crystallinity of quartz particles for various diameters with a disordered surface layer of 0.03 μm ^[10] is also shown. The average Raman spectroscopy values are significantly higher than those from XRD for the two impactor stages covering the smallest particles (1 to 0.5 μm and 0.5 to 0.25 μm). The p values from the t tests are 0.13, 0.02, <0.01 and <0.01 for the 10- to 2.5- μm , 2.5- to 1- μm , 1- to 0.5- μm and 0.5- to 0.25- μm impactor stages, respectively (Table 2). The XRD results obtained in this research are comparable with those obtained by Page,^[12] who measured samples of a grade of quartz dust known as Min-U-Sil 10 (Figure S6).

3.1 | Stone cutting and polishing tests

Paired XRD and Raman spectroscopy results were obtained from a total of 119 emission test samples, which included 72 impactor and 47 respirable and thoracic samples. In total, there were 24 XRD values below the lowest estimated LOD of 1 μg and four Raman spectroscopy values below the highest estimated LOD of 0.21 μg . The mass percentages of crystalline silica and other crystalline mineral components in the sandstone and engineered (resin-containing), diorite and sintered stones used in the

XRD			
Angle of reflection (2θ)	20.9	26.6	50.1
Measurement of blank filters	11 μg	1 μg	13 μg
By calculation. From the variability of the background scatter	14 μg	3 μg	21 μg
Raman			
Measurement of blank filters	0.210 μg		
By calculation. From the variability of the background scatter	0.085 μg		

Abbreviation: XRD, X-ray diffraction.

TABLE 1 Limits of detection (LODs) for the XRD and Raman spectroscopy methods when measuring quartz on clean blank filters, ashed and deposited in a 15-mm-diameter area on a silver filter, and when calculating the LOD for quartz from the variability in the background scatter

TABLE 2 Particle size statistics measured by laser diffraction for fractions of aerosolised quartz reference material A9950, and the bulk powders of A9950 and Quin B, the average percentage of quartz measured with standard deviation and the *t*-test probability that the XRD and Raman reported values for the per cent crystallinity

Particle size range	Mean diameter (μm)	Median diameter (μm)	Technique	Number of samples (<i>n</i>)	Average per cent crystallinity and standard deviation (1 σ)	<i>t</i> -test probability (<i>p</i>)
Impactor Stage 4 0.25 to 0.5 μm	0.6	0.54	XRD	4	27.6 ± 8.0	<0.01
			Raman	4	54.9 ± 7.7	
Impactor Stage 3 0.5 to 1 μm	0.88	0.85	XRD	4	72.4 ± 4.5	<0.01
			Raman	4	83.5 ± 2.4	
Impactor Stage 2 1 to 2.5 μm	1.34	1.31	XRD	4	89.8 ± 5.0	0.02
			Raman	3	101 ± 3.0	
Impactor Stage 1 2.5 to 10 μm	3.43	2.93	XRD	4	105 ± 4.7	0.13
			Raman	3	99.2 ± 3.0	
Quin B (respirable fraction)	3.03	2.59	XRD	3	99.9 ± 0.7	0.97
			Raman	3	99.9 ± 2.1	
A9950	4.85	4.20	XRD	3	107 ± 2.0	0.01
			Raman	3	100 ± 1.8	
Quin B	7.20	7.20	XRD	3	112 ± 0.2	<0.01
			Raman	3	92.2 ± 4.2	

Abbreviation: XRD, X-ray diffraction.

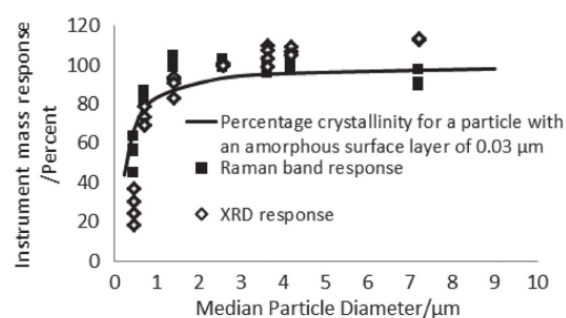


FIGURE 3 Relative Raman spectroscopy and X-ray diffraction (XRD) responses when measuring size fractions of the quartz reference material A9950

emission tests are shown in Table 3. Results comparing the instrument response and estimated mass of crystalline silica measured by XRD and Raman spectroscopy in each Sioutas particle size fraction for the samples collected from the cutting and polishing of engineered stone and sandstone are shown in Figure 4 for power cutting and Figure 5 for polishing. Results for diorite and sintered stones are in Figure S7 (cutting) and Figure S8 (polishing). The results for XRD are shown in the charts on the left-hand side, and the Raman spectroscopy measures, reported on the same samples, are shown in the

charts on the right-hand side. The solid lines in the charts in these figures represent the instrument response. The broken lines on these charts represent the calculated values for the mass of quartz particles when the mass correction factor was applied. The XRD mass response correction factors were 0.95, 1.11, 1.38 and 3.62, and the Raman spectroscopy mass response correction factors were 1.00, 0.98, 1.20 and 1.82 for the 10- to 2.5-μm, 2.5- to 1-μm, 1- to 0.5-μm and 0.5- to 0.25-μm impactor stages, respectively.

For cutting stone, the range of loadings on the impactor samples was from 1600 to 700 μg for the 10- to 2.5-μm stage down to 122 to 72 μg for the 0.5- to 0.25-μm stage. When polishing, the range of loadings on the impactor filters was from 787 to 330 μg for the 10- to 2.5-μm stage down to 37 to 19 μg for the 0.5- to 0.25-μm stage. For the samples from cutting, two XRD values were less than the LOD (1 μg) for the smallest size fraction; for the sintered stone and diorite samples (and hence the missing data points in Figure S7), only one Raman spectroscopy measurement reported an LOD when measuring the same samples. For the samples collected from polishing, 14 XRD values were below the LOD. In contrast, Raman spectroscopy was not able to report two results from the polishing activity. The two Raman spectroscopy measurements were on samples collected from the sintered stone (Figure S8). One Raman spectroscopy measurement was

Material	Mass per cent crystalline silica (quartz) SiO ₂	Other mineral phases Per cent crystalline content
Sandstone	62	Albite (NaSi ₃ O ₈) 7.5% Kaolinite (Al ₂ Si ₂ O ₅ (OH) ₄) 2.2%
Engineered stone R1	67	Albite (NaSi ₃ O ₈) 14%
Engineered stone R2	89	Rutile (TiO ₂) 2.2%
Diorite	7.2	Anorthite (CaAl ₂ Si ₂ O ₈) 51% Diopside (MgCaSi ₂ O ₆) 35% Mica (KAl ₂ (AlSi ₃ O ₁₀)(OH) ₂) 2.4% Hornblende ((Ca,Na) ₂ (Mg,Fe,Al) ₅ (Al, Si) ₈ O ₂₂ (OH) ₂) 3.4%
Sintered stone S1	6.9	Zircon (ZrSiO ₄) 16% Mullite (3Al ₂ O ₃ 2SiO ₂) 12%

TABLE 3 Composition of crystalline minerals in the stone samples

Sandstone

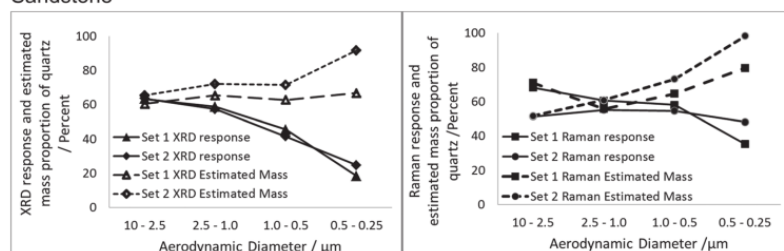
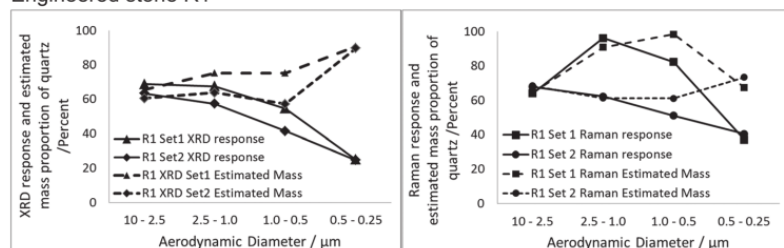
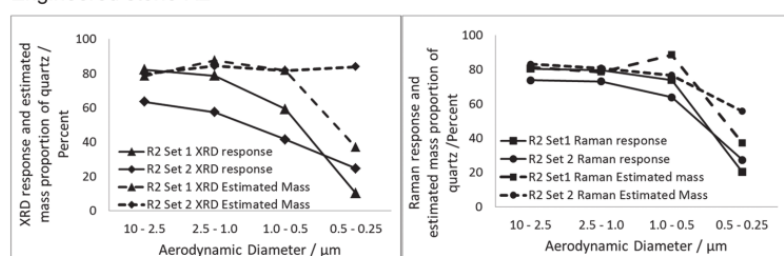


FIGURE 4 Cutting of artificial and natural stones. Relative instrument response and estimated mass proportions of quartz obtained by X-ray diffraction (XRD) and Raman spectroscopy when measuring size fractions collected by the Sioutas impactor sampler

Engineered stone R1



Engineered stone R2



below the LOD, and the other had too much fluorescence in each spectrum. The sample with too much fluorescence was from the impactor filter collecting the 10- to

2.5- μ m particle size fraction and had more than 1 mg of dust. The highest loaded impactor samples (around 1 mg) were affected by excessive occurrence of detector

saturation. A subsample, with less loading, was obtained for some samples by suspending the dust from the filter in isopropanol, taking an aliquot of the suspension and filtering this suspension to produce a sample with a lower particle density than was previously measured. Figures 6–8 compare the correlations between mass values for crystalline silica obtained by XRD and Raman spectroscopy when measuring the impactor (Figure 6), respirable (Figure 7) and thoracic samples (Figure 8), during the cutting and polishing of the stones. Both the x and y axes are \log_{10} scale. The dotted lines on the charts in Figures 6–8 represent the ideal 1:1 relationship. The

paired XRD and Raman spectroscopy results from the impactor samples were corrected for changes in response due to particle size by multiplying the measured value with the mass correction factor for its size fraction. The coefficient for the slope of 0.97 for the impactor samples was not significantly different from the ideal relationship 1.00 (95% confidence level for the range of slope values was 0.94 to 1.00). Eight XRD values, for the respirable and thoracic dust samples from polishing, were not reported because they were less than the LOD of $1\ \mu\text{g}$, whereas only three values were not reported when measured using Raman spectroscopy (LOD of $0.21\ \mu\text{g}$).

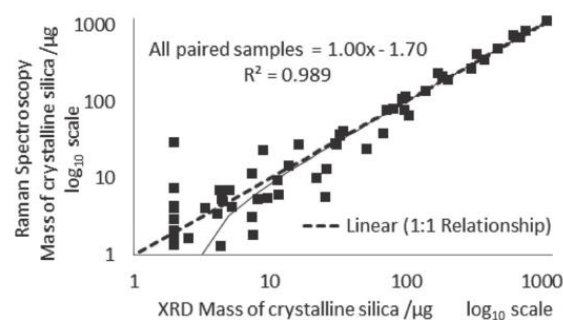
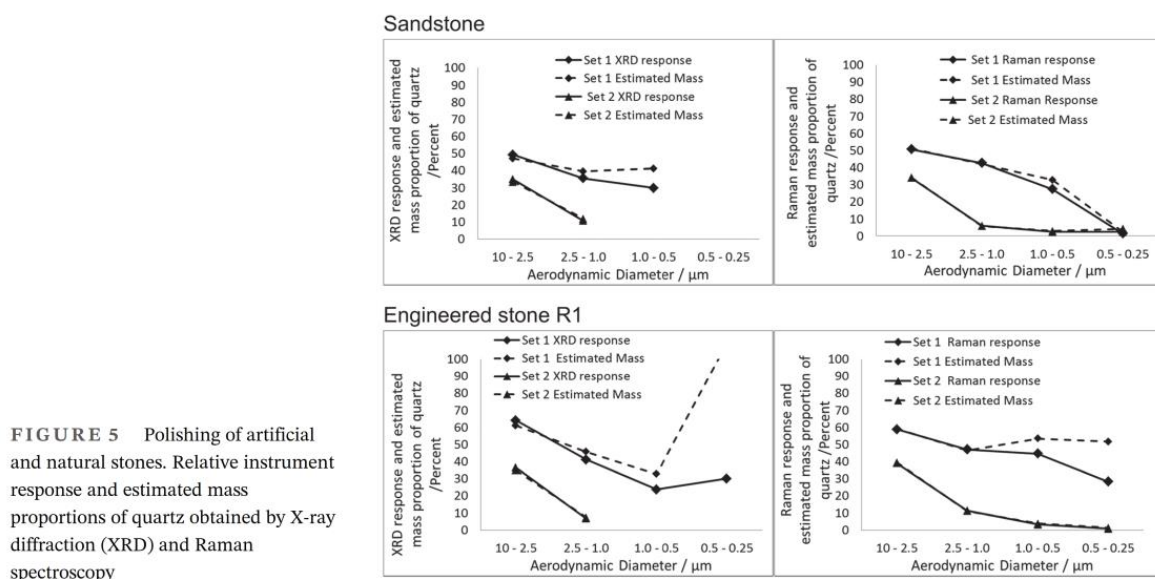


FIGURE 6 A comparison of Raman and X-ray diffraction (XRD) measurements of crystalline silica in the fractions of aerosol collected by the Sioutas impactor for all samples (from cutting and polishing). The results are corrected for the change in measurement XRD and Raman response for small diameter particles (less than $1\ \mu\text{m}$ in diameter) due to the reduction in crystallinity

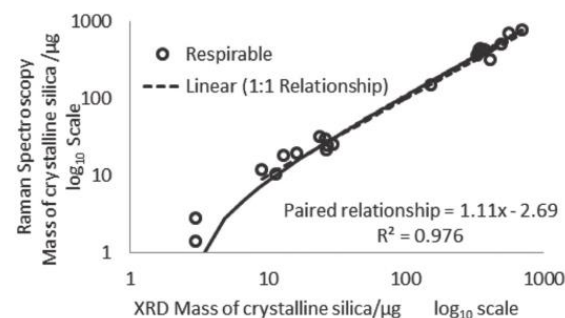


FIGURE 7 The respirable fraction. A comparison of Raman and X-ray diffraction (XRD) measurements of crystalline silica collected from cutting and polishing of sandstone, engineered stone, diorite stone and sintered stone

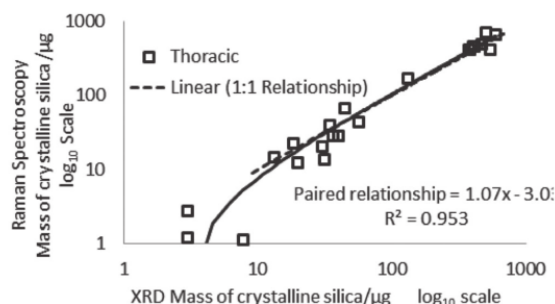


FIGURE 8 The thoracic fraction. A comparison of Raman and X-ray diffraction (XRD) measurements of crystalline silica collected from cutting and polishing of sandstone, engineered stone, diorite stone and sintered stone

Coefficients of determination for the paired relationships were 0.97 and 0.95 with slope values of 1.11 and 1.06 for the respirable and thoracic samples, respectively. The slope value for the RCS analyses was significantly different from the ideal value of 1.00 at the 95% level of confidence (the range of values within a 95% level of confidence was 1.03 to 1.19) but not for the thoracic samples (the range of slope values within a 95% level of confidence was 0.96 to 1.17).

4 | DISCUSSION

4.1 | The use of Raman spectroscopy for exposure measurement

Raman spectroscopy has a clear benefit over XRD in terms of its ability to measure samples with lower masses of quartz and its sensitivity when measuring particle sizes less than 1 µm (Figure 3). Its LOD is between 0.085 and 0.210 µg, which is 14 times lower than that calculated for the most sensitive XRD reflection. The benefit of applying a Raman spectroscopy method based on the averaged accumulated spectra from multiple micro-area measurements is that the occasional spectra with fluorescence or detector saturation can be ignored, because the average value is fairly consistent (Figure S3), so long as sufficient measurements are recorded. Nearly every sample had an occasional spectrum where saturation of the detector occurred, which was discounted for the calculation of the average value. Excess fluorescence prevented the measurement of just one single sample in the 119 that were measured in these tests. This particular sample of zircon had a high mass loading (greater than 1 mg) in the 10- to 2.5-µm fraction. Loadings greater than 1 mg are not frequently encountered for

occupational hygiene sampling of RCS. The low incidence of measurement failure on these challenging samples and good correlation of Raman spectroscopy and XRD measurements (Figures 6–8) demonstrates the robustness of the Raman spectroscopy method for samples from stone working activities. The results from the impactor samples (Figures 4 and 5) show that, in general, Raman will give results for samples containing crystalline silica that are similar to those measured by XRD. Most paired XRD and Raman spectroscopy results are close to the ideal relationship of 1.00 (Figure 7), despite some additional variability from the lowest impactor stage samples. The calculated mass proportions of quartz particulate are similar for each particle size fraction from cutting and polishing, although the values from cutting are closer to the proportion of crystalline silica in the bulk material than for polishing. The variability in the estimated mass values obtained for the impactor stage with the lowest particle size fraction could be due to (a) measurement errors for low masses of crystalline silica in the presence of significant mineral interference (e.g., for the diorite samples with only 7% quartz in an anorthite matrix) and (b) correction errors caused by some migration of particles from the third to the fourth impactor stage. Particle bounce from one stage to another is a phenomenon that can occur when the impaction collection mediums are heavily loaded.^[38]

Spectra and scans showed that Raman spectroscopy is of greater benefit than XRD when measuring samples containing zircon (ZrSiO₄). Zircon is fully resolved when using Raman spectroscopy (Figure S9) and potentially more accurately measured, whereas it is a significant interference for the main quartz reflection at 26.6° when using XRD (Figure S10). There is also interference of the Raman band shift for quartz at 464 cm⁻¹ from some common feldspar mineral components like albite, anorthite and microcline; however, these were resolved using the peak fitting software in the Raman spectroscopy instruments WIRE™ operating program (Figure S11). The mapping process also allows for occasional Raman spectrum with too much interference to be omitted, because the mean density of particles over the filter surface should be reasonably consistent. XRD has similar issues with interference from silicate minerals^[39] (Figure S12).

A significant issue for Raman spectroscopy is the presence of rutile (titanium oxide, TiO₂). Rutile was found as a contaminant in the engineered stone samples (about 0.5% to 2%), although it is not usually present in other workplace samples for RCS measurement. Rutile bands were difficult to resolve from quartz and may have contributed to some high Raman spectroscopy values

(+10% to +20%) when compared with XRD results. Despite these potential issues, the slope coefficient between Raman spectroscopy and XRD measurements for crystalline silica, from cutting and polishing stone, is close to the ideal of 1.00. One disadvantage for practical work is that Raman spectroscopy is not able to cope with excess filter residue as well as XRD. Occasional incidents of visible excess filter residue were thought to be the cause for the single points significantly below the trend line for the 1:1 relationship in Figures 7 and 8. However, excess filter residue after ashing is probably not significant when dealing with more routine samples in the United Kingdom. The GK 2.69 samplers used 37-mm-diameter filters in anticipation of some high loadings of aerosol, whereas most respirable samplers in the United Kingdom use 25-mm-diameter filters that substantially reduce the amount of material (by about 55%).

A high background level in the Raman spectrum was a significant issue for the first set of samples of engineered stone (R1) prepared for measurement, which was attributed the use of an old set of silver filters with a rougher scratched surface. The measurement time had to be reduced to permit analysis, which resulted in broader Raman bands and curved backgrounds, which makes the fitting of the band profile difficult when using the software and a linear background correction.

4.2 | Response due to particle size and sample depth

The calibration encompassed samples with a range of particle densities from scattered particles in each field of view to multilayers (Figure S4).

Figure 2 indicates that the Raman band intensity is proportionally related to the volume of particles (N) within the cross-sectional area of the laser (A) (Equation 2) when the loading is below 1000 μg .

At low particle densities, the depth of the sample (d) is effectively the particle diameter and the absorption (α) is from the particle itself, because other particles are not close enough to influence the Raman scattering. Therefore, the scattering coefficient (s) will depend on the volume of particles within the illuminated cross-sectional area. The character of the Raman band intensity changes at higher mass loadings from one where there are relatively small variations in depth to one where more particles are packed in multilayers within the volume of the focused laser. Factors like absorption and multiple scattering, of laser, Rayleigh and emitted Raman photons (Equation 1) by adjacent particles, are more prevalent and will contribute to the Raman scattering collected by the optics. The increase in Raman scattering coincides

with significant attenuation for XRD measurements, which (for calibration samples) is attributed with point at which sufficient multilayers of particles are present to prevent XRD radiation from fully penetrating into the sample.^[36] Figure 2 also shows that the intensity has not achieved its maximum penetration depth, because it has not yet reached a plateau.^[28]

The relative response for the Raman band at 464 cm^{-1} is fairly constant for particles with diameters from about 1 to $7\text{ }\mu\text{m}$ (Figure 3) and closely follows the predicted proportion of crystalline material for particles with an amorphous/disordered structural surface layer of $0.03\text{-}\mu\text{m}$ depth, as described by Foster and Walker^[10] and Nagelschmidt et al.^[14] This demonstrates the relationship between the Raman area band response and the crystallinity of the particle. This finding is expected because the area intensity for both XRD and Raman spectroscopy^[40] is closely related to the molecular symmetry in the crystal structure.

For example, the principal Raman shift at 464 cm^{-1} is related to the oxygen (O) motion in the plane of Si–O–Si atoms of silicon (Si) and oxygen.^[41] Sato and McMillan^[41] demonstrated that it is the oxygen atoms that contribute most to the intense Raman band shift for quartz at 464 cm^{-1} , whereas the silicon atoms remain relatively stationary within their structural arrangement. Raman spectroscopy was significantly more sensitive when measuring particle size fractions below $1\text{ }\mu\text{m}$. It is possible that the Si–O–Si plane of molecular symmetry extends further into the surface layer of quartz and that some Raman scattering will still be emitted from Brillouin zones within the more disordered structure.^[40]

Most practical studies^[30,32,33,42,43] show an increase in Raman band intensity with decreasing particle size. However, Chio et al.^[31] found that the response increased with particle size when studying grains of quartz. Moreover, Hu et al.^[42] demonstrated a curved relationship for one crystalline polymorph where the Raman band response increases as particle size decreases and reaches a plateau before decreasing with decreasing particle size for the smallest particles. Hu et al.^[42] and Chio et al.^[31] studied relatively large particle sizes ($64\text{- to }215\text{-}\mu\text{m}$ and $11\text{- to }250\text{-}\mu\text{m}$ grain size, respectively), and both proposed that the analysis volume was a major influence affecting the measurement response and particle size; that is, particle size effects were reduced for larger particle sizes by increasing the laser sampling volume. This hypothesis is supported by the Monte Carlo simulations of Raman scattering in solids and powders studied by Duy et al.^[44] Duy et al.^[44] examined pellets and powders of pure lactose with different particle sizes ($38\text{ to }382\text{ }\mu\text{m}$ in diameter) using three different instrumental arrangements. Modelling the scattering of photons showed that

the scattering centre moves deeper into the particle and has a broader direction of scatter as the particle size increases. Duy et al.^[44] found that, in practice, the relationship between response and particle size was dependent on the geometric etendue of the instrument. The number of photons counted could increase with particle size when the detector area was much larger than the illumination area ($\times 4.2$) but could also decrease when the two areas were more similar ($\times 1.6$) because the laterally scattered photons on larger particles were not detected as efficiently. Previous method development work showed a decrease in measurement sensitivity when using the quartz reference material with the largest particle size (Quin B),^[24] suggesting that the instrument arrangement proposed for the measurement method was not efficiently collecting the laterally scattered photons for the very largest particles in this instance. In this research, reported herein, the minimum area of the focused spot was $4.5 \mu\text{m}^2$, which is slightly less than the median diameter of the particles of Quin B ($7 \mu\text{m}$). Moving to a lower magnification objective to increase the collection of laterally scattered photons will not improve the intensity of the Raman scatter, because the lower magnification with low numerical aperture has a smaller angle of light collection.^[45]

Fine grains studied in this work are smaller than those previously investigated and will scatter photons in a relatively localised area close to the particles' surface, which will be efficiently collected by the detector when using the current optics applied by the method proposed by Stacey et al.^[24]; that is, the proportion of laterally dispersed photons is small for particles in this study. These conditions may account for the plateau for Raman band intensity observed in this research, for fractions of quartz particles with median diameters between 1 and $7 \mu\text{m}$.

5 | CONCLUSION

Raman spectroscopy is a promising alternative to XRD for measurement of RCS and has a much lower LOD of around $0.2 \mu\text{g}$. The technique is highly correlated with XRD, when measuring the respirable and thoracic health-related particle size fractions of aerosols, generated from the cutting and polishing of natural and artificial stones, and demonstrates the useful application of Raman spectroscopy when analysing workplace exposure samples from stonemasonry activities. In particular, Raman spectroscopy has a distinct advantage over XRD when measuring crystalline silica in samples containing significant levels of zircon (about 50%).

The Raman band response for crystalline silica increases with mass loading of aerosols when using a

standard sized deposition area. The point at which the Raman band response increases, more than the slope for a linear relationship, coincides with the mass at which the XRD response attenuates as a result of X-ray absorption, that is, matrix absorption due to multiple layers. In effect, the XRD results would under-predict when the Raman spectroscopy measurements start to over-predict the 'true' value. This suggests that there was a relationship between X-ray absorption and scattering of Raman photons when the measurement conditions used in this study were applied.

The Raman band response is closely related to the predicted crystallinity of the quartz particle. A slight drop in intensity at $7 \mu\text{m}$ is probably due to the geometric etendue of the instrument.

ACKNOWLEDGEMENTS

Thanks to Ian Pengelly, Laurie Davies, Margaret Wade and Susan Hambling who reviewed the article, to Matthew Jackson and Alwyn Sowerby for the gravimetric, Jack Mellor who did some XRD analysis on the bulk materials and Lidia Malecka who helped graphically redraw some spectra (all Health and Safety Executive).

DISCLAIMER

The opinions expressed in this article are those of the authors alone and do not necessarily represent the policy or views of the Health and Safety Executive.

ORCID

Peter Stacey  <https://orcid.org/0000-0002-2689-2890>

REFERENCES

- [1] HSE, *EH75 Respirable Crystalline Silica, Variability in Fibrogenic Potency and Exposure-Response Relationships for Silicosis*, Health and Safety Executive, Richmond, Surrey, United Kingdom **2003**. Report No. ISBN:9780717621910.
- [2] L. Rushton, S. J. Hutchings, L. Fortunato, C. Young, G. S. Evans, T. Brown, R. Bevan, R. Slack, P. Holmes, S. Bagga, J. W. Cherrie, M. van Tongeren, *Br. J. Cancer* **2012**, 107(Suppl 1), S3.
- [3] T. Brown, J. W. Cherrie, M. Van Tongeren, L. Fortunato, S. Hutchings, L. R. *The Burden of Occupational Cancer in Great Britain Lung Cancer*, Health and Safety Executive, Bootle, Liverpool **2012**.
- [4] NIOSH, *Health Effects of Occupational Exposure to Respirable Crystalline Silica*, Publications Dissemination, 4676 Columbia Parkway, Cincinnati, OH 45226-1998, Department of Health and Human Services, Centers for Disease Control and Prevention, National Institute for Occupational Safety and Health, United States **2002** Contract No.: Publication No. 2002-129.
- [5] CEN, *EN 481:1993 Workplace Atmospheres—Size Fraction Definitions for Measurement of Airborne Particles*, European Committee for Standardisation, Brussels **1993**.
- [6] M. B. Ranade, M. C. Woods, F. L. Chen, L. J. Purdue, K. A. Rehme, *Aerosol Sci. Technol.* **1990**, 13(1), 54.

- [7] B. Brunekreef, S. T. Holgate, *The Lancet* **2002**, 360(9341), 1233.
- [8] HSE, *Methods for the Determination of Hazardous Substances, MDHS 101/2 Crystalline Silica in Respirable Airborne Dust, Direct On-Filter Analyses by Infrared Spectroscopy and X-Ray Diffraction*, Health and Safety Executive (HSE), Norwich, United Kingdom: Crown **2014**.
- [9] P. Stacey, E. Kauffer, J.-C. Moulut, C. Dion, M. Beauparlant, P. Fernandez, R. Key-Schwartz, B. Friede, D. Wake, *Ann. Occup. Hyg.* **2009**, 53(6), 639.
- [10] R. D. Foster, R. F. Walker, *Analyst* **1984**, 109(9), 1117.
- [11] J. Dodgson, W. Whitaker, *Ann. Occup. Hyg.* **1973**, 16(4), 373.
- [12] S. J. Page, *AIHA Journal* **2003**, 64(1), 30.
- [13] R. L. Gordon, G. W. Harris, *Nature* **1955**, 175(4469), 1135.
- [14] G. Nagelschmidt, R. L. Gordon, O. G. Griffin, *Nature* **1952**, 169(4300), 539.
- [15] E. J. King, *Occup. Med.* **1947**, 4(1), 26.
- [16] P. B. Dempster, P. D. Ritchie, *Nature* **1952**, 169(4300), 538.
- [17] D. V. Petrov, *J. Optic A: Pure Appl. Optics* **2007**, 9(8), S139.
- [18] G. Schweiger, *J. Aerosol Sci.* **1990**, 21(4), 483.
- [19] D. C. Doughty, S. C. Hill, *J. Quant. Spectrosc. Radiat. Transfer* **2017**, 188, 103.
- [20] P. Vargas Jentzsch, B. Kampe, V. Ciobotă, P. Rösch, J. Popp, *Spectrochim. Acta, Part a* **2013**, 115, 697.
- [21] P. Stacey, K. T. Mader, C. Sammon, *J. Raman Spectrosc.* **2017**, 48(5), 720.
- [22] L. Zheng, P. Kulkarni, M. E. Birch, K. Ashley, S. Wei, *Anal. Chem.* **2018**, 90, 6229.
- [23] J. A. Lynch, Q. T. Birch, T. H. Ridgway, M. E. Birch, *Ann. Work Expo. Health* **2018**, 62(5), 604.
- [24] P. Stacey, F. Clegg, J. Morton, C. Sammon, *Anal. Methods* **2020**, 12, 2757.
- [25] G. Gouadec, P. Colombar, *Prog. Cryst. Growth Charact. Mater.* **2007**, 53(1), 1.
- [26] S. Osswald, V. N. Mochalin, M. Havel, G. Yushin, Y. Gogotsi, *Phys. Rev. B* **2009**, 80(7), 075419.
- [27] B. Schrader, G. Bergmann, *Fresenius Zeitschrift Anal. Chem.* **1967**, 225(2), 230.
- [28] B. Schrader, A. Hoffmann, S. Keller, *Spectrochim. Acta, Part a* **1991**, 47(9), 1135.
- [29] D. A. Gómez, J. Coello, S. Maspoch, *Vib. Spectrosc.* **2019**, 100, 48.
- [30] M. V. Pellow-Jarman, P. J. Hendra, R. J. Lehnert, *Vib. Spectrosc.* **1996**, 12(2), 257.
- [31] C. H. Chio, S. K. Sharma, P. G. Lucey, D. W. Muenow, *Appl. Spectrosc.* **2003**, 57(7), 774.
- [32] H. Wang, C. K. Mann, T. J. Vickers, *Appl. Spectrosc.* **2002**, 56(12), 1538.
- [33] P. Kristova, L. J. Hopkinson, K. J. Rutt, *J. Phys. Chem. A* **2015**, 119(20), 4891.
- [34] C. Misra, M. Singh, S. Shen, C. Sioutas, P. M. Hall, *J. Aerosol Sci.* **2002**, 33(7), 1027.
- [35] P. Stacey, *Powder Diffr.* **2019**, 34(3), 251.
- [36] M. Mecchia, C. Pretorius, P. Stacey, M. Mattenklott, E. Incocciati, X-ray absorption effect in aerosol samples collected on filter media, in *Silica and Associated Respirable Mineral Particles*, (Eds: M. Harper, T. Lee), ASTM International, West Conshohocken, PA, United States of America **2013** 139.
- [37] A. D. Maynard, *J. Aerosol Sci.* **1999**, 30(9), 1227.
- [38] M. Chang, S. Kim, C. Sioutas, *Atmos. Environ.* **1999**, 33(15), 2313.
- [39] ISO B. 16258-1, *Workplace Air—Analysis of Respirable Crystalline Silica Using X-Ray Diffraction. Part 1. Direct-on-Filter Method (ISO)* ISO, editor, British Standards Institution, Chiswick, London **2015**.
- [40] D. Tuschel, *Spectroscopy* **2017**, 32(3), 26.
- [41] R. K. Sato, P. F. McMillan, *J. Phys. Chem.* **1987**, 91(13), 3494.
- [42] Y. Hu, H. Wikström, S. R. Byrn, L. S. Taylor, *Appl. Spectrosc.* **2006**, 60(9), 977.
- [43] A. Sparén, M. Hartman, M. Fransson, J. Johansson, O. Svensson, *Appl. Spectrosc.* **2015**, 69(5), 580.
- [44] P. K. Duy, S. Chun, H. Chung, *Anal. Chem.* **2017**, 89(22), 11937.
- [45] D. Tuschel, *Spectroscopy* **2017**, 32(9), 14.

SUPPORTING INFORMATION

Additional supporting information may be found online in the Supporting Information section at the end of this article.

How to cite this article: Stacey P, Hall S, Stagg S, Clegg F, Sammon C. Raman spectroscopy and X-ray diffraction responses when measuring health-related micrometre and nanometre particle size fractions of crystalline quartz and the measurement of quartz in dust samples from the cutting and polishing of natural and artificial stones. *J Raman Spectrosc.* 2021;1–13. <https://doi.org/10.1002/jrs.6110>

Supplementary Information

Raman spectroscopy and X-ray diffraction responses when measuring health-related micrometre and nanometre particle size fractions of crystalline quartz and its measurement in samples from cutting and polishing of natural and artificial stones.

Peter Stacey, Samantha Hall, Steven Stagg, Francis Clegg and Christopher Sammon

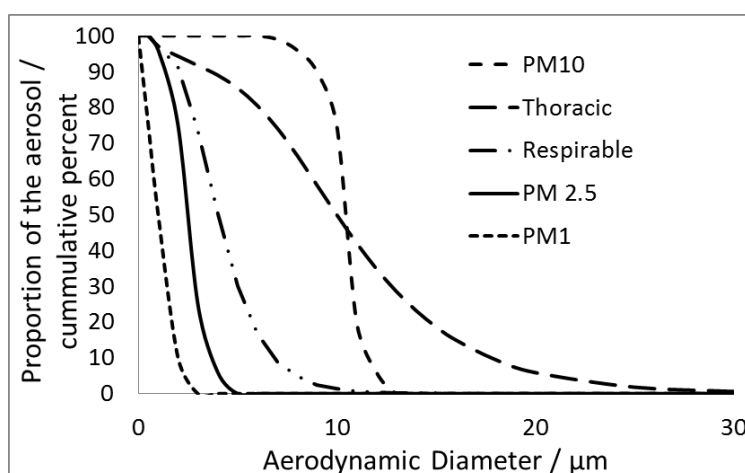


Fig S1. Diagram showing the differences between thoracic, respirable, PM10 and PM2.5 health related particle size definitions for occupational and environmental aerosol sampling.

Raman measurement conditions

An In-Via Raman microscope (Renishaw Ltd, Gloucester, UK) with near infrared laser (785 nm) excitation, CCD camera, and a grating with 1200 l mm^{-1} was used to collect Raman spectra between 314 and 906 cm^{-1} . Raman spectra were collected from 50 to 90 points inside a single predetermined area using x 20 microscope objective with a numerical aperture of 0.4. A schematic representation of the typical area selected by an operator from within which the instrument would collect spectra without further operator influence is shown in Fig S2.

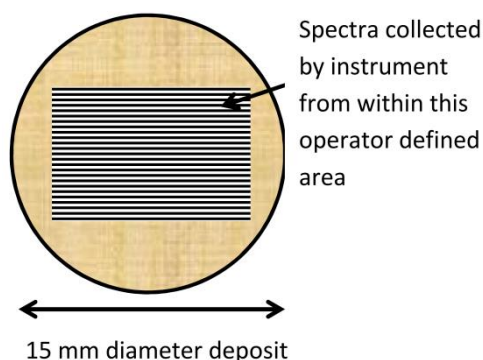


Fig S2: A schematic representation of a typical operator defined area for the Raman spectrometers' automated collected of spectra with an automated stage and laser focusing.

An automated microscope stage and focus facilitated an operator free data collection process. The automated focus was set to operate for every third field of view position. The laser was focused on the sample surface to obtain a sharp image. The area of the focused laser imaged by the microscope camera was an oval with diameters of 80 μm and 120 μm .

Step size between sampling points to collect spectra was not identical for each sample although each step was generally 600 μm to 800 μm . The diffraction minimum area of the focused laser was about 4.5 μm^2 , with a spatial lateral resolution of 1.2 μm . The integrated areas under the Raman band response at 464 cm^{-1} for α -quartz was measured by fitting a Gaussian model using the standard algorithms in the manufacturer's WiRE™ 4 software package for each spectrum collected. A background spectrum was not subtracted from the sample point spectra. Spectra were collected using the same laser power at each sampling point. At low mass loadings, each spectrum was collected by the instrument at 100 % power with three accumulations of seven seconds. The laser (Renishaw Ltd) had a power rating of 300 mW at source with 110 mW on the sample (without attenuation). Sampling times were reduced at higher loadings when the most spectra became saturated. The area obtained for the spectrum taken from each field of view was corrected for a reduced counting time by multiplying it by the count time used in the calibration (7 s) and dividing by the counting time applied for each spectrum. The average peak area response was calculated for each sample. Some spectra that were shown to

have saturated the detector were excluded from this calculation because they were unusable. Spectra with no band response above background at 464 cm^{-1} were recorded as zero. Trend lines were drawn to compare the average area counts and mass. A silicon (Si) wafer was measured before the analysis of a test sample and used as an external standard to compensate for daily fluctuations in laser intensity. The integrated area from the silicon wave number shift at 520 cm^{-1} was measured with a x 50 objective at 10 % laser power for 1 s. The average area measurement, calculated for each calibration and test sample, was corrected for fluctuations in laser intensity using the ratio between the area count collected when the silicon was first measured and the average collected on the day of the filter measurement. The stability of the average area count is shown in Fig S3. The cumulative average area measurement from each field of view collected within an analysis area on a sample is shown for four filters; one from each of the four stages in the Sioutas impactor collecting size fractions of $10\text{ }\mu\text{m}$ to $2.5\text{ }\mu\text{m}$ (570 μg deposit), $2.5\text{ }\mu\text{m}$ to $1\text{ }\mu\text{m}$ (350 μg deposit) $1\text{ }\mu\text{m}$ to $0.5\text{ }\mu\text{m}$ (188 μg deposit) and $0.5\text{ }\mu\text{m}$ to $0.25\text{ }\mu\text{m}$ (120 μg deposit). The variability of the average area measurement, including the most variable results at the start of the scan, ranged from 4 % to 9 %. This indicates that there is scope to reduce the sample analysis time for samples with a mass of α -quartz above 100 μg .

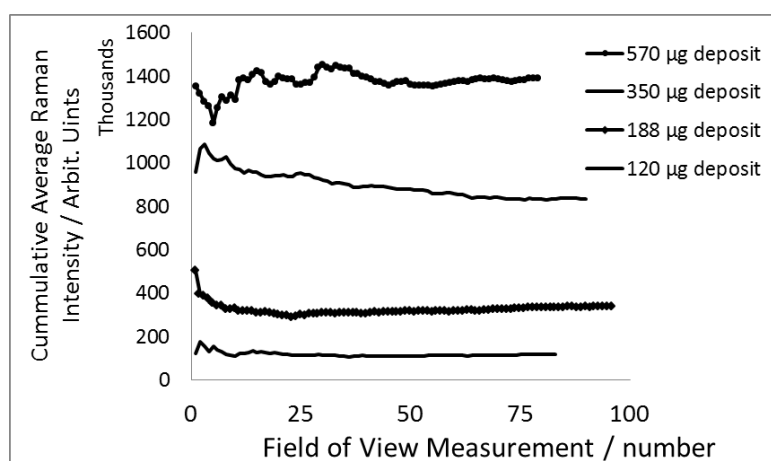


Figure S3. Stability of the cumulative average area counts for four filters containing α -quartz standard A9950 collected from each stage of a Sioutas impactor of $10\text{ }\mu\text{m}$ to $2.5\text{ }\mu\text{m}$, $2.5\text{ }\mu\text{m}$ to $1\text{ }\mu\text{m}$, $1\text{ }\mu\text{m}$ to $0.5\text{ }\mu\text{m}$ and $0.5\text{ }\mu\text{m}$ to $0.25\text{ }\mu\text{m}$.

X-ray Diffraction measurements

The quantity of α -quartz in test samples was also determined using an X-pert Pro MPD instrument (PANalytical Ltd, Cambridge, UK) with focusing Bragg-Brentano geometry. The instrument used the second set of standard instrumental conditions described in Table A1 of the International Standards Organization (ISO) standard method ISO 16258-1; 2015.³⁷ The instrument was fitted with a broad focus copper tube set at 50 kW and 45 mA, automatic scattering and receiving slits set to provide an illumination length of 18 mm, and an array detector with the detection area set at 2.12 degrees 2θ . The area of the three most intense XRD intensities of quartz at 2θ angles of, 20.9, 26.6 and 50.1 degrees 2θ were measured for 600 s, 420 s and 600 s respectively, for each 0.03 2θ degree interval over the two degree range centred on the measurement intensity position. The total sample analysis time was about 30 minutes. Tube intensity drift was corrected using the measurement of an aluminium plate as an external standard. The average of the two most consistent results obtained from each reflection was used for the comparison with the Raman results to compensate for the presence of XRD interference from other silicates.

Limits of detection

Raman spectroscopy

Limits of detection (LOD) for Raman were determined in two ways. Firstly, ten clean 37 mm diameter PVC filters were ashed, and each residue was recovered, and deposited into a 15 mm diameter area on a silver filter. Raman spectra were collected from 90 different fields of view from each silver filter with the ashed residue of the PVC filter, and any detected noise at about $464 \pm 4 \text{ cm}^{-1}$ was measured. The average area count was calculated for each blank sample and converted into a mass using the trend line coefficients determined for mass and Raman response. The LOD was calculated by multiplying the standard deviation of the ten results by 3. The LOD was also tested following another procedure.^{85, 172} The standard deviations of the background noise of 90 Raman spectra from five of the silver filters containing the ashed residue of the clean PVC filters were calculated using a Matlab, 2011a computational script

(Mathworks, Cambridge, UK). The script was applied to plot a line of best fit using a polynomial equation between 400 cm^{-1} to 520 cm^{-1} wave numbers i.e. the range which encapsulates the Raman Si-O-Si band. The calculated standard deviations of the data points from the best fit line were multiplied by 3 to estimate a 99% level of confidence of the blank. This provides an estimate of the LOD from the noise of the background in a single spectrum.

X-ray diffraction

LODs were calculated for the three main XRD intensities for α -quartz at 20.9, 26.6 and 50.1 degrees 2θ . The ten 37 mm diameter PVC filters measured by Raman were also measured using XRD. A one degree base line was drawn through the middle of the background noise centred on the midpoint under each XRD intensity position using Dataviewer™ software (PANalytical Ltd). The area intensity of the noise above each base line was recorded and a standard deviation was calculated for all ten area measurements for each intensity position. Each standard deviation was multiplied by 3 to obtain the 99 % level of confidence for the blank. This provides the lowest LOD estimate where the probability of false negatives is 50%. The LOD was also determined using the method described previously for which the average noise under each reflection position was modelled in five samples using a polynomial curve.¹⁷² The standard deviation of the noise collected for each XRD scan was then calculated. The LOD, in terms of area counts per second, was estimated by multiplying the standard deviation of the noise by 1.66. This provides the area intensity that has an approximate intensity height to noise ratio of 3, where noise is three standard deviations. The LOD was then checked measuring samples of aliquots from a suspension with known mass values. The average standard deviation was multiplied by the mass response trend line coefficients to obtain a mass value. The intensity for the mass value of $3\text{ }\mu\text{g}$ has an average corrected height intensity which is about 3.1x the noise.

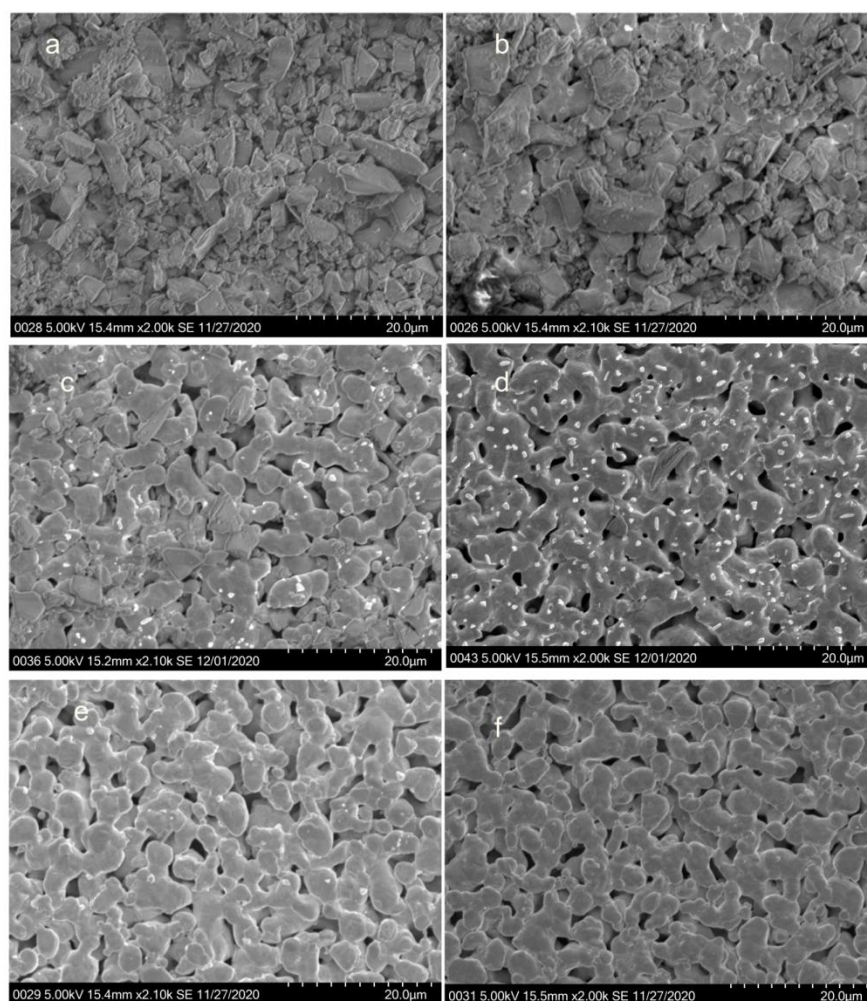


Figure S4. Scanning Electron Microscope pictures for the density of, a) 1000 μg ; b) 500 μg ; c) 100 μg ; d) 15 μg ; e) 7.5 μg and f) 0 μg of HSE α -quartz reference material A9950 deposited onto silver filters with a 0.45 μm pore size. The scale on the bottom right hand side of each photograph is 20 μm . Photograph 'b' showed some gaps between particles, photograph 'c' showed some particles in most field of view, photograph 'd' showed only one of two particles in each field of view. Particles are densely packed at high and scattered at low mass loadings.

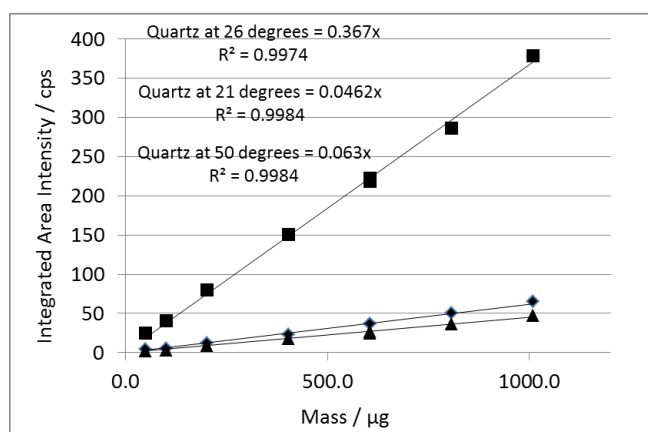


Figure S5. Calibration for the XRD when measuring aliquots of the United Kingdom's, Health and Safety Executive respirable crystalline silica standard A9950 pipetted into a 15 mm diameter area on a silver filter.

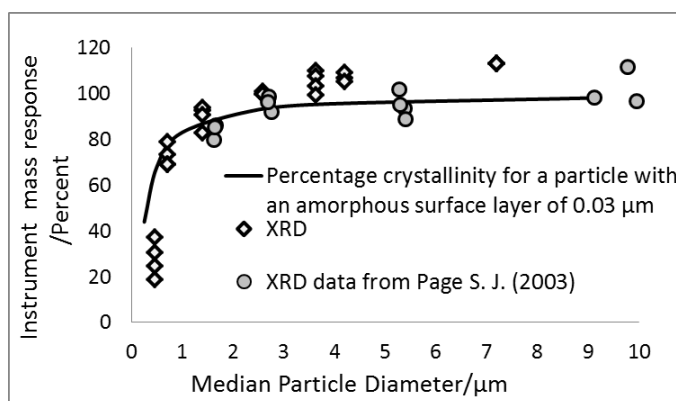
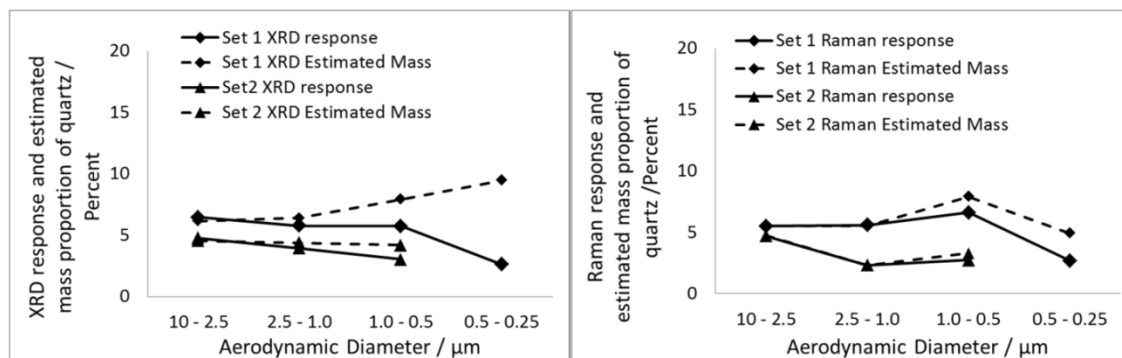


Figure S6. The relative XRD response with particle size obtained in this research compared with results obtained from Page S (2003).¹⁴⁸

Diorite stone



Sintered stone S1

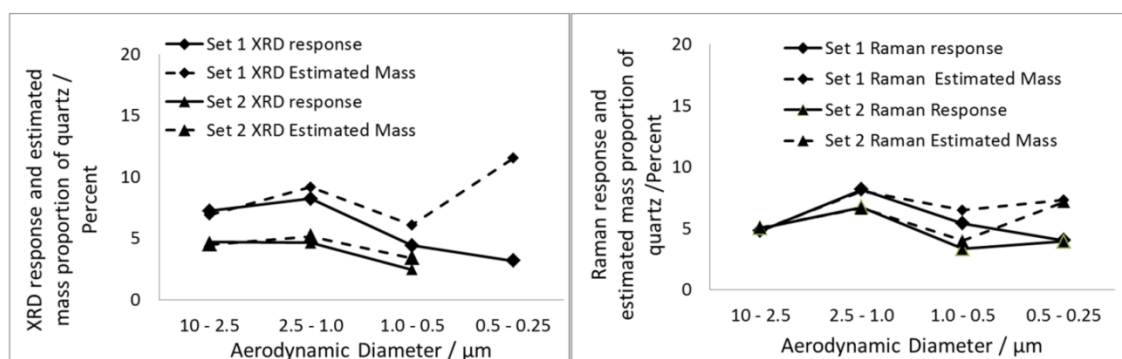
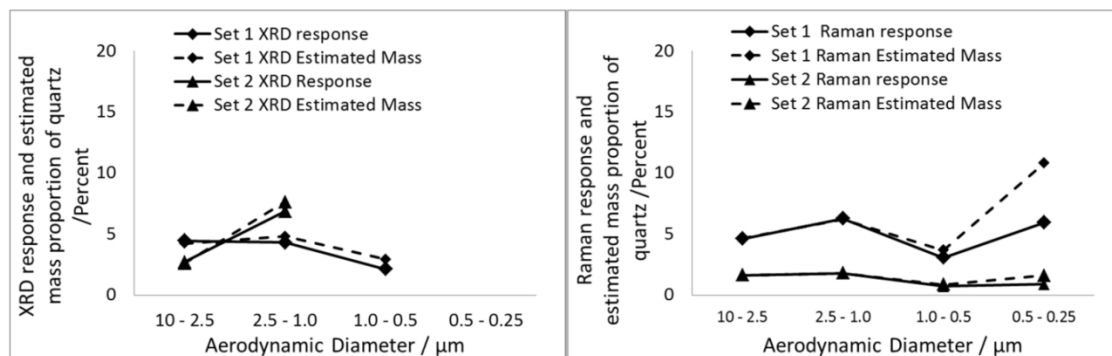


Figure S7. A comparison of X-ray diffraction and Raman measurements from different particle size fractions from samples collected from the Sioutas impactor during cutting of Diorite and sintered stones

Diorite stone



Sintered stone

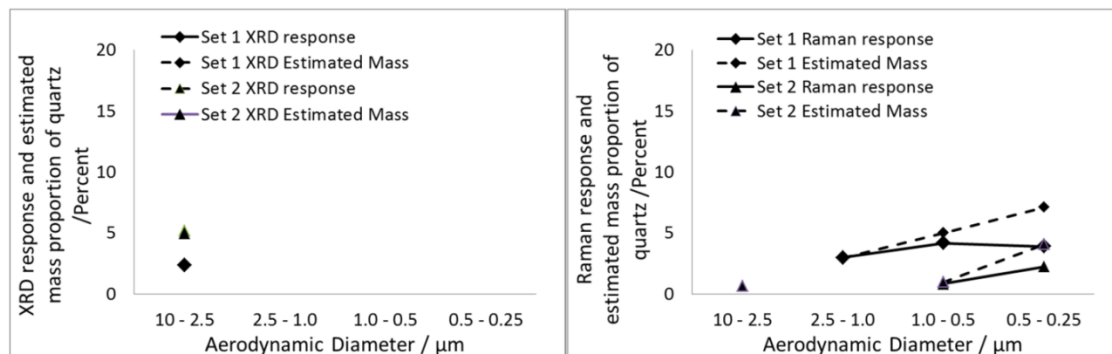


Figure S8. A comparison of X-ray diffraction and Raman measurements from different particle size fractions from samples collected from the Sioutas impactor during polishing of Diorite and sintered stones.

Raman bands and X-ray diffraction intensities

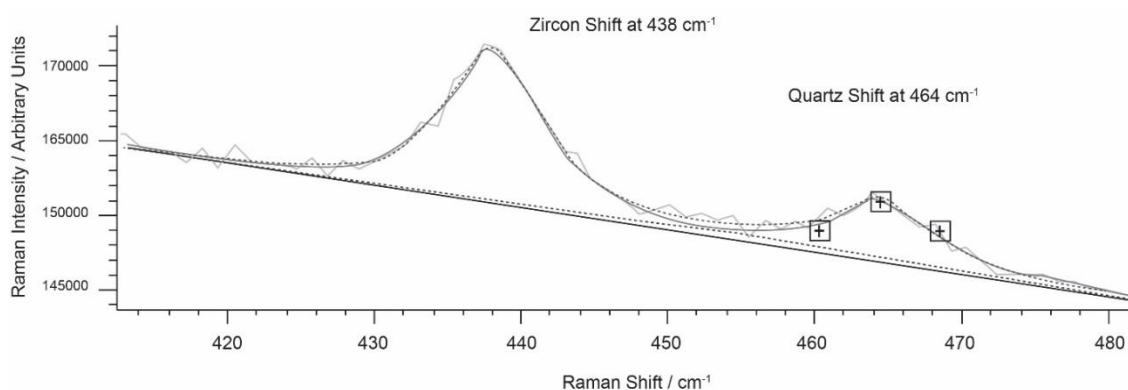


Figure S9. The Raman spectra for α -quartz with zircon taken in a single field of view at 40 x magnification. The dotted lines show the fitted profile using the default option in the instruments WIRETM software.

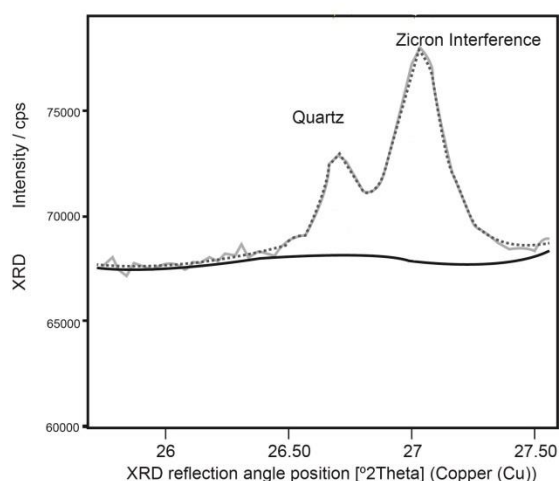


Figure S10. An XRD scan for the principle intensity of α -quartz at 26.6 degrees 2θ in the presence of a significant quantity of zircon. The dotted lines show the fitted profile using a profile fitting algorithm supplied with the instruments software XpertTM Highscore software.

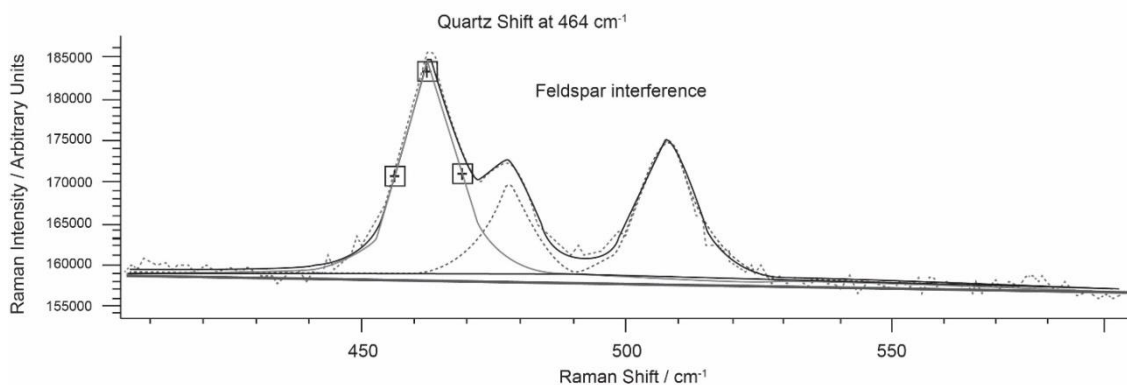


Figure S11. A Raman spectrum taken from a single field of view showing α -quartz in the presence of feldspar at x40 magnification. The dotted lines show the fitted profile using the default option in the instruments WIRE™ software.

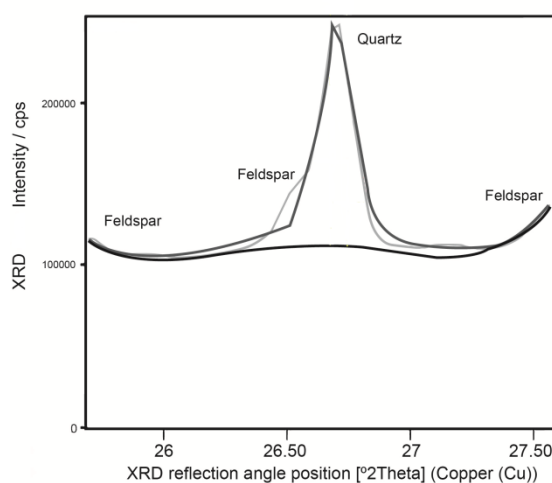


Figure S12. An XRD scan for the principle intensity of α -quartz at 26.6 degrees 2θ in the presence of a significant quantity of a Feldspar mineral. The black lines show the fitted profile using a profile fitting algorithm supplied with the instruments software Xpert™ Highscore software.

Chapter. 6 A comparison between partial least squares and principal component regressions for analysis of particulate in coal dust.

Multicomponent measurement of respirable quartz, kaolinite and coal dust using Fourier Transform Infrared spectroscopy (FTIR): A comparison between partial least squares and principal component regressions.

Peter Stacey, Francis Clegg, and Christopher Sammon

Published: - UK Government Licence

Annals of Work Exposures and Health, Volume 66, Issue 5, June 2022, Pages 644–655, <https://doi.org/10.1093/annweh/wxab081>

Infrared analysis is quick (less than 4 mins), less expensive than XRD and is a potentially portable instrument. Its main limitation is the potential for absorbencies from other silicate minerals to be coincident with those of α -quartz. The goal of this work was to investigate differences between two common chemometric methods, to compare with the performance of UK regulatory approach and to ascertain if the chemometric methods could potentially provide a sufficiently reliable measurement of more than one component.

Original Article

Multicomponent Measurement of Respirable Quartz, Kaolinite and Coal Dust using Fourier Transform Infrared Spectroscopy (FTIR): A Comparison Between Partial Least Squares and Principal Component Regressions

Peter Stacey^{1,2,*}, Francis Clegg² and Christopher Sammon²

¹Health and Safety Executive, Harpur Hill, Buxton, Derbyshire, SK17 9JN, United Kingdom; ²Sheffield Hallam University, Materials and Engineering Research Institute, Sheffield, S1 1WB, United Kingdom.

*Author to whom correspondence should be addressed. E-mail: peter.stacey@hse.gov.uk

Submitted 12 March 2021; revised 4 September 2021; editorial decision 5 September 2021; revised version accepted 10 September 2021.

Abstract

Exposure to respirable crystalline silica (RCS) is potentially hazardous to the health of thousands of workers in Great Britain. Both X-ray diffraction (XRD) and Fourier transform infrared (FTIR) spectroscopy can be used to measure RCS to assess exposures. The current method outlined in the Health and Safety Executive's (HSE) Methods for the Determination of Hazardous Substances (MDHS) guidance series is 'MDHS 101 Crystalline silica in respirable airborne dust - Direct-on-filter analyses by infrared spectroscopy or x-ray'. This describes a procedure for the determination of time-weighted average concentrations of RCS either as quartz or cristobalite in airborne dust. FTIR is more commonly employed because it is less expensive, potentially portable and relatively easy to use. However, the FTIR analysis of RCS is affected by spectral interference from silicates. Chemometric techniques, known as Partial Least Squares Regression (PLSR) and Principal Component Regression (PCR), are two computational processes that have the capability to remove spectral interference from FTIR spectra and correlate spectral features with constituent concentrations. These two common chemometric processes were tested on artificial mixtures of quartz and kaolinite in coal dust using the same commercially available software package. Calibration, validation and prediction samples were prepared by collecting aerosols of these dusts onto polyvinylchloride (PVC) filters using a Safety in Mines Personal Dust Sampler (SIMPEDS) respirable cyclone. PCR and PLSR analyses were compared when processing the same spectra. Good correlations between the target values, measured using XRD, were obtained for both the PCR and PLSR models e.g. 0.98–0.99 (quartz), 0.98–0.98 (kaolinite) and 0.96–0.97 (coal). The level of agreement between PCR and PLSR was within the 95% confidence value for each analyte. Slight differences observed between predicted PCR and PLSR values were due to

What's Important About This Paper?

Incidence of worker ill health caused by exposure to aerosols containing hazardous particulate, like respirable crystalline silica (RCS), remains an issue of international concern. Fourier Transform Infrared (FTIR) instruments are relatively inexpensive, portable and potentially measure many agents simultaneously, but interference can limit accuracy. This work explores the use of two chemometric data processing methods—principal component and partial least squares regression—that use commercially available software, to strip out interference from FTIR spectra. Both methods improved the accuracy of RCS measurement and provided a more complete characterization of a worker's exposure to a number of substances with a single measurement on one sample.

the number of optimal principal components applied to each chemometric process. The presence of kaolinite in these samples caused an 18% overestimation of quartz, for the FTIR, when following MDHS 101 without a chemometric method. Chemometric methods are a useful approach to obtain interference-free results for the measurement of RCS from some workplace environments and to provide a multicomponent analysis to better characterise exposures of workers.

Keywords: quartz, respirable crystalline silica, coal dust, kaolinite, principal component regression, partial least squares regression

Introduction

Crystalline silica is a generic name for a group of minerals that have the same chemical composition of silicon (Si) and oxygen (O) but with different crystalline structures known as polymorphs. The most common polymorphs of crystalline silica is quartz. Respirable dust is a health-related term for aerodynamic sizes of particles that enter the alveoli of the lung. The respirable definition includes particles with aerodynamic diameters of less than 16 μm and a median of 4 μm (CEN, 1993). Inhalation of respirable crystalline silica (RCS) is a potential hazard to the health of 560,000 workers in Great Britain (Brown *et al.*, 2012) because exposure to aerosols containing RCS can cause lung diseases like silicosis (HSE, 2003), lung cancer (Brown *et al.*, 2012) and chronic obstructive pulmonary disease (COPD) (Bergdahl *et al.*, 2004). One established approach to assess exposures is to measure a portion of the aerosol entering the breathing zones of workers. The workplace exposure limit for an 8-h time-weighted average exposure to RCS during a working shift in Great Britain is currently 100 $\mu\text{g m}^{-3}$ (HSE, 2005). Samples of aerosol are collected onto a filter using a respirable sampler. The most common respirable sampler used by the Health and Safety Executive is the Safety in Mines Personal Dust Sampler (SIMPEDS) which uses a cyclone action at a flow rate of 2.2 L min⁻¹. The two most common analytical techniques universally employed for RCS measurement of aerosol particulate on filters are x-ray diffraction (XRD) and Fourier transform infrared spectroscopy (FTIR). FTIR instruments measure

the absorption of infrared energy from Si–O vibrations, whereas XRD measures the reflections from the crystalline structure of the silica. Infrared measurements of RCS are more affected by potential mineral interference from other silicates present in the sample than XRD, because silicate mineral structures contain similar tetrahedral arrangements of Si and O atoms and so have similar Si–O vibrations. In addition, crystalline silica polymorphs and amorphous forms of silica also have similar convergent FTIR spectra patterns (Bye, 1994) affecting accurate quantification. FTIR instruments are more widely used to measure RCS in aerosol dust collected onto filters because they are currently much cheaper than using XRD and some models are more portable.

The development of portable (often battery powered) and low-cost infrared instruments enables the potential for the measurement of end-of-shift samples at the worksite (Cauda *et al.*, 2016). Portable instruments have an advantage since the hygienist can potentially measure and report exposure results soon after a work shift or work task is completed. The time taken to improve emission controls and lower airborne RCS concentrations emitted from the process can be significantly reduced, since it is not necessary to wait for a result from an external laboratory, which can take several weeks. On-site instruments rely on the application of a direct on-aerosol filter measurement method, which is the standard RCS analysis approach used in the series of methods developed by the Health and Safety Executive (HSE) in Great Britain (Foster and Walker, 1984, HSE, 2014) known as Methods

for the determination of hazardous substances (MDHS 101: Respirable crystalline silica by infrared and x-ray. Hence, the MDHS 101 measurement approach for RCS involves the analysis of the dust deposited on the aerosol sampling filter without any attempt to treat the dust to remove interference. Early work (Pickard *et al.*, 1985) demonstrated no significant difference in direct on-aerosol filter FTIR results compared with a direct on-aerosol-filter XRD method when measuring the same samples from foundries, brickworks and potteries. However, other researchers (Lee *et al.*, 2013) measuring quartz in coal dust samples, found significant interference from kaolinite when using indirect methods (0.2–23%); where the dust is recovered from the aerosol filter and concentrated onto a smaller filter for analysis (MSHA, 1994). In Great Britain, analysis of samples of coal for quartz followed an indirect infrared potassium bromide (KBr) disc analysis approach involving a furnace to heat the dust and decompose the kaolinite (Dodgson and Whitaker, 1973). However, this process involves the potential for sample loss during sample handling and processing. Currently, skilled judgement from a trained analyst is needed to interpret FTIR spectra with spectral interference. The subjective nature of this may add to the variability of results. The increased availability of low-cost FTIR portable equipment for on-site measurement may diversify the range of people involved in the interpretation of results, including those in roles who are not previously trained for this task. The potential for chemometric methods to accurately measure without the need for further spectral interpretation may lead to a ‘black-box’ approach facilitating an instant and less expensive analysis of a worker’s exposure. Currently, the chemometrics model may need a check to verify that it works in a particular workplace because it is not yet known if they universally applicable. However, the addition of workplace-specific samples, where target values are derived from a reference laboratory, could resolve any site-specific issues.

The purpose of this article is to compare the performance of both partial least squares regression (PLSR) and principal component regression (PCR) for the measurement of quartz collected on aerosol sampling filters and to compare the XRD method with the FTIR method in MDHS 101. Coal dust itself is also a potential cause of lung disease (Ross and Murray, 2004) so we also assessed if the parameters selected by the chemometric models can also quantify other major and potentially hazardous components of these samples.

Chemometric methods

Current regulatory analytical methods for the measurement of RCS using infrared instruments (NIOSH, 2004,

HSE, 2014) measure the peak height, from the base line to the maxima, of the characteristic absorbance bands for quartz at 800 cm^{-1} and 780 cm^{-1} . These methods use the Beer–Lambert Law assumption which states the attenuation of absorbance is directly proportional to the concentration of the substance and a constant known as the molar extinction coefficient. The model for the calibration is based on a simple regression between two sets of coordinates, where x is the mass of the analyte and y is the measured response. This approach is applied because most calibrations are conducted on test samples containing pure RCS (quartz or cristobalite). Correction due to the presence of other components is addressed at a later stage in the analytical method.

Chemometrics is a mathematical process that can examine the whole FTIR spectrum and access the influence of different infrared active components with overlapping absorbance from interferences (Breen *et al.*, 2008, Weakley *et al.*, 2014). The application of chemometric models to resolve the influence of amorphous silica on the quantification of crystalline silica in an FTIR spectrum was first applied in the 1990’s by Bye (1994), who employed PLSR to resolve artificial mixtures of crystalline silica (quartz and cristobalite) and amorphous silica. More recently, (Miller *et al.*, 2016) used PLSR to resolve the influence of kaolinite from the measurement of quartz on coal dust samples when using portable infrared instruments.

Chemometric techniques, like PLSR and PCR, are based on a technique known as Principal Component Analysis (PCA). The PCA is a way of reducing large amounts of data to a limited number of characteristic vector quantities (Jolliffe and Cadima, 2016). Spectral data, consisting of a series of paired points representing an absorbance at specific wavenumbers, is an ideal format for PCA. This technique is usually applied when there are multiple variables in both x and y . In this case discussed herein, y represents the multiple combinations of different constituents (masses of coal dust, kaolinite and quartz) and x are multiple versions of absorbencies from the resulting scans obtained. The PCA process introduces new coordinates by maximising the co-variance of these data and reducing the multiple points of x or y to vectors known as principal components (PC). The technique essentially provides vector coordinates for the bands that have a magnitude in the assembled spectra and are most important for each component. The PCA can provide a vector value (score) for each matrix component by fitting a line to the variables and determining the distance of a point to an origin. In PCR, the first stage of the process is to determine the direction of each absorbance from the mean value. This

PCR process then establishes a relationship for each substance in the matrix between the calibration spectra (associated with mass of coal dust, kaolinite, and quartz) with the most correlated vector values. The difference between PCR and PLSR is that PCR interrogates only the spectral information i.e. the absorbencies, whereas PLSR examines both spectral and concentration data (Hemmateenejad *et al.*, 2007). Both processes analyse multiple regressions to test the resulting models, however, PLSR contains separate calibrations for each component. PLSR has been widely used with infrared instruments to measure complex mixtures of components including recent studies investigating the measurement of quartz in Pittsburgh coal dust (Miller *et al.*, 2016) and a PLSR using a modified Monte Carlo process to eliminate unimportant spectral variables (Weakley *et al.*, 2014). The performance of PCR and PLSR has been studied and the differences between results are not generally considered significant although PLSR is generally preferred for FTIR analysis. The main difference is that the PLSR calibration often requires fewer latent variables for its prediction (Wentzell and Vega Montoto, 2003) which may increase the PLSR models efficiency when measuring mass values close to the background, since this reduces the likelihood of over modelling the background noise.

Method

Overview of the analytical process

A schematic representation of the analytical measurement process used in this study is shown in Figure 1.

The PVC filter is itself a spectral component that affects absorbance, so current direct on-aerosol filter analysis methods for quartz (e.g. MDHS 101) involve the subtraction of a spectrum of an unused PVC filter (HSE, 2014; Hart *et al.*, 2018). Before sample collection, unused PVC filter blanks were analysed using FTIR to determine their spectral profile. The unused filters were then weighed. Aerosols were generated and the filters were loaded with test mixtures following the description outlined below. Gravimetric analysis was performed to assess the total gravimetric mass of the loaded material and to later calculate the mass of coal dust. XRD was used to determine the mass of quartz and kaolinite in the test mixtures and the samples were later scanned using FTIR. The XRD measured values for the quartz and kaolinite were used as the target values assigned to each sample for use in the chemometric modelling and for comparison with FTIR values determined using MDHS 101.

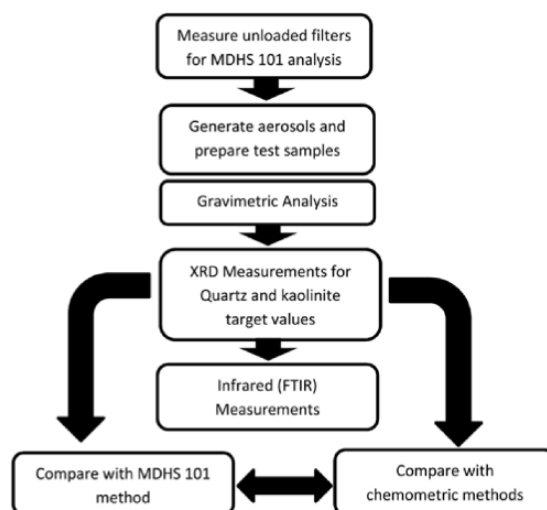


Figure 1. The analytical process.

Sample preparation

Several approaches for the preparation of calibration standards are possible; however, to be predictive of samples from different workplaces, the calibration and validation mixtures must contain representative proportions of relevant components i.e. the constituent minerals.

In this study, artificial mixtures were generated so that each component of interest could be evaluated and quantifiable. The proportions of each significant component were altered to decrease any collinearity within the model and increase the variability of component concentrations. Test filters containing mixtures of respirable dust were prepared following the method described in MDHS 101 (HSE, 2014) and Stacey (2019). Aerosols of a single constituent or mixtures of constituent minerals were generated in a glass dust cloud generator of the type shown in MDHS 101 (HSE, 2014). The test dust was placed in the bowl at the bottom of the generator and aerosolised using a short burst of pressurised air. The apparatus was earthed (grounded) to reduce the agglomeration of particles due to charge. Test samples of these aerosols were collected onto 25 mm diameter 5 µm pore size PVC filters (SKC Ltd, Blandford Forum, Dorset, UK) using a SIMPEDS (Casella UK Ltd, Bedford, United Kingdom) at a flow rate of 2.2 L min⁻¹. The flow rate through the respirable sampler was calibrated to its nominal value using a TSI 4100 flow calibrator (TSI Inc, Shoreview, USA). The bulk powders used for aerosol generation and their origin are listed in Table 1. Mineral samples can potentially contain other trace minerals as contaminants, which may affect the reliability of their quantification. Each powder was scanned using XRD

Table 1. Respirable powders included in the study and their origin.

Powder	Origin
Respirable Quartz	HSE reference power A9950, Buxton, United Kingdom (UK)
Kaolinite	Georgia, United States of America
Coal Dust (Coal 1)	Durrans Graded Coal Dust 30, James Durrans & Sons Ltd, Sheffield, UK
Coal Dust (Coal 2)	Council for Scientific and Industrial Research (CSIR), Pretoria, South Africa

to assess the presence of other potential mineral components. XRD scans for coal dust from a variety of sources are shown in [Figure S1 \(Supplementary Information\)](#). Coal dusts identified as Polish, South African, Pittsburgh (United States of America), Coal Rank 502 (a coke coal) and Durrans were measured. The South African coal dust differs from the others because it was collected from ventilation filters in a mine, whereas the other samples were collected from pulverised coal. The mineral composition was similar for each coal dust. Quartz (SiO_2), kaolinite ($\text{Al}_2\text{Si}_2\text{O}_5(\text{OH})_4$), a mica type named muscovite 2M1 or 3T ($\text{KAl}_2(\text{AlSi}_3\text{O}_{10})(\text{OH})_2$), pyrite (Fe_2S) and some trace reflections that could be associated with calcite (CaCO_3), and a microcline (KAlSi_3O_8) were identified in the majority of samples. The most significant reflections were for quartz and kaolinite. The coal identified as Polish was relatively quartz-free although it had noticeable kaolinite reflections. Durrans coal was selected for further work because it had lower quartz and kaolinite reflections. FTIR scans for Durrans coal deposited onto a PVC filter are shown in [Figure 2](#) and compared with an unused filter.

Determination of the sample 'assigned' independent target value

XRD following the MDHS 101 method ([HSE, 2014](#)) was used as the reference method for the assigned values since XRD is less influenced by the presence of kaolinite as interference. The quantity of quartz and kaolinite in all samples was determined using an X-pert Pro MPD x-ray diffractometer (Malvern PANalytical Ltd, Cambridge, UK) with focusing Bragg-Brentano geometry. The XRD measurement conditions are described in the [supplementary information](#). The calibrations for quartz and kaolinite are shown in [Figures S2 and S3 \(Supplementary information\)](#).

The mass of coal was determined by subtracting the mass values for quartz and kaolinite from the gravimetric mass of the dust loaded onto each PVC filter. Filter weighing was conducted using a XP2U Mettler microbalance with a readability of $1\text{ }\mu\text{g}$ (Mettler-Toledo Ltd, Leicester, United Kingdom) in a balance room with controlled temperature and humidity maintained at 25°C and 50% relative humidity. Static charge was eliminated from the PVC filters before weighing using an Haug deioniser (Mettler-Toledo Ltd, Leicester, United Kingdom).

FTIR analysis

A Perkin Elmer Frontier FTIR instrument was used with Quant software (Perkin Elmer UK Ltd, Beaconsfield, UK). The standard conditions in MDHS 101 were used for FTIR analysis ([HSE, 2014](#)). Thirty-two scans were collected from 560 cm^{-1} to 1000 cm^{-1} with a resolution of 4 cm^{-1} . A previous study ([Miller et al., 2016](#)) used a resolution of 2 cm^{-1} but this takes longer and was found to make little or no difference to sensitivity ([Figure S4, Supplementary Information](#)). With a scan speed of 2 cm s^{-1} the total sample measurement time was less than 4 min. Spectral effects due to external factors were compensated for by running a background scan prior to analysis of each batch of filters.

Background correction

The first-order derivative background treatment was compared with the spectral subtraction approach of MDHS 101 using PVC filters containing pure quartz standard A9950; to assess if the first-order derivative approach could replace the current procedure. The same standards were used for calibration and prediction and both approaches used the Beer-Lambert approach where the absorbance is proportional to the concentration. The only difference between the two approaches was the processing of the spectra before analysis. The absolute and relative differences were compared.

The chemometric process

The chemometric process involved the collection and measurement of three independent sets of samples; one for calibration, one for validation of the model and another to serve as a prediction set to assess how well the models compare. The calibration test samples included samples of pure analyte and combinations of mixtures of the constituent components (quartz, kaolinite and Durrans coal dust). The validation and prediction samples generally included all three constituents, although a small number of samples were included with, no kaolinite, just kaolinite and some samples containing only quartz obtained from the AIR

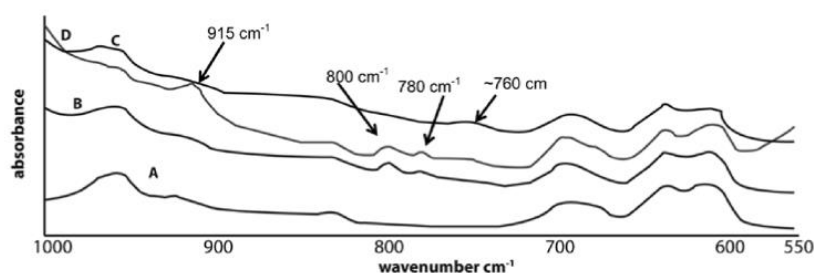


Figure 2. FTIR scans between 560 cm^{-1} and 1000 cm^{-1} wavenumbers showing a unloaded blank PVC filter (A), a PVC filter loaded with about 1.3 mg of Durran's coal dust and a mass of quartz (B), a PVC filter loaded with 1 mg of Durran's coal dust (C), and a sample of about 1.3 mg of coal dust from South Africa (D).

proficiency testing (PT) programme (LGC Ltd, Teddington, UK). AIR PT is a quality assurance programme that distributes samples to assess the proficiency of laboratories measuring contaminants in workplace atmospheres. Durran's coal dust (Coal 1) was used for the preparation of calibration and validation samples. Prediction samples to test the models also included coal dust from a South African mine (Coal 2). A list of the samples, loaded masses and their constituent proportions are presented in [Tables S2 to S4 \(Supplementary Information\)](#). The same samples were used for the PCR and the PLSR model.

Processing parameters

The spectral range was constrained in favour of obtaining a scan of the area of interest for the measurement of quartz. [Miller *et al.* \(2016\)](#) found that wavenumbers between 560 cm^{-1} and 1000 cm^{-1} contained the wavenumbers of most significance for the measurement of quartz in coal dust. There were few spectral wavenumber ranges that were not affected by the mineral constituents. The measured spectrum in the analysis was not subdivided further (e.g. to specifically reduce the proportion of redundant spectra to improve kaolinite or coal dust measurement). Unlike other work ([Weakley *et al.*, 2014](#), [Miller *et al.*, 2016](#)), the spectrum of the loaded test sample was not corrected by subtraction of a spectrum of an unused PVC filter. A first-order derivative was applied to each scan to normalise the influence of the spectral bands from the filter material. A beneficial effect of the application of the first-order derivative is to suppress off-sets (i.e. variation about the expected vibrational absorbencies). The most common reason for this to occur in this work was the difference in absorbance due to the depth of the PVC filter and the sample loading i.e. the smaller the sample loading the more spectral interference from the filter. A second-order derivative was attempted because this process is potentially more sensitive to low analyte mass values; however, it tended to underestimate the higher loadings and was not used because it was not applicable

to the wider analytical range. No further weighting or normalisation was applied for processing the spectrum before applying the PLSR or PCR model.

All data were centred around the mean for the principal component analysis. The PCR model was centred around the mean for y (absorbance) and the PLSR model was centred around the mean for both x (constituents and masses) and y (constituents and absorbance). The maximum possible number of components was not restricted. The commercial software uses a validation protocol during the calibration stage, as well as an independent validation stage after calibration, to assess its predictive ability. Each calibration spectrum is sequentially removed and predicted from the recalculated model. The prediction error is a measure of all the differences obtained by the model during the calibration validation process. The validation set included both samples prepared with Durran's and South African coal dust and the results were corrected for a slight bias for kaolinite which the software applied to all analytes.

The influence of the number of principal components on the values reported for quartz in the prediction set was investigated using the PCR model. The similarity between values predicted by PCR with different numbers of PCs and the XRD assigned values were assessed from the 95% level of confidence intervals for the slope and intercept of their regressions obtained from Excel (Microsoft Corp, United States). Ideally, the slope value should not be significantly different from 1.00 and the intercept should not be significantly different from zero. The similarity between the PCR and the PLSR models was also determined in the same way, once the models were established with numbers of PCs that were a close match to the XRD assigned values.

Results and discussion

Calibration results

There were 62 and 19 samples in the calibration and validation sets, respectively. Statistical estimates generated

by the software for the quantification of each component using all 62 samples are shown in Table 2.

The calculated values from PCR and PLSR calibration and validation sets compared with the assigned value of quartz determined using XRD are shown in Figure 3.

A set of thirty samples used in the prediction set containing quartz in artificial mixtures with added kaolinite and South African coal dust (Coal 2) were prepared and evaluated against their measured quartz values (Table S3 supplementary information).

Evaluation of the number of principal components (PC)

The software package computationally processed the PCR model for quartz with six PCs, however, the software options for PCR allowed the user to specify the number of principle components for each analyte. Therefore different numbers of principle components were assessed to check if six was the best for prediction as well as to assess trends in the prediction values. Prediction values, obtained by processing PCR calibration with different numbers of PCs (3 to 7), were plotted against the assigned target values (Figure S5, Supplementary Information). The regression and average differences are provided in Table S1 (Supplementary Information). Changing the number of PCs alters the slope and intercepts coefficients. The slope of the regression line between the predicted model value and the assigned XRD value for the trend line with five PCs was one of two PCRs that were not significantly different from the ideal 1:1 trend line slope from the measured XRD values indicating a close statistical relationship (95% confidence interval of the slope was from 0.99 to 1.11). The average difference was $-6.5 \mu\text{g}$ with values for the slope and intercept of 1.05 and $-10.7 \mu\text{g}$, respectively. Predicted values from the PCR model with three PCs were also not significantly different from the XRD assigned values. The model with 3 PCs had the least

average difference with the XRD values ($0.86 \mu\text{g}$) and a better fitted linear relationship with the target values (Slope = 0.996 and Intercept = $1.1 \mu\text{g}$). The PCR model with five PCs was selected for further work to compare with the equal number of PCs selected by the PLSR method.

Prediction close to the XRD limit of detection (LOD)

Six prediction samples of South African coal (shown in Figure 4) dust contained very low masses of quartz ($7.7\text{--}9.5 \mu\text{g}$). These samples provided an opportunity to test whether the reduction in the number of PCs improved the LOD for quartz. Large negative values for these six samples (about $-20 \mu\text{g}$) occurred when the number of PCs was high ($n = 7$), which is associated with the larger intercept of this model (Table S1, Supplementary Information). However, poor predictions can also occur if the number of PCs is too low since the variances in data might not be represented (Breen *et al.*, 2008). For the 5 PC model, the predicted quartz values for the six samples were close to zero and ranged from $-6.1 \mu\text{g}$ to $1.1 \mu\text{g}$ (average was $-1.5 \mu\text{g}$), suggesting that the method is unable to reliably predict very low masses of quartz close to the XRD limit of detection of about $8 \mu\text{g}$. When using 3 PCs, the predicted were closer to the XRD target values (average absolute difference was $2 \mu\text{g}$ compared with $8 \mu\text{g}$), indicating 3 PCs were better match with the XRD target values.

The need for blank matching

An added advantage of the chemometric software package was the opportunity to apply derivatives to normalise the spectra before processing, i.e. tangent lines to the graph of the function at that point. The comparability of the predicted values obtained from the models with the linear 1:1 relationship demonstrates that the derivatisation did not have a negative impact on the results. A separate experiment compared eight results

Table 2. Calibration data for quartz, kaolinite and coal dust.

Model	Analyte	Number of principal components	Percentage of explained variance	Estimated prediction error (μg)
Principal component regression	Quartz	5	99.5%	12.6
	Kaolinite	5	98.4%	17.6
	Coal dust	10	97.1%	36.5
Partial least squares regression	Quartz	5	99.6%	11.6
	Kaolinite	1	96.8%	24.4
	Coal Dust	5	94.8%	50.5

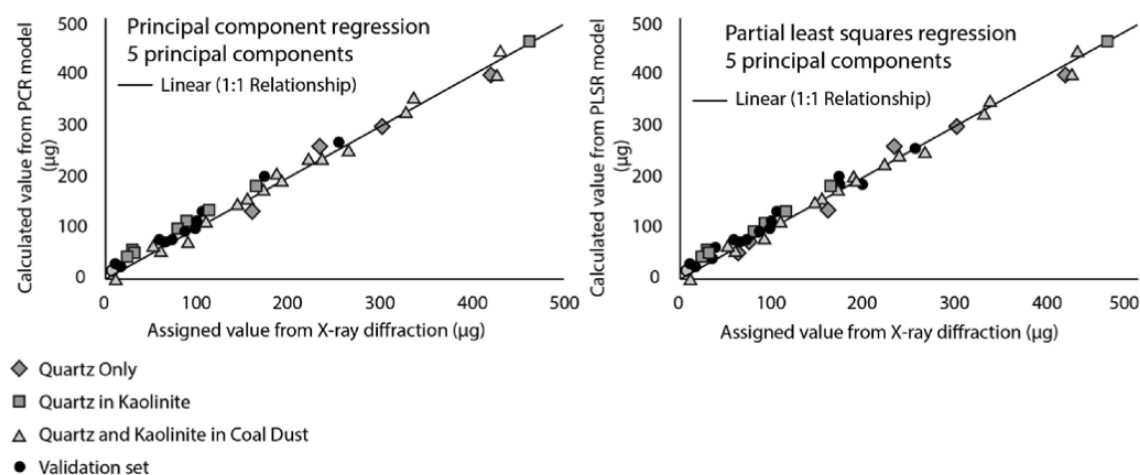


Figure 3. Calibration and validation calculated values for quartz.

from two Beers law models; one following MDHS 101 with blank filter subtraction and the other using a first-order derivative background treatment (Table S4, Supplementary Information). Most differences when comparing these background treatment approaches were relatively small (–3% to –7%). Other studies (Weakley *et al.*, 2014, Miller *et al.*, 2016) removed the spectral bands from the filter by subtracting the spectrum recorded from a clean unused filter. However, such blank subtraction proved unnecessary and risks the occurrence of spectral artefacts remaining; which may hinder the determination of trace levels of other components. The derivatisation removes the need for loaded samples to be matched with blank filters before analysis simplifying the analytical process and may also further reduce the cost of analysis. Blank matching can be the most laborious part of the FTIR analytical process specified in MDHS 101.

Comparison with the MDHS 101 method

A comparison of the predicted quartz concentrations obtained from the samples in the PCR calibration set containing coal dust and kaolinite was made with those values obtained following MDHS 101 method (Figure 5). MDHS 101 uses a calibration based on the Beer-Lambert law i.e. the absorbance response is directly proportional to the concentrations of quartz present in the calibration standards of pure quartz collected onto filters.

To calculate the corrected peak height absorbance, a baseline correction under the quartz absorbance at 780 cm^{-1} and 800 cm^{-1} was applied. This followed the current guidance in the MDHS to ‘draw baselines on the blank corrected spectra tangential to the absorbance

minima at about 730 cm^{-1} and 830 cm^{-1} and did not have any special regard to the presence of kaolinite. The trend line intercept for the comparison of XRD measured quartz values with the infrared values, determined following MDHS 101 method, was not significantly different from zero (95% level of confidence was from –10 to +33). The trend with results from the Beer–Lambert law calibration was linear with a significant positive bias (about +18% at the current workplace exposure limit in Great Britain) and with a slightly poorer coefficient of determination (0.97). The range of bias was from 0% to 23% and exactly matches that found by (Lee *et al.*, 2013) when using peak height measurement with the National Institute for Occupational Safety and Health (NIOSH) infrared method 7603 (NIOSH, 2004), which is similar to the regulatory method P7 for the Mines Safety and Health Administration (MSHA) (MSHA, 1994). An RCS concentration value that is 18% higher than the ‘true’ exposure concentration might result in unnecessary further corrective action to control exposures. A plot of the percentage difference between the measured XRD values and the results obtained using FTIR and following MDHS 101 with the varying proportions of quartz and kaolinite showed a negatively sloped relationship (Figure S6, Supplementary Information). The larger proportions of kaolinite (with ratios close to 1:1 with quartz) were responsible for the largest relative errors. The trend line relationship between the percentage differences from the XRD assigned values and the ratio of quartz and kaolinite was $-11.3 \times (\text{ratio quartz/kaolinite}) + 47.8$ with a coefficient of determination of 0.41. The slope of the trend line was significantly different from zero indicating that the relationship is real (the 95% level of confidence of the slope was from –4.1 to –18). No significant relationship

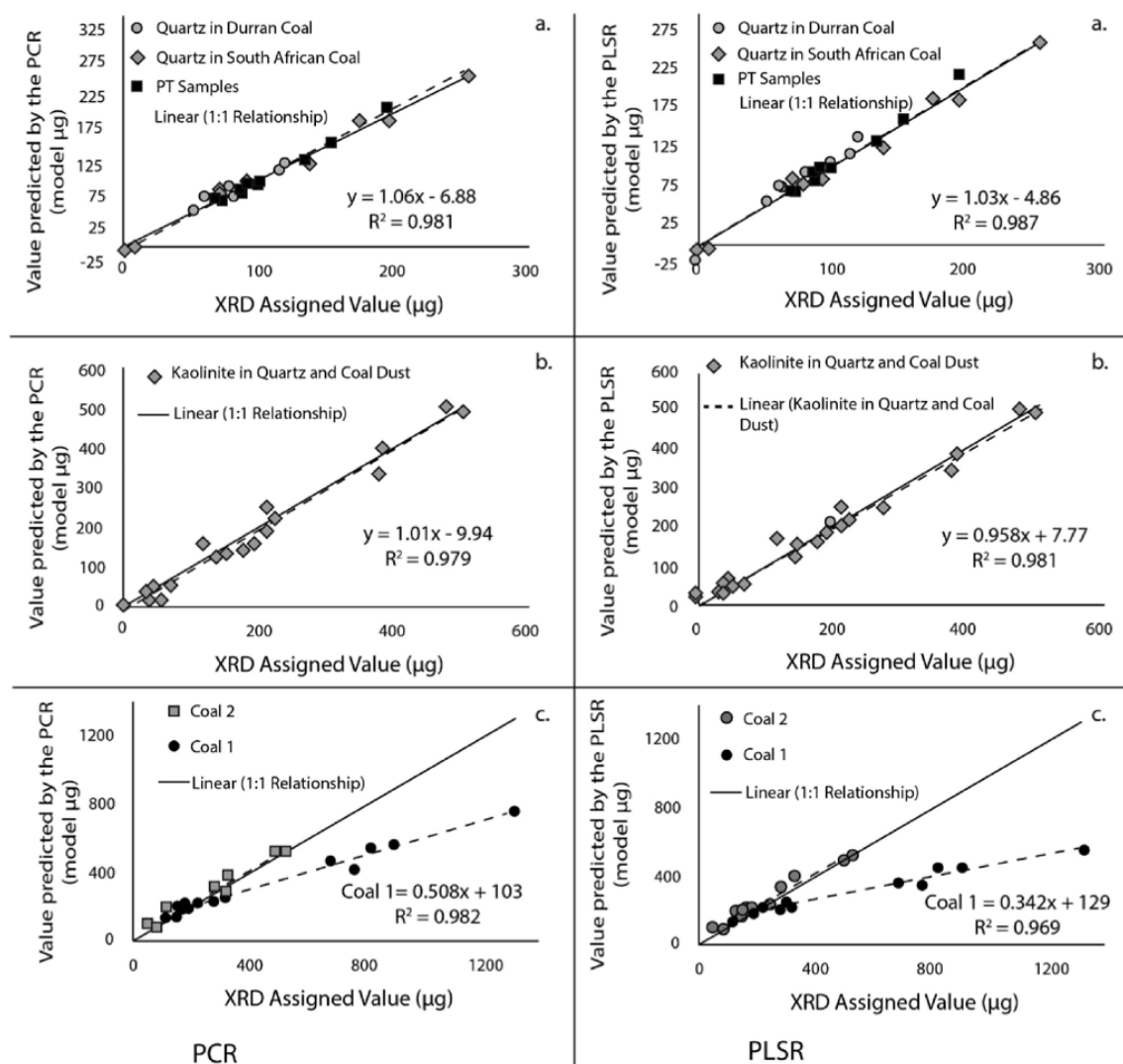


Figure 4. Predicted FTIR values for quartz (a), kaolinite (b) and coal dust (c) from the PCR (left hand side charts) and PLSR (right hand side charts) analysis chemometric models compared with assigned values measured by XRD.

between the percentage differences was found for varying proportions of coal dust in the calibration samples as the confidence interval for the slope included zero (the 95% level of confidence was from -28 to $+59$).

The comparison between PCR and PLSR

The two chemometric methods (PCR and PLSR) produced similar predicted values when compared with the XRD values. Figure 4 compares the predicted values of twenty-eight samples from the PCR and PLSR with the XRD assigned values. All results show good correlations with the assigned values except for coal dust. The coefficients of determination for quartz, kaolinite, South

African coal dust (Coal 2) and Durrans coal dust (Coal 1) were 0.99, 0.98, 0.96 and 0.95 for the PCR method and 0.98, 0.98, 0.96 and 0.97 for the PLSR method, respectively, demonstrating that they are statistically related with mass of analyte. In this work, the two coal dust types appeared to have a different relationship to each other (Figure 4) when the loading is greater than $380 \mu\text{g}$ with high coefficients of determination, i.e. the samples from the different types (ranks) of coal dust are potentially predictable and a correction factor could be applied. For example, the average PCR difference from the target value for coal dust 1 was $169 \mu\text{g}$ whereas it was $26 \mu\text{g}$ for coal dust 2. Different types (ranks) of

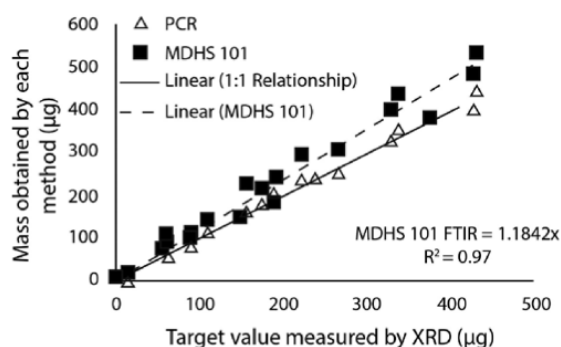


Figure 5. Comparison between predicted PCR results for quartz and those obtained using FTIR following MDHS 101 (Beer–Lambert relationship) and the background subtraction correction for the absorption from the PVC filter.

coal do have different organic contents (He *et al.*, 2017) which may explain the differences observed by the chemometric modelling at higher mass loadings. He *et al.* (2017) characterised thirteen types of coal from lignite to the more crystalline anthracite and found that they have very similar absorption bands that vary in intensity. The main IR active region for coal, in the spectral range used in this study, is between 700 cm^{-1} and 900 cm^{-1} . These IR active bands for coal are associated with aromatic C–H (several bands within 670 cm^{-1} to 900 cm^{-1}) out of plane bending (Coates, 2006, He *et al.*, 2017) and coincide with those for quartz (800 cm^{-1} and 780 cm^{-1}) and the hydroxyl (Al–OH) stretching vibrations of kaolinite at 915 cm^{-1} (Madejová and Komadel, 2001, Lee *et al.*, 2013). However, the only perceptible spectral differences in the FTIR scan of a clean PVC filter and one loaded with Durrans coal (Coal 1) is a broad band at about 760 cm^{-1} and an increase in absorbance from 990 cm^{-1} to 1000 cm^{-1} , which is probably associated with hydroxide group bending from the additional kaolinite found in the South African coal (Coal 2). These differences indicate that components other than kaolinite and quartz within the coal are potentially distinctive to the type of coal. The hydrocarbon content might also have an influence on the observed spectrum and a chemometric FTIR method may provide an opportunity to more fully characterise a worker’s personal exposure. To achieve this, the scan range may need an extension above 1000 cm^{-1} (He *et al.*, 2017). It is possible that the spectra of different kaolinites might also vary, however, Lee *et al.* (2013) demonstrated that most kaolinite will have a similar IR response for the 915 cm^{-1} band unless they are chemically treated (acid washed) or a slight variant of kaolinite (halloysite, which contains more hydroxyl groups). Therefore, the coal dust models described by this study could be corrected for

different coal dusts because the two other quantifiable components have a relatively consistent absorbance per unit mass.

The masses of quartz and kaolinite are predicted by the models with reasonable levels of precision. The following standard deviations include the difference from the assigned target value. For the PCR model, the standard deviation of percentage differences between the PCR predicted value and the assigned value by XRD was 7.9%, 14.1% and 38.5% for quartz, kaolinite and coal dust, respectively. Eight samples from two rounds of the AIR proficiency testing (PT) programme were added for prediction as well as two samples containing pure quartz prepared using a SIMPEDS sampler. The pure quartz samples, including the two sets of four from the AIR PT, obtained a percentage standard deviation of 4.4% from the target values (range of results was 0.7–11%). The standard deviations of percentage differences were 19.6% for coal dust from South Africa and 36.8% for the Durrans coal dust, i.e. there was more variability for the FTIR results when using PCR about the expected target values, for coal dust and Durrans coal when compared to quartz and kaolinite.

For the PLSR model, the standard deviations of percentage differences were, 8.0%, 13.8% and 35.4% for quartz, kaolinite and coal dust, respectively. The South African coal dust was 23% and the Durrans coal dust was 27%. The standard deviation of percent differences for the same AIR PT samples and quartz standards was 7.0% (range of percent differences was from 0.6% to 10.5%).

The agreement between quartz standards prepared using the SIMPEDS and the AIR proficiency testing (PT) samples is good. The AIR PT samples are prepared using the British Cast Iron Research Association (BCIRA) respirable sampler, which is different from the SIMPEDS sampler used in this work and has a slightly different sampling bias. The deposit of dust on the aerosol filter can alter the sensitivity of the measurement, however, the close agreement was observed for results from these samplers in an international comparison (Stacey *et al.* 2014).

A direct comparison of regression coefficients for the PCR and PLSR models, where x are the values predicted by PLSR and y are the predicted values from PCR when processing the same thirty samples, is shown in Table 3 and plots are provided in Figure S7 (supplementary information).

Table 3, Figure 4 and Figure S7 show that there is generally good relationship with a linear model between results generated by the PCR and PLSR models, except for coal dust. There are some slight differences in the predictions of the two methods. Firstly, the ideal value of 1.00 demonstrating perfect correlation is significantly different for kaolinite and coal dust at the 95% level of confidence.

Table 3. Regression coefficients obtained from a comparison of PCR and PLSR results.

Analyte	Regression coefficient (r^2)	Slope	95% level of confidence for the slope coefficient	Intercept (μg)	95% level of confidence for the intercept coefficient
Quartz	0.997	0.98	0.94–1.01	1.39	–1.5 to + 5.5
Kaolinite	0.997	1.04	1.01–1.07	–15.6	–9.6 to –22
Coal dust	0.969	1.23	1.11–1.37	–52.9	–97 to –17

Coal dust has a bias of about +23% indicating that the PCR is reporting higher values than the target values (see Figure 4). The difference for the intercept and slope coefficients is probably due to the number of PCs applied by each model (e.g. a low number (1 principle component) was selected by the software for the PLSR and a higher number (5) was selected for the PCR model used for kaolinite). However, for each analyte, 92.5% of differences between individual values were within the 95% level of agreement (Bland and Altman, 2003) indicating that there was no practical difference in results reported between models.

A potential flaw, when generating samples onto a filter from an aerosol, is that it is difficult to control the collection of the exact proportions of the minerals of interest (quartz and kaolinite). The proportions for quartz in the calibration and validation sets (generally more than 18%) tended to match the top end of the range (2–30%) found by Miller *et al.* (2016) when measuring samples from six coal mines in the United States; which may compromise the model's predictions for samples with low proportions of quartz.

Conclusions

The results reported herein demonstrate the need for matrix-specific calibration standards when measuring quartz from workplace atmospheres with FTIR where other components are present that will influence the spectra close to the absorbance for quartz. Both PLSR and PCR models were found to provide values comparable with XRD when following the XRD part of the MDHS 101 for the measurement of constituents in coal dust with matrix matched standards, which was more accurate than the current FTIR MDHS 101 approach.

The advantage of these chemometric models is that they offer the potential for multicomponent analysis to provide more comprehensive knowledge of a workers' exposure to the workplace atmosphere and not only a single individual component in the matrix. They also have the potential to provide a black box capability that requires less knowledge or experience to interpret spectra. The next stage of this work will be to examine the universal applicability of these models for predicting quartz in a range of workplace environments.

The use of the first derivative to normalise spectra before processing removes the need for the blank filter subtractions for each spectrum. This will significantly reduce the complexity of a direct on-filter analysis approach.

There are only slight differences between results obtained by the PCR and PLSR methods. Selection of the number of PCs has an important effect on the slope of the relationship between the 'true' value and the value predicted by the chemometric models applied to the FTIR data. It was useful to have the capability to further optimise the number of PCs for the PCR approach and to check its impact on the predicted values by testing the significance of coefficients and differences obtained from a regression with the assigned target XRD values. The software selected 6 PCs, for the PCR; however, 5 or 3 PC provided predicted values that were more comparable with the target values. This capability might be a useful consideration when developing models based on PCR using commercially available software.

Supplementary Data

Supplementary data are available at *Annals of Work Exposures and Health* online.

Acknowledgements

Thanks to Ian Pengelly, Laurie Davies, Margaret Wade, Clare McNicholas and Susan Hambling at HSE who conducted the internal HSE technical and editorial reviews and Dr Chisholm (NIOSH) for his assistance when examining the effect of different FTIR instrument resolutions on the signal to noise ratio (Figure S4).

Disclaimer

The work presented in this article was funded by the Health and Safety Executive (HSE) in the United Kingdom (Project PH00760). The opinions expressed in this article are those of the authors and do not necessarily reflect HSE policy.

Data availability

The data underlying this article are available in the article and in its online supplementary material. The raw data will be shared on reasonable request to the corresponding author.

References

- Bergdahl IA, Torén K, Eriksson K, *et al.* (2004) Increased mortality in COPD among construction workers exposed to inorganic dust. *Eur Res J*; 23: 402.
- Bland JM, Altman DG. (2003) Applying the right statistics: analyses of measurement studies. *Ultrasound Obstet Gynecol*; 22: 85–93.
- Breen C, Clegg F, Herron MM, *et al.* (2008) Bulk mineralogical characterisation of oilfield reservoir rocks and sandstones using diffuse reflectance Infrared Fourier Transform Spectroscopy and partial least squares analysis. *J Petroleum Sci Eng*; 60: 1–17.
- Brown T, Cherrie JW, Van Tongeren M, *et al.* (2012) The burden of occupational cancer in Great Britain Lung cancer. HSE Research Report RR858 Bootle, Liverpool: Health and Safety Executive.
- Bye E. (1994) Chemometrics in Aerosol Analysis: Quantitative Analysis of silica dust mixtures by multivariate calibration applied to Infrared Spectroscopy. *Ann Occupat Hygiene*; 38: 519–25.
- Cauda E, Miller A, Drake P. (2016) Promoting early exposure monitoring for respirable crystalline silica: Taking the laboratory to the mine site. *J Occupat Environ Hygiene*; 13: D39–D45.
- CEN. (1993) EN 481:1993 *Workplace atmospheres — Size fraction definitions for measurement of airborne particles*. Brussels: European Committee for Standardisation.
- Coates J. (2006) Interpretation of infrared spectra, a practical approach. In Mckelvy, R. A. M. A. M. L. editor. *Encyclopedia of Analytical Chemistry*. Online Library: John Wiley & Sons.
- Dodgson J, Whitaker W. (1973) The determination of quartz in respirable dust samples by infrared Spectrophotometry—I: The potassium bromide disc method. *Ann Occupat Hygiene*; 16: 373–87.
- Foster RD, Walker RF. (1984) Quantitative determination of crystalline silica in respirable-size dust samples by infrared spectrophotometry. *Analyst*; 109: 1117–27.
- Hart JF, Autenrieth DA, Cauda E, *et al.* (2018) A comparison of respirable crystalline silica concentration measurements using a direct-on-filter Fourier transform infrared (FT-IR) transmission method vs. a traditional laboratory X-ray diffraction method. *J Occupat Environ Hygiene*; 15: 743–54.
- He X, Liu X, Nie B, Song D. (2017) FTIR and Raman spectroscopy characterization of functional groups in various rank coals. *Fuel*; 206: 555–63.
- Hemmateenejad B, Akhond M, Samari F. (2007) A comparative study between PCR and PLS in simultaneous spectrophotometric determination of diphenylamine, aniline, and phenol: Effect of wavelength selection. *Spectrochim Acta Part A: Mol Biomol Spectros*; 67: 958–65.
- HSE. (2003) EH75 Respirable Crystalline Silica, variability in fibrogenic potency and exposure-response relationships for silicosis. Health Safety Execut.
- HSE. (2005) EH40/2005 *Workplace exposure limits, containing the list of workplace exposure limits for use with the control of substances hazardous to health regulations (as amended)*. Norwich, United Kingdom, Health and Safety Executive, Crown.
- HSE. (2014) *Methods for the determination of hazardous substances, MDHS 101/2 crystalline silica in respirable airborne dust, direct on-filter analyses by infrared spectroscopy and X-Ray diffraction*. Norwich, United Kingdom, Crown: Health and Safety Executive (HSE).
- Jolliffe IT, Cadima J. (2016) Principal component analysis: a review and recent developments. *Philos Trans R Soc A: Math Phys Eng Sci*; 374: 20150202.
- Lee T, Chisholm WP, Kashon M, *et al.* (2013) Consideration of Kaolinite interference correction for quartz measurements in Coal Mine Dust. *J Occupat Environ Hygiene*; 10: 425–34.
- Madejová J, Komadel P. (2001) Baseline studies of the clay minerals society source clays: Infrared methods. *Clays Clay Miner*; 49: 410–32.
- Miller AL, Weakley T, Griffiths P, *et al.* (2016) Direct-on-Filter α -Quartz Estimation in respirable Coal Mine dust using transmission Fourier transform infrared spectrometry and partial least squares regression. *Appl Spectrosc*; 71: 1014–24.
- MSHA. (1994) *Infrared determination of quartz in respirable coal mine dust: Method P-7*. Pittsburgh, PA: MSHA: Mine Safety and Health Administration (MSHA).
- NIOSH. (2004) *Quartz in coal mine dust by Infrared (redemption) Method 7603*. Cincinnati: Department of Health and Human Services, National Institute for Occupational Safety and Health (NIOSH).
- Pickard KJ, Walker RF, West NG. (1985) A comparison of X-Ray diffraction and infra-red Spectrophotometric methods for the analysis of α -Quartz in Airborne Dusts*. *Ann Occupat Hygiene*; 29: 149–67.
- Ross MH, Murray J. (2004) Occupational respiratory disease in mining. *Occupat Med*; 54: 304–10.
- Stacey P. (2019) A study to assess the performance of an “X-ray powder diffraction with Rietveld” approach for measuring the crystalline and amorphous components of inhalable dust collected on aerosol sampling filters. *Powder Diffract*; 34: 251–9.
- Stacey P, Mecchia M, Verpaele S, *et al.* (2014) Differences between samplers for respirable dust and the analysis of quartz—an international study. In Harper M, Lee T, editors. *Silica and associated respirable mineral particles*. West Conshohocken, PA: ASTM International. pp. 73–102.
- Weakley AT, Miller AL, Griffiths PR, *et al.* (2014) Quantifying silica in filter-deposited mine dusts using infrared spectra and partial least squares regression. *Anal Bioanal Chem*; 406: 4715–24.
- Wentzell PD, Vega Montoto L. (2003) Comparison of principal components regression and partial least squares regression through generic simulations of complex mixtures. *Chemomet Intell Laboratory Syst*; 65: 257–79.

Supplementary Information

Multicomponent measurement of respirable quartz, kaolinite and coal dust using Fourier Transform Infrared spectroscopy (FTIR): A comparison between partial least squares and principal component regressions.

Peter Stacey^{*,++}, Francis Clegg⁺⁺, and Christopher Sammon⁺⁺.

^{*}Health and Safety Executive, Harpur Hill, Buxton, Derbyshire, SK17 9JN, United Kingdom

⁺⁺Sheffield Hallam University, Materials and Engineering Research Institute, Sheffield, S1 1WB United Kingdom

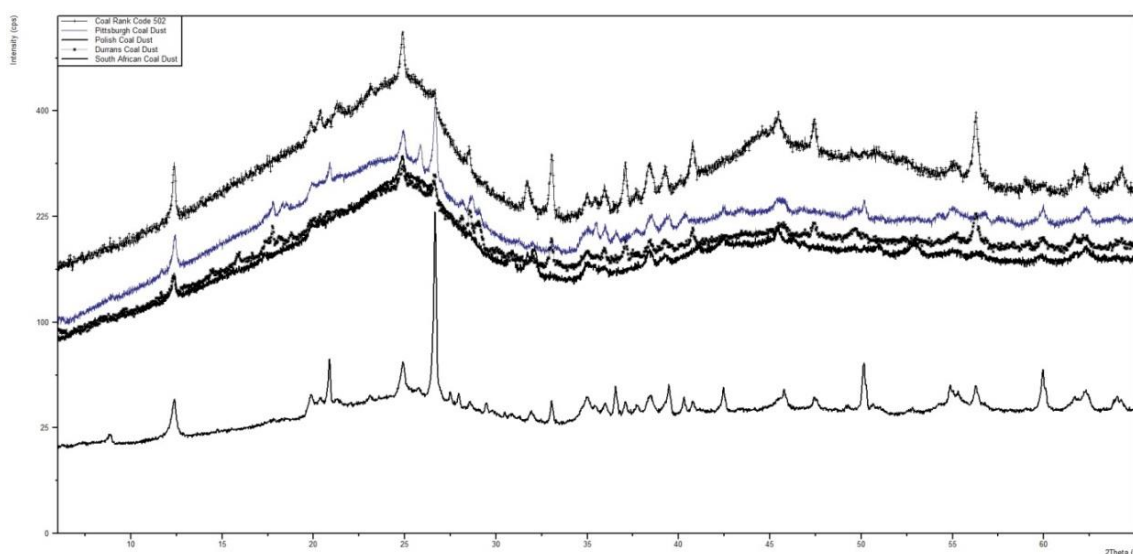


Figure S1. X-ray diffraction scans from a selection of powdered coals.

X-ray diffraction analysis for the determination of the assigned target values.

Measurement conditions

For quartz, the instrument used the second set of standard instrumental conditions described in Table A1 of the International Standards Organization (ISO) standard method ISO 16258-1; 2015 (ISO, 2015). The instrument was fitted with a broad focus copper tube set at 50 kW and 45 mA, automatic scattering and receiving slits set to provide an illumination length of 18 mm, and an array detector with the detection area set at a 2θ range of 2.12 degrees. The area of the three most intense XRD diffraction positions of α -quartz at 2θ angles of, 20.9, 26.6 and 50.1 degrees were measured for 600 seconds, 420 s and 600 s, respectively, for each 0.03 2θ degree interval over the two degree range centered on the measurement intensity. The total sample analysis time was

about 30 minutes. Tube drift was corrected using the measurement of an aluminium plate as an external standard. The average of the two most consistent results obtained from the three intensities was used as the quartz 'assigned' target value when significant interference was present that affected one of the XRD reflections.

For kaolinite, the area of the two most intense intensities free from quartz interference at 2θ positions of 12.2 and 25 degrees were used for quantification. A scan of a sample was collected from 6 to 60 degrees in steps of 0.02 and 60 s per step. The total scan time was 25 minutes. Each measurement intensity was quantified using a 2θ range of two degrees. The average of the two results obtained from each of the kaolinite measurement reflections was used as the kaolinite 'independent' value.

X-ray diffraction calibration charts are shown in Figures S2 and S3 overleaf.

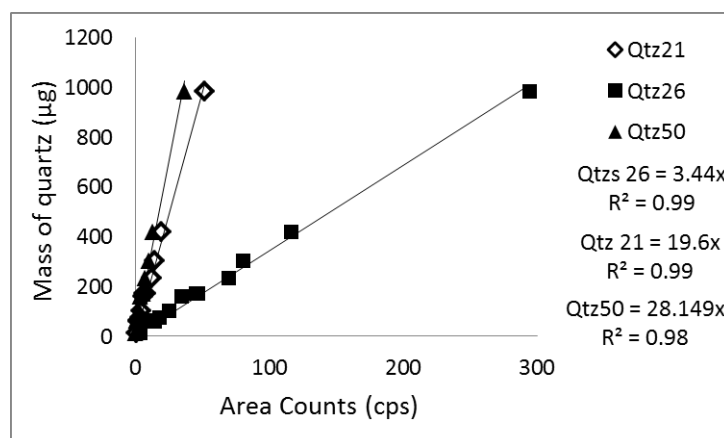


Figure S2. Trend line for the relationship between mass of α -quartz standard A9950 collected on a filter using the SIMPEDS respirable sampler and X-ray diffraction area response for the principal quartz intensities at 2θ degrees of 20.9 (Qtz21), 26.6 (Qtz26) and 50.1 (Qtz50).

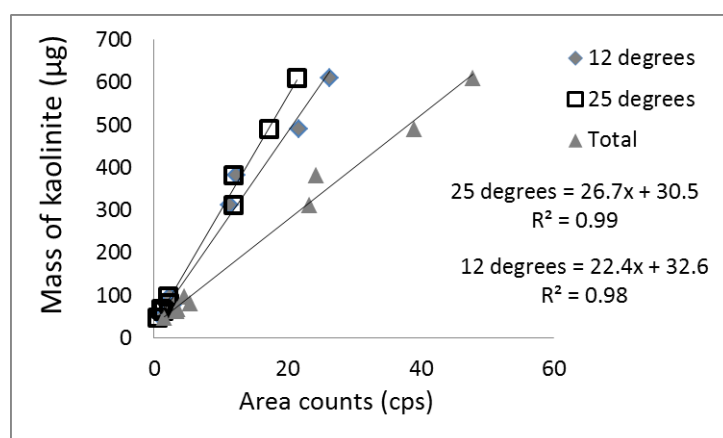


Figure S3. Trend line for the relationship between mass of kaolinite standard (Georgia, USA) collected on a filter using the SIMPEDS respirable sampler and X-ray diffraction area response for the principal kaolinite intensities at 2θ positions of 12 and 25 degrees.

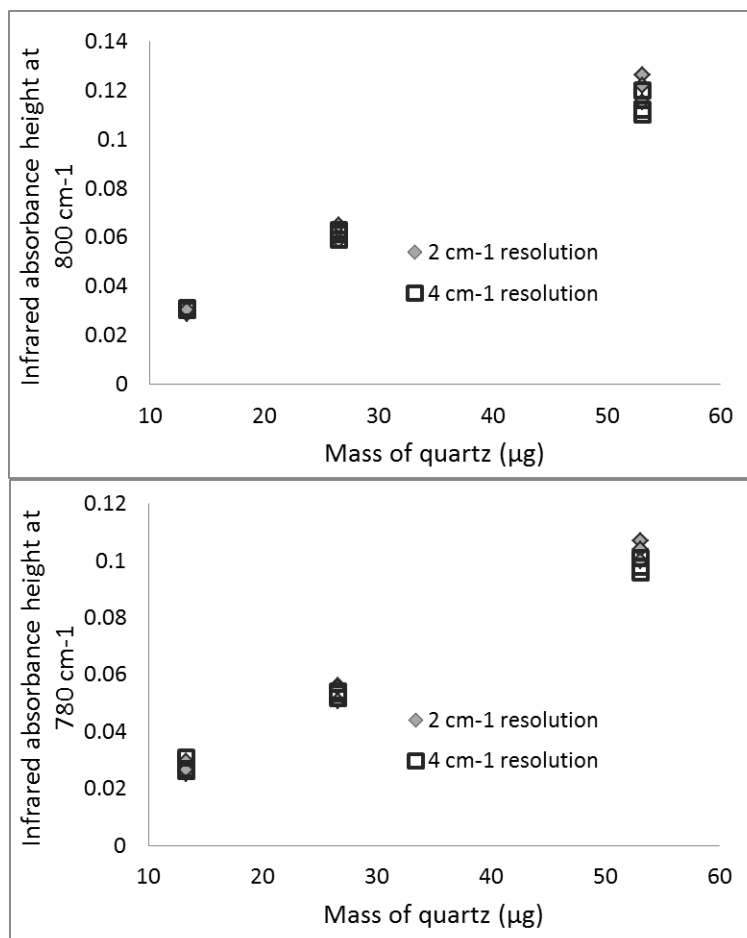


Figure S4. Infrared absorbance at 800 cm^{-1} and 780 cm^{-1} , when measuring three replicate aliquots α -quartz at three different mass loadings deposited onto polyvinylchloride filters at two different spectral resolutions of 4 cm^{-1} and 2 cm^{-1} .

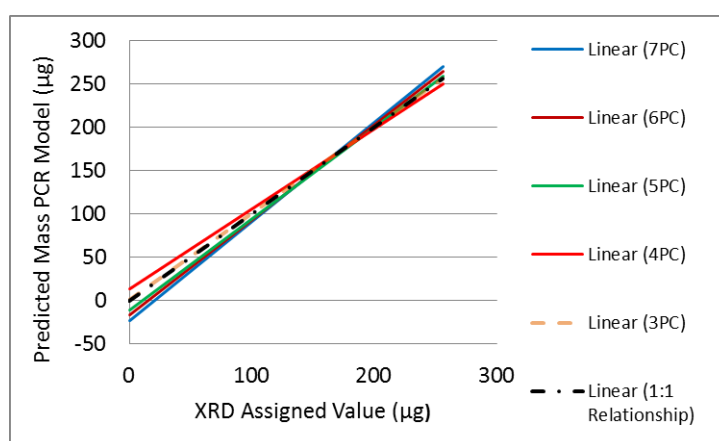


Figure S5. Change in the slope of the relationship between the predicted mass and the XRD assigned value for quartz as the number of principal components are changed from 3 to 7.

Table S1. Regression coefficients and average difference for the principal component regression model shown in Figure S5 with 3 to 7 principal components (PC).

PC	Slope coefficient	Intercept coefficient (μg)	Average absolute difference (μg)
7	1.14	-23.0	17.2
6	1.09	-16.3	12.5
5	1.05	-10.7	9.4
4	0.927	13.2	12.1
3	0.996	1.16	5.6

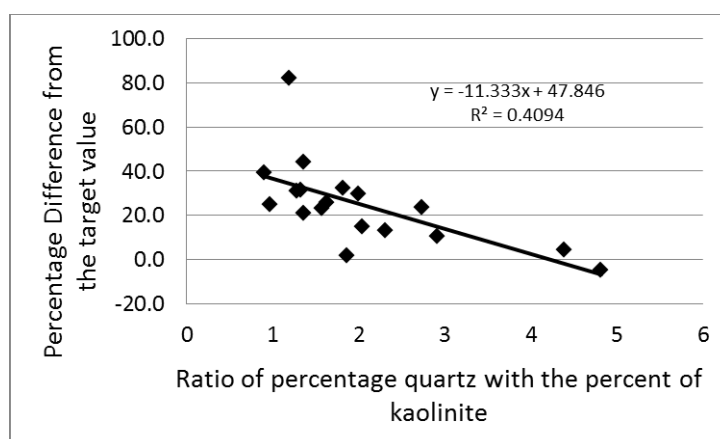


Figure S6. Chart showing the relationship between the proportion of kaolinite in the sample and its effect in on the magnitude of the error for the reported value when using infrared with MDHS 101.

Table S2. Composition and total gravimetric mass of samples used for the calibration set

Total Gravimetric Mass (μg)	Percent proportion of constituent mineral		
	Quartz	Kaolinite	Coal Dust
314.3	0.7	11.0	88.3
698.0	20.8	4.7	74.4
204.7	27.1	14.9	58.0
420.3	26.2	20.4	53.4
247.2	24.9	27.7	47.3
665.0	28.9	17.8	53.3
731.7	30.4	22.8	46.8
879.0	37.4	27.5	35.1
423.0	41.2	26.1	32.7
428.7	20.7	7.1	72.2
844.3	21.1	4.4	74.5
487.7	18.1	18.6	63.3
882.3	18.1	15.2	66.7
584.7	26.7	19.6	53.7
901.3	37.4	18.7	44.0
845.7	27.8	17.4	54.8
679.3	39.1	19.2	41.7
1010.7	42.2	18.2	39.6
1348.3	32.0	11.7	56.3
419.9	100		
302.5	100		
160.7	100		
99.9	100		
170.7	100		
234.5	100		
75.0	100		
171.8	100		
10.9	100		
60.6	100		
985.2	100		
62.9	100		
327.1		100	
107.1		100	
88.7		100	
99.7		100	
53.3		100	
88.9		100	
72.3		100	

60.9		100	
403.2		100	
478.3		100	
218.1		100	
55.4		100	
611.1		100	
489.5		100	
311.3		100	
382.4		100	
97.5		100	
67.2		100	
48.2		100	
81.5		100	
62.7		100	
518.4	89.6	10.4	
214.7	77.2	22.8	
120.9	64.2	35.8	
169.1	67.4	32.6	
183.6	49.9	50.1	
85.9	37.1	62.9	
202.0	39.8	60.2	
107.6	31.7	68.3	
222.4	26.3	73.7	
121.4	21.9	78.1	

Table S3. Total gravimetric mass and proportions of constituents in the samples used for the validation set.

Total Gravimetric Mass (μg)	Percent proportion of constituent mineral		
	Quartz	Kaolinite	Coal Dust
100	100.0		
75	100.0		
74	18.3		81.7
142	28.0		72.0
98	19.2	46.0	34.7
192	17.6	44.7	37.7
143	26.3	37.8	36.0
339	26.1	60.9	12.9
277	38.9	32.3	28.7
169	37.1	27.4	35.4
238	42.1	31.0	26.9
176	19.3	39.6	41.1
181	34.2	37.9	27.9
362	27.8	25.8	46.3
205	32.8	46.8	20.4
1205	16.4	40.1	43.5
851	20.7	44.8	34.5
534	21.3	42.6	40.0
1255	20.4	40.4	39.2

Table S4. Total gravimetric mass and proportions of constituents in the samples used for the prediction set.

Total Gravimetric Mass (μg)	Percent proportion of constituent mineral		
	Quartz	Kaolinite	Coal Dust
939.6		4.8	95.2
801.7		4.9	95.1
417.1	24.0		76.0
397.8	30.6		69.4
532.5	21.8	22.3	55.8
308.7	17.2	45.7	37.2
437.2	15.3	41.8	42.9
536.3	17.3	42.3	40.3
123.1		32.0	68.0
152.1	6.1		93.9
204.6	3.8	19.9	76.3
222.0	4.1	21.2	74.8
250.5	3.8		96.2
150.5	5.7		94.3
270.2	26.6	54.4	19.0
380.7	18.8	39.9	41.2
403.1	20.5	48.6	30.9
851.0	20.7	44.8	34.5
427.0	20.4	42.4	37.2
493.4	18.6	44.0	37.4
578.3	13.9	37.2	48.9
853.8	16.4	45.2	38.4
1204.8	16.4	40.1	43.5
1254.5	20.4	40.3	39.3
74.0	100.0		
99.9	100.0		
101.0	100.0	Proficiency testing samples	
135.0	100.0		
99.9	100.0		
74.0	100.0		
92.6	100.0		
86.7	100.0		
155.2	100.0		
196.6	100.0		

Comparison of background correction methods

Table S4 compares the results obtained when using the blank filter subtraction process outlined in MDHS 101 and with a first derivative processing of the scan to normalise the spectral background from the filter. Beers law models were developed for each background correction process. Each model was developed using the same calibration filters. Results from eight independent samples containing α -quartz standard are listed below.

Table S5. A comparison of results from two background correction processes.

Sample	Mass recorded by each method		Absolute difference (μg)	Percentage Difference
	Blank filter subtraction	First derivative processing		
T3	413 μg	401 μg	-12.0	-2.9 %
T4	94.5 μg	89.0 μg	-5.5	-5.8 %
T5	75.6 μg	71.2 μg	-4.4	-5.8 %
T6	465 μg	453 μg	-12	-3.2 %
T10	112 μg	106 μg	-6.0	-5.3 %
T13	45.6 μg	42.5 μg	-3.1	-6.8 %
T14	91.8 μg	85.6 μg	-6.2	-6.7 %
T16	15.8 μg	11.6 μg	-4.2	-26 %

Correction to: Multicomponent measurement of respirable quartz, kaolinite and coal dust using Fourier Transform Infrared spectroscopy (FTIR): A comparison between partial least squares and principal component regressions.

Peter Stacey, Francis Clegg, and Christopher Sammon

Comparability of differences between the MDHS 101 and the principal component regression (PCR) methods.

The statement in results section that the differences between the MDHS 101 method and the XRD values of 0% to 23 % exactly matched those found by Lee et al., (2013) for the peak height was not correct. The differences between the MDHS 101 method and the XRD values were mostly between -4.7% and 44%. This range of percentage differences remains comparable with those found by Lee et al., (2013) for the range of differences of FTIR measurements of spiked quartz in samples of kaolinite without correction which were from 0.06% to 45%.

Chapter. 7 Application of a Principal Component Regression (PCR) chemometric method for the quantification of RCS (quartz), in coal dusts.

Application of a Fourier Transform Infrared (FTIR) Principal Component Regression (PCR) Chemometric Method for the Quantification of Respirable Crystalline Silica (Quartz), Kaolinite, and Coal in Coal Mine Dusts from Australia, UK, and South Africa.

Peter Stacey, Francis Clegg , Gary Rhyder and Christopher Sammon

Annals of Work Exposures and Health, Volume 66, Issue 6, July 2022, Pages 781–793,

<https://doi.org/10.1093/annweh/wxab119>

Current citations = 1 (November 2022)

The purpose of this article was to test a chemometric model with a range of real samples from a range of workplaces working with coal dusts and to assess its performance in terms of its limits of detection, and uncertainty when measuring these samples.

Original Article

Application of a Fourier Transform Infrared (FTIR) Principal Component Regression (PCR) Chemometric Method for the Quantification of Respirable Crystalline Silica (Quartz), Kaolinite, and Coal in Coal Mine Dusts from Australia, UK, and South Africa

Peter Stacey^{1,2,*}, Francis Clegg², Gary Rhyder³ and Christopher Sammon²

¹Health and Safety Executive, Science Division, Harpur Hill, Buxton, Derbyshire SK17 9JN, UK; ²Materials and Engineering Research Institute (MERI), Sheffield Hallam University, Sheffield S1 1WB, UK; ³Pickford & Rhyder Consulting Pty Ltd, PO Box 975, Ryde, NSW 1680, Australia

*Author to whom correspondence should be addressed. Tel: +44-02030282151; e-mail: peter.stacey@hse.gov.uk

Submitted 25 August 2021; revised 18 November 2021; editorial decision 10 December 2021; revised version accepted 15 December 2021.

Abstract

This article describes the approach used to assess the performance of a Fourier transform infrared (FTIR) and principal component regression (PCR) chemometric method when measuring respirable quartz, kaolinite, and coal in samples from a variety of mines from different countries; relative to target assigned values determined using X-ray diffraction (XRD). For comparison, FTIR results using the partial least squares regression (PLSR) method are also available. Bulk dusts from 10 Australian mines were scanned using XRD and grouped into three sets based on the levels of quartz, kaolinite, and feldspar within their crystalline mineral composition. Prediction samples were generated from 5 of these Australian mine dusts, Durrans coal dust, 2 mine dusts from the UK, and a single South African mine dust (71 samples in total) by collecting the aerosolized respirable dust onto 25-mm diameter polyvinylchloride filters using the Safety in Mines Personal Dust Sampler (SIMPEDS) operating at 2.2 l min⁻¹. The predicted values from the FTIR chemometric methods were compared with assigned target values determined using a direct on-aerosol filter XRD analysis method described in Method for the Determination of Hazardous Substances (MDHS) 101. Limits of detection (LOD) and uncertainty values for each analyte were calculated from a linear regression between target and predicted values. The uncertainty was determined using the calibration uncertainty equation for an unweighted regression. FTIR results from PCR and PLSR are very similar. For the PCR method, the LOD for quartz, kaolinite, and coal were 5, 20, and 71 µg, respectively. For quartz, an LOD

What's Important About This Paper?

Fourier transform infrared instruments are relatively inexpensive, portable, and potentially measure many chemical agents simultaneously, including crystalline silica, but interference can limit accuracy. Accurate measurements of respirable crystalline silica are important because of their relationship with potential risk of worker ill-health. This article describes a chemometric method, a principal component regression model derived using laboratory generated samples, that reduces the influence of interference in the spectrum to determine component concentrations. The method was used to establish detection limits for crystalline silica in mine dusts, and the study demonstrated that the method can meet international performance criteria.

of 5 μg corresponds to an airborne quartz concentration of 10 $\mu\text{g m}^{-3}$, assuming a 4-h sampling time and collection flow rate of 2.2 l min^{-1} . The FTIR measurement met the expected performance criteria outlined in ISO 20581 when sampling quartz for more than 4 h using a flow rate of 2.2 l min^{-1} at a concentration of 0.1 mg m^{-3} (100 $\mu\text{g m}^{-3}$), the current workplace exposure limit in Great Britain. This method met the same performance criteria when measuring exposures at the Australian Workplace Exposure Standard (WES) concentration of 0.05 mg m^{-3} , although in this case a sampling period greater than 8 h was needed.

Keywords: chemometrics; coal; kaolinite; limit of detection; principal component regression; quartz; respirable crystalline silica; uncertainty

Introduction

The expanded uncertainty is a measure of the reliability of a reported value. It is calculated as the product of the combined standard deviations of all the steps that could contribute to its variability multiplied by a coverage factor (usually 2) as an estimate of the 95% confidence interval. The objective, in this work, is to assess the performance of a principal component regression (PCR) chemometric model for Fourier transform infrared (FTIR) analysis of respirable quartz, kaolinite, and coal against international performance standards for occupational hygiene methods, where there are requirements to work within specific levels of expanded uncertainty. In this article, the expanded uncertainty is derived from measurements on samples from workplace environments working with dusts from coal mines.

Crystalline silica is a generic name for minerals with the same elemental composition of silicon and oxygen (SiO_2) but different crystal structures known as polymorphs. The quartz polymorph of crystalline silica is often present as a contaminant in coal and frequently found as a major component in the geological stratum that occurs next to coal seams.

Occupational exposure to aerosols containing respirable crystalline silica (RCS) is a major health issue. The word respirable refers to the particle size fraction that penetrates into the alveoli of the human lung (CEN, 1993). When inhaled, respirable-sized particles of crystalline silica can cause diseases like silicosis (HSE, 2003)

and lung cancer (Rushton *et al.*, 2012). High exposures to RCS can occur in mines due to the use of powered tools to access the seams and extract the coal, and the confined working space which restricts the dispersion and hence dilution of the aerosol. Coal dust itself is also a potential hazard to the health of a worker via inhalation and can cause pneumoconiosis (Ross and Murray, 2004).

In Great Britain (GB) and Australia, samples of workplace aerosol are frequently collected and measured to assess if worker exposures are below workplace exposure limits (WEL). In GB the 8-h WEL for RCS is currently 0.1 mg m^{-3} i.e. 100 $\mu\text{g m}^{-3}$ (HSE, 2005b), whilst in Australia the Workplace Exposure Standard (WES) for RCS is 0.05 mg m^{-3} i.e. 50 $\mu\text{g m}^{-3}$. Samples of aerosol are obtained by drawing a volume of air through a respirable sampler and onto a filter or foam. The respirable sampler is located within the breathing zone of a worker and separates larger non-respirable particles in the sampled aerosol from the smaller respirable fraction. The most common approach is to use a cyclone sampler, where the smaller respirable particles, known as the respirable fraction, are collected onto the filter or foam from the centre of the vortex and the larger non-respirable particles, with larger masses and moments of inertia, move across the air flow and impact onto the body of the sampler. The collected respirable fraction aerosol is then analysed to determine the quantity of respirable hazardous substance (in this case quartz or coal), collected from a known volume of air.

X-ray diffraction (XRD) and FTIR are two analytical techniques that are commonly employed for the measurement of aerosol sampling filters containing RCS (Pickard *et al.*, 1985; HSE, 2014). Raman spectroscopy is also available (Zheng *et al.*, 2018; Stacey *et al.*, 2020) but is a relatively new technique for this type of analysis, and not yet widely used for routine work. Infrared analysis is used more widely than XRD because the instrumentation required is significantly cheaper, easier to use and maintain and provides a quicker analysis (less than 4 min in total). However, both XRD and Raman spectroscopy methods have greater specificity than FTIR as their measurement responses are more directly related to the crystalline structure of quartz present in the samples (Stacey *et al.*, 2021c).

Recent developments in technology have led to the miniaturization of FTIR instruments; which are now portable (Crocombe, 2018; Ashley *et al.*, 2020) and able to be carried to different locations to facilitate end-of-shift, or even end-of-task testing (Cauda *et al.*, 2016). This allows the analysis to be carried out on-site, rather than at a purpose-built laboratory, making results available more quickly and enabling more rapid implementation of any remedial action required to reduce exposures. However, the need for experienced interpretation of FTIR spectra for many workplace samples is a significant limitation on the widespread adoption of this new technology.

Infrared bands at 800 and 780 cm^{-1} are measured for quartz, which is the most common polymorph of RCS. The basic structure of the crystalline unit cell of quartz consists of tetrahedral arrangements of silicon (Si) and oxygen (O) atoms. The tetrahedral arrangement of Si and O is also shared by a larger group of minerals known as silicates, which also have similar absorbance to quartz in the infrared fingerprint range between 500 and 1000 cm^{-1} and so there is some absorbance which is coincident with the 780 and 800 cm^{-1} wavenumbers (Foster and Walker, 1984). Therefore, some absorbance which occurs at infrared bands 780 and 800 cm^{-1} may be attributable to the presence of other silicate minerals, which can affect the accuracy of results. Kaolinite is a silicate that is also a major interference in many workplace samples and is often found in dusts from coal mines (Lee *et al.*, 2013; OSHA, 2015).

Chemometric methods are computational processes that can interrogate spectra to reduce the influence of interference and correlate features in the FTIR spectrum to component concentrations. Several recent studies have explored the use of chemometric and other methods to reduce the effect of interfering minerals on the quartz measurement (Weakley *et al.*, 2014; Miller

et al., 2016; Hart *et al.*, 2018; Salehi *et al.*, 2020). Two common chemometrics methods are partial least squares regression (PLSR) and PCR. Both methods are based on a principal component analysis. Only slight differences between predicted results were found between these chemometric methods, when a similar number of principal components were applied (Stacey *et al.*, 2021a).

Methods

The chemometrics process requires three independent sets of samples—the calibration, validation, and prediction sets. In this study, the calibration and validation sets are based on (and extended upon herein) the preparation of samples with artificial mixtures of the three major components (quartz, kaolinite, and coal). The calibration and validation samples are mostly the same as those used in a previous study (Stacey *et al.*, 2021a). A calibration set defines the relationship between the target values and the magnitude of the vectors for principal components in their spectra. Validation samples are used to determine predicted values from the calibration and check the number of principal components with the minimum variance and the models' biases. A third set of samples known as the prediction set are used to independently challenge the model's capabilities in predicting the quantities of analytes present. To assess the potential for its universal applicability, the performance of the FTIR PCR method, calibrated using artificial mixtures of pure quartz, kaolinite, and Durrans coal dust, was evaluated when measuring samples generated from a wide variety of mine dusts. The chemometric model may over or under model the spectra and potentially produce erroneous results when the mass or proportions of analyte are outside the calibration or validation range or when mineral interferences are present that were not considered. The ability to prepare a range of mixtures with an artificial process is an advantage (when developing a model for its universal application) since these mixtures can be generated to represent the levels and combinations of significant components found in most workplace atmospheres. Quartz, kaolinite, and coal are the most significant components in most dusts from coal mines.

Ten samples of bulk dust collected from coal mines in New South Wales and Western Australia were provided by Pickford and Rhyder Consulting Pty Ltd, Australia. An X-pert pro MPD X-ray diffraction instrument (Malvern Panalytical, Ltd, Malvern, UK) was used to obtain qualitative scans of these bulk samples to identify specific components within these samples. The instrumental parameters for these qualitative measurements

are provided in [Supplementary Information](#) (available at *Annals of Work Exposures and Health* online). These dusts were categorized into three groups (shown in [Fig. 1](#)) based on the crystalline composition and the magnitude in response (high, medium, or low) of the most significant crystalline components using scatter analysis (Xpert Highscore™, Malvern Panalytical Ltd, Malvern, UK). [Table 1](#) describes the sources of the dusts used for the generation of the prediction samples and their composition. [Table 1](#) reports the significant components, although other reflections were also present in the XRD scans indicating the presence of unidentified trace components. Other notable potential mineral components in dust from Australian coal mines include pyrite (Fe_2S), calcite (CaCO_3), and dolomite ($\text{CaMg}(\text{CO}_3)_2$).

Only dolomite is expected to potentially be present in a significant quantity (greater than 10%) ([Ward et al., 1999](#)). XRD scans of the coal mine dusts from the UK are shown in [Supplementary Information](#) (available at *Annals of Work Exposures and Health* online).

The procedure for the generation of prediction samples is described in [Stacey et al. \(2021a\)](#), however, no pure quartz or kaolinite powder was added to the bulk dust mixtures. Aerosols were generated in a glass jar and the respirable dust was collected onto a 25-mm diameter PVC filter using a Safety in Mines Personal Dust Sampler (SIMPEDS) operating at a flow rate of 2.2 l min^{-1} (Casella, Bedford, UK). The flow rate through the respirable sampler was calibrated using a TSI 4100 flow metre (TSI Inc., USA). Two bulk samples from Group 1,

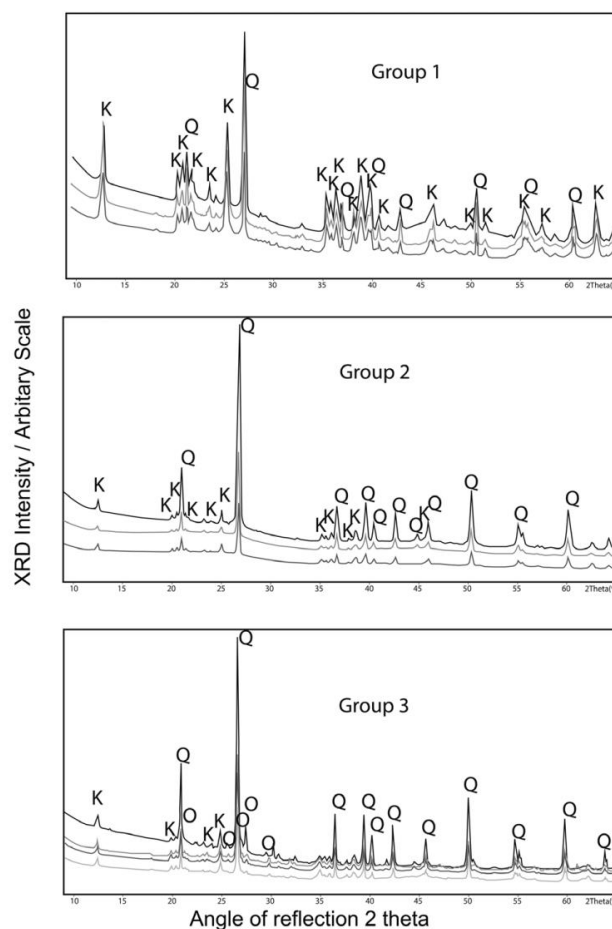


Figure 1. XRD scans of dust samples from Australian coal mines grouped into three sets based on their crystalline composition. The symbol Q denotes XRD reflections attributable to quartz, K denotes XRD reflections attributable to kaolinite, and O denotes XRD reflected attributed to orthoclase or 'ordered' microcline Feldspar minerals. Minor trace reflections attributed to muscovite 2M1 are not shown.

Table 1. Significant crystalline mineral composition and identification of the mine dusts for samples used in the predictions sets.

Identification	Bulk samples	Number of prediction samples	Significant crystalline composition
Australian Group 1	Bulks 8 and 10	12	Quartz (SiO_2), kaolinite ($\text{Al}_2\text{Si}_2\text{O}_5(\text{OH})_4$), trace—mica (muscovite 2M1, $\text{KAl}_2(\text{AlSi}_3\text{O}_{10}(\text{OH})_2$)
Australian Group 2	Bulks 1 and 2	9	Quartz (SiO_2), minor—kaolinite ($\text{Al}_2\text{Si}_2\text{O}_5(\text{OH})_4$)
Australian Group 3	Bulk 9	6	Quartz (SiO_2), minor—kaolinite ($\text{Al}_2\text{Si}_2\text{O}_5(\text{OH})_4$), feldspar possibly microcline or orthoclase (KAlSi_3O_8)
UK Coal 1		10	Graphite (C), minor—quartz (SiO_2), kaolinite ($\text{Al}_2\text{Si}_2\text{O}_5(\text{OH})_4$), illite ($\text{K}_{0.65}\text{Al}_2(\text{Al}_{0.65}\text{Si}_{3.35}\text{O}_{10}(\text{OH})_2$), pyrite (Fe_2S)
UK Coal 2		5	Graphite (C), trace—quartz (SiO_2), kaolinite ($\text{Al}_2\text{Si}_2\text{O}_5(\text{OH})_4$), analcime ($\text{NaAlSi}_2\text{O}_6$), dolomite ($\text{CaMg}(\text{CO}_3)_2$)
South African Durrans (low quartz)		16	Described in Stacey et al. (2021b)
		13	Minor—quartz (SiO_2) and kaolinite ($\text{Al}_2\text{Si}_2\text{O}_5(\text{OH})_4$)

2 bulk samples from Group 2, and 1 bulk sample from Group 3 (containing the highest response from the feldspar mineral) were used to generate 12, 9, and 6 samples, respectively, of aerosolized respirable dust for collection on filters. A total of 16 prediction samples were obtained from the South African mine dust with added kaolinite and quartz from the previous study ([Stacey et al., 2021b](#)) were included and 15 prediction samples from 2 coal seams from a single mine in Wales, in the UK. An additional set of 13 prediction samples (separate to other low quartz content Durrans samples added to the calibration and validation sets) of Durrans coal dust were also prepared to provide an additional check of the models prediction capabilities with low proportions (1–25%) of quartz A9950 and quartz-free kaolinite (Georgia, USA).

Independent target ‘assigned’ values

The procedures used to determine the target values for quartz, kaolinite, and coal are described in [Stacey et al. \(2021a\)](#) and in [Supplementary Information](#) (available at *Annals of Work Exposures and Health* online). In brief, the target mass values for quartz and kaolinite were obtained using a direct on-aerosol-filter XRD method described in the Health and Safety Executive’s (HSE) Method for the Determination of Hazardous Substances (MDHS) 101 ([HSE, 2014](#)). The mass of coal was estimated by subtracting the XRD values for kaolinite and quartz from the value for the mass of respirable dust measured gravimetrically using a balance with a

readability of 1 μg (Mettler-Toledo Ltd, Leicester, UK). Therefore, the target value for coal potentially includes other non-quantified substances in the mine dust.

The XRD measurement was verified, when large proportions of kaolinite (an interference) were present, with an indirect furnace-based method, similar to that described in the National Institute for Occupational Safety and Health (NIOSH) method 7500 ([NIOSH, 2004](#)). Calibrations for the indirect method were prepared using a SIMPEDS to collect amounts of aerosol of the HSE quartz standard A9950 ([Stacey et al., 2009](#)) onto 25-mm diameter PVC filters. The PVC filters were then ashed in a furnace and the residue was recovered and filtered onto 0.45- μm pore size silver filters (SKC Ltd, Blandford, UK). A furnace temperature of 450°C rather than the 600°C specified in NIOSH 7500 was used to provide an opportunity to assess if clays other than kaolinite were present. Kaolinite will dehydroxylate to form an amorphous meta-kaolinite or mullite at this temperature and thus kaolinite is removed from the sample, whereas potential contaminant clays like dickite and illite, with reflections at similar XRD positions as kaolinite, decompose at higher temperatures. The temperature of 450°C successfully removed the coal and reduces the potential for the formation of wollastonite from the presence of any significant calcite.

Infrared analysis

A Perkin Elmer Frontier FTIR instrument was used with Quant software (Perkin Elmer UK Ltd, Beaconsfield, UK).

The standard conditions in MDHS 101 were used for FTIR analysis (HSE, 2014). Thirty-two scans were collected from 560 to 1000 cm^{-1} with a resolution of 4 cm^{-1} . Spectral effects due to external factors (e.g. CO_2 and H_2O) were compensated for by running a background scan prior to analysis of each batch of filters. A first-order derivative was used to process each spectrum before applying the PCR computational process using the Quant software.

The chemometrics process

The chemometrics model determines the spectral features in a scan that correlate best with concentration for the quantification or identification of a component. The process centres spectral data to its mean value and derives a new set of coordinates called eigenvectors from x and y ordinates for wavenumber and absorbance. The eigenvectors showing the maximum variance on different samples are those that are more closely associated with each individual component, and are reduced to a limited number of components that have the largest influence on the spectral profile i.e. the principal components.

For PCR, each sample is processed until the best possible correlation is obtained from a regression between the values determined for the principal components (known as scores) from a combination of a number of components in the spectral profile and the mass of analyte.

The process is developed further for PLSR, where not only the above is applied, but the scores that determine the maximum variability of the spectral data are also explained by scores generated from the variability of the combinations of sample constituents and mass of analyte and then both sets of data are correlated to find the maximum covariance. PLSR models can potentially be derived that use fewer principal components than the PCR model, because the concentration of a component can be given a low weighting if the derived scores poorly describe the observed variability in the spectra. This may reduce the variability of results obtained when the models are challenged with dusts from different atmospheres; since there is a lower potential for the spectral components to be affected by interference. However, the commercial software offers the potential for the user to optimize the number of principal components for the PCR model. This was done for quartz and kaolinite using the strategy described in Stacey *et al.* (2021b).

Estimation of precision and the measurement uncertainty

An assessment of the expanded measurement uncertainty is essential to quantify the reliability of the method for a particular measured value and to assess if the method meets international performance requirements.

To calculate the expanded uncertainty, the analytical method uncertainty is combined with that for the aerosol sampling, which is estimated as 10.1% in ISO 24095 (ISO, 2009). These uncertainty components are combined as the square root of the sum of the squared individual uncertainty values which is then multiplied by a coverage factor of 2 to obtain an expanded uncertainty for the whole measurement process (ISO, 2016).

For each analyte, analytical method uncertainties were calculated by applying an approach to estimate it from the calibration relationship, to the unweighted regression relationships between the predicted and assigned target values (Fig. 2). The equation to find uncertainty of an individual measured value from calibration data is given in equation (1).

$$U(X_{\text{pred}}) = \sqrt{\frac{S^2}{b_i^2} \cdot \left(\frac{1}{1} + \frac{1}{n} + \frac{(X_{\text{pred}} - \bar{X})^2}{(\sum (X_i^2) - (\sum X_i)^2/n)} \right)} \quad (1)$$

where $U(X_{\text{pred}})$ is the estimated uncertainty on the predicted value of X_p , and where in this case, X is the target assigned value of the analyte derived using XRD direct on-filter method, \bar{X} is the mean value of all X and X_i are the individual values of X and ' n ' is the number of samples. S^2 is the mean residual difference in the value predicted by the model (Y) between the observed (Y_{obs}) and the calculated $Y(Y_{\text{cal}}) \sum \frac{(Y_{\text{obs}} - Y_{\text{cal}})^2}{n-2}$, b_i is the slope of best fit for the linear regression (EURACHEM, 2000). To assess the appropriateness of using an unweighted regression, the standard analytical method uncertainties were plotted with the absolute percentage differences for each individual predicted value. In theory, about 60% of absolute differences should be within the analytical method standard uncertainty. Standard deviations of the percentage difference from the target assigned values were also calculated for each analyte in the prediction sample sets.

Limits of detection

The limits of detection (LOD) were calculated from the standard error of the intercept and slope coefficient of the regression between the predicted and assigned target values for each analyte.

$$\text{LOD} = 3.3 \times (c/b_i) \quad (2)$$

where c is the standard error of the intercept from the regression and b_i is the slope of the trend line.

Results and discussion

Optimization for the chemometrics models

The measurements of aerosol filter samples sent from Australia (separate to those used for the prediction sets),

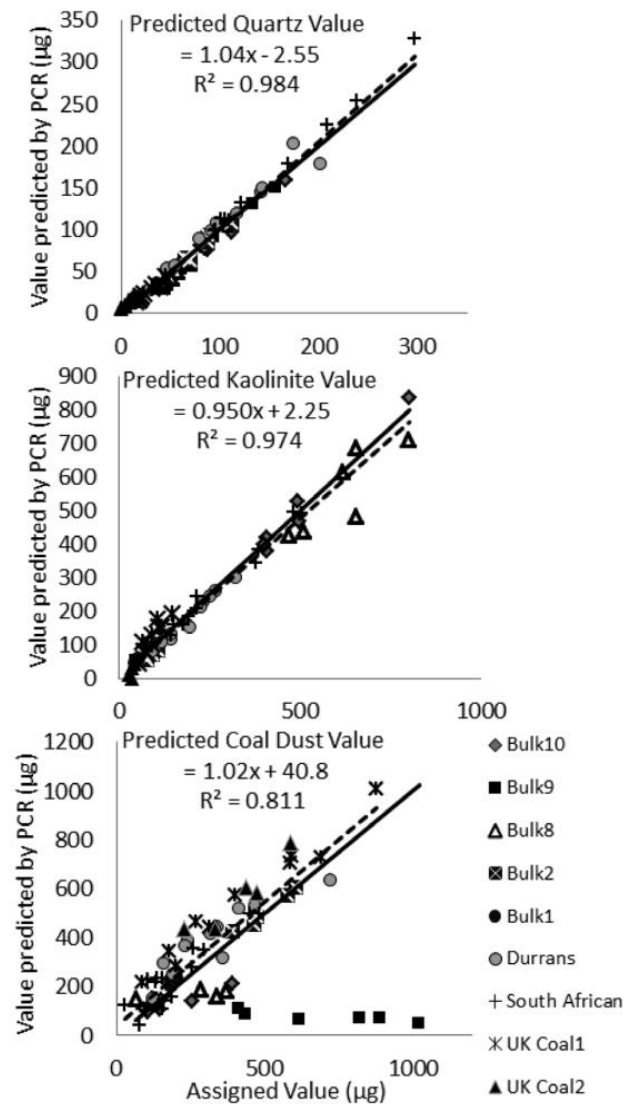


Figure 2. Predicted values for quartz (top), kaolinite (middle) measured using FTIR with PCR method compared against the assigned target value measured using direct on-aerosol filter XRD analysis and coal dust (bottom) which was compared against the remaining mass of respirable dust (assumed as all coal dust). The straight line drawn on the chart is the ideal 1:1 relationship. The dotted line is the linear trend line for the relationship between the two measurement approaches. The trend line equation for coal dust excludes samples from Bulk 9 with the feldspar mineral.

and evaluated for this study using XRD, identified that most respirable dusts from coal mines contained less than 20% quartz whilst some samples had more than 50% kaolinite. These values were outside the range of most calibration and validation samples prepared for the previous PCR or PLSR models (Stacey *et al.*, 2021a). The proportion of kaolinite in some of the Australian aerosol filter samples was more than that found in some British mines (up to 40%) in the 1970s (Dodgson and Whitaker, 1973).

The following changes were introduced to optimize the models for Australian coal mine dusts. Firstly, an additional 13 samples, of artificial mixtures of Durrans coal dust, kaolinite, and 1–10% of HSE quartz standard A9950, were added to the calibration and validation sets. Secondly, the XRD calibration range for quartz was investigated and reduced from 1000 to 400 μg to reduce the influence of a few calibration points with higher loadings when measuring low quartz values. New

calibration coefficients were derived for quartz and new target values were assigned to each calibration and validation sample. The spectrum range for processing was reduced to from 1000 to 966 cm^{-1} to improve the consistency of predicted values for kaolinite.

The average proportions of quartz, kaolinite, and coal in the prediction samples containing dust from Australian coal mines were 11.5% (range 4.9–23%), 37% (range 4.8–84%), and 51% (8.5–89%), respectively. The average proportions in the prediction samples containing dust from UK mines were 4.2% (range 3.5–5.8%), 15.9% (range 11.7–24.6%), and 80% (range 69.6–84.6%) in UK Coal 1 and 0.7% (range 0–1.1%), 4.5% (range 0–8.6%), and 94.8% (range 90.5–100%) in UK Coal 2 for quartz, kaolinite, and coal, respectively. Durrans coal dust contained artificially mixed proportions of quartz (3–33%) and kaolinite (21–39%). A list of proportions for each prediction sample is shown in [Supplementary Information](#) (available at *Annals of Work Exposures and Health* online).

The PCR model

Figures comparing the values calculated by the PCR for the calibration and validation samples with their assigned target values are provided in [Supplementary Information](#) (available at *Annals of Work Exposures and Health* online) as [Fig. S3](#) for quartz, [Fig. S4](#) for kaolinite, and [Fig. S5](#) for coal. Statistics from the software recalculation of the PCR model are shown in [Table 2](#).

[Fig. 2](#) compares the predicted values obtained from the PCR model with the target values for quartz, kaolinite, and coal.

Verification of the assigned target values

Assigned target values for quartz were checked on 10 filters using XRD and a separate indirect recovery XRD method when the proportion of kaolinite in the sample was high (above 50%); since significant interference could occur for the principal and secondary quartz reflections at 2 theta degrees of 26.6 and 20.9. The average difference and standard deviation from the PCR predicted values from the target values were $-10.4 \pm 6.2\%$, and the difference from the indirect XRD analysis

method involving the furnace recovery process was $-7.7 \pm 6.6\%$. The means are not significantly different with a *t*-test probability (*P*) value for equal variance of 0.38, which is more than 0.05.

Precision, limit of detection, and uncertainty

For the PCR model, the average percent difference from the assigned target value was 0.78, -1.57 , and 13.4% for quartz, kaolinite, and coal, respectively, with standard deviations of 15.4, 17.5, and 63.8%. While for the PLSR model, for the purposes of the comparison, the average percent difference from the assigned target value was 4.03, 0.02, and 65.1% for quartz, kaolinite, and coal, respectively, with standard deviations of 15.8, 18.8, and 60.2%.

The percentage difference from each assigned target value for quartz, showing the spread and bias of individual results, is in [Fig. 3](#).

Values for the LODs were 5.0 μg (quartz), 25 μg (kaolinite), and 71 μg (coal) for the PCR and 4.7 μg (quartz), 29 μg (kaolinite), and 96 μg (coal) for the PLSR method, respectively. None of the values for coal include results from Bulk 9. The values for quartz are close to the LOD and limit of quantification of 3 and 10 μg , respectively, for the FTIR method reported in MDHS 101 (HSE, 2014). The approach used to calculate the LOD for XRD in the MDHS 101 method is different from the chemometrics approach applied to FTIR because it is determined by making repeat measurements on clean filters. An LOD of 5 μg corresponds to a quartz concentration of 10 $\mu\text{g m}^{-3}$, assuming a 4-h sample collected at a flow rate of 2.2 l min^{-1} .

The estimated standard uncertainty of these measurements (which should be equivalent to about 1 SD of values) from the PCR model for quartz, kaolinite, and coal are plotted in [Fig. 4](#) together with the absolute percentage difference of the individual results from the assigned target values. About 60–70% of the absolute percent difference values are below the standard uncertainty trend line for each analyte (quartz, 61%, kaolinite, 70%, and coal, 62%). Ideally, the estimate should represent 60% results; so 70% is a slightly cautious estimation of the analytical method uncertainty for kaolinite

Table 2. Statistics for the PCR models for quartz, kaolinite, and coal in artificial mixtures of Durrans coal dust.

Analyte	Number of principal components	Percent of explained variance (%)	Standard error of the regression (μg)	Standard error of the predictions (μg)
Quartz	3	99.5	9.1	9.6
Kaolinite	2	96.9	25	25
Coal	18	99.7	15	32

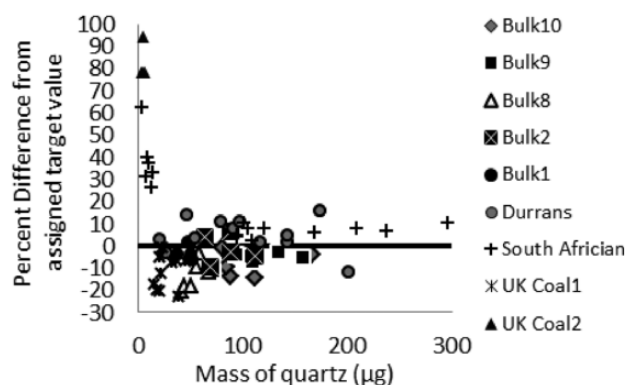


Figure 3. Precision of the FTIR and PCR method when measuring quartz in coal dust samples from various sources with three principal components.

measurements. A small number of extreme values were excluded from the calculation of the standard uncertainty relationships where the residual difference for the predicted value was greater than a z score of 3 (quartz = 2, kaolinite = 3, and coal = 1).

Uncertainties were higher for kaolinite and coal than for quartz (Fig. 4). For coal, the variability was due to differences between the sources of the mine dusts (Fig. 2), the relatively few prominent distinguishing features in its spectra (Stacey *et al.*, 2021a), and the uncertainty of the gravimetric measurements themselves.

The chemometric models for coal are calibrated with a coal dust that is relatively free of other components, whilst real samples also contain minor or trace levels of other substances (Table 1, Fig. 1, and Supplementary Fig. S1, available at *Annals of Work Exposures and Health* online) included in the gravimetric analysis, besides quartz and kaolinite. This may introduce some additional uncertainty for the assigned value for coal. In addition, a principal component value of 18 for coal is relatively high and may result in over modelling, which may poorly predict samples that are independent from the calibration and validation. However, smaller numbers of principle components increased the differences between the predicted and assigned values for coals from different bulk samples. A typical example is demonstrated for the results obtained using the PLSR model with seven principal components (Supplementary Fig. S8, available at *Annals of Work Exposures and Health* online). The larger number of principal components potentially compensates for any spectral differences attributable to a specific characteristic of the coal in the mine dust e.g. the higher crystallinity coals from the UK.

For kaolinite, the low XRD intensity for the principal reflections, relative to quartz, influenced the uncertainty precision for the target values; however, higher relative

errors were also obtained for some mass values above 500 μg (Fig. 2, Bulk 8). Samples with amounts of illite (such as the UK coal samples) reported consistently higher results for kaolinite. The PLSR model was affected to a greater extent (Supplementary Fig. S7, available at *Annals of Work Exposures and Health* online). This difference is potentially due to similar O–H absorbance near those for kaolinite at 915 cm^{-1} , the presence of poorly crystalline clays, or interference from dolomite; which has an absorbance close to that for kaolinite at 900 cm^{-1} .

The values of uncertainty for quartz are of particular interest because of its health concern and its relatively low occupational WEL, namely 0.1 mg m^{-3} ($100\text{ }\mu\text{g m}^{-3}$) in GB and 0.05 mg m^{-3} ($50\text{ }\mu\text{g m}^{-3}$) in Australia. The trend line equation for quartz (Fig. 4) indicates that the analytical uncertainty is about 6.7% (1 SD) when measuring a mass of $103\text{ }\mu\text{g}$ collected from an aerosol containing $100\text{ }\mu\text{g m}^{-3}$ of quartz, using a standard respirable sampler operating at 2.2 l min^{-1} for a full 8-h working shift. The standard uncertainty for the analytical method increases to 13% when the sampling time is reduced to 4 h. This is also the uncertainty if measuring half the mass, namely a mass of $53\text{ }\mu\text{g}$ of quartz from an aerosol containing $50\text{ }\mu\text{g m}^{-3}$ of quartz using a standard respirable sampler operating at 2.2 l min^{-1} for a full 8-h working shift.

A value of 33% was obtained for the expanded uncertainty at $53\text{ }\mu\text{g}$ (representative of an aerosol of $50\text{ }\mu\text{g m}^{-3}$). This expanded uncertainty value is close to the $\pm 30\%$ performance requirement specified in the international standard ISO 20581 for measuring occupation exposure limits (ISO, 2016). Measurements will meet the ISO 20581 expanded uncertainty requirement for measurement at the GB WEL if the sample is collected for about 4 h 30 min with existing equipment or a higher

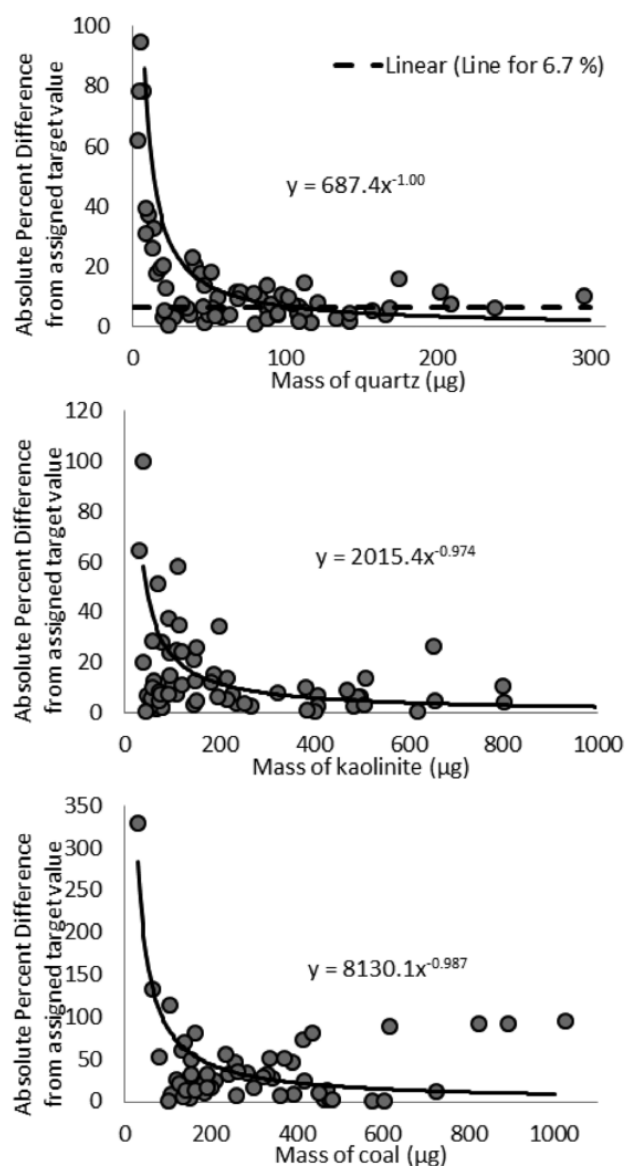


Figure 4. Calculated uncertainties for quartz, kaolinite, and coal dust predictions using the FTIR and PCR method. The trend line is the analytical method uncertainty calculated using the formula for determining analytical uncertainty from calibration data. The dots represent the absolute relative difference for individual results from the assigned target value.

flow rate sampler is used at about 4 l min^{-1} to sample more than 528 l of the workplace atmosphere. Different respirable samplers may also have different deposition profiles for the collected aerosol (ISO, 2015). If a higher flow rate sampler is used with this PCR model, it will be necessary to check that the sensitivity is the same as that obtained from the SIMPEDS; which was used to prepare the calibration and validation standards.

The WEL for respirable kaolin in GB is higher than that for RCS at 2 mg m^{-3} (i.e. 2000 μg m^{-3}) (HSE,

2005b) where the predicted analytical precision would be about 1.2%. In this case, the uncertainty would be purely limited by the variability of the sampling apparatus. Internationally, exposure limits for respirable dust in coal mines vary from about 400 to 3000 μg m^{-3} (IFA, 2021). GB has deemed respirable dust, when present at a concentration in air equal to, or greater than, 4 mg m^{-3} (4000 μg m^{-3}) as a time-weighted average over an 8-h period, to be a substance hazardous to health and so the Control of Substances Hazardous to Health (COSHH)

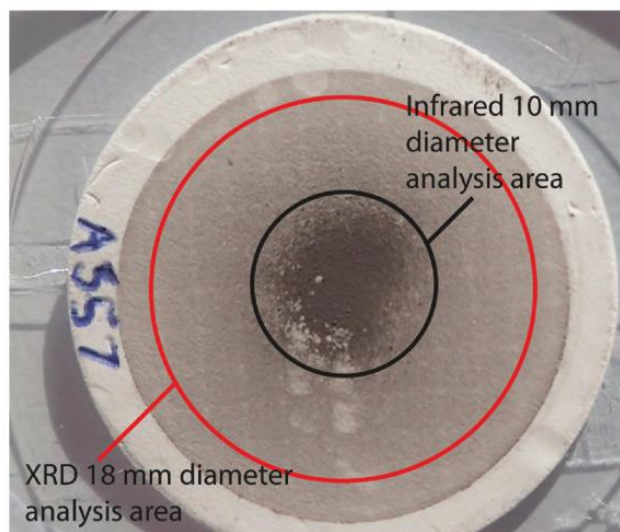


Figure 5. A filter containing respirable coal dust with some dust lost from the filter's centre. A circle with a diameter of approximately 18 mm in diameter is drawn on the filter to represent the estimated analysis area for the XRD measurement and a similar circle of approximately 10 mm in diameter is drawn for the FTIR analysis area.

regulations apply (HSE, 2005a). Most exposure standards for respirable dust in coal mines are based on measuring the total respirable dust captured using gravimetric analysis. A PCR measurement might not be appropriate to assess exposure to a respirable coal mine dust standard since it employs a different metric to more specifically quantify the coal, and results for the respirable fraction would be lower than that reported in historical data. The specific PCR measurement does, however, provide hygienists, other occupational health professionals, regulators, and duty holders with better detailed information about the nature of the exposure, i.e. the proportions of major constituents (e.g. quartz and kaolinite present in the coal dust).

Practical issues

In a limited number of samples (Fig. 4), the comparability between XRD target values and FTIR results was compromised due to the potential for loss of dust from the centre of the aerosol filters containing coal mine dust (Fig. 5) at mass loadings around or greater than 0.5 mg. Losses occurred during transport from the sampling location to the laboratory, when removing the filter from its cassette for analysis, transfer to and from a filter holder for the FTIR and prolonged exposure in the infrared beam. Fig. 5 shows the typical image for loss of coal mine dust from the centre of an aerosol filter. The clear patches towards the centre are areas where the dust has fallen off. This is a particular problem for FTIR analysis since the analysis area for these instruments is

typically 6–10 mm. The FTIR results will be lower than the XRD value because the XRD is able to analyse a wider area (about 18 mm in diameter) and so the loss of dust is proportionally less.

Filter handling and transport is an important part of the analytical process for samples containing coal; since dust can be lost from the filter's centre, which is the within the area measured by the FTIR instrument. Filter cassettes designed to minimize handling may have an important role in reducing the potential for dust loss. It would be advantageous to measure the samples as close to the worksite as possible to reduce the potential for losses of dust during transport. Portable FTIR instruments are one option that would facilitate the analysis of samples at the site by hygienists or duty holders. Calibrations between these portable FTIR instruments were shown to be comparable (Ashley *et al.*, 2020) which implies that a single chemometric method may also be transferable between instruments.

Conclusion

The PCR model accurately measured quartz and kaolinite in dusts from a range of coal mines, from different countries and Australian states, containing a variety of different minerals, coal types, and proportions of these minerals in their matrix.

The expanded uncertainty of measurements for quartz, kaolinite, and coal when using the FTIR and PCR method either met or were close to the international

performance requirements for occupational exposure measurements at airborne concentrations equivalent to current GB and Australian WEL.

For quartz, the expanded measurement uncertainty meets the requirements of ISO 20581 at the GB WEL concentration of 0.1 mg m^{-3} ($100 \text{ } \mu\text{g m}^{-3}$) when sampling for 4.5 h using a respirable sampler operating at 2.2 l min^{-1} . An 8-h sampling period would be needed when measuring an RCS aerosol at the Australian WEL concentration of 0.05 mg m^{-3} ($50 \text{ } \mu\text{g m}^{-3}$), which would be suitable when monitoring mine workers since sampling generally occurs for their whole working shift (often about 8–12 h).

The LOD for quartz of $5.0 \text{ } \mu\text{g}$ is comparable with those published for direct on-aerosol filter measurement methods like that for XRD in MDHS 101, where the limit of detection is determined by analysis of clean unused filters and the calibration relationship is by the measurement of a pure quartz standard. A limit of detection of $5.0 \text{ } \mu\text{g}$ equates to a quartz concentration of $10 \text{ } \mu\text{g m}^{-3}$, (which is 1/10th of the current GB exposure limit of 0.1 mg m^{-3}) assuming a 4-h sample collected at a flow rate of 2.2 l min^{-1} .

Supplementary Data

Supplementary data are available at *Annals of Work Exposures and Health* online.

Funding

The work presented in this article was funded by the Health and Safety Executive (HSE) in the UK.

Disclaimer

The opinions expressed in this article are those of the authors and do not necessarily reflect the views of the Health and Safety Executive (HSE). There is no commercial relationship between Pickford & Rhyder Consulting Pty Ltd and the HSE.

Acknowledgements

Thanks to Ian Pengelly, Shirley Haslett, Laurie Davies, Margaret Wade, Clare McNicholas, and Susan Hambling at HSE who conducted the internal HSE technical and editorial reviews. Cliff Seymour, Trevor Lowe, and Vincent Fowler [all Her Majesty's Inspectorate for Health and Safety (Mines)] for their help with the project and for identifying and collecting challenging sources of UK coal dust and Kate Jones (HSE) who helped identify potential partners in Australia.

Data availability

Data will be shared on reasonable request to the corresponding author.

References

- Ashley EL, Cauda E, Chubb LG *et al.* (2020) Performance comparison of four portable FTIR instruments for direct-on-filter measurement of respirable crystalline silica. *Ann Work Expo Health*; 64: 536–46.
- Cauda E, Miller A, Drake P. (2016) Promoting early exposure monitoring for respirable crystalline silica: taking the laboratory to the mine site. *J Occup Environ Hyg*; 13: D39–45.
- CEN. (1993) *EN 481:1993 workplace atmospheres—size fraction definitions for measurement of airborne particles*. Brussels, Belgium: European Committee for Standardisation.
- Crocombe RA. (2018) Portable spectroscopy. *Appl Spectrosc*; 72: 1701–51.
- Dodgson J, Whitaker W. (1973) The determination of quartz in respirable dust samples by infrared spectrophotometry—I: the potassium bromide disc method. *Ann Occup Hyg*; 16: 373–87.
- EURACHEM. (2000) *Quantifying uncertainty in analytical measurement*. Sugiez, Switzerland: Cooperation on International Traceability in Analytical Chemistry (CITAC).
- Foster RD, Walker RF. (1984) Quantitative determination of crystalline silica in respirable-size dust samples by infrared spectrophotometry. *Analyst*; 109: 1117–27.
- Hart JF, Autenrieth DA, Cauda E *et al.* (2018) A comparison of respirable crystalline silica concentration measurements using a direct-on-filter Fourier transform infrared (FT-IR) transmission method vs. a traditional laboratory X-ray diffraction method. *J Occup Environ Hyg*; 15: 743–54.
- HSE. (2003) *EH75 respirable crystalline silica, variability in fibrogenic potency and exposure-response relationships for silicosis*. Suffolk, UK: Health and Safety Executive Books.
- HSE. (2005a) *The control of substances hazardous to health regulations 2002 (as amended)*. Norwich, UK: Health and Safety Executive, Crown.
- HSE. (2005b) *EH40/2005 workplace exposure limits, containing the list of workplace exposure limits for use with the control of substances hazardous to health regulations (as amended)*. Norwich, UK: Health and Safety Executive, Crown.
- HSE. (2014) *Methods for the determination of hazardous substances, MDHS 101/2 crystalline silica in respirable airborne dust, direct on-filter analyses by infrared spectroscopy and X-ray diffraction*. Norwich, UK: Health and Safety Executive (HSE), Crown.
- IFA. (2021) GESTIS-Substance Database. International limit values for chemical agents (occupational exposure limits, OELs) [Online]. Sankt Augustin, Germany: Institut fuer Arbeitsschutz der Deutschen Gesetzlichen Unfallversicherung (IFA). Available at <https://www.dguv.de/ifa/gestis/gestis-internationale-grenzwerte-fuer-chemische-substanzen-limit-values-for-chemical-agents/index-2.jsp>. Accessed 6 January 2022.
- ISO. (2009) *ISO 24095:2009. Workplace air—guidance for the measurement of respirable crystalline silica*. Geneva, Switzerland: International Standards Organisation. ISBN 978 0 580 58960 7.

- ISO. (2015) 16258-1. *Workplace air—analysis of respirable crystalline silica using X-ray diffraction. Part 1. Direct-on-filter method*. London, UK: British Standards Institution.
- ISO. (2016) *BSI ISO 20581 workplace air—general requirements for the performance of procedures for the measurement of chemical agents*. Geneva, Switzerland: International Organization for Standardization.
- Lee T, Chisholm WP, Kashon M *et al.* (2013) Consideration of kaolinite interference correction for quartz measurements in coal mine dust. *J Occup Environ Hyg*; 10: 425–34.
- Miller AL, Weakley T, Griffiths P *et al.* (2016) Direct-on-filter α -quartz estimation in respirable coal mine dust using transmission Fourier transform infrared spectrometry and partial least squares regression. *Appl Spectrosc*; 71: 1014–24.
- NIOSH. (2004) *Silica, crystalline, by XRD (filter redeposition) Method 7500*. Department of Health and Human Services, National Institute for Occupational Safety and Health. Available at <https://www.cdc.gov/niosh/docs/2003-154/default.html>. Accessed 6 January 2022.
- OSHA. (2015) *Method ID142. Crystalline silica. Quartz and cristobalite*. Sandy, UT: Industrial Hygiene Chemistry Division, OSHA Salt Lake Technical Center.
- Pickard KJ, Walker RF, West NG. (1985) A comparison of X-ray diffraction and infra-red spectrophotometric methods for the analysis of α -quartz in airborne dusts. *Ann Occup Hyg*; 29: 149–67.
- Ross MH, Murray J. (2004) Occupational respiratory disease in mining. *Occup Med*; 54: 304–10.
- Rushton L, Hutchings SJ, Fortunato L *et al.* (2012) Occupational cancer burden in Great Britain. *Br J Cancer*; 107: S3–7.
- Salehi M, Zare A, Taheri A. (2020) Artificial neural networks (ANNs) and partial least squares (PLS) regression in the quantitative analysis of respirable crystalline silica by Fourier-transform infrared spectroscopy (FTIR). *Ann Work Expo Health*; 65: 346–57. doi:10.1093/annweh/wxaa097.
- Stacey P, Clegg F, Morton J *et al.* (2020) An indirect Raman spectroscopy method for the quantitative measurement of respirable crystalline silica collected on filters inside respiratory equipment. *Anal Methods*; 2757–71. doi:10.1039/D0AY00165A.
- Stacey P, Clegg F, Sammon C. (2021a) Multicomponent measurement of respirable quartz, kaolinite and coal dust using Fourier transform infrared (FTIR) with commercially available chemometric software: a comparison between partial least squares and principal component regressions. doi:10.1093/annweh/wxab081.
- Stacey P, Clegg F, Sammon C. (2021b) Multicomponent measurement of respirable quartz, kaolinite and coal dust using Fourier transform infrared spectroscopy (FTIR): a comparison between partial least squares and principal component regressions. *Ann Work Expo Health*.
- Stacey P, Hall S, Stagg S *et al.* (2021c) Raman spectroscopy and X-ray diffraction responses when measuring health-related micrometre and nanometre particle size fractions of crystalline quartz and the measurement of quartz in dust samples from the cutting and polishing of natural and artificial stones. *J Raman Spectrosc*; 52: 1095–107.
- Stacey P, Kauffer E, Moulut JC *et al.* (2009) An international comparison of the crystallinity of calibration materials for the analysis of respirable alpha-quartz using X-ray diffraction and a comparison with results from the infrared KBr disc method. *Ann Occup Hyg*; 53: 639–49.
- Ward CR, Spears DA, Booth CA *et al.* (1999) Mineral matter and trace elements in coals of the Gunnedah Basin, New South Wales, Australia. *Int J Coal Geol*; 40: 281–308.
- Weakley AT, Miller AL, Griffiths PR *et al.* (2014) Quantifying silica in filter-deposited mine dusts using infrared spectra and partial least squares regression. *Anal Bioanal Chem*; 406: 4715–24.
- Zheng L, Kulkarni P, Birch ME *et al.* (2018) Analysis of crystalline silica aerosol using portable Raman spectrometry: feasibility of near real-time measurement. *Anal Chem*; 90: 6229–39.

Correction to: Application of a Fourier Transform Infrared (FTIR) Principal Component Regression (PCR) chemometric method for the quantification of respirable crystalline silica (quartz), kaolinite and coal in coal dusts from Australia, United Kingdom and South Africa.

Peter Stacey*++, Francis Clegg++, Gary Rhyder# and Christopher Sammon++.

*Health and Safety Executive, Science Division, Harpur Hill, Buxton, Derbyshire, SK17 9JN, United Kingdom

++Sheffield Hallam University, Materials and Engineering Research Institute, Sheffield, S1 1WB United Kingdom

#Pickford & Rhyder Consulting Pty Ltd, PO Box 975, Ryde NSW 1680, Australia.

The focus of this article was on the principal component regression (PCR) chemometrics model, however, some results for the partial least squares regression (PLSR) were also provided for comparison. The average and standard deviations of the percentage differences from the assigned target values for kaolinite and coal dust with the PLSR model did not include results from the most recently added data. Table 1 is provided below with corrected values for all data excluding values below the limits of detection. For comparison, results for the PCR model are also included.

In addition, there was a difference in the limit of detection calculated for kaolinite when using the PCR model, which changed from 25 µg to 20 µg.

Table 1. For each analyte and chemometric model, averages and standard deviations of the percentage differences from the assigned target values.

Chemometric Model	Statistic	Analyte		
		Quartz	Kaolinite	Coal
PLSR	Average	4.0%	13.6%*	37.5%*
	Standard deviation	15.8%	36.3%*	67.4%*
PCR	Average	0.78%	-1.57%	15.5%
	Standard deviation	15.4 %	17.5%	62.3%

*denotes values with a significant change

Supplementary Information

Application of a Fourier Transform Infrared (FTIR) Principal Component Regression (PCR) Chemometric Method for the Quantification of Respirable Crystalline Silica (Quartz), Kaolinite, and Coal in Coal Mine Dusts from Australia, UK, and South Africa.

Peter Stacey^{***}, Francis Clegg⁺⁺, Gary Rhyder[#] and Christopher Sammon⁺⁺.

X-ray diffraction conditions for the qualitative scans shown in Figure 1.

A scan of a 10 mm diameter pellet of pressed coal dust powder was taken using an X-pert pro MPD X-ray diffraction instrument with Bragg–Brentano focusing geometry. Each material was scanned from a 2 theta angle of six degrees to a 2 theta angle of 70 degrees at a rate of 0.03 degrees per step of 120 s. The instrument used a line from a broad focus copper tube operated at 50 kW and 45 mA with 10 mm mask in front of a one degree fixed divergence slit which irradiated sample spinning at 1 rotation per second. A nickel filter was placed in front of the copper tube. An array detector was used with a detection area set at 2.12 degrees.

X-ray diffraction analysis for the determination of the assigned target values.

Measurement conditions for quantitative analysis

For quartz, the instrument used the second set of standard instrumental conditions described in Table A1 of the International Standards Organization (ISO) standard method ISO 16258-1; 2015 (ISO, 2015). The instrument was fitted with a broad focus copper tube set at 50 kW and 45 mA, automatic scattering and receiving slits set to provide an illumination length of 18 mm, and an array detector with the detection area set at a 2 θ range of 2.12 degrees. The area of the three most intense XRD positions of α -quartz at 2 θ angles of, 20.9, 26.6 and 50.1 degrees were measured for 600 seconds, 420 s and 600 s, respectively, for each 0.03 2 θ degree interval over the two degree range cantered on the measurement intensity. The total sample analysis time was about 30 minutes. Tube drift was corrected using the measurement of an aluminium plate as an external standard. The average of the results obtained from the three intensities was used as the quartz 'assigned' value.

For kaolinite, the area of the two most intense diffraction positions free from quartz interference at 2θ degrees of 12.2 and 25 were used for quantification. A scan of a sample was collected from 6 to 60 degrees in steps of 0.02 and 60 s per step. The total scan time was 25 minutes. Each measurement intensity was quantified using a 2θ range of two degrees. The average of the two results obtained from each of the kaolinite measurement intensities was used as the kaolinite 'independent' value.

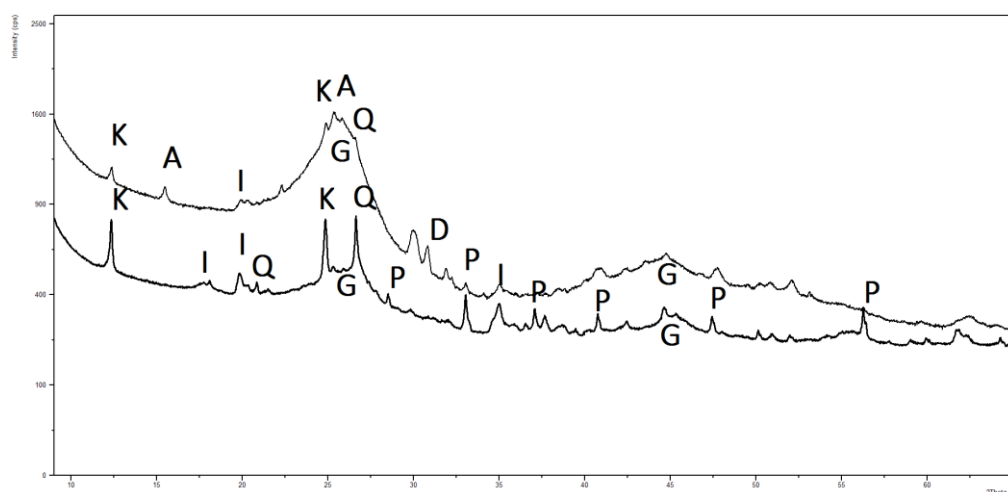


Figure S1. X-ray diffraction scans for two coal dusts from the United Kingdom. The bottom scan is UK coal 1 and the top scan is UK coal 2. The top scan is offset by 1.4. The following letters denote the intensities that are attributable to a mineral in the coal dust. Only significant phases are identified. K denotes Kaolinite ($\text{Al}_2\text{Si}_2\text{O}_5(\text{OH})_4$), I denotes Illite ($\text{K}_{0.65}\text{Al}_2(\text{Al}_{0.65}\text{Si}_{3.35}\text{O}_{10})(\text{OH})_2$), Q denotes α -quartz (SiO_2), P denotes pyrite (Fe_2S), G denotes a graphite (C, anthracite) D denotes dolomite ($\text{CaMg}(\text{CO}_3)_2$) and A is for Analcime ($\text{NaAlSi}_2\text{O}_6$)

Analyte	Number of principal components	Percent Explained Variance	Standard error for the calibration	Standard error of the prediction
Quartz	3	99.5 %	9.1 μg	9.4 μg
Kaolinite	6	99.2 %	13 μg	13 μg
Coal	7	99.6 %	24 μg	27 μg

Table S1. Number of principal components and statistics for the PLSR method

The PLSR model used the sample calibration and validation samples with the same assigned target values as the PCR. The spectra were processed in the same way. The only difference in treatment was the type of chemometric model applied to the spectra.

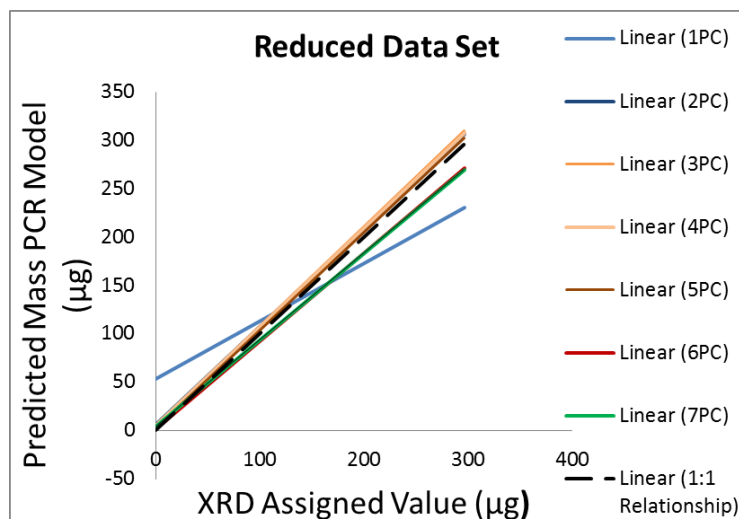


Figure S2. Change in slope and intercept with number of principal components for the reduced calibration set for quartz when using the FTIR PCR method relative to the XRD assigned value.

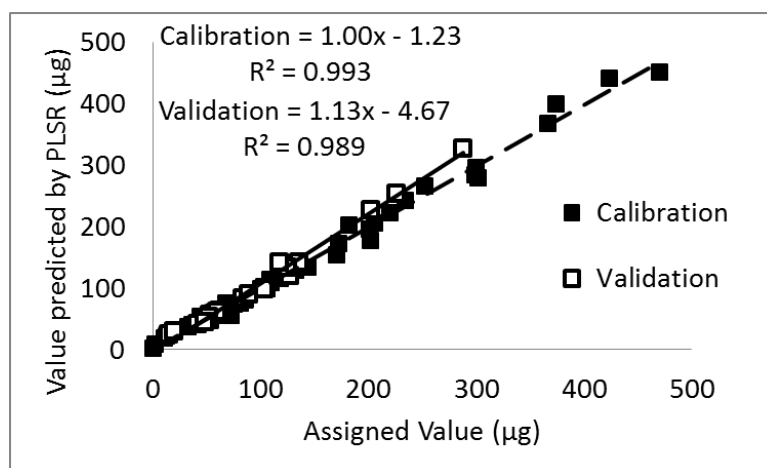


Figure S3. Quartz, a comparison of the values predicted by the FTIR PCR method and the target XRD assigned values obtained from the calibration and validation samples

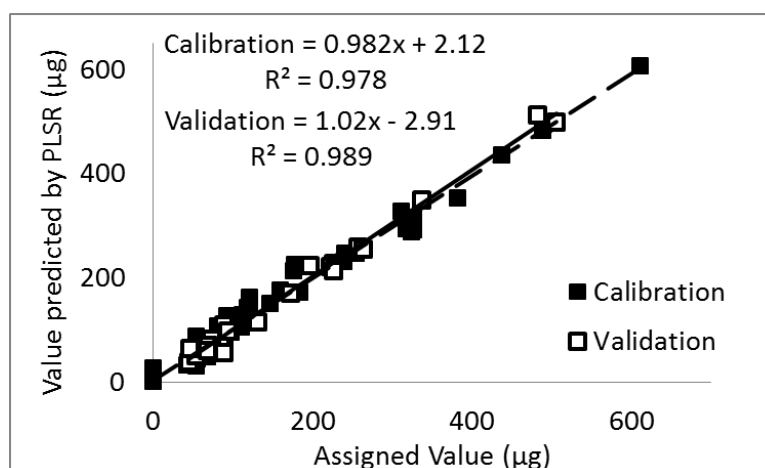


Figure S4. Kaolinite, a comparison of the values predicted by the FTIR PCR method and the target XRD assigned values obtained from the calibration and validation samples

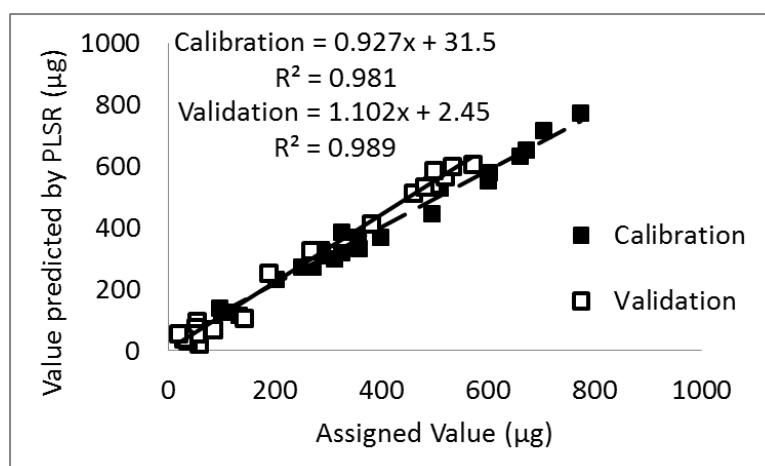


Figure S5. Durrans coal dust, a comparison of the values predicted by the FTIR PCR method and the target XRD assigned values obtained from the calibration and validation samples

Figures S6 to S8 compare the predicted values obtained from the PLSR model with the target values for quartz, kaolinite and coal assigned to the samples generated from the bulk powders. Samples were generated from Bulk 1, Bulk 2, Bulk 8 Bulk 9, Bulk 10, UK Coal 1 and UK coal 2. Also shown are the results for 13 additional samples with artificial mixtures of Durrans coal dust, kaolinite and HSE quartz standard. Durrans coal dust was mixed with the HSE quartz standard A9950 and pure kaolinite powder. In addition, 16 samples from a South African coal used in previous work were also included in the evaluation.

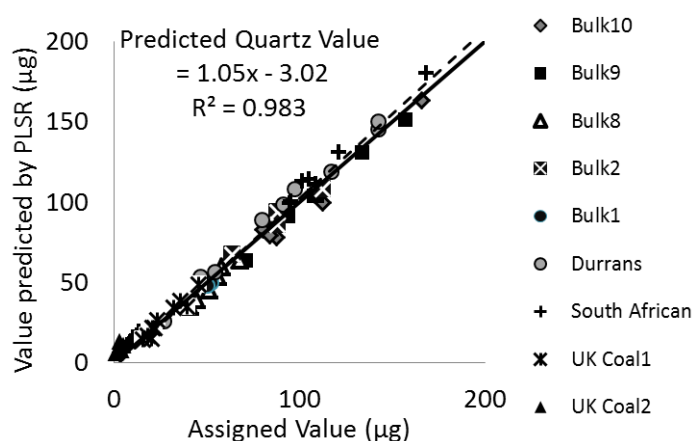


Figure S6. Quartz measured using direct -on-aerosol filter FTIR with PLSR method compared against the measured assigned value using XRD at HSE's Science and Research centre. The linear line represents the ideal 1:1 relationship.

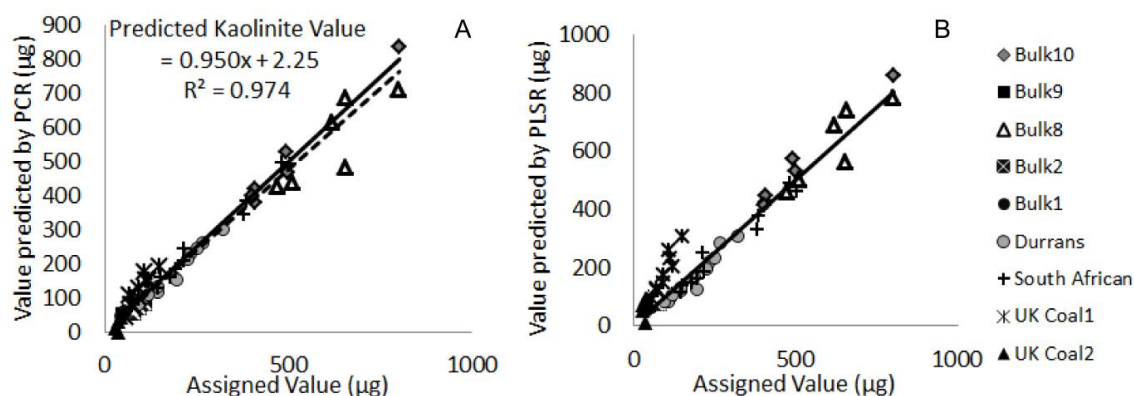


Figure S7. Kaolinite measured using direct -on-aerosol filter FTIR with PCR method (A) using 2 principal components and the PLSR method (B) using 6 principal components. The x axis is the measured assigned value using XRD at HSE's Science and Research centre. The linear line represents the ideal 1:1 relationship.

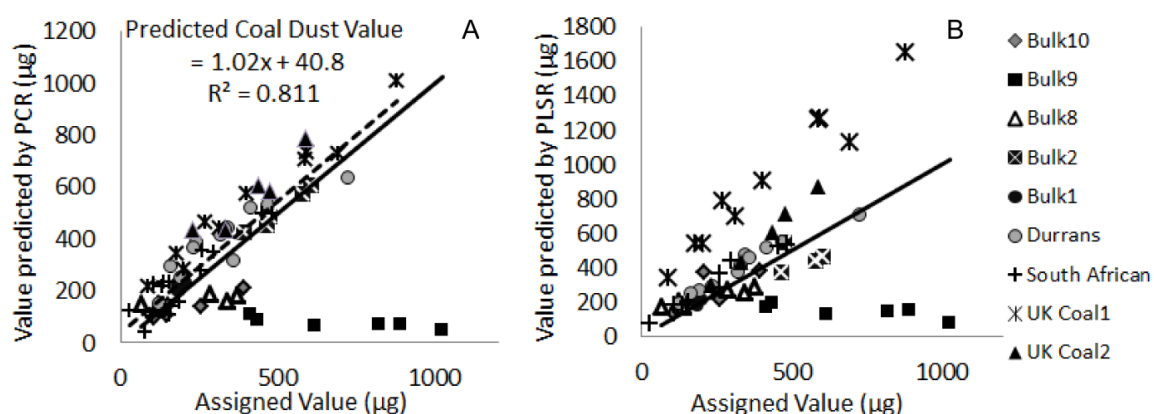


Figure S8. Coal dust measured using direct -on-aerosol filter FTIR: A comparison between the PCR method (A) using 18 principal components and the PLSR method (B) using 7 principal components a. The linear line represents the ideal 1:1 relationship.

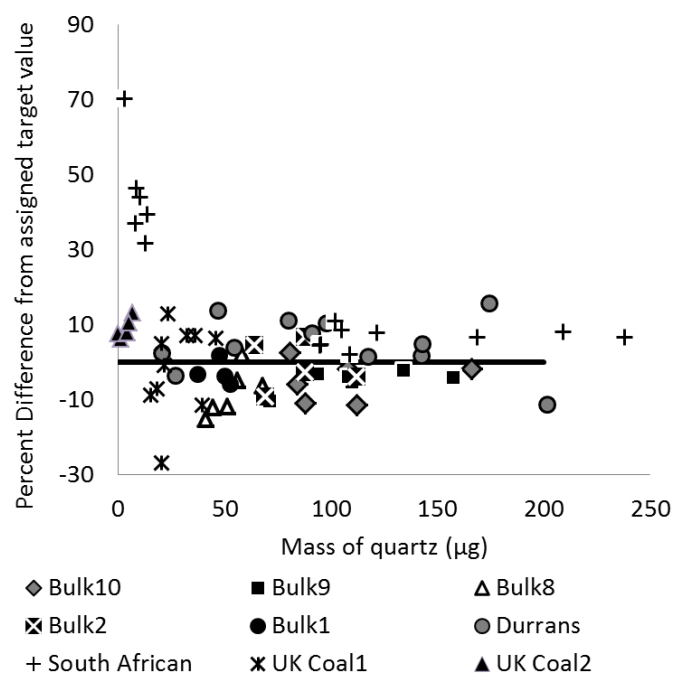


Figure S9. Precision of the PLSR method when measuring quartz in coal dust samples from various sources with 3 principal components.

Table S1. Proportions of each analyte in each prediction sample

Sample Identification	Percentage of analyte		
	Quartz	Kaolinite	Coal Dust
Bulk 1 S1	13.40	17.47	69.13
Bulk 1 S2	15.16	18.41	66.43
Bulk 1 S3	16.94	19.77	63.29
Bulk 1 S4	16.63	19.96	63.42
Bulk 1 S5	12.64	14.44	72.92
Bulk 2 S1	10.50	11.95	77.55
Bulk 2 S2	11.36	13.23	75.41
Bulk 2 S3	13.22	14.41	72.36
Bulk 2 S4	13.49	13.34	73.16
Bulk 8 S1	4.98	60.67	34.35
Bulk 8 S2	5.33	61.19	33.48
Bulk 8 S3	5.90	74.97	19.13
Bulk 8 S4	6.05	74.27	19.68
Bulk 8 S5	5.10	69.91	24.99
Bulk 8 S6	6.64	84.87	8.49
Bulk 9 S1	10.65	8.10	81.25
Bulk 9 S2	21.24	13.02	65.74
Bulk 9 S3	22.81	13.93	63.26
Bulk 9 S4	6.17	4.87	88.95
Bulk 9 S5	12.17	7.60	80.23
Bulk 9 S6	10.10	7.77	82.13
Bulk 10 S1	12.19	59.00	28.81
Bulk 10 S2	10.64	63.03	26.33
Bulk 10 S3	10.83	58.63	30.54

Sample Identification	Percentage of analyte		
	Quartz	Kaolinite	Coal Dust
Bulk 10 S4	11.75	69.79	18.46
Bulk 10 S5	11.61	64.54	23.85
Bulk 10 S6	11.82	64.30	23.88
Durrans S1	1.82	26.42	71.76
Durrans S2	3.14	39.49	57.36
Durrans S3	7.29	37.53	55.18
Durrans S4	8.68	37.09	54.23
Durrans S5	12.00	33.17	54.83
Durrans S6	13.51	32.01	54.48
Durrans S7	31.34	31.02	37.65
Durrans S8	29.61	30.31	40.07
Durrans S9	33.18	31.08	35.75
Durrans S10	27.31	26.76	45.93
Durrans S11	28.46	24.16	47.39
Durrans S12	25.54	21.32	53.14
Durrans S13	17.05	37.18	45.77
South African S2	19.50	40.09	40.41
South African S3	23.55	40.34	36.12
South African S4	32.59	54.41	13.00
South African S5	23.31	39.93	36.76
South African S6	24.18	42.37	33.46
South African S7	23.40	43.98	32.62
South African S8	24.32	48.56	27.12
South African S9	25.58	44.77	29.65

Sample Identification	Percentage of analyte		
	Quartz	Kaolinite	Coal Dust
South African S10	3.73	0.00	96.27
South African S11	7.08	0.00	92.92
South African S12	5.20	0.00	94.80
South African S13	9.10	0.00	90.90
South African S14	6.73	0.00	93.27
South African S15	7.44	0.00	92.56
UKCoal1 S1	5.81	24.6	69.6
UKCoal1 S2	5.22	19.8	75.0
UKCoal1 S3	4.20	19.1	76.7
UKCoal1 S4	4.00	12.3	83.7
UKCoal1 S5	3.57	14.4	82.0
UKCoal1 S6	3.65	11.7	84.6
UKCoal1 S7	4.17	14.0	81.9
UKCoal1 S8	3.59	12.7	83.7
UKCoal1 S9	3.95	11.8	84.2
UKCoal1 S10	3.79	18.5	77.7
UK Coal2 S1	0.51	0.00	99.5
UK Coal2 S2	0.00	0.00	100.0
UK Coal2 S3	1.12	6.05	92.8
UK Coal2 S4	0.91	7.77	91.3
UK Coal2 S5	0.97	8.56	90.5

Chapter. 8 Discussion and conclusions

8.1 Discussion

A new technique for the regulatory measurement of respirable crystalline silica needs to demonstrate:

- a) An ability to specifically measure crystalline silica (e.g. to distinguish between crystalline and amorphous phases).
- b) An ability to be quantitative and demonstrate a correlation between instrument response and the mass of RCS particulate collected onto a filter.
- c) It's potential to accurately quantify RCS (quartz or cristobalite) in samples from workplaces with different characteristics e.g. different particle size distributions and matrices.

Ideally, for the measurement of RCS, a new technique also needs to demonstrate better performance in terms of limits of detection and measurement uncertainty when compared with the established methods of FTIR and XRD.

The capabilities of a Raman microscopy mapping method to provide a quantitative regulatory measurement for RCS with a low limit of detection in a range of matrices were demonstrated in Chapters 3, 4 and 5.

8.1.1 Quantitative measurement of RCS

The feasibility study, described in Chapter 3, was the first article that demonstrated the potential for a quantitative Raman spectroscopy measurement of RCS on silver filters. Another feasibility study examining the potential to use Raman spectroscopy for near real time quantitative analysis of aerosols of RCS was also published by the National Institute for Occupational Safety and Health (NIOSH) in the United States, a year later.¹⁷⁶ Subsequently, the HSE and Sheffield Hallam University were invited to participate in a laboratory comparison as a prerequisite for the inclusion of a Raman spectroscopy method in the NIOSH manual of analytical methods; which is an internationally recognised resource of methods for occupational hygiene

analyses. Raman spectroscopy is a potential candidate for use as a near real-time instrument because it provides a very sensitive measurement when the sample is concentrated into a small deposit area.^{176, 177} A Raman measurement system has recently (2021) been developed by a Swiss company for end-of-shift monitoring.¹⁷⁸ The measurement system used in Chapters 3 to 5 was a Raman microscope with automated stage movement and an autofocus microscope objective. The microscope lens improves the Raman response because it focuses the laser energy into a defined area for the efficient collection of the emitted photons (Figure 17). The selection of the appropriate numerical aperture objective is a compromise between Raman band intensity and the measured sample volume. Raman band intensity is reduced when measuring larger sample volumes with lower numerical apertures (section 1.6.8.5). A mapping process (Figure S2, Chapter 5) facilitated by the automatic stage:

- a) Increases the proportion of the measured sample to improve precision.
- b) Reduces operator selectivity of the fields of view and the potential for operator bias.

The representativeness of spectral collection is an important consideration. For a single spectrum, collected using a microscope, the minimum focal volume of the laser is defined by the numerical aperture of the objective lens (Section 1.6.8.5) and wavelength of the laser. In theory, the minimum diameter of a focal area is given by:

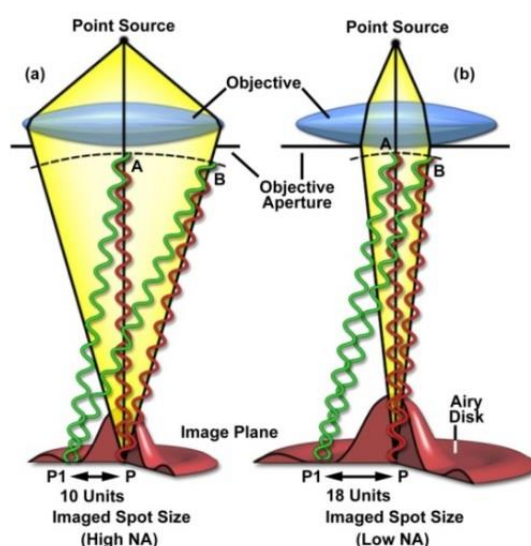
$$d = \frac{1.22\lambda}{NA} \quad (23)$$

Where d is its diameter, λ is the laser wavelength in μm and NA is the numerical aperture of the objective.

With a depth of focus in air (df) of about:

$$df = \frac{4\lambda}{NA^2} \quad (24)$$

The largest diameters and focal depths are found for the longest wavelengths. In theory, the minimum focal diameter and depth of focus are $2.4\text{ }\mu\text{m}$ and about $19.6\text{ }\mu\text{m}$ for a x20 objective with a numerical aperture of 0.4, when using a $0.785\text{ }\mu\text{m}$ laser used in this work. The area represents a small proportion of a typical sample deposit area of 10 mm or 15 mm. However, Everall observed that there is a large out-of-focus contribution of photons collected by the objective.¹⁷⁹ Values of d and df do not consider laser wave fronts and imperfections in the focusing of laser light into the focal point (lens aberrations) or energy passing beyond the focal plane. Wave fronts from the circular objective lens, form rings of constructive and destructive interference around an area of most intensity. The minima, due to destructive interferences of wavelengths, are more distinct with higher numerical aperture objectives (Figure 27).



Reproduced with the permission of Nikon instruments Ltd

Figure 27. A representation of the size of an airy disc for high and low numerical aperture objectives showing the extension beyond the wavelength limited focal area and destructive interference occurring at P1.

Interactions can also occur with the sample or filter substrate. Some laser photons will penetrate the sample layer and interact with the substrate beneath, which produces its own phonons and Rayleigh scattering. Penetration of light into the substrate will depend on the absorbance of the material. In a powder,

multiple reflections from the air particle interface will contribute to the penetration of light.¹⁸⁰ Metal filters used in this work will enhance backscattering since they are highly reflective.¹⁸¹ The penetration of photons into metal is low, however, the filter surface is porous and undulating (Chapter 5, Figure S4), which may enhance internal reflectance and scatter.¹⁸⁰ Images indicate that the sample area emitting photons differs from that captured by the objective. Figure 28 (A) shows an image taken with a Keyence VHX6000 digital microscope of the effect of the laser when making mapping measurements across the surface of a polytetrafluorethylene filter coated with a thin layer of aluminium. The aluminium was deposited from plasma. The same objective and measurement parameters were applied as described in Chapters 3, 4 and 5. For Figure 28A, the laser has 'removed' the aluminium off the filter's surface. The length of each area affected by the laser is 100 μm . Figure 28B shows an image of a hole created by the laser through a thin gold coated polycarbonate filter placed on a reflective silver filter. In this case only 10% power was applied rather than 100%. The area in the centre of the hole showing the silver filter is about 60 μm x 80 μm .

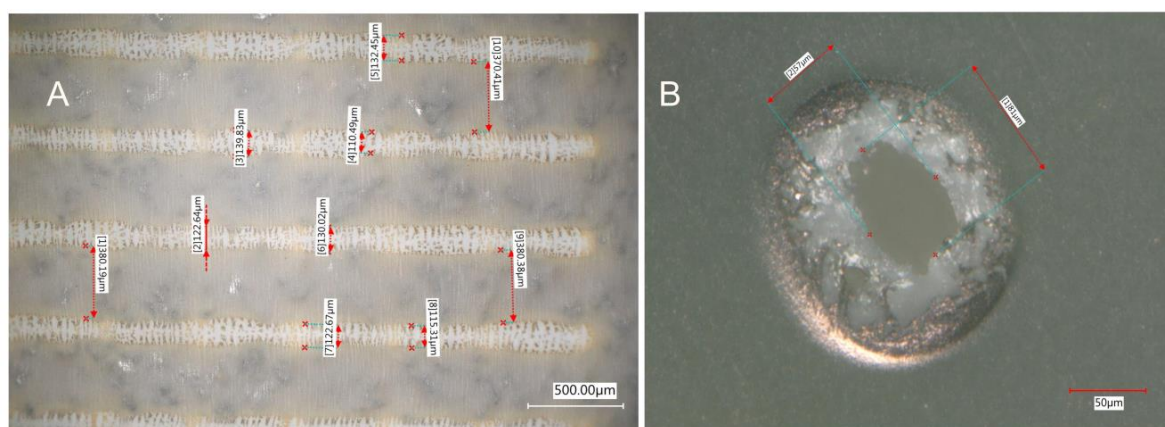


Figure 28. (A) The pattern observed when aluminium was removed from the surface of a polytetrafluorethylene filter when its surface was mapped using a 785 nm laser at 100 % power for three accumulations of 7 seconds at each position with a x20 objective and numerical aperture of 0.4. (B) The hole formed in a gold coated polycarbonate filter placed on a silver filter when measured with the same parameters at 10 % power.

The area contributing photons to the objective is smaller. Figure 29 shows the results an experiment where a quartz plate (2 mm depth) was mapped in 1 μm increments using a x20 objective with a numerical aperture of 0.4 at 100% power. A line of measurements was taken from the quartz to the surface of a thin foil.

The diameter of maximum intensity is observed as the slope of decreasing band intensity as the measurements move over the foil.

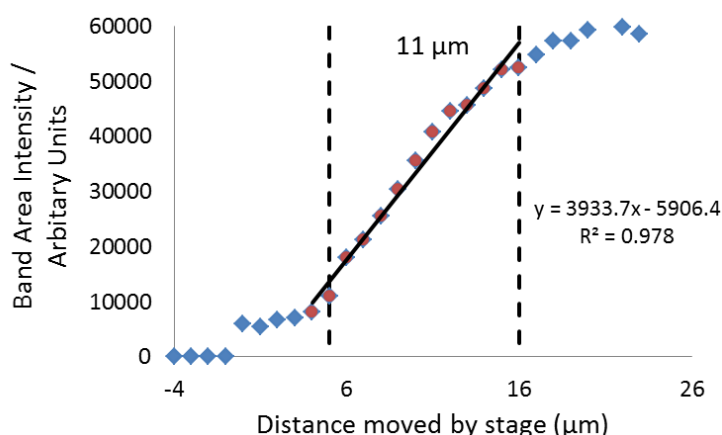


Figure 29. The approximate diameter of the area contributing most photons collected by a x20 objective (NA 0.4) (between the dotted lines) when measuring the surface of a quartz plate in 1 μm steps over a metal foil.

The area of the sample contributing most intensity is about 11 μm in diameter, although, some photon contribution originates from positions much further than this distance. This experiment indicates that substrate interactions can significantly increase the origin of the photons collected by the objective and it's probable that the angular range at which the objective collects photons is a significant constraint.⁹⁵ The area mapped remains a small proportion of the total sample and, therefore, for precise measurements, it is important that the uniformity of the sample deposit is considered.

A consistent particle density per mass loading of the deposit was maintained using a filtration process with bespoke funnel and masks with matching internal diameters to reduce the spread of deposit. The calculation of an average

integrated band area from multiple spectra achieved a relatively consistent value with small variability (Figure 30). The standard deviation of the cumulative average values for a 15 mm diameter deposit are shown since this deposit area provided the lowest particle density. For a 15 mm diameter deposit, the percentage standard deviation of the cumulative average from the 50th to the 90th spectra ranged from 1% at 1000 μg to 9% at 14 μg . A percentage of 2% was obtained at 14 μg by limiting the calculation to the values between the 80th and 90th spectra.

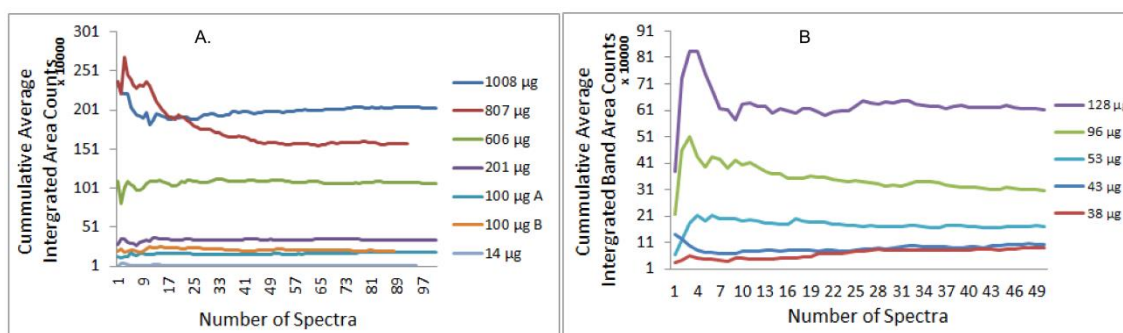


Figure 30. The cumulative average Raman band integrated area for the measurement of quartz powder A9950 over a 15 mm diameter deposit on silver filters (A) and the measurement of quartz collected with the HSE miniature sampler onto 13 mm diameter quartz fibre filters (B).

It was found that, the mapping process and the recording of an average area response from accumulated spectra is an advantage in instances of interference including the effects of fluorescence (Chapters 3 to 5). Interferences exert less influence when the density of particles is spread across the surface of a filter, as a thin layer (where the effects of absorption are not observable due to the reduced proximity or density of particles). Fewer particles are within the analysis volume of the focused laser spot at low mass loadings. Exceptionally problematic spectra can be removed from the averaging calculation, so long as sufficient spectra are included, since the average particle density for these measured volumes should be fairly consistent (Figure 30). Analysts can also employ strategies when the particle density is too high. Additional sample preparation can either reduce the concentration or increase the deposit area (Chapter 5). One advantage is that Raman intensity is directly

proportional to the deposit area; assuming the same measurement parameters are used and subject to the consideration of the presence of interferents¹⁷⁶ (Figure S2. supplementary information, Chapter 5); so the same calibration is potentially applicable to different deposit diameters. For example, calibrations for RCS measurements, collected several years apart, were coincident when corrected for the different deposit diameters of 5 mm and 10 mm (Figure S2, Chapter 4).

A linear correlation between instrument response and mass of analyte was demonstrated for several diameters of deposit onto 0.45 μm pore size silver filters. These deposits were, 5 mm 10 mm and 15 mm in diameter. Two instances where the measurement diverged from a linear correlation were:

- a) Due to the influence of absorption of the Raman photons when measuring loadings of 20% quartz in hematite in a 5 mm diameter deposit (Chapter 3).
- b) Due to multilayers of sample when measuring more than 1 mg of quartz in a 15 mm diameter deposit (Chapter 5)

8.1.2 Influence of absorption

Coloured particles, such as iron oxides, absorb Raman photons and can reduce expected band intensity from RCS particles, when in close proximity. X-ray diffraction measurements have similar issues when using copper radiation and measuring RCS in a matrix of iron compounds¹⁸² (section 1.5.3.1). Hematite is one of the most frequently encountered coloured iron compounds in workplace samples, which can either be emitted as part of the workplace aerosol (brick dust) or be formed in an analytical process which ashes the aerosol filter (the oxidation of iron compounds in respirable coal or foundry dust). Chapter 3 demonstrated a critical mass (particle density) below which absorbance of Raman photons is not significant when measuring RCS in a matrix of hematite. The Raman band intensity was significantly reduced when measuring more than 5 μg of quartz in an artificial mixture containing 80 % hematite, deposited into a 5 mm diameter circular area. Increasing the deposit area to reduce the particle density may help reduce the effect of Raman absorption (Chapter 5). In

principle, a 15 mm diameter deposit would increase the critical mass at which absorption is significant by 9 times; however, the increased area can also reduce measurement sensitivity if the same measurement parameters are applied. Alternatively, a higher magnification objective will, provide greater Raman band intensity and have a smaller sampling volume (and so is less likely to include other absorbing particles). Higher magnification objectives were not evaluated in this work and a specialised method to measure samples from these environments may need development. Fortuitously, workplace aerosols would rarely contain as much as 80% hematite; however, the capability of Raman to measure workplace samples with highly coloured sample deposits (e.g. brick or foundry dust) has yet to be demonstrated.

8.1.3 Influence of particle density

It was found that the band area intensity did not deviate from a linear relationship with mass when an $8.2 \mu\text{g}.\text{mm}^2$ density of respirable quartz particles were uniformly spread over the surface of a filter (Chapter 5). In these circumstances, Equation 20 could be simplified to:

$$I = \frac{\Phi}{A} s \quad (25)$$

This equation will also hold true for real samples before consideration of other sample effects; such as absorption.

For quartz, this density of sample equates to a $4.7 \mu\text{m}$ depth of particles assuming the median diameter of the HSE standard quartz A9950 is $1.39 \mu\text{m}$ and these particles are deposited uniformly in a 15 mm diameter deposit (with hexagonal packing). The point at which the response increases per unit mass is where the sample is approximately 3 to 4 layers of particles deep. At this level of particle density, the plane of focus has moved from or close to the substrate surface to the surface of the particles. The additional contribution of Rayleigh and Raman scattered photons to the sample volume from adjacent particles and scatter at the particle and air surface interface¹⁸⁰ may increase Raman response when photons travel through these multiple layers (Chapter 5). Coincidentally, significant (about 10%) attenuation of XRD response occurs at

about the same particle density⁶⁰ which, in this case is primarily associated with the depth at which penetration of X-rays starts to significantly affect the measurement response due to absorption. In other work, Schrader *et al.* showed a linear increase of Raman response with sample depth (in mm) for powders of various particle diameters which reached a plateau more quickly for smaller particles.⁸⁸ This is not the same as observed in this work. In this work, there is a linear Raman response which is proportional to the mass of analyte which then increases when a particular particle density is achieved. The plateau for multi-layered particles (in mm) represents the point at which further Raman scattering of a sample is no longer achievable, and is observed at a greater sample depth.

8.1.4 Improvements in the limit of detection (LOD)

Chapters 3, 4 and 5 and recent work by NIOSH^{176, 177} demonstrated the capability of Raman spectroscopy to provide a LOD that is lower than current established XRD and FTIR methods. Table 7 compares LOD results obtained in this study for Raman spectroscopy and XRD (shaded areas) with recent work from NIOSH for Raman spectroscopy and FTIR. In this work, improvements in LOD were found for all analytical techniques (XRD, Raman spectroscopy and FTIR); when compared with published values for current analytical methods (Table 4). For XRD, FTIR, and Raman the lower LOD in terms of mass is due to the concentration of the sample into an area where the instruments provide more sensitive measurements (Chapters 4 and 5). The noise does not change since all the measurements are collected with the same parameters. For FTIR, the sample is concentrated into the diameter of the emission from the FTIR source (which is usually 6 to 8 mm in diameter). For XRD, more intensity was obtained when the sample deposit diameter is 15 mm or less.¹⁸³ For Raman microscopy, like other optical techniques, a band response is obtainable from a very small area of the deposit which represents a small volume of particulate.

8.1.4.1 *Limits of detection determined by XRD.*

BS EN 1540 for workplace exposure states that the LOD is the 'lowest amount that is detectable with a given level of confidence'. In addition, the EN 1540 standard also notes that this can be achieved from three standard deviations measurement of blank filters, whilst accepting that the error of false negatives at this point is potentially 50%.¹⁸⁴ This point represents the lowest possible intensity response where a decision can be made that the analyte is present or not. It does not represent the mass that would be reliably detected as it is not observable on every occasion. This value was used to compare the lowest LOD achievable by XRD in ideal conditions with that obtained using Raman spectroscopy using a similar approach (Chapter 5).

Alternatively, the limit of detection for method evaluation is typically defined as an intensity height that is 3x the background noise and represents the point where probability of false negatives is less than 1%. Observed intensity between the two represents the range of mass values where there remains a possibility of a false negative when measuring calibration type samples with no interference.

For a method evaluation LOD, noise was calculated as three standard deviations of the differences between the observed background intensity and a polynomial line drawn along the midpoint of the background. For the most sensitive XRD intensity at 26.6 degrees measuring a 15 mm diameter deposit, three standard deviations of the background noise (1.99 counts/second) provided an estimate for an ideal corrected intensity height for a ratio of 3x the noise of (5.97 counts/second). For XRD, an area intensity is a much smaller number than the intensity height in terms of count rate because the x axis is in terms of tenths of a degree. Therefore, the relationship between corrected height and corrected area for the calibration material was calculated ($\text{Area} = 0.156 \times \text{height} + 0.115$). For the measurement conditions applied, an initial estimate of the area intensity was obtained by multiplying a standard deviation of the noise by 1.66¹⁷² and then the ratio was tested by measurement. Figure 31 shows the test of the estimated XRD mass of 3 μg for an intensity height ratio of about 3 for the measurement of quartz A9950 deposited onto a 15 mm

diameter area. The average noise to corrected peak height ratio for three replicate samples at 3.3 μg was 3.3. In comparison, the lowest detectable mass with a 50% level of confidence for false negatives determined from measurements of blank filters or solely from three standard deviations of the noise was 1.1 μg .

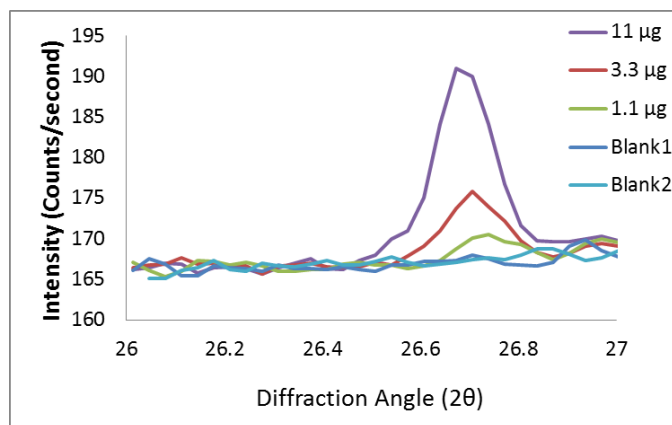


Figure 31. A test of the X-ray diffraction limit of detection from 11 μg to 1 μg for the measurement of quartz standard A9950 deposited into an 15 mm diameter area onto 0.45 μm pore size silver filters.

In practice the LOD is much higher than these figures when measuring real workplace samples. It is often necessary to confirm the presence RCS with the observation of the secondary intensities due to the number of interferences that coincide with the most sensitive. The value of 3 μg reported in Table 7 is slightly less than that previously recorded in literature of 5 μg when using the NIST 1878a quartz standard which applies a 15 mm diameter deposit.⁵⁷ The mass values for the intensities recorded at these LODs were calculated without using intercept, which was assumed as zero. The value of zero was within the 95% level of confidence for the intercept coefficient and the calculated mass values were closer to the known masses from the test samples. Including the intercept brings the mass values for the LOD closer to that published in the NIOSH method 7500.⁵⁷

There remains uncertainty, about the application of the calibration coefficients to calculate an LOD in terms of mass and concern that the intercept coefficient may introduce a bias from the 'true' value; which was also noted by previous reseachers.¹⁸⁵

For example, in Chapter 4, it was observed that, for XRD, the application of both the intercept (c) and slope regression (m) coefficients for the linear calibration relationship ($y = mx + c$), rather than just the slope coefficient, can play a role in reducing the comparability of XRD results with Raman spectroscopy when close to its LOD. XRD intensity for quartz at 2 θ degrees of 26.6 was observed below the calculated LOD of 5.6 μg for a 10 mm diameter deposit; when a calibration intercept coefficient was applied to calculate mass because it was significantly different from zero. The LOD excluding the intercept coefficient was 2.0 μg . In principle, the LODs for FTIR and XRD are not expected to be significantly different from an ideal intercept of zero when the sample deposit is completely included within the areas of most analytical sensitivity. A negative intercept may occur when analyte mass exists outside the analysis area and is not contributing to the measured response (e.g. when measuring RCS on a 25 mm diameter aerosol filter following the direct on-filter measurement approach). Intercepts should be less probable for deposits of 10 mm in diameter since the area providing most intensity for XRD is about 15 mm in diameter. Therefore the lower mass value of 2 μg was probably a better estimate for the LOD in this case.

The current HSE method uses the direct on-aerosol filter analysis approach which is less time consuming and potentially cheaper; however, respirable samplers are not yet designed to contain 15 mm diameter filters. Whilst smaller diameter aerosol filters or deposit areas may allow lower limits of detection, the critical mass at which sample absorption occurs, due to the depth of deposit, will decrease. This may be an issue for some types of samples with a minor content of RCS⁶⁰ because the measurement may under-record the true mass of analyte due to matrix absorption.

Table 7. Limits of detection obtained in this work compared with other recent studies.

Technique	Description	Number of measurements	Calculated limits of detection (μg)
X-ray Diffraction	Indirect 15 mm diameter area on silver filters	10	1 to 3
	Direct on 13 mm diameter PVC aerosol	10	2.3 (1.5 to 3)
	Indirect 10 mm diameter area on silver	8	2.0*
Raman	Indirect 15 mm diameter area on silver	10 x 90	0.21
	Indirect 10 mm diameter area on silver	10 x 90	0.26
	Aliquots 5 mm diameter area ⁸⁵	5 x 50 spectra	0.049
	1, 1.5 and 3 mm diameter areas ¹⁷⁶	3 x 15 spectra	0.055 to 3
Infrared	Direct on 9 mm diameter PVC aerosol filter ¹⁸⁶	12	0.5 to 1.5
	Cascade laser focused into 1.7 mm area deposit ¹⁸⁷	Not Known	0.33

Note: Shaded areas denote the LODs determined in this work. LOD values for XRD are all calculated with a zero intercept coefficient.

*Lowest XRD mass observed was 1 μg and 2 μg is the value of the LOD when an intercept coefficient is set to zero to calculate the mass. The average LOD is 5.6 μg when the intercept coefficient is applied with the slope coefficient to calculate a mass value.

8.1.4.2 *Limits of detection for Raman spectroscopy methods*

For the Raman microscope method, the LODs reported in Table 7 were determined from three standard deviations of measurements made on blank filters.¹⁸⁴ The filters contained residues of clean PVC filters that were processed through a plasma asher. LODs determined using this approach were more representative of the analysis of samples than those obtained from measuring calibration type filters. All analyses used the same measurement conditions on the various diameters of sample deposit. LODs were also determined from three standard deviations of the variability of the spectral noise, which were lower than those in Table 7. When using a mapping method, the variability increases for both the number of spectra with observable Raman bands and the average band intensity collected as the particle density decreases. LODs calculated from three standard deviations spectral noise are representative of

what is potentially detectable in single spectrum, although, they are not necessarily realistic for the particle density detectable with the mapping method from a specified number of spectra. In practice, an analyst may need to observe more than a single observation to be confident that the method LOD is achieved. In Poisson counting statistics, (commonly used in electron microscopy methods) the equivalent of three observations are needed to achieve a 99 % level of confidence.

For Raman spectroscopy, it was not possible to verify the LODs by preparing samples of known masses. The pipetting of aliquots at these loadings would be variable and no reference method exists that could verify the amount of analyte. An assessment of the validity of the method LOD is obtainable from measured samples. For example, for the 5 mm deposit method, the lowest calibration standards of 0.250 μg recorded an average of 192,000 counts and 7 spectra whilst two process blanks reported significant measurements of about 0.130 μg from 3 spectra. It is therefore feasible that one spectrum or a small number of spectra are recorded from 50 fields with a band intensity area equating to the method LOD of 0.05 μg .

As an additional measure the LODs for the 5 mm and 15 mm diameter deposits were checked following a similar strategy outlined for the XRD measurement. The range of noise was estimated by multiplying the median standard deviation of the scatter from a polynomial line fitted to the midpoint of the background from 476 scans by 3. The ideal corrected height for band intensity (for intensity with 1% probability of false negatives) was estimated by multiplying the range of noise by 3.0. The band area was estimated from the trend line equation of values of band height and band area for low intensity bands observed at 464 cm^{-1} . Estimates for the 5 mm and 15 mm diameter deposits were 0.037 μg and 0.199 μg respectively. In absolute terms, these values are very close to those reported in the articles (Table 7).

In comparison to the standard FTIR and XRD methods, Raman spectroscopy obtained the lowest LOD for all diameters of deposit. When applying the same measurement parameters, reducing the sample deposit area increases the sample concentration, which leads to a proportional increase in sensitivity.

However, increasing concentration may also increase the potential for absorption (all techniques), fluorescence (XRD and Raman spectroscopy), and for interference (all techniques) from other particles (section 1.7.8). The effect of interference on the LOD is not yet quantified for Raman spectroscopy; however, chemometric models or multicomponent calibrations are a promising solution for removing interference from FTIR spectra (Chapters 6 and 7) which could also be used for Raman spectroscopy. In practice, the analyst may have to balance the desired LOD with an optimum particle density for measurement.

8.1.5 Measurement of samples collected from inside a respirator

There are industrial processes that may expose workers to high RCS concentrations above the WEL, even when good control practice is applied and respiratory protective equipment (RPE) is then also required to further reduce exposures. Chapter 4 describes the successful application of a Raman spectroscopy method to measure samples collected inside respirators to potentially determine the actual exposure of workers when wearing respirators or workplace inward leakage ratios. Respirators are normally tested under laboratory conditions to achieve a nominal standard of protection; however they are expected to have a poorer performance when worn in the workplace. An assigned protection factor (APF) is a performance rating attributed to a respirator when worn in workplace conditions and is a ratio of the proportion of anticipated leakage of workplace dust particles. For example, an APF of 20 is a rating assigned to a classification of respirator commonly used to protect workers from emissions of RCS called a filtering face-piece 3 (FFP3). An APF of 20 implies the respirator is capable of reducing the aerosol concentration by at least twenty-fold, so that the in-respirator concentration is expected to be $1/20^{\text{th}}$ of that outside. Other respirators with higher numbered APF ratings are also used to protect workers from RCS, which would potentially further reduce the mass available for measurements. The measurement challenge is further complicated because workers are advised to take a break when wearing tight fitting respirators for more than an hour, which will reduce the sampling time and mass of dust collected by an in-respirator sampler. An achievement in this work (Chapter 4), is that the LOD for Raman spectroscopy was potentially sufficient for in-respirator sampling to permit a sampling period of 1 h when the

worker was exposed to the WEL (over an 8 h shift) with a respirator performing to an APF of 20.

8.1.6 *Comparison with particle number and mass metrics*

Chapter 4 provided an opportunity to compare mass and number concentration inward leakage ratios. The exposure of a worker wearing a respirator is difficult to assess since in-respirator measurements are not generally available, however, it may be estimated by applying a correction to the results obtained from personal samples taken outside the respirator. The correction is based on the APF which is calculated from the 5th percentile of workplace data; however, few workplace studies have been conducted and none specifically for RCS exposures. The development of a miniature respirable sampler to fit inside a respirator may permit the study of analyte specific inward leakage ratios when worn in the workplace.⁴⁶ Particle number counting is the metric generally used by instruments for tests to assess the fit of RPE on a worker, since they provide a very sensitive measurement, although, the derived inward leakage ratios might not directly correspond to a worker's exposure in terms of mass, which is needed for comparison with a WEL. Chapter 4 uses three instruments to compare three metrics (Table 8).

Table 8. Metrics and particle diameter range for instruments used to compare inward leakage ratios.

Instrument	Metric	Particle diameter range
Portacount™	Particle number concentration	0.02 µm to 1 µm
MiniWRAS™	Particle number and particle mass concentration*	0.01 µm to 32 µm
Raman spectroscopy	Mass of crystalline silica	Respirable range 100% collected from 1 µm and below with a median at 4 µm and 0.1 % at 16 µm

*Mass concentration is calculated from the particle density and assumes the aerosol is relatively pure

Several effects were observed. Firstly, there was a correlation between the mass median aerodynamic diameter (MMAD) outside and inside the respirator

with a coefficient of determination of 0.89 when measured using the miniWRAS. This correlation could indicate the MMAD of particles inside a respirator is predictable; however, this has not yet been confirmed for workplace data. Secondly, the proportion of RCS inside the RPE decreased with reducing mass concentration of RCS in the test chamber. The reducing RCS proportion could be attributable to measurement bias. The respirable dust is measured gravimetrically with a relatively high LOD and a positive bias for the total mass at values close to the LOD would reduce the calculated proportion of RCS. This reduction of the percentage of RCS is potentially a demonstration of a limitation of using techniques with a relatively high LOD. Thirdly, at higher ILRs, the RCS mass-based values or miniWRAS mass and number ILRs were not comparable with the number concentration values collected with the Portacount™ instrument (Chapter 4, Figure 10). Fundamental differences between each metric and the measured particle size range of each instrument are probably the cause of differences in the measured concentrations and ILRs. Mass measurements are biased towards the largest particles since these contain the most mass. For example, one spherical particle of 10 µm contains the same mass as 1000 particles of 1 µm in diameter with the same density. The Portacount™, which is used in RPE fit testing, collects a very limited particle size range, when compared with the other instruments (Table 8), which may account for the differences observed for relatively high inward leakage ratios. Low numbers of larger particles leaking into the respirator at low concentrations of ILR (less than 3) resulted in more comparable values between the miniWRAS and the other methods listed in Table 8. Higher in-respirator concentrations may increase the frequency of the measurement of larger particles which may result in differences because they contain significantly more mass as a result of their larger particle volumes. Although, these data are limited, it's possible that instruments with a wider particle diameter measurement range are needed to measure RPE inward leakage performance in the workplace for comparison with WELs in terms of mass. These instruments with wider particle size measurement ranges would need to be compared with the established measurement approaches, especially with those methods that can measure the analyte of concern.

8.1.7 Comparability of Raman with XRD measurements of RCS

XRD and Raman spectroscopy are considered complementary.¹⁸⁸ Chapters 4 and 5 demonstrate that there are similarities in the nature of the response detected by each respective instrument; although the XRD response is related to the scattering of X-rays and the Raman response results from atomic vibrations. In a crystalline solid, the instrument response of both is determined by the atomic structure. For Raman spectroscopy, the atomic vibrations initiated by the laser are represented by a phonon wave of vibrating nuclei through the lattice. Any scattered Raman photon received by the detector is projected through the centre of a Brillouin zone in the reciprocal crystal lattice, since this represents the volume for the largest amplitudes of the molecular vibrations. For XRD, the X-ray radiation is scattered by a plane of atoms through the reciprocal lattice. Larger atoms cause more scatter. In X-ray diffraction, the Brillouin zone represents the area for diffraction vectors that fulfil the requirements of the Bragg equation (Equation 5) $n\lambda = 2d\sin\theta$. Therefore, the detected response from both techniques is projected through the reciprocal lattice (the Brillouin zone) and for RCS both responses are dependent on the crystallinity of the material⁸⁴ and the size of the particle (Chapter 5). This is the similarity that connects both instruments. The behaviour of the measurement responses for both techniques are similar before taking into account the different mechanisms associated with absorption of Raman photons and XRD absorption of copper radiation by contaminant particles. For both techniques, the measurement response is narrow and intense when measuring a material with a high degree of crystallinity and becomes broader and flatter as the crystallinity decreases and the atomic structure becomes more disordered. Therefore, integrated area rather than band height must be applied for Raman measurements of RCS to provide more consistent measurements comparable with XRD values (Chapter 5). The limitations of the collection optics and not the focal volume are considered the main explanation for lower Raman band responses (Chapter 5) when measuring dust with larger particle diameters (greater than 7 μm).⁹⁵

Good comparability of results between XRD and Raman spectroscopy was achieved for RCS analysis of 119 aerosol samples from emissions derived from cutting and polishing of natural and artificial stones (Chapter 5). Some of these

matrices were challenging because they contained high proportions of potentially interfering minerals and low proportions of quartz (5% to 10%). On average, Raman spectrometry reported slightly higher values (about +11% for RCS and about 6 % for the thoracic crystalline silica) than the XRD analysis when measuring the same samples. Further analysis, presented here, shows that the variability of results at low measured values were explained by the type of stone or the higher LOD of the XRD. Figure 32 presents the results for the impactor samples by stone type (Chapter 5, Figure 6). Samples with relatively minor interferences (sandstone or engineered stone) obtained very comparable results (coefficients of determination = 0.99). Comparison of Raman measurements against the LOD of the XRD (results around 2 μg in Figure 32) was one exception. Figure 32 shows that many of the Raman results were less than the XRD values for the Diorite and more than the XRD values for the sintered stone samples. Coefficients of determination and trend line coefficients are shown in Table 9.

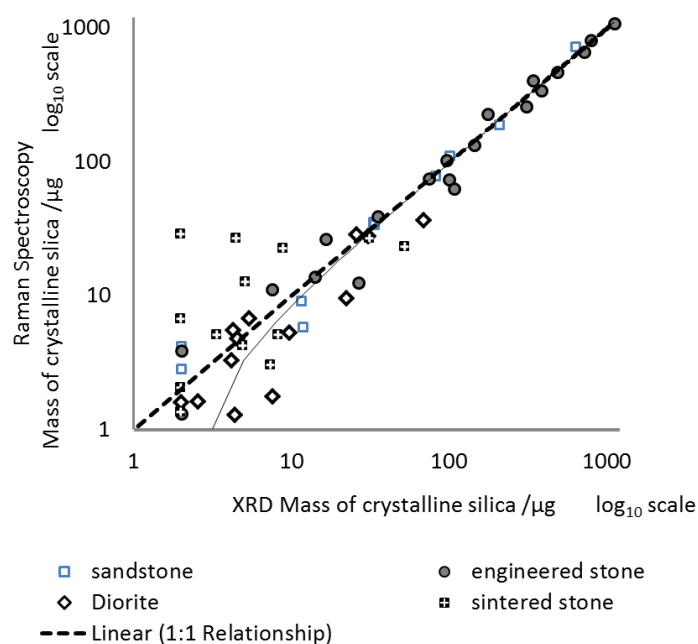


Figure 32. Comparison between X-ray diffraction (XRD) and Raman spectroscopy measurements of respirable crystalline silica collected on impactor samples by stone type (sandstone, engineered stone, diorite and sintered stone).

Table 9. Trend line coefficients and coefficients of determination for a comparison of XRD with Raman measurements of RCS on Sioutas impactor samples from four stone types.

Stone Type	Raman Mass measurement range (µg)	Trend line coefficients	Coefficient of determination
Sandstone	0.73 µg to 719 µg	$y = 1.13x - 6.33$	0.996
Engineered stone	1.3 µg to 1082 µg	$y = 0.987x - 0.529$	0.990
Diorite	LOD (0.21µg) to 36.7 µg	$y = 0.598x + 1.17$	0.843
Sintered	LOD (0.21µg) to 26.7 µg	$y = 0.401x + 7.03$	0.255

There are several reasons for the poor correlations between results from samples of Diorite and sintered stones.

- Firstly, the diorite and sintered stones contained less than 10% crystalline silica and 66% of the reported XRD LOD values were for these stones.
- Secondly, all of the reported mass values were below 50 µg; where the reliability (uncertainty) of the XRD measurements was poorer and approaches its limit of quantification.¹³⁰
- Thirdly, both these stones contained significant mineral interferences for XRD. For example, the diorite contained a Feldspar mineral known as anorthite (Figure 20) and the sintered stone contained Zircon (Figure S10, supplementary information, Chapter 5).

There are two advantages for Raman spectroscopy. Firstly, a Raman band profile fitting option was available with the manufacturers WIRE™ software, which was able to model and compensate for the effect of coincident bands (Figure S11, supplementary information, Chapter 5); whereas, for XRD the current practice was to correct the background positions using expert judgement. Profile fitting routines are available for XRD, although they are not commonly used for analysis of RCS on filters due to the difficulties of resolving low intensity coincident reflections.¹⁸⁹ Secondly, the Raman bands for zircon and quartz in the sintered stones are fully resolved (Figure S9, supplementary information, Chapter 6) whereas they are coincident for XRD; hence many XRD results are higher than those for Raman spectroscopy.

8.1.8 *Dealing with spectral interferences*

The effect of interference on the uncertainty of RCS measurements is not included in uncertainty evaluations from method validation studies because of the wide variety of workplace atmospheres and proportions of components. Therefore, few articles quantify its effect (section 1.7.8) which can, in some circumstances, be significant for both XRD and FTIR. Instruments like FTIR have advantages because they are cheaper, provide a fast analysis, easy to operate and maintain, are potentially portable and can provide a multicomponent analysis (Chapters 6 and 7). These advantages may facilitate their wider use, although their effectiveness in the presence of interference is thought to be poorer than XRD. A substance of particular interest is the clay silicate, kaolinite; which interferes with quartz, and is commercially quarried in Great Britain as china or ball clay. Kaolinite was the most common interference found in workplace samples when using FTIR.⁶⁸ Chapter 6 demonstrated a significant bias (average = + 18%) for RCS measurements in kaolinite and coal mine dust with the current FTIR MDHS 101 method and using a single component Beer-Lambert law calibration. Application of a PCR chemometric model significantly improved the comparability of results with the XRD method and reduced bias caused by the kaolinite. The same developed chemometric models can also be potentially applied to the analysis of samples of pure china or ball clay.

Multivariate approaches, like chemometrics, investigate the whole spectral region and are able to deconstruct the magnitude of the influence of interference. Whilst some recent work has been done using PLSR models for the measurement of quartz (section 1.8) none has sought to develop multicomponent analysis to include other potentially hazardous substances in the same material. Chapters 6 and 7 demonstrated the successful application of the PCR and PLSR chemometric models to the prediction of quartz, kaolinite and coal in coalmine dusts.

A key element that distinguishes an analyte of interest is the number of principle components since these values usually represent the features in spectra that are most attributable to that analyte. A large number may over model the

spectrum and risk association with spectra features attributable with other analytes. For Chapter 7, 18 principal components were derived for coal dust by the PCR model, which is more than the number of discernible spectral features in the spectral range. By comparison, the number of principal components (3 and 2) for quartz and kaolinite matched the most significant spectral features for these minerals. However, the relatively high number of principal components from the PCR coal model provided more values that matched the mass on the filter attributable to the coal dust mass, whereas, PLSR model tended to over predict the coal values using 7 principal components. Both the PCR and PLSR models distinguished between the anthracitic and the poorly crystalline coals with high kaolinite. Differences between coal types (source of the coal) were more evident for the PLSR model. The type of coal can vary from mine to mine. Each type of coal may have spectral features within the spectral range that are distinctive. The higher number of principal components for the PCR model potentially compensates for the more prominent spectral features found for some coal types. For example, a distinct spectral feature at about 900 cm^{-1} for the anthracitic coal dusts. The large number of components may reduce these distinctions.

The main finding for Chapter 6 was that there were no significant differences between predictions from the PCR and PLSR when a similar number of principal components (PCs) were used for each model. The advantage of PLSR to determine a calibration using fewer PCs than the PCR process was compensated for by the manufacturer's software, which provided a PC number selection option for processing the PCR. An additional process was implemented to check for the most appropriate number of PCs. A comparison of the significance of the intercept and slope from regressions of the predicted and measured target values reasonably indicated the optimum PC number. Optimum PCs were indicated when the slope and intercept comparing the predicted and assigned target values for a set of samples were not significantly different from one and zero. These PCs were different from those initially calculated by the software for the PCR calibration. Use of a derivative spectral processing option also helped reduce the background associated with the aerosol filter and removed the need for the measurement of a clean unused

filter for spectral subtraction, which may help reduce the cost, complexity, and time of analysis. These findings are likely to inform the revision of the HSE method MDHS 101.

The development of a PCR or PLSR model using artificial mixtures of three main components in coal mine dust was a key feature of this work (Chapters 6 and 7). Use of artificial mixtures was found to be an efficient way of developing a widely applicable model, because a combination of different proportions can be generated in laboratory conditions. Use of real workplace samples is problematic because of the difficulty of measuring a 'true' value in the presence of interference and the cost of visiting a variety of work sites to collect representative samples. Rationally, it is not necessary to measure every combination of mine dust to identify the appropriate number of PCs and generate a new calibration. In addition, it is not always necessary to consider minor components (less than 10 % in the bulk material) because they are not necessarily collected at low loadings (less than 1 mg) or significantly affect the spectral bands of the analyte of interest. To test this, samples, generated from a range of coalmines from Australia, South Africa and the United Kingdom were used to challenge the performance of the PCR model, developed with artificial mixtures of the main components (Chapter 7). Modifications were required to train the model for circumstances at the extreme range of mixtures. These modifications involved the addition of more calibration and validation samples with low quartz proportions and mixtures with very high proportions of kaolinite.

An innovative approach was applied to characterise the performance of the PCR and compare this to international performance criteria for regulatory occupational hygiene measurements. The uncertainty equation relating to a calibration was used to determine the analytical method uncertainty when applied to regressions of the FTIR PCR method predicted and measured or 'known' values. An example of its application is provided for some key RCS exposure concentrations that were proposed as international exposure standards.¹³⁰ Filter loadings of 26 µg, 53 µg and 103 µg would be the masses of analyte collected on an aerosol filter for key RCS concentration values of 0.025 mg.m⁻³, 0.05 mg.m⁻³ and 0.1 mg.m⁻³ respectively; if using a respirable

sampler at a flow rate of $2.2 \text{ L}\cdot\text{min}^{-1}$ over a full 8 h shift. The analytical method uncertainty for these key masses is 26%, 13% and 6.5% respectively when using the FTIR PCR method. These values for the analytical method uncertainty indicate that the international requirements for expanded uncertainty (when multiplied by 2 to estimate the 95 % level of confidence) are exceeded for masses of quartz collected on filters equating to concentrations of $0.025 \text{ mg}\cdot\text{m}^{-3}$, and when it is combined with the sampling uncertainty estimate of 10.1% prescribed in ISO 24095 for the nominal flow rate. Expanded uncertainty for an RCS concentration of $0.05 \text{ mg}\cdot\text{m}^{-3}$ is close to the international requirements and probably acceptable in practice for full shift (8 h) sampling. Therefore, it is important to sample for as much of the full shift as possible to obtain the most reliable results when assessing potential RCS exposures around $0.05 \text{ mg}\cdot\text{m}^{-3}$. The analytical method uncertainty estimates in Chapter 7 are based on the measurement of real samples with matrix interferences rather than the estimates based on the analysis of samples of pure quartz which is usually the case. In comparison, the average within laboratory precision for the FTIR direct on-aerosol filter method is 5.3% when measuring filters of pure quartz in a PT programme; where the lowest loading was about $80 \text{ }\mu\text{g}$.¹³² This suggests that the estimate of uncertainty with real samples with interference is reasonable, when compared with the precision at $100 \text{ }\mu\text{g}$ of RCS for the PCR method. However, there remains a contribution of additional variability compared with the measurement of quartz alone and it may still be possible to improve the chemometric model. A major limitation of this work is the time needed to prepare standards and assess the assigned 'true' value. This time intensive process limited the number of samples produced to test the models. The XRD measurements, used in this work to set the assigned values, will also contribute to the higher than expected uncertainty. The XRD technique is just as variable as the FTIR measurements;^{132, 139} calibration coefficients can cause noticeable changes in target values when the calibration range is altered (Chapter 7) and intercept coefficients for the XRD can cause bias at low RCS masses (Chapter 4). Some institutes adopt a logarithmic trend line between mass and XRD response for low loadings because it is thought the true relationship at these loadings is curved.⁵⁶ To reduce uncertainty further, there is a need for a highly

sensitive, precise reference technique that is relatively unaffected by interference.

8.1.9 Regulatory measurement at concentrations lower than the current WEL in Great Britain.

In many countries, there is pressure to further reduce exposure limits for RCS because there is no known concentration at which a health effect is not observed in some proportion of the working population. However, the reliability of measurements at proposed RCS concentrations lower than the current WEL in GB has not always been considered sufficient¹³⁰ for regulatory purposes.

The expanded uncertainty is a key indicator of a method's suitability to provide values to assess against exposure limits.¹²⁴ For practical reasons, many method validation studies in this topic area only examine the performance with samples of pure quartz or cristobalite. Sample contamination, with interfering components, will add to the variability of these analyses; so estimates of method performance, such as uncertainty precision, are less accurate for some matrices (e.g. granite dust). Recovery methods can improve measurement sensitivity by providing the opportunity to concentrate the sample but may also increase variability (section 1.7.4). Higher flow rate respirable dust samplers could improve uncertainty estimates', for concentrations lower than 0.1 mg.m^{-3} , as they collect more mass on a filter; however there are none that offer a flow rate at or above 4 L.min^{-1} , that currently work with a direct on-aerosol filter measurement approach. Replacement of existing equipment to use higher flow rate samplers is also potentially costly for hygienists. When using XRD or FTIR, none of the existing uncertainty or method performance estimates would be sufficient for research to investigate in-respirator or lung tissue measurements of RCS, where there is a need to accurately measure more than 10x below the LODs of the current analytical methods.

Raman spectroscopy has demonstrated its potential to provide measurements of RCS at lower exposure concentrations than are currently achievable when using existing recognised methods (Chapters 3, 4, and 5). Very similar analytical method uncertainty (intermediate precision) values were obtained for

XRD and Raman spectroscopy, when measuring the same filters with a 10 mm diameter deposit (Chapter 4). This suggests the expanded uncertainty between XRD and Raman spectroscopy is very similar despite the increase in sensitivity of the Raman technique. The advantage of Raman spectroscopy is its lower LOD which helps this technique potentially meet all the requirements of ISO 20581 at lower RCS concentrations; subject to a number of specific criteria. Chapter 4 postulated that an RCS concentration of 0.01 mg.m^{-3} for full shift an 8-hour sample could potentially fulfil all the international requirements for a regulatory measurement if the deposit is about 10 mm in diameter, if samples are classifiable as thin layered (less than a couple of microns in depth), they are free from interferents and the sampling uncertainty is not greater than 10.1% (based on the nominal flow rate). However, Raman band measurements from individual spectra at low mass loadings (less than $5 \text{ }\mu\text{g}$) on samples free from interference were of relatively low intensity. More practically, Raman spectroscopy could be the technique of choice, when assessing exposure concentrations as low as the Occupational Safety and Health Administration (OSHA) action level for RCS of 0.025 mg m^{-3} , since the required measurement range from 0.1x to 2x the exposure standard is well within this technique's capabilities.

Further development is needed for the routine application of Raman spectroscopy. There are many types of workplace atmospheres and industry sectors where exposure to RCS occurs. Any new method needs to demonstrate its universal applicability or the limitations of its applicability. This is to ensure that it is not incorrectly applied to particular circumstances or workplaces (e.g. due to interferents) and reports erroneous results that lead to incorrect actions to control RCS exposures. This is ethically important because of the relationship between an RCS exposure measurement and the potential for worker ill-health. The performance of Raman spectroscopy when measuring workplace samples containing hematite (e.g. from brick manufacture, some construction samples or from foundries) remains a gap in knowledge that needs investigating since these are particularly challenging samples. In addition, a demonstration of the comparability of results between national laboratories when measuring these

more challenging samples would also further establish the capability of the Raman technique for industry and establish its wider use.

Chemometric methods using PCR and PLSR also offer the potential to improve confidence in the performance of the FTIR or Raman techniques when measurements are made in the presence of interference. Chapters 6 and 7 demonstrated their application for multicomponent analysis of quartz, kaolinite and coal in complex mixtures of coal mine dust. Ideally, application of the chemometric method should reduce the variability and bias of the analytical method. The additional bias and variability caused by the influence of kaolinite on the measurement of quartz following the current MDHS 101 method is shown in Chapter 7. Chapters 6 and 7 both demonstrate the potential for these mathematical multivariate calibration processes to reduce bias. The uncertainty estimates for the chemometric methods are promising, although, there remains some additional contribution to uncertainty from the presence of interferences.

8.2 The potential for further improvements for RCS measurements and future work.

Raman spectroscopy remains a field where advances are in development to further improve measurement sensitivity and suppress fluorescence, if it should occur from a particular sample or spectrum. Inert noble metal nanoparticles, spread over the surface of a sample or as part of a substrate, provide localised electromagnetic fields for Surface Enhanced Raman spectroscopy (SERS), which increases band intensity¹⁹⁰ by $\times 10^4$ to $\times 10^6$. A suitable SERS substrate may further facilitate its application for a direct on-aerosol filter measurement approach or for near real-time measurements of RCS. It is reported that these SERS effects depend on the quality and consistency of distribution of the enhancing material in its required state^{190, 191} which might not be sufficient for accurate quantitative analysis. Although, a recent multi-laboratory study obtained total precision estimate of about 13% to 28% when measuring an analyte on solid gold or silver substrates using a 785 nm laser.¹⁹² Tip Enhanced Raman Spectroscopy (TERS) overcomes some of the issues of SERS because it can apply the enhanced effect more uniformly across the surface of a sample.¹⁹¹ TERS employs a small tip (about 10 nm), coated with a noble metal, which is positioned close to the surface of particles. The electromagnetic field of the noble metal coated tip is designed to resonate with the choice of laser wavelength employed for excitation. This permits a consistent application of the induced electromagnetic field to each sampling position¹⁹¹ and potentially provides a consistent response per volume of material measured. Substrates for SERS have also progressed.¹⁹¹ Consistently applied and stable SERS mediums were sprayed by printing ink jets onto paper filter substrates and analysed using a near infrared laser.¹⁹³ These printable mediums may facilitate the development of a direct on-aerosol filter measurement approach, when applied to the filters used for aerosol sampling. However, the addition of these materials may also reduce the size of the filter pores and increase pump backpressure during sampling. Relatively inexpensive and readily available fused quartz (amorphous) or alumina aerosol sampling filters may provide a suitable framework to support SERS active coatings. Continuous aluminium films may also provide a cheaper alternative for SERS, compared with the gold

and silver, and could, potentially, be spray-coated onto these aerosol filters. Aluminium films were found to provide strong enhancement when used with the 785 nm laser wavelength, which was thought to be due to the presence of the oxide layer.¹⁹⁴

In this work, detector saturation occurred in the occasional spectra from a mapping measurement but rarely prevented a measurement result since sufficient spectra were collected from other fields of view. Detector saturation occurs more frequently at high loadings close to 1 mg. It is possible that fluorescence, which can cause detector saturation, is not a widespread problem that affects workplace samples; however, this has not yet been fully established. Enhancement of the Raman signal, with use of SERS or TERS, may also help because the fluorescence becomes a proportionally smaller part of the photons detected. Another approach to improving sensitivity is to use a shorter wavelength laser (e.g. UV) as the scattering is inversely proportional to the wavelength of the laser. However, shorter wavelength lasers have a greater propensity to induce fluorescence, when susceptible particles are also present; which can swamp the detector with more photons resulting in detector saturation. The more commonly employed Stokes Raman band shift is measured and more affected by fluorescence, which itself is a change to a longer wavelength, than anti-Stokes Raman bands. Anti-stokes Raman scattering has recently been the subject of study.¹⁹⁵ Approaches that take advantage of the differences in the nature of the two photon producing effects (Raman scattering and fluorescence) are also potentially able to resolve sample fluorescence. Fast pulsed lasers, with Kerr gates, take advantage of the time difference between the emission of the Raman photon (in pico-seconds) and the time lagged nature of the fluorescence effect, however, there are additional losses of intensity through the optics and Kerr gates. Other methods use wavelength phase modulation with high frequency ultrasound or from the laser source to differentiate between the Raman photon emission and the longer wavelength fluorescence based on the known decay times for each photon effect.¹⁹⁵ The more applicable of these approaches is probably the use of two narrowly spaced laser wavelengths from the same laser. The Raman spectrum is based on the shifted combination of these laser wavelengths whereas the

fluorescence is dependent on the individual wavelengths of the laser¹⁹⁵ which may reduce the magnitude of fluorescence by shifting the excitation energy for the Raman effect.

FTIR measurements could also be developed further. A much faster analysis total time is a key advantage for FTIR compared with XRD and Raman spectroscopy. An improvement in uncertainty precision could be obtained by increasing the area of the measured sample (Figure 5, Chapter 7) with multiple measurements and still obtain an analysis result in under 10 minutes. Two separate but partially coincident independent measurements could also reduce the uncertainty by $\sqrt{2}$. Although, this may require modification of the sample holder in the FTIR to move the sample slightly horizontally in the beam to obtain two independent values rather than two measurements of the same position. Multiple measurements of sub-fractions from the sample may also potentially reduce the influence of particle size on the FTIR absorbance (section 1.7.6).

The chemometric methods now need further development to improve their universal applicability and encourage their widespread use. To this end, it is more useful to have a single model applicable to all the possible combinations of workplace atmospheres, so there are no limitations for its application. It is possible a single principal component vector, which would be less susceptible to interference, that may satisfactorily predict RCS results for all types of samples from different workplace atmospheres; however, this is still to be evaluated. It's more likely that a series of processes will be needed to first determine the type of workplace atmosphere from a spectrum. For example, a principal component analysis may have to perform a cluster analysis to classify the sample and then process it through a particular PCR or PLSR process. Computational artificial neural networks may have a role in facilitating this type of analysis without the need for involvement of laboratory-based measurement specialists.¹⁹⁶ For construction tunnelling, mining or quarrying, these processes could be coupled with artificial intelligence (self-learning) processes to handle on-site data from multiple sources to look for patterns in exposure levels or trends in geology and anticipate higher exposures before they occur. This innovation could have a major impact to reduce exposures since currently

instruments are not able to anticipate high exposure events. Near real time measurements are potentially possible especially when the sample is collected into a smaller diameter area than is usually measured for current aerosol sampling.¹⁸⁷ The characterisation of the performance of these methods to measure more complex and challenging feldspar concentrations (granite dusts, section 1.7.7) remains a knowledge gap that would potentially help establish the applicability of these chemometric methods to most workplace atmospheres since these are very challenging matrices for both XRD and FTIR (section 1.7.7).

A study with Feldspar minerals would further demonstrate the usefulness of chemometric models or multicomponent calibrations for routine measurement of RCS in complex matrices; since Feldspar interference can be particularly challenging when using XRD and FTIR. Such a study could provide a 'road map' to support separate industry sectors to improve their own RCS measurements. A series of chemometric FTIR methods developed and validated in a number of reference laboratories would potentially help ensure the consistency of workplace RCS measurements, since these chemometric methods are potentially transferable from instrument to instrument.

For XRD, the limit of detection was improved by concentrating the deposit into 15 mm. Further improvements might be obtained if instruments had smaller focusing diameters which would bring the detector and source closer to the sample. Currently, the distance to detector can be between 180 mm to 240 mm for laboratory based instruments. Shorter focal distances are available with benchtop instruments and may offer improvements in sensitivity.¹⁹⁷

8.3 Conclusion

The research described in this thesis, relating to the development of a different technique (Raman spectroscopy) and potential further refinements to existing established methods (XRD and FTIR), has advanced the science of RCS measurement to support occupational hygiene assessments. There are now more options for reliable measurements at key concentrations below the current WEL where a health risk remains. This work has achieved its principal objectives which were to:

- Investigate the potential of Raman spectroscopy to measure dust collected on filters containing RCS obtained from a miniature aerosol sampler developed by a team at the Health and Safety Executive.
- To investigate the performance of Raman spectroscopy:
 - a) when measuring aerosol particles from natural and industrial processes of the most common polymorphs of crystalline quartz and cristobalite;
 - b) when measuring different particle size fractions within the respirable range;
 - c) when measuring samples collected from behind respirators.
- To compare the performance of XRD and FTIR analytical techniques specified in international methods for RCS.
- To investigate the use of de-convolution data processing techniques to remove the effect of interfering components to improve both the existing and novel approaches.

Raman spectroscopy was investigated and many aspects of its performance measuring RCS were characterised. Raman spectroscopy is a viable new technique with limits of detection that are capable of measuring RCS specific respirator inward leakage concentrations with short sampling times, given for example a tight fitting respirator might be worn for an hour or less. Furthermore,

a quantitative measurement of RCS particulate collected onto a filter using Raman spectroscopy is possible for a range of conditions.

The Raman spectroscopy work demonstrated a quantitative linear correlation between mass of analyte and response for various diameters of deposit area (5 mm to 15 mm) and when using a mapping approach to collect spectra from a more representative proportion of the sample. It was found that the depth of the sample deposit was not a factor influencing Raman response when measuring quartz A9950 and the sample was a thin layer (about 3.7 layers of particles 1.39 μm in diameter). The equation for Raman intensity could potentially be modified for aerosol particulate on filter surfaces to exclude depth of deposit. Additional Rayleigh and Raman scattering was considered the cause of a divergence from the linear regression, at loadings greater than 1 mg for a deposit area of 15 mm in diameter; where Raman intensity increased with the increase of filter loadings where XRD response would be attenuated by absorption. This divergence may occur at lower mass loadings for smaller diameter deposits. It's possible that this effect will occur for other respirable-sized powders.

The mapping approach and use of the cumulative average integrated band area was found to be robust when occasional instances of fluorescence or interference occur. The occasional spectra with too much interference can be removed from an average Raman band area calculation for the Raman response from accumulated spectra, if sufficient representative spectra are collected from the sample.

The robustness of the Raman method developed in this work was confirmed when measuring 119 realistic samples from stonemasonry work. Generally, the mass values and proportions of quartz in the samples when measured using Raman spectroscopy were highly correlated with XRD, which was used as a reference method. Raman spectroscopy was shown to be potentially better than XRD when the measurements were not as highly correlated.

Crystallinity of quartz particles was found to be a dominate factor influencing the Raman response. The Raman response closely matched the theoretical crystallinity of particles of various diameters. In addition, the reported mass

values from Raman and XRD were similar when measuring quartz dusts of different particle diameters.

Reduction in the size of the deposit area was found to improve the limit of detection for all the analytical techniques. Raman spectroscopy obtained the lowest LODs ($\sim 0.25 \mu\text{g}$) when compared with established XRD and FTIR methods.

The development and application of a Raman analytical method was demonstrated for the measurement of RCS specific inward leakage ratios, which will form the basis of experiments to further compare mass and number concentration inward leakage ratios for respirators to assess their protective performance. Initial results on limited samples suggest that instruments with wider measurement ranges than those currently employed for fit testing should be used for workplace studies to compare with WELs. Further work is needed to confirm this finding.

This work demonstrated the potential for chemometric processes combined with FTIR to provide a multicomponent analysis of more than one hazardous component from a single filter. This potentially facilitates better quality information about the exposure of workers to dusts, since this approach can evaluate exposure to more than one hazardous substance. Respirable coal and quartz dust are the examples given in the two articles; although, these chemometric methods might also be useful for other mixed dust scenarios e.g. wood and other minerals in construction dust carpentry or amorphous and crystalline silica.

Chemometric methods were found to have a valuable role to play in reducing the bias of FTIR measurements with interference and for improving the confidence in the reliability of RCS measurements when measuring concentrations as low as, 0.05 mg.m^{-3} . These chemometric models are potentially universally applicable when samples are included in the calibration and validation that are representative of the extreme range of circumstances encountered.

This research demonstrated the use of unweighted calibration uncertainty to estimate the analytical method uncertainty for the chemometric FTIR principal component regression method. This was applied to the predictions for quartz, kaolinite and coal measurements in mine dusts particulate from Australia, South Africa and the United Kingdom collected onto aerosol filters. The equation for calibration uncertainty was found to be a useful approach to employ when it is difficult to prepare replicate samples for precision estimates. The overall expected proportion of samples for a standard uncertainty of measurements (60%) was close to the number that would be included within the calculated estimates of standard analytical method uncertainty using the calibration uncertainty equation. This approach is less time consuming than preparing and measuring replicates and may also be useful to use to supplement or verify limited precision data.

Raman spectroscopy provides excellent potential for sufficiently sensitive measurements which are capable of supporting an evaluation of short-term task-specific activities in the workplace. Some practical limitations remain to be able to apply Raman spectroscopy measurements for the direct on-aerosol filter measurement approach and to confirm that the technique is capable of measuring the wide variety of mixtures of RCS dusts found in workplaces. In particular, brick and foundry dust samples will need further examination as these types of samples might potentially be challenging due the presence of photon absorbing particles and Raman band interferents.

References

1. Taylor, S. R.; McLennan, S. M., *The continental crust: Its composition and evolution*. Blackwell Scientific Pub., Palo Alto, CA: 1985; p Medium: X; Size: Pages: 328.
2. Martin, M., Crystalline Silica: Occurrence and use. *Indoor and Built Environment* **1999**, 8 (2), 82-88.
3. Donaldson, K.; Borm, P. J. A., The quartz hazard: A variable entity. *The Annals of Occupational Hygiene* **1998**, 42 (5), 287-294.
4. Deer, W.; Howie R; Zussman J, *An Introduction to the Rock Forming Minerals*. Longman Group Ltd: London, United Kingdom, 1978.
5. Chisholm, J. E., Determination of cristobalite in respirable airborne dust using X-ray diffraction. *Analytica Chimica Acta* **1994**, 286 (1), 87 - 95.
6. Horwell, C. J.; Williamson, B. J.; Llewellyn, E. W.; Damby, D. E.; Le Blond, J. S., The nature and formation of cristobalite at the soufrière hills volcano, montserrat: implications for the petrology and stability of silicic lava domes. *Bulletin of Volcanology* **2013**, 75 (3), 696.
7. Dyson, D. J.; Butler, M. A.; R.J., H.; Fisher, R.; G.W., H., The de-vitrification of alumino-silicate ceramic fibre materials - the kinetics of the formation of different crystalline phases. *Ann. occup. Hyg* **1997**, 41 (5), 561 - 590.
8. Fernández Rodríguez, P.; Díaz Huerta, V.; Madera García, J.; Martínez-Blanco, D.; Blanco, J. A., Crystalline silica in quartz agglomerates: a study of bulk materials and an evaluation of the respirable levels in workplace atmospheres. Harper, M.; Lee, T., Eds. ASTM International: West Conshohocken, PA, 2013; pp 54-72.
9. Keat, P., A new crystalline silica. *Science* **1954**, 120 (3113), 328-330.
10. Bragg, W. H., The X-ray spectra given by crystals of sulphur and quartz. *Proceedings of the Royal Society of London. Series A, Containing Papers of a Mathematical and Physical Character* **1914**, 89 (614), 575-580.
11. Saksena, B. D., Analysis of the Raman and Infrared spectra of α -quartz. *Proc. Indian Acad. Sci.* **1940**, 12A, 93-139.
12. Worrall, D. M., *Clays and Ceramic Raw Materials*. Springer Netherlands: 1986.
13. Dollase, W. A., Reinvestigation of the structure of low cristobalite. *Zeitschrift fur Kristallographie* **1965**, 121, 369-377.
14. CEN, EN 481:1993 Workplace atmospheres — Size fraction definitions for measurement of airborne particles. Euopean Commitee for Standardisation: Brussels, 1993.
15. HSE EH75 *Respirable Crystalline Silica, Variability in fibrogenic potency and exposure-response relationships for silicosis*; ISBN 978 0 7176 2191 0; Health and Safety Executive: Richmond, Surrey, United Kingdom., 2003.

16. Greenberg, M. I.; Waksman, J.; Curtis, J., Silicosis: A Review. *Disease-a-month* **2007**, *53* (8), 394-416.
17. NIOSH *Health effects of occupational exposure to respirable crystalline silica*; Department of Health and Human Services, Centers for Disease Control and Prevention, National Institute for Occupational Safety and Health: Publications Dissemination, 4676 Columbia Parkway, Cincinnati, OH 45226–1998, United States, 2002.
18. Guha, N.; Straif, K.; Benbrahim-Tallaa, L., The IARC Monographs on the carcinogenicity of crystalline silica. *Med Lav* **2011**, *102* (4), 310-320.
19. Brown T; Cherrie JW; Van Tongeren M; Fortunato L; Hutchings S; L, R. *The burden of occupational cancer in Great Britain. Lung cancer*, Health and Safety Executive: Bootle, Liverpool, 2012.
20. Guha, N.; Straif, K.; Tallaa, L., The IARC Monographs on the carcinogenicity of crystalline silica. *Med Lav* **2011**, *102*, 310-20.
21. Rushton, L.; Hutchings, S. J.; Fortunato, L.; Young, C.; Evans, G. S.; Brown, T.; Bevan, R.; Slack, R.; Holmes, P.; Bagga, S.; Cherrie, J. W.; Van Tongeren, M., Occupational cancer burden in Great Britain. *British Journal of Cancer* **2012**, *107* (Suppl 1), S3-S7.
22. Union, E., Directive (EU) 2017/2398 of the European Parliament and of the Council of 12 December 2017 amending Directive 2004/37/EC on the protection of workers from the risks related to exposure to carcinogens or mutagens at work In 32004L0037, Official Journal of the European Union: Brussels, Belgium, 2017.
23. Wagner, G. R., Asbestosis and silicosis. *The Lancet* **1997**, *349* (9061), 1311-1315.
24. Hoy, R. F.; Baird, T.; Hammerschlag, G.; Hart, D.; Johnson, A. R.; King, P.; Putt, M.; Yates, D. H., Artificial stone-associated silicosis: a rapidly emerging occupational lung disease. *Occupational and Environmental Medicine* **2018**, *75* (1), 3-5.
25. Bradshaw., L.; Bowen., J.; Fishwick., D.; Powell., S. *Health surveillance in silica exposed workers*; Health and Safety Executive, Science Division: HSE Books, Norwich, United Kingdom, 2010.
26. Clouter, A.; Brown, D.; Höhr, D.; Borm, P.; Donaldson, K., Inflammatory effects of respirable quartz collected in workplaces versus standard DQ12 quartz: Particle Surface Correlates. *Toxicological Sciences* **2001**, *63* (1), 90-98.
27. Pavan, C.; Fubini, B., Unveiling the variability of “Quartz Hazard” in light of recent toxicological findings. *Chemical Research in Toxicology* **2017**, *30* (1), 469-485.
28. Vallyathan, V.; Kang, J. H.; Van Dyke, K.; Dalai, N. S.; Castranova, V., Response of alveolar macrophages to in vitro exposure to freshly fractured versus aged silica dust: The ability of prosil 28, an organosilane material, to coat silica and reduce its biological reactivity. *Journal of Toxicology and Environmental Health* **1991**, *33* (3), 303-315.

29. Jacobsen, M.; Rae, S.; Walton, W. H.; Rogan, J. M., The relation between pneumoconiosis and dust-exposure in British coal mines. *Inhaled Part* **1970**, 2, 903-919.
30. T. Ogden., History of Occupational Hygiene Part 8. What coal taught us about dust measurement. Silica, Coal Dust and TB. *Exposure* 2020.
31. Rogan, J. M.; Attfield, M. D.; Jacobsen, M.; Rae, S.; Walker, D. D.; Walton, W. H., Role of dust in the working environment in development of chronic bronchitis in British coal miners. *Br J Ind Med* **1973**, 30 (3), 217-26.
32. Miller, B. G.; Hagen, S.; Love, R. G.; Soutar, C. A.; Cowie, H. A.; Kidd, M. W.; Robertson, A., Risks of silicosis in coalworkers exposed to unusual concentrations of respirable quartz. *Occupational and Environmental Medicine* **1998**, 55 (1), 52-58.
33. HSE, *The Control of Substances Hazardous to Health Regulations 2002 (as amended)*. Health and Safety Executive, Crown: Norwich, United Kingdom, 2005.
34. HSE, *The Control of Substances Hazardous to Health Regulations 2002. Approved Code of Practice and guidance*. 6th ed.; HSE Books,: The Stationery Office, Norwich, United Kingdom, 2013.
35. HSE, HSG 173 Monitoring Strategies for Toxic Substances. (HSE), T. H. a. S. E., Ed. The Stationary Office: HSE Books, Sudbury, Suffolk, United Kingdom, 2006.
36. Stacey, P.; Mecchia, M.; Verpaele, S.; Pretorius, C.; Key-Schwartz, R.; Mattenklott, M.; Eypert-Blaison, C.; Thorpe, A.; Roberts, P.; Frost, G., *Differences between samplers for respirable dust and the analysis of quartz—An international study*. ASTM International: West Conshohocken, PA, 2014; p 30.
37. ISO. BSI, ISO 16258- 1. Workplace Air - Analysis of Respirable Crystalline Silica using X-ray Diffraction. Part 1. Direct-on-filter Method British Standards Institution: Chiswick, London, 2015.
38. Marple, V.; Rubow, K.; Olson, B., Inertial, Gravitational, Centrifugal, and Thermal Collection Techniques. In *Aerosol Measurement: Principles, Techniques and Applications.*, Willeke, K.; Baron, P., Eds. Van Nostrand Reinhold: New York, United States of America, 1993.
39. Vincent, J., *Aerosol Sampling: Science and Practice*. John Wiley & Sons Ltd.: Bath, United Kingdom., 1989.
40. Harris, G. W.; Maguire, B. A., A gravimetric dust sampling instrument (Simpeds): Preliminary results. *The Annals of Occupational Hygiene* **1968**, 11 (3), 195-201.
41. Higgins, R. I.; Dewell, P., A gravimetric size-selecting personal dust sampler. In *Inhaled Particles and Vapours*, Davies, C. N., Ed. Pergamon: 1967; pp 575-586.
42. Soo, J.-C.; Lee, T.; Kashon, M.; Kusti, M.; Harper, M., Quartz in Coal Dust Deposited on Internal Surface of Respirable Size Selective Samplers. *Journal of Occupational and Environmental Hygiene* **2014**, 11 (12), D215-D219.

43. Blackford, D. B.; Harris, G. W.; Revell, G., The reduction of dust losses within the cassette of the SIMPEDS personal dust sampler. *The Annals of Occupational Hygiene* **1985**, 29 (2), 169-180.
44. Kenny, L.; Chung, K.; Dilworth, M.; Hammond, C.; Jones, J. W.; Shreeve, Z.; Winton, J., Applications of low-cost, dual-fraction dust samplers. *The Annals of Occupational Hygiene* **2001**, 45 (1), 35-42.
45. Stacey, P.; Thorpe, A.; Mogridge, R.; Lee, T.; Harper, M., A new miniature respirable sampler for in-mask sampling: Part 1—Particle size selection performance. *The Annals of Occupational Hygiene* **2016**, 60 (9), 1072-1083.
46. Mogridge, R.; Stacey, P.; Forder, J., A new miniature respirable sampler for in-mask sampling: Part 2—Tests performed inside the mask. *The Annals of Occupational Hygiene* **2016**, 60 (9), 1084-1091.
47. Nevalainen, A.; Willeke, K.; Liebhaber, F.; Pastuszka, J., Bioaerosol Sampling. In *Aerosol Measurement: Principles, Techniques, and Applications*, Willeke, K.; Baron, P., Eds. Van Nostrand Rienhold, New York, United States of America., 1993.
48. HSE, *EH40/2005 Workplace exposure limits, Containing the list of workplace exposure limits for use with the Control of Substances Hazardous to Health Regulations (as amended)*. Health and Safety Executive, Crown, Norwich, United Kingdom, 2005.
49. NIOSH, *Chapter R Determination of Airborne Crystalline Silica*. Department of Health and Human Services, National Institute for Occupational Safety and Health (NIOSH). Cincinnati, United States, 2004; Vol. Publication 94-113.
50. Miles, W. J.; Hamilton, R. D., Chemical methods of analysis for crystalline silica: A critical literature review. *Analytica Chimica Acta* **1994**, 286 (1), 3-7.
51. Das, A. K.; Sweet, T. R., Crystalline silica analysis in minerals by mixed flux fusion followed by atomic absorption spectrophotometry. *American Industrial Hygiene Association Journal* **1978**, 39 (9), 762-766.
52. NIOSH, *Silica, Crystalline by UV/Vis Method 7601*. Department of Human Health Services, National Institute for Occupational Safety and Health (NIOSH): Cincinnati, United States, 2004.
53. Eller, P. M.; Feng, H. A.; Song, R. S.; Key-Schwartz, R. J.; Esche, C. A.; Groff, J. H., Proficiency Analytical Testing (PAT) silica variability, 1990–1998. *American Industrial Hygiene Association Journal* **1999**, 60 (4), 533-539.
54. Miles, W. J., Issues and controversy: The measurement of crystalline silica; review papers on analytical methods. *American Industrial Hygiene Association Journal* **1999**, 60 (3), 396-402.
55. HSE, *Methods for the Determination of Hazardous Substances, MDHS 101/2 Crystalline silica in respirable airborne dust, Direct On-Filter Analyses by Infrared Spectroscopy and X-ray Diffraction*. Crown: Health and Safety Executive (HSE), Norwich, United Kingdom, 2014.

56. OSHA, Method ID142. Crystalline Silica. Quartz and Cristobalite Industrial Hygiene Chemistry Division, Ed. OSHA Salt Lake Technical Center, Sandy UT 84070-6406, United States., 2015.
57. NIOSH, *Silica, Crystalline, by XRD (filter redeposition) Method 7500*. Department of Health and Human Services, National Institute for Occupational Safety and Health: 2004.
58. Connolly, J. Introduction to X-ray Powder Diffraction www.fp.fkp.nat.uni.erlangen.de/advanced-laboratory-course/selection-of-experiments/MSc-Zusatzmaterial/M41_More_information_for_the_interested.pdf.
59. Liu, J.; Saw, R.; Kiang, Y. H., Calculation of effective penetration depth in X-ray diffraction for pharmaceutical solids. *Journal of pharmaceutical sciences* **2010**, 99, 3807-14.
60. Mecchia, M.; Pretorius, C.; Stacey, P.; Mattenklott, M.; Incocciati, E., *X-ray absorption effect in aerosol samples collected on filter media*. ASTM International: West Conshohocken, PA, United States of America, 2013.
61. Smith, D. K., Evaluation of the detectability and quantification of respirable crystalline silica by X-ray powder diffraction methods. *Powder Diffraction* **2013**, 12 (4), 200-227.
62. LeRoux, J.; Lennox, D. H.; Kay, K., Direct quantitative X-ray analysis by diffraction-absorption technique. *Analytical Chemistry* **1953**, 25 (5), 740-743.
63. Ritz, M.; Vaculíková, L.; Plevová, E.; Matýsek, D.; J, M., Determination of chlorite, muscovite, albite and quartz in claystones and clay shales by infrared spectroscopy and partial least-squares regression. *Acta Geodynamica et Geomaterialia* **2012**, 9.
64. ISO. BSI, ISO 16258- 2. *Workplace Air - Analysis of Respirable Crystalline Silica using X-ray Diffraction. Part 2. Indirect Method* British Standards Institution: Chiswick, London, 2015.
65. Stacey, P.; Kauffer, E.; Moulut, J.-C.; Dion, C.; Beauparlant, M.; Fernandez, P.; Key-Schwartz, R.; Friede, B.; Wake, D., An International Comparison of the Crystallinity of Calibration Materials for the Analysis of Respirable alpha-Quartz Using X-ray Diffraction and a Comparison with Results from the Infrared KBr Disc Method. *Annals of Occupational Hygiene* **2009**, 53 (6), 639-649.
66. Stach, R.; Barone, T.; Cauda, E.; Krebs, P.; Pejic, B.; Daboss, S.; Mizaikoff, B., Direct infrared spectroscopy for the size-independent identification and quantification of respirable particles relative mass in mine dusts. *Analytical and Bioanalytical Chemistry* **2020**, 412.
67. Atkins, P. W., *Physical Chemistry*. Second Edition ed.; Oxford University Press: Walton Street, Oxford, OX2 6DP, United Kingdom, 1982.
68. Foster, R. D.; Walker, R. F., Quantitative determination of crystalline silica in respirable-size dust samples by infrared spectrophotometry. *Analyst* **1984**, 109 (9), 1117-1127.

69. Bye, E., Chemometrics in aerosol analysis: Quantitative analysis of silica dust mixtures by multivariate calibration applied to Infrared spectroscopy. *The Annals of Occupational Hygiene* **1994**, 38 (inhaled_particles_VII), 519-525.
70. Nielsen, J. R., THE RAMAN EFFECT. *School Science and Mathematics* **1929**, 29 (6), 581-589.
71. Raman, C. V.; Krishnan, K. S., A new type of secondary radiation. *Nature* **1928**, 121 (3048), 501-502.
72. Fabelinskiĭ, I. L., Seventy years of combination (Raman) scattering. *Physics-Uspekhi* **1998**, 41 (12), 1229-1247.
73. Bard, D. Raman spectroscopic characterisation of inorganic fibres and particles and their coverage by wetting agents. 1998.
74. Paul, W. Raman microscopy studies of carbon particles from diesel particulate matter and coal dust. Sheffield Halam University, Sheffield, 2001.
75. Ferraro, J. R.; Nakamoto, K.; Brown, C. W., *Introductory Raman Spectroscopy*. Elsevier Science & Technology: San Diego, UNITED STATES, 2003.
76. Elcombe, M. M., Some aspects of the lattice dynamics of quartz. *Proceedings of the Physical Society* **1967**, 91 (4), 947-958.
77. Scott, J. F.; Porto, S. P. S., Longitudinal and transverse optical lattice vibrations in quartz. *Physical Review* **1967**, 161 (3), 903-910.
78. Swainson, I. P.; Dove, M. T.; Palmer, D. C., Infrared and Raman spectroscopy studies of the α - β phase transition in cristobalite. *Physics and Chemistry of Minerals* **2003**, 30 (6), 353-365.
79. Cherukuri, S. C.; Pye, L. D.; Chakraborty, I. N.; Condrate, R. A.; Ferraro, J. R.; Cornilsen, B. C.; Martin, K., The vibrational spectra and normal coordinate analysis of ^{28}Si - and ^{29}Si -substituted α -cristobalite. *Spectroscopy Letters* **1985**, 18 (2), 123-137.
80. Placzek, G., *The Rayleigh and Raman Scattering*. UCRL Translation No 526 (L) Physis, Lawrence Radiation Laboratory ed.; Akademische Verlagsgesellschaft: Leipzig, 1934; Vol. 2.
81. Sato, R. K.; McMillan, P. F., An infrared and Raman study of the isotopic species of α -quartz. *The Journal of Physical Chemistry* **1987**, 91 (13), 3494-3498.
82. Bates, J. B., Raman spectra of α and β cristobalite. *The Journal of Chemical Physics* **1972**, 57 (9), 4042-4047.
83. Sherwood, P. M. A., *Vibration spectroscopy of solids* Cambridge University Press: Cambridge, 1972.
84. Tuschel, D., Why are the raman spectra of crystalline and amorphous solids different? *Spectroscopy* **2017**, 32 (3), 26-33.
85. Stacey, P.; Mader, K. T.; Sammon, C., Feasibility of the quantification of respirable crystalline silica by mass on aerosol sampling filters using Raman microscopy. *Journal of Raman Spectroscopy* **2017**, 48 (5), 720-725.

86. Giles, J. H.; Gilmore, D. A.; Denton, M. B., Quantitative analysis using Raman spectroscopy without spectral standardization. *Journal of Raman Spectroscopy* **1999**, 30 (9), 767-771.
87. Schrader, B.; Bergmann, G., Die intensität des ramanspektrums polykristalliner substanzen. *Fresenius' Zeitschrift für analytische Chemie* **1967**, 225 (2), 230-247.
88. Schrader, B.; Hoffmann, A.; Keller, S., Near-Infrared Fourier transform Raman spectroscopy: Facing absorption and background. *Spectrochimica Acta Part A: Molecular Spectroscopy* **1991**, 47 (9), 1135-1148.
89. Jawhari, T.; Hendra, P. J.; Willis, H. A.; Judkins, M., Quantitative analysis using Raman methods. *Spectrochimica Acta Part A: Molecular Spectroscopy* **1990**, 46 (2), 161-170.
90. Pellow-Jarman, M. V.; Hendra, P. J.; Lehnert, R. J., The dependence of Raman signal intensity on particle size for crystal powders. *Vibrational Spectroscopy* **1996**, 12 (2), 257-261.
91. Wang, H.; Mann, C. K.; Vickers, T. J., Effect of powder properties on the intensity of Raman scattering by crystalline solids. *Appl. Spectrosc.* **2002**, 56 (12), 1538-1544.
92. Hu, Y.; Wikström, H.; Byrn, S. R.; Taylor, L. S., Analysis of the effect of particle size on polymorphic quantitation by Raman spectroscopy. *Appl. Spectrosc.* **2006**, 60 (9), 977-984.
93. Townshend, N.; Nordon, A.; Littlejohn, D.; Myrick, M.; Andrews, J.; Dallin, P., Comparison of the determination of a low-concentration active ingredient in pharmaceutical tablets by backscatter and transmission Raman spectrometry. *Analytical Chemistry* **2012**, 84 (11), 4671-4676.
94. Chio, C. H.; Sharma, S. K.; Lucey, P. G.; Muenow, D. W., Effects of particle size and laser-induced heating on the raman spectra of alpha quartz grains. *Appl. Spectrosc.* **2003**, 57 (7), 774-783.
95. Duy, P. K.; Chun, S.; Chung, H., Characterization of Raman scattering in solid samples with different particle sizes and elucidation on the trends of particle size-dependent intensity variations in relation to changes in the sizes of laser illumination and detection area. *Analytical Chemistry* **2017**, 89 (22), 11937-11943.
96. Bowie, B. T.; Griffiths, P. R., Determination of the resolution of a multichannel Raman spectrometer using Fourier transform Raman spectra. *Appl. Spectrosc.* **2003**, 57 (2), 190-196.
97. Shin, K.; Chung, H., Wide area coverage Raman spectroscopy for reliable quantitative analysis and its applications. *Analyst* **2013**, 138 (12), 3335-46.
98. Pelletier, M. J., Quantitative analysis using Raman spectrometry. *Appl. Spectrosc.* **2003**, 57 (1), 20A-42A.
99. Tuschel, D., The effect of microscope objectives on the Raman spectra of crystals. *Spectroscopy* **2017**, 32 (9), 14-23.
100. Kingma K, H. R., Raman spectroscopic study of microcrystalline silica. *American Mineralogist* **1994**, 79, 269-273.

101. Wang A, J. B., Haskin L Raman spectroscopy as a method for mineral identification on lunar robotic exploration missions. *Journal of Geophysical Research* **1995**, 100 (E10), 21,189 - 21,199
102. Pop, D.; Constantina, C.; Tătar, D.; Kiefer, W., Raman spectroscopy on gem-quality microcrystalline and amorphous silica varieties from Romania *Studia UBB Geologia* **2004**, 49 (1), 41-52.
103. Noguchi N, S. K., Masuda K, Quantitative analysis of binary mineral mixtures using Raman microspectroscopy: Calibration curves for silica and calcium carbonate minerals and application to an opaline silica nodule of volcanic origin. *Journal of Mineralogical and Petrological Sciences* **2009**, 104.
104. Deng, C.; Brooks, S. D.; Vidaurre, G.; Thornton, D. C. O., Using Raman microspectroscopy to determine chemical composition and mixing state of airborne marine aerosols over the pacific ocean. *Aerosol Science and Technology* **2014**, 48 (2), 193-206.
105. Doughty, D. C.; Hill, S. C., Automated aerosol Raman spectrometer for semi-continuous sampling of atmospheric aerosol. *Journal of Quantitative Spectroscopy and Radiative Transfer* **2017**, 188, 103-117.
106. Ghosal, S.; Macher, J. M.; Ahmed, K., Raman Microspectroscopy-based identification of individual fungal spores as potential indicators of indoor contamination and moisture-related building damage. *Environmental Science & Technology* **2012**, 46 (11), 6088-6095.
107. Halvorson, R. A.; Vikesland, P. J., Surface-Enhanced Raman Spectroscopy (SERS) for environmental analyses. *Environmental Science & Technology* **2010**, 44 (20), 7749-7755.
108. Ji, Z.; Dai, R.; Zhang, Z., Characterization of fine particulate matter in ambient air by combining TEM and multiple spectroscopic techniques--NMR, FTIR and Raman spectroscopy. *Environ Sci Process Impacts* **2015**, 17 (3), 552-60.
109. Lutin, A.; Bulatov, V.; Jadwat, Y.; Wood, N. H.; Feller, L.; Schechter, I., Fourier transform spectral imaging microscopy (FT-SIM) and scanning Raman microscopy for the detection of indoor common contaminants on the surface of dental implants. *Talanta* **2015**, 134, 514-23.
110. Soewono, A.; Rogak, S., Morphology and Raman spectra of engine-emitted particulates. *Aerosol Science and Technology* **2011**, 45 (10), 1206-1216.
111. Potgieter-Vermaak, S. S.; Van Grieken, R., Preliminary Evaluation of Micro-Raman spectrometry for the characterization of individual aerosol particles. *Appl. Spectrosc.* **2006**, 60 (1), 39-47.
112. Catelani, T.; Pratesi, G.; Zoppi, M., Raman characterization of ambient airborne soot and associated mineral phases. *Aerosol Science and Technology* **2014**, 48 (1), 13-21.
113. Grafen, M.; Nalpantidis, K.; Platte, F.; Monz, C.; Ostendorf, A., multivariate characterization of a continuous soot monitoring system based on Raman spectroscopy. *Aerosol Science and Technology* **2015**, 49 (10), 997-1008.

114. Mertes, S.; Dippel, B.; Schwarzenböck, A., Quantification of graphitic carbon in atmospheric aerosol particles by Raman spectroscopy and first application for the determination of mass absorption efficiencies. *Journal of Aerosol Science* **2004**, 35 (3), 347-361.
115. Popovicheva, O.; Kireeva, E.; Persiantseva, N.; Timofeev, M.; Blatt, H.; Ivleva, N. P.; Niessner, R.; Moldanova, J., Microscopic characterization of individual particles from multicomponent ship exhaust. *Journal of Environmental Monitoring* **2012**, 14 (12), 3101-3110.
116. Stefaniak, E. A.; Buczynska, A.; Novakovic, V.; Kuduk, R.; Grieken, R. V., Determination of chemical composition of individual airborne particles by SEM/EDX and micro-Raman spectrometry: A review. *Journal of Physics: Conference Series* **2009**, 162 (1), 012019.
117. Bumrah, G. S.; Sharma, R. M., Raman spectroscopy – Basic principle, instrumentation and selected applications for the characterization of drugs of abuse. *Egyptian Journal of Forensic Sciences* **2016**, 6 (3), 209-215.
118. Hirschfeld, T.; Chase, B., FT-Raman Spectroscopy: Development and justification. *Appl. Spectrosc.* **1986**, 40 (2), 133-137.
119. Fran, A., Considerations of grating selection in optimizing a Raman spectrograph. *Spectroscopy* **2013**, 28 (10).
120. Wang, Y.; McCreery, R. L., Evaluation of a diode laser/charge coupled device spectrometer for near-infrared Raman spectroscopy. *Analytical Chemistry* **1989**, 61 (23), 2647-2651.
121. Chase, B., A new generation of Raman instrumentation. *Appl. Spectrosc.* **1994**, 48 (7), 14A-19A.
122. Andersen, M. E.; Muggli, R. Z., Microscopical techniques in the use of the molecular optics laser examiner Raman microprobe. *Analytical Chemistry* **1981**, 53 (12), 1772-1777.
123. CEN, EN 482:2012+A1:2015 Workplace exposure. General requirements for the performance of procedures for the measurement of chemical agents. Comité Européen De Normalisation: Brussels, Belgium, 2015.
124. ISO, BSI ISO 20581 Workplace air — General requirements for the performance of procedures for the measurement of chemical agents. International Organization for Standardization: Geneva, Switzerland, 2016.
125. ISO, ISO 19087:2018 Workplace air — Analysis of respirable crystalline silica by Fourier-Transform Infrared spectroscopy. International Organisation for Standardisation, : Geneva, Switzerland, 2018.
126. NIOSH, *Quartz in coal mine dust by Infrared (redeposition) Method 7603*. Department of Health and Human Services, National Institute for Occupational Safety and Health (NIOSH): Cincinnati, United states, 2004.
127. HSE, *HSG173 Monitoring strategies for toxic substances*. Health and Safety Executive, Crown: The Stationery Office, PO Box 29, Norwich NR31GN United Kingdom, 2006.
128. Cauda, E.; Chubb, L.; Reed, R.; Stepp, R., Evaluating the use of a field-based silica monitoring approach with dust from copper mines. *Journal of Occupational and Environmental Hygiene* **2018**, 15 (10), 732-742.

129. Swanson, J.; Pham, L.; Xue, J.; Durbin, T.; Russell, R.; Miller, W.; Kittelson, D.; Jung, H.; Johnson, K., Uncertainty in gravimetric analysis required for LEV III light-duty vehicle PM emission measurements. *SAE International Journal of Engines* **2018**, 11 (3), 349-362.
130. Stacey, P., Analytical performance criteria - Measurements of silica in air: Reliability at new and proposed occupational exposure limits. *Journal of Occupational and Environmental Hygiene* **2007**, 4 (1), D1-D4.
131. Bartley, D. L., Definition and assessment of sampling and analytical accuracy. *The Annals of Occupational Hygiene* **2001**, 45 (5), 357-364.
132. Stacey, P.; Tylee, B.; Bard, D.; Atkinson, R., The performance of laboratories analysing alpha-quartz in the Workplace Analysis Scheme for Proficiency (WASP). *Annals of Occupational Hygiene* **2003**, 47 (4), 269-277.
133. Cox, L. A.; Van Orden, D. R.; Lee, R. J.; Arlauckas, S. M.; Kautz, R. A.; Warzel, A. L.; Bailey, K. F.; Ranpuria, A. K., How reliable are crystalline silica dust concentration measurements? *Regulatory Toxicology and Pharmacology* **2015**, 73 (1), 126-136.
134. OSHA *Preliminary Economic Analysis and Initial Regulatory Flexibility Analysis, Supporting document for the Notice of Proposed Rulemaking for Occupational Exposure to Crystalline Silica*; Occupational Safety and Health Administration, Department of Labor, United States., 2013.
135. Eyfert-Blaison, C.; Moulut, J.-C.; Lecaque, T.; Marc, F.; Kauffer, E., Validation of the analysis of respirable crystalline silica (quartz) in foams used with CIP 10-R samplers. *Annals of Occupational Hygiene* **2011**, 55 (4), 357-368.
136. Nebbia, R.; Genta, G.; Zuliani, P.; Patrucco, M.; Pira, E.; Galetto, M., Measurement of respirable crystalline silica concentration by X-ray diffraction: Evaluation of metrological performances. *Measurement* **2021**, 183, 109839.
137. CEN, B., EN 689:2018. Workplace Exposure - Measurement of exposure by inhalation to chemical agents - Strategy for testing compliance with occupational exposure limit values. British Standards Institution (BSI): Chiswick, London, 2018.
138. ISO, ISO 24095:2009. Workplace air - Guidance for the measurement of respirable crystalline silica. International Standards Organisation Geneva, Switzerland, ISBN 978 0 580 58960 7, 2009.
139. Harper, M.; Sarkisian, K.; Andrew, M., Assessment of respirable crystalline silica analysis using proficiency analytical testing Results from 2003-2013. *Journal of occupational and environmental hygiene* **2014**, 11, D157-63.
140. Lee, R. J.; Van Orden, D. R.; Cox, L. A.; Arlauckas, S.; Kautz, R. J., Impact of muffle furnace preparation on the results of crystalline silica analysis. *Regulatory Toxicology and Pharmacology* **2016**, 80, 164-172.
141. Harper, M.; Key-Schwartz, R. J., Letter to the Editor: Preparation of respirable crystalline silica samples for subsequent analysis. *Regulatory Toxicology and Pharmacology* **2017**, 83, 100-102.
142. Lee, T.; Chisholm, W. P.; Kashon, M.; Key-Schwartz, R. J.; Harper, M., Consideration of kaolinite interference correction for quartz measurements in

- coal mine dust. *Journal of Occupational and Environmental Hygiene* **2013**, 10 (8), 425-434.
143. Kauffer, E.; Masson, A.; Moulut, J. C.; Lecaque, T.; Protois, J. C., Comparison of direct (X-ray diffraction and Infrared Spectrophotometry) and Indirect (Infrared Spectrophotometry) methods for the analysis of α -quartz in airborne dusts. *The Annals of Occupational Hygiene* **2005**, 49 (8), 661-671.
144. Chisholm, J., Comparison of quartz standards for X-ray diffraction analysis: HSE A9950 (Sikron F600) and NIST SRM 1878. *Annals of Occupational Hygiene* **2005**, 49 (4), 351-358.
145. Gordon, R. L.; Harris, G. W., Effect of particle-size on the quantitative determination of quartz by X-ray diffraction. *Nature* **1955**, 175 (4469), 1135-1135.
146. Kauffer, E.; Moulut, J. C.; Masson, A.; Protois, J. C.; Grzebyk, M., Comparison by X-ray Diffraction and Infrared spectroscopy of two samples of α quartz with the NIST SRM 1878a α quartz. *The Annals of Occupational Hygiene* **2002**, 46 (4), 409-421.
147. Pickard, K. J.; Walker, R. F.; West, N. G., A Comparison Of X-ray diffraction and infra-red spectrophotometric methods for the analysis of α -quartz in airborne dusts. *The Annals of Occupational Hygiene* **1985**, 29 (2), 149-167.
148. Page, S. J., Comparison of coal mine dust size distributions and calibration standards for crystalline silica analysis. *AIHA Journal* **2003**, 64 (1), 30-39.
149. Dodgson, J.; Whitaker, W., The determination of quartz in respirable dust samples by infrared spectrophotometry—I: The potassium bromide disc method. *The Annals of Occupational Hygiene* **1973**, 16 (4), 373-387.
150. Nagelschmidt, G.; Gordon, R. L.; Griffin, O. G., Surface of finely-ground silica. *Nature* **1952**, 169 (4300), 539-540.
151. King, E. J., Solubility Theory of Silicosis. A Critical Study. *Occupational Medicine* **1947**, 4 (1), 26-49.
152. Dempster, P. B.; Ritchie, P. D., Surface of finely-ground silica. *Nature* **1952**, 169 (4300), 538-539.
153. Anderson, P. L., Free silica analysis of environmental samples—a critical literature review. *American Industrial Hygiene Association Journal* **1975**, 36 (10), 767-778.
154. Gómez, D. A.; Coello, J.; MasPOCH, S., The influence of particle size on the intensity and reproducibility of Raman spectra of compacted samples. *Vibrational Spectroscopy* **2019**, 100, 48-56.
155. Hall, S.; Stacey, P.; Pengelly, I.; Stagg, S.; Saunders, J.; Hambling, S., Characterizing and comparing emissions of dust, respirable crystalline silica, and volatile organic compounds from natural and artificial stones. *Annals of Work Exposures and Health* **2021**.
156. MSHA, Infrared determination of quartz in respirable coal mine dust: Method P-7. Mine Safety and Health Administration (MSHA). Pittsburgh, Pa.: MSHA., 1994.

157. Altree-Williams, S.; Lee, J.; Mezin, N. V., Quantitative X-ray diffractometry on respirable dust collected on nuclepore filters. *The Annals of Occupational Hygiene* **1977**, *20* (2), 109-126.
158. Ojima, J., Determining of crystalline silica in respirable dust samples by infrared spectrophotometry in the presence of interferences. *Journal of Occupational Health* **2003**, *45* (2), 94-103.
159. Roggo, Y.; Chalus, P.; Maurer, L.; Lema-Martinez, C.; Edmond, A.; Jent, N., A review of near infrared spectroscopy and chemometrics in pharmaceutical technologies. *Journal of Pharmaceutical and Biomedical Analysis* **2007**, *44* (3), 683-700.
160. Breen, C.; Clegg, F.; Herron, M. M.; Hild, G. P.; Hillier, S.; Hughes, T. L.; Jones, T. G. J.; Matteson, A.; Yarwood, J., Bulk mineralogical characterisation of oilfield reservoir rocks and sandstones using Diffuse Reflectance Infrared Fourier Transform Spectroscopy and Partial Least Squares analysis. *Journal of Petroleum Science and Engineering* **2008**, *60* (1), 1-17.
161. Weakley, A. T.; Miller, A. L.; Griffiths, P. R.; Bayman, S. J., Quantifying silica in filter-deposited mine dusts using infrared spectra and partial least squares regression. *Analytical and Bioanalytical Chemistry* **2014**, *406* (19), 4715-4724.
162. Jolliffe, I. T.; Cadima, J., Principal component analysis: a review and recent developments. *Philosophical Transactions of the Royal Society A: Mathematical, Physical and Engineering Sciences* **2016**, *374* (2065), 20150202.
163. Hemmateenejad, B.; Akhond, M.; Samari, F., A comparative study between PCR and PLS in simultaneous spectrophotometric determination of diphenylamine, aniline, and phenol: Effect of wavelength selection. *Spectrochimica Acta Part A: Molecular and Biomolecular Spectroscopy* **2007**, *67* (3), 958-965.
164. Bjørsvik, H.-R.; Bye, E., Multivariate calibration applied to infrared spectroscopy for quantitative determination of crystalline and amorphous silica. *Appl. Spectrosc.* **1991**, *45* (5), 771-778.
165. Cauda, E.; Miller, A.; Drake, P., Promoting early exposure monitoring for respirable crystalline silica: Taking the laboratory to the mine site. *Journal of Occupational and Environmental Hygiene* **2016**, *13* (3), D39-D45.
166. Miller, A. L.; Drake, P. L.; Murphy, N. C.; Noll, J. D.; Volkwein, J. C., Evaluating portable infrared spectrometers for measuring the silica content of coal dust. *Journal of Environmental Monitoring* **2012**, *14* (1), 48-55.
167. Ashley, E. L.; Cauda, E.; Chubb, L. G.; Tuchman, D. P.; Rubinstein, E. N., Performance comparison of four portable FTIR instruments for direct-on-filter measurement of respirable crystalline silica. *Annals of Work Exposures and Health* **2020**, *64* (5), 536-546.
168. Miller, A. L.; Weakley, T.; Griffiths, P.; Cauda, E.; Bayman, S., Direct-on-filter α -quartz estimation in respirable coal mine dust using transmission Fourier transform infrared spectrometry and partial least squares regression. *Appl. Spectrosc.* **2016**, *71* (5), 1014-1024.

169. Pampeña, J. D.; Cauda, E. G.; Chubb, L. G.; Meadows, J. J., Use of the field-based silica monitoring technique in a coal mine: A Case Study. *Mining, Metallurgy & Exploration* **2020**, 37 (2), 717-726.
170. Martin, J.; Beauparlant, M.; Lesage, J.; Van Tra, H., Development of a quantification method for quartz in various bulk materials by X-ray diffraction and the Rietveld method. *Powder Diffraction* **2012**, 27 (1), 12-19.
171. Zhou, X.; Liu, D.; Bu, H.; Deng, L.; Liu, H.; Yuan, P.; Du, P.; Song, H., XRD-based quantitative analysis of clay minerals using reference intensity ratios, mineral intensity factors, Rietveld, and full pattern summation methods: A critical review. *Solid Earth Sciences* **2018**, 3 (1), 16-29.
172. Stacey, P., A study to assess the performance of an "X-ray powder diffraction with Rietveld" approach for measuring the crystalline and amorphous components of inhalable dust collected on aerosol sampling filters. *Powder Diffraction* **2019**, 1-9.
173. Stacey, P.; Lee, T.; Thorpe, A.; Roberts, P.; Frost, G.; Harper, M., Collection efficiencies of high flow rate personal respirable samplers when measuring arizona road dust and analysis of quartz by X-ray diffraction. *Annals of Occupational Hygiene* **2014**, 58 (4), 512-523.
174. Stacey, P.; Thorpe, A.; Echt, A., Performance of high flow rate personal respirable samplers when challenged with mineral aerosols of different particle size distributions. *The Annals of Occupational Hygiene* **2016**, 60 (4), 479-492.
175. Chisholm, W. P.; Lee, T.; Chirila, M., Determination of crystalline silica in dust at low concentrations by low-temperature infrared spectrometry. *Annual book of ASTM standards. Section 11, Water and environmental technology. ASTM Committee E-35 on Pesticides* **2013**, 2013.
176. Zheng, L.; Kulkarni, P.; Birch, M. E.; Ashley, K.; Wei, S., Analysis of crystalline silica aerosol using portable Raman spectrometry: Feasibility of near real-time measurement. *Analytical Chemistry* **2018**, 90, 6229 - 6239.
177. Wei, S.; Johnson, B.; Breitenstein, M.; Zheng, L.; Snawder, J.; Kulkarni, P., Aerosol analysis using handheld Raman spectrometer: On-site quantification of trace crystalline silica in workplace atmospheres. *Annals of Work Exposures and Health* **2021**.
178. StatPeel Products Identifier S1. Silica Monitoring. <https://www.statpeel.com/products/identifier-s1/> Last Viewed 27/11/22.
179. Everall, N. J., Confocal Raman microscopy: common errors and artefacts. *Analyst* **2010**, 135 (10), 2512-2522.
180. Fischer, P.; Romano, V.; Weber, H. P.; Karapatis, N. P.; Boillat, E.; Glardon, R., Sintering of commercially pure titanium powder with a Nd:YAG laser source. *Acta Materialia* **2003**, 51 (6), 1651-1662.
181. Lohumi, S.; Kim, M.; Qin, J.; Cho, B.-K., Improving sensitivity in Raman imaging for thin layered and powdered food analysis Utilizing a reflection mirror. *Sensors* **2019**, 19.
182. Mos, Y. M.; Vermeulen, A. C.; Buisman, C. J. N.; Weijma, J., X-ray Diffraction of iron containing samples: The importance of a suitable configuration. *Geomicrobiology Journal* **2018**, 35 (6), 511-517.

183. Stacey, P.; Thorpe, A. *Testing of high flow rate respirable samplers to assess the technical feasibility of measuring 0.05mg m⁻¹ respirable crystalline silica*; Health and Safety Executive 2010.
184. CEN, B., EN 1540 Workplace Exposure - Terminology. British Standards Institution: Chiswick, London, 2021.
185. HSE, *Methods for the Determination of Hazardous Substances, MDHS 101/1 Crystalline silica in respirable airborne dust, Direct On-Filter Analyses by Infrared Spectroscopy and X-ray Diffraction*. 1 ed.; Crown: Health and Safety Executive (HSE), Norwich, United Kingdom, 2005.
186. Lee, T.; Lee, L.; Cauda, E.; Hummer, J.; Harper, M., Respirable size-selective sampler for end-of-shift quartz measurement: Development and performance. *Journal of Occupational and Environmental Hygiene* **2017**, 14 (5), 335-342.
187. Wei, S.; Kulkarni, P.; Ashley, K.; Zheng, L., Measurement of crystalline silica aerosol using quantum cascade laser-based Infrared spectroscopy. *Scientific Reports* **2017**, 7 (1), 13860.
188. Rondahl, S. H.; Pointurier, F.; Ahlinder, L.; Ramebäck, H.; Marie, O.; Ravat, B.; Delaunay, F.; Young, E.; Blagojevic, N.; Hester, J. R.; Thorogood, G.; Nelwamondo, A. N.; Ntsoane, T. P.; Roberts, S. K.; Holliday, K. S., Comparing results of X-ray diffraction, μ -Raman spectroscopy and neutron diffraction when identifying chemical phases in seized nuclear material, during a comparative nuclear forensics exercise. *J Radioanal Nucl Chem* **2018**, 315 (2), 395-408.
189. Elton, N. J.; Smith, D. K., *Silica*. CRC Press: 1999; pp 450 - 451.
190. Langer, J.; Jimenez de Aberasturi, D.; Aizpurua, J.; Alvarez-Puebla, R. A.; Augu  , B.; Baumberg, J. J.; Bazan, G. C.; Bell, S. E. J.; Boisen, A.; Brolo, A. G.; Choo, J.; Cialla-May, D.; Deckert, V.; Fabris, L.; Faulds, K.; Garc  a de Abajo, F. J.; Goodacre, R.; Graham, D.; Haes, A. J.; Haynes, C. L.; Huck, C.; Itoh, T.; K  ll, M.; Kneipp, J.; Kotov, N. A.; Kuang, H.; Le Ru, E. C.; Lee, H. K.; Li, J.-F.; Ling, X. Y.; Maier, S. A.; Mayerh  fer, T.; Moskovits, M.; Murakoshi, K.; Nam, J.-M.; Nie, S.; Ozaki, Y.; Pastoriza-Santos, I.; Perez-Juste, J.; Popp, J.; Pucci, A.; Reich, S.; Ren, B.; Schatz, G. C.; Shegai, T.; Schl  cker, S.; Tay, L.-L.; Thomas, K. G.; Tian, Z.-Q.; Van Duyne, R. P.; Vo-Dinh, T.; Wang, Y.; Willets, K. A.; Xu, C.; Xu, H.; Xu, Y.; Yamamoto, Y. S.; Zhao, B.; Liz-Marz  n, L. M., Present and Future of Surface-Enhanced Raman Scattering. *ACS Nano* **2020**, 14 (1), 28-117.
191. Orlando, A.; Franceschini, F.; Muscas, C.; Pidkova, S.; Bartoli, M.; Rovere, M.; Tagliaferro, A., A Comprehensive review on Raman Spectroscopy applications. *Chemosensors* **2021**, 9 (9), 262.
192. Guccione, P.; Lopresti, M.; Milanese, M.; Caliandro, R., Multivariate analysis applications in X-ray diffraction. *Crystals* **2021**, 11 (1), 12.
193. Yu, W. W.; White, I. M., Inkjet Printed surface enhanced Raman spectroscopy array on cellulose paper. *Analytical Chemistry* **2010**, 82 (23), 9626-9630.

194. Mogensen, K. B.; Gühlke, M.; Kneipp, J.; Kadkhodazadeh, S.; Wagner, J. B.; Espina Palanco, M.; Kneipp, H.; Kneipp, K., Surface-enhanced Raman scattering on aluminum using near infrared and visible excitation. *Chemical Communications* **2014**, 50 (28), 3744-3746.
195. Wei, D.; Chen, S.; Liu, Q., Review of fluorescence suppression techniques in Raman Spectroscopy. *Applied Spectroscopy Reviews* **2015**, 50 (5), 387-406.
196. Salehi, M.; Zare, A.; Taheri, A., Artificial Neural Networks (ANNs) and Partial Least Squares (PLS) regression in the quantitative analysis of respirable crystalline silica by Fourier-transform infrared spectroscopy (FTIR). *Annals of Work Exposures and Health* **2020**, 65 (3), 346-357.
197. Ohbuchi, A.; Konya, T.; Fujinawa, G., Improved bench-top X-ray diffractometer for crystalline phase analysis of cement. *Powder Diffraction* **2013**, 28 (4), 249-253.

Appendix 1

Article information

Copyright

All the articles in this thesis were published under an open access licence where the copyright is retained by the Crown. Confirmation that these articles could also be reproduced in their entirety was obtained from Wiley, The Royal Society of Chemistry and Oxford Journals. Copies of the correspondence are available from the author.

Contribution of other authors attributed in the articles

Chapter 3. Feasibility of the quantification of respirable crystalline silica by mass on aerosol sampling filters using Raman microscopy.

Kirsten Mader. Analysis of samples for uncertainty estimates and review of drafts.

Christopher Sammon. Director of studies, analysis of samples for uncertainty estimates, review and authorisation of the drafts.

Chapter 4. An indirect Raman spectroscopy method for the quantitative measurement of respirable crystalline silica collected on filters inside respiratory equipment.

Francis Clegg and Jackie Morton. Contribution to the design and planning of experiments, review of drafts.

Christopher Sammon. Director of studies, contribution to the design and planning, review and authorisation of the drafts.

Chapter 5. Raman spectroscopy and X-ray diffraction responses when measuring health-related micrometre and nanometre particle size fractions of crystalline quartz and the measurement of quartz in dust samples from the cutting and polishing of natural and artificial stones.

Samantha Hall and Steven Stagg. Organisation of wind tunnel tests and collection of samples.

Francis Clegg. Discussion of results and reviewing drafts

Christopher Sammon. Director of studies, planning, review and authorisation of the drafts.

Chapter 6, Multicomponent measurement of respirable quartz, kaolinite and coal dust using Fourier Transform Infrared spectroscopy (FTIR): A comparison between partial least squares and principal component regressions.

Francis Clegg. Specialist advice, quality check of the models and some data, and technical review of drafts

Christopher Sammon. Director of studies, contribution to the planning, review and authorisation of the drafts.

Chapter 7. Application of a Fourier Transform Infrared (FTIR) Principal Component Regression (PCR) Chemometric Method for the Quantification of Respirable Crystalline Silica (Quartz), Kaolinite, and Coal in Coal Mine Dusts from Australia, UK, and South Africa.

Francis Clegg. Specialist advice, quality check of the models and some data, and technical review of drafts

Garry Rhyder. Collection of samples, contribution to design and review of drafts

Christopher Sammon. Director of studies, contribution to the planning, review and authorisation of the drafts.

